Unravelling the Multiscale Temporal Modulations in Seizure Features using Long-term iEEG Recordings

Mariella Panagiotopoulou

A thesis submitted for the degree of
Doctor of Philosophy

School of Computing
Newcastle University
Newcastle upon Tyne
United Kingdom

July 2, 2024

I would like to dedicate this thesis to my family.

Abstract

Epilepsy poses a significant treatment challenge due to its dynamic nature, characterised by fluctuations in pathological brain activity and symptoms. Seizures can manifest in different ways, resulting in diverse spatial and temporal patterns of features within individual patients. While researchers have extensively studied fluctuations over different timescales in seizure occurrence, the presence of similar fluctuations in other seizure features and the expression of the underlying fluctuations in pathological brain regions remain unclear.

To address these gaps, I investigated cyclical patterns of seizure network evolutions and seizure duration (used as proxy for seizure severity) in refractory focal epilepsy patients. Using long-term intracranial EEG (iEEG) recordings, I analysed how seizure features change over time within subjects. Initially, I explored whether temporal fluctuations in iEEG band power over seconds to days could explain variability in seizure evolutions. Within each subject, a combination of ultradian, circadian and some slower fluctuations accounted for most of the diversity in seizure evolution. Then, I explored how seizure severity changes over time using iEEG band power cycles. Combinations of multiple band power cycles explained most of the variability in seizure duration. These findings suggest that cycles over multiple timescales in interictal iEEG properties, such as band power, may modulate seizure features and serve as markers for seizure-modulating processes. I then examined the functional expression of band power cycles in both pathological and healthy brain regions. Interestingly, ultradian and circadian cycles were diminished in brain regions identified as pathological, indicating that brain pathology may alter biological rhythms on similar timescales.

In summary, my research contributes to the understanding of temporal changes in seizure features. Disentangling the dynamic nature of the disease and specifically the seizure modulating factors could improve personalised epilepsy treatments for seizure control. Furthermore, by predicting not only seizure occurrences but also their dynamics, evolutions, severity, and symptoms, my work expands the scope of alternative treatments. Fluctuations in iEEG features may serve as biomarkers for monitoring treatment response and enabling on-demand treatment options. Finally, investigat-

ing the relationship between altered cycles and pathology could unveil the biological rhythm's role in ictogenesis and epileptogenesis.

Declaration

I hereby declare that the contents of this thesis comprise the output of my own work except where specific reference is made to the work of others. No part of this thesis has been submitted for a degree or qualification in Newcastle University, or any other institution.

Mariella Panagiotopoulou

July 2, 2024

Publications

Parts of my thesis work have either been published in peer-reviewed journals or are currently drafted to be submitted for publication. In detail, the publication status of work included in the three research chapters of my thesis can be summarised as follows:

1. **Panagiotopoulou, M.**, Papasavvas, C.A., Schroeder, G.M., Thomas, R.H., Taylor, P.N., & Wang, Y. (2022). 'Fluctuations in EEG band power at subject-specific timescales over minutes to days explain changes in seizure evolutions'. Human Brain Mapping, 43(8), 2460–2477. https://doi.org/10.1002/hbm.25796.

   This publication formed the content of Chapter 2. In this project, I performed all aspects of data analysis, produced all data visualisations, and wrote all of the content for this publication, while receiving guidance and input from my supervisors and other co-authors. The code for this publication is available in the following link: https://zenodo.org/record/5798022#.YqyC1BPMI0Q.

2. **Panagiotopoulou, M.**, Schroeder, G.M., Blickwedel, J., Chowdhury, F.A., Diehl, B., de Tisi, J., Duncan, J.S., Cronie, A., Falconer, J., Faulder, R., Leach, V., Livingstone, S., Thomas, R.H., McEvoy, A.W., Miserocchi, A., Taylor, P.N. & Wang, Y. (2023). 'Seizure duration is associated with multiple timescales in interictal iEEG band power'.

   This work formed the content of Chapter 3 and is currently drafted for being submitted for publication. For this work, I performed the preprocessing, analysis and visualisation of the data. Additionally, I have written the content related to this chapter based on suggestions and guidance from my supervisors and other co-authors.

3. **Panagiotopoulou, M.**, Thornton, C., Schroeder, G.M., Chowdhury, F.A., Diehl, B., Duncan, J.S., McEvoy, A.W., Miserocchi, A., de Tisi, J., Taylor, P.N. & Wang, Y. (2023). 'Diminished circadian and ultradian rhythms in pathological brain tissue in human in vivo'.

This work formed the content of Chapter 4 and is currently drafted for being submitted for publication. For this work, I performed the preprocessing, analysis and visualisation of the data. Furthermore, I have written the content related to this chapter based on suggestions and guidance from my supervisors and other co-authors.

In addition to my thesis work, I have made contributions to the following papers and preprints that have been published:

1. Wang, Y., Schroeder, G.M., Horsley, J.J., **Panagiotopoulou, M.**, Chowdhury, F.A., Diehl, B., Duncan, J.S., McEvoy, A.W., Miserocchi, A., de Tisi, J. & Taylor, P.N. (2023) 'Temporal stability of intracranial EEG abnormality maps for localizing epileptogenic tissue', Epilepsia. https://onlinelibrary.wiley.com/doi/10.1111/epi.17663.

   For this work, I performed the preprocessing of the long-term iEEG and contributed in discussions regarding visualisation of the results.

2. Gascoigne, Waldmann, L., Schroeder, G. M., **Panagiotopoulou, M.**, Blickwedel, J., Chowdhury, F., Cronie, A., Diehl, B., Duncan, J. S., Falconer, J., Faulder, R., Guan, Y., Leach, V., Livingstone, S., Papasavvas, C., Thomas, R. H., Wilson, K., Taylor, P. N., & Wang, Y. (2023). 'A library of quantitative markers of seizure severity', Epilepsia (Copenhagen), 64(4), 1074–1086. https://doi.org/10.1111/epi.17525.

   I contributed to this work in terms of conceptualisation, methodology, formal analysis and writing.

3. Schroeder, G.M., Karoly, P.J., Maturana, M., **Panagiotopoulou, M.**, Taylor, P.N., Cook, M.J., & Wang, Y. (2022). 'Chronic iEEG recordings and interictal spike rate reveal multiscale temporal modulations in seizure states'. https://arxiv.org/abs/2201.11600.

   In this work, I contributed to discussions regarding the methodology, analysis and was involved in writing.

Acknowledgements

First and foremost, I would like to express my gratitude to my supervisors, Yujiang Wang and Rhys Thomas, for their valuable help and guidance through my research work. Also, I would like to express my sincere gratitude to the entire group of people constituting the Center for Doctoral Training in Cloud Computing for Big Data, but especially to Jennifer Wood and my fellow PhD students for their help and friendship.

I would also like to thank the Computational Neurology, Neuroscience, and Psychiatry Lab, School of Computing (CNNP Lab) for their support and valuable insights on my research work. All CNNP lab members provided outstanding feedback, ideas and thoughts regarding my work throughout my PhD research. I want also to give my deepest appreciation to Chris Papasavvas for his mentorship at my first steps as a PhD student and our discussions on different ideas regarding my first research project. I must also thank Gabrielle Marie Schroeder for her valuable ideas on different aspects of my research journey, such as writing process, effective visualisations and most importantly her research work that formed an inspiration and a major pillar for the completion of my first research project.

I would also like to extend my thanks to our collaborators at University College London Hospital (UCLH) for the epilepsy monitoring unit data. I am grateful for their comments and insights especially for my second project. Also, I am sincerely grateful to our UCLH collaborators for providing the data allowing me to conduct two additional analyses that formed the second and third chapters of my PhD thesis.

Additionally, I am grateful to the Engineering and Physical Sciences Research Council for funding my research [grant number EP/L015358/1].

Finally, I would like to thank my family, for their support and patience throughout my PhD journey.

Abbreviations

AED antiepileptic drug

ASM antiseizure medication

ANT-DBS deep brain stimulation of the anterior nucleus of the thalamus

AUC area under the curve

CCA canonical correlation analysis

CEEMDAN complete ensemble EMD with adaptive noise

CT computed tomography

CV-MSE cross-validation mean square error

ECoG electrocorticography

EEG electroencephalography

EEMD ensemble EMD

EMD empirical mode decomposition

EZ epileptogenic zone

FDR false discovery rate

FFT fast fourier transform

fMRI functional magnetic resonance imaging

FTBTC focal to bilateral tonic clonic

GGC Glasgow and Clyde center

HFO high frequency oscillations

IBE International Bureau for Epilepsy

IED interictal epileptiform discharge

iEEG intracranial EEG

ILAE International League Against Epilepsy

IMF intrinsic mode function

LASSO least absolute shrinkage and selection operator

LOOCV leave one out cross validation

MEMD multivariate empirical mode decomposition

MRI magnetic resonance imaging

MSE mean square error

MTLE mesial temporal lobe epilepsy

NA-MEMD noise-assisted MEMD

NMF negative matrix factorization

NNSVD-LRC non-negative singular value decomposition with low-rank correction

NREM non-rapid eye movement

OLS ordinary least squares

PET positron emission tomography

REM rapid eye movement

PSD power spectral density

RMSE root mean squared error

RNS responsive neurostimulation

ROI region of interest

SCN suprachiasmatic nucleus

sEEG stereotaxic-EEG

SEEG stereoelectroencephalography

SOZ seizure onset zone

SPECT single-photon emission computerized tomography

SVD singlular value decomposition

SUDEP sudden unexpected death in epilepsy

SWEC Sleep-Wake-Epilepsy-Center

VNS vagus nerve stimulation

UCLH University College London Hospital

Contents

List of Figures

List of Tables

Chapter 1. Epilepsy as a Dynamic Disease

Contents

1.1 Introduction

The history of epilepsy days back almost 4500 years (Patel and Moshé, 2020), when identified as a clinical condition based on symptoms and signs that have been observed and reported in documents. Epilepsy was thought to be a mystical disease (Patel and Moshé, 2020), as the causes of this condition were unknown and empowered by the religious beliefs at that time (Patel and Moshé, 2020). Hippocrates was the first one to describe the disease as a neurological disease. By the beginning of 18$^{\text{th}}$ century, epilepsy was determined as an *idiopathic* disease originating in the brain. Along the years, several terms linked to their beliefs at the time were used to describe epilepsy, such as sacred disease (Greek: ιερά νόσος), an illness sent by the gods, "lunacy" (Greek: σεληνιασμός), possession by evil spirits or "demons", "falling sickness" (Panteliadis et al., 2017). The etymology of seizure or epilepsy is derived from the Greek word 'ελαμβάνειν', which means "to be taken hold of", "to be seized" (Patel and Moshé, 2020). However, nowadays this word is used by the scientific community not only for seizures, but rather to determine any severe and abrupt event. Thus, seizures related to epilepsy are called *epileptic seizures*.

During the late 19$^{\text{th}}$ and early 20$^{\text{th}}$ century the scientific community made a shift from the belief that epilepsy was a mystical disease. Advances in science led to a better understanding of the disease, as different types of epilepsy (Fisher et al., 2017) were described and electroencephalography (EEG) became an important tool for investigation by researchers (Panteliadis et al., 2017). Thus, epilepsies and seizures were better described as etiologies and different types of seizures, as well as epilepsy syndromes becoming better understood.

Epilepsy has been established as a chronic neurological disease characterised by the recurrence of spontaneous and unprovoked seizures. An *epileptic seizure* is an instantaneous, transient alteration of the normal electrical functioning of the brain caused by an imbalance between inhibitory and excitatory activity (Stafstrom and Carmant, 2015). Based on the International League Against Epilepsy (ILAE) and the International Bureau for Epilepsy (IBE) (Fisher et al., 2017), an *epileptic seizure* is defined clinically as "a transient occurrence of signs and/or symptoms due to abnormal excessive or synchronous neuronal activity in the brain" (Fisher et al., 2005, p. 471).

Clinical symptoms accompanying an epileptic event reflect the brain area/s in which the seizure initiated and evolved through time. These signs can be evident as numbness, jerking movements, loss of memory and consciousness, odd sensations and feelings, and many others. The presence of a single seizure does not imply that an individual is epileptic, as he/she may not experience seizures again during their lifetime. The state of recurring seizures is one of the fundamental aspects that define *epilepsy*. The pathogenic process of a normal brain becoming epileptic is termed as *epileptogenesis*. Typically, a seizure can last a few seconds or minutes. However, seizures can be prolonged lasting usually more than five minutes. These seizures are called status epilepticus and can cause severe brain injuries or even lead to death.

The quality of life for patients with epilepsy can be significantly affected by the epileptic events. In most cases they need to rely on carers for ensuring they will not encounter mild or severe injuries in case of a seizure episode. Also, they face restrictions in terms of several fundamental aspects of everyday life, such as ability to drive, finding employment, career choice, social interactions and others (Smeets et al., 2007; Jacoby, 2002). Lastly, they may experience cognitive dysfunction or/and psychological problems as a result of their condition (Devinsky and Lai, 2008).

Epilepsy is not a single disease or syndrome (Wirrell et al., 2022), but rather covers a variety of syndromes characterised by a range of different types of seizures such as focal-onset or generalised-onset seizures (Fisher et al., 2017). An *epilepsy syndrome* is defined as "a characteristic cluster of clinical and electroencephalographic features, often supported by specific etiological findings (structural, genetic, metabolic, immune, and infectious)" (Wirrell et al., 2022, p. 1334); it reflects a number of different aspects that need to be consistent, such as the clinical symptoms that accompany the seizure episodes, a defined seizure type, age of onset, EEG seizure patterns, response to antiseizure medications (ASMs), any known factors triggering the events and genetics (Stafstrom and Carmant, 2015). The complex nature of this disease is mirrored in the multiple causes that have been identified, such as stroke, traumatic brain injury, infections, autoimmune diseases as well as genetic conditions; each resulting to a chronic state of brain dysfunction (Löscher and Klein, 2021). However, the underlying mechanisms of epilepsy are only partially understood.

Epilepsy currently has no cure, so pharmacological recommendations for the symp-

tomatic treatment of epilepsy still form core therapy for patients with epilepsy. As such, one of the first lines of treatment for controlling seizures can be achieved with ASMs (also referred to as anticonvulsant or antiepileptic drugs (AEDs)) by preventing or significantly suppressing the initialisation and propagation of seizures or reducing their severity. This is evident for almost 70% of patients suffering with epilepsy. Despite the availability of numerous ASMs that employ different mechanisms for diminishing the electrical activity of the brain, seizures found to be resilient/resistant to treatment are found in 30% of patients (Chen et al., 2018; Perucca et al., 2020; Janmohamed et al., 2020) (termed as refractory epilepsy, i.e. seizures cannot be suppressed by two or more ASMs or any other therapies (Stafstrom and Carmant, 2015)). Patients with refractory focal epilepsy often undergo surgery (Rosenow, 2001); the epileptogenic tissue (thought to be the origin of seizures) is localised and removed surgically. However, for $\sim 60-70\%$ of patients surgery fails to render a patient seizure-free or provide a short-term benefit (de Tisi et al., 2011). Importantly, a portion of patients suffering from drug-resistant epilepsy might not be eligible candidates for surgery, as the epileptogenic zone might lie on brain areas that form part of the eloquent cortex; the eloquent cortex comprises of cortical areas that are responsible for critical functions, and thus removal or even perturbation of those areas might cause serious neurological deficits. In patients who are not eligible for a surgery or the surgery was not successful, vagus nerve stimulation (VNS) (Ben-Menachem, 2002; Lin and Wang, 2017) can be an alternative treatment. However, it is not effective to completely abolishing seizures, but rather might contribute to the reduction of frequency or duration of seizures (Zamponi et al., 2011) in 45-65% of the patients (Toffa et al., 2020).

Due to the ineffectiveness of current treatments in a considerable amount of patients, there is a need for better treatment of epilepsy; especially as $\sim 1\%$ of the population is suffering from epilepsy around the world. To this end, new treatments are currently heavily researched and developed, such as neurostimulation techniques, including deep brain stimulation, brain stimulation and brain-responsive neurostimulation (such as RNS) (Jarosiewicz and Morrell, 2021; Lin and Wang, 2017). A better understanding of the underlying excitatory and inhibitory mechanisms could enhance our knowledge regarding the factors that lead to the *epileptogenesis* and hence enable researchers and clinicians to improve current treatment techniques or develop new therapeutic solutions.

Epilepsy is not a static disease. As the disease progresses, seizures themselves change within the same patient. A repertoire of distinct patterns arise at the onset of seizures even for patients with the same type of epilepsy (Lagarde et al., 2019; Perucca et al., 2014). Diversity in cortical excitability differentiates how seizures spread across the brain (Badawy et al., 2007). These changes may occur at brain regions distant from the epileptogenic zone for a number of seizures (Lagarde et al., 2019; Saggio et al., 2020). Ictal activity comprises of different spectral characteristics (Pacia and Ebersole, 1997; Alarcon et al., 1995; Jiménez-Jiménez et al., 2015; Litt et al., 2001) and propagates in various types (Karoly, Kuhlmann, Soudry, Grayden, Cook and Freestone, 2018; Cook et al., 2016; Freestone et al., 2017). Duration of seizures varies based on the seizure type, but also within seizures of the same type (Jenssen et al., 2006). Clinical symptoms (semiology) of seizures change over time as well (Noachtar and Peters, 2009).

Thus, seizure features and electrographic seizure patterns reveal a time-dependent trait. It is likely that the mechanisms underlying seizure activity to be also time-varying. Importantly, if we find and characterise distinct patterns of variability in seizure features, such as rhythms across a hierarchy of timecsales, then we might be able to identify and distinguish the physiological mechanisms underlying seizures that reveal similar patterns. This can be indicative of the provoking factors that not only involved in seizure initiation, but also determine the duration, spread and severity of seizures within a single patient. Two important questions can be raised: 1) Do seizures occur in time randomly? and 2) How do seizures change over time in terms of their duration, seizure spread, seizure trajectory patterns (seizure dynamics), seizure severity? Recently, the availability of ultra long-term EEG recordings has demonstrated the prevalence of daily (circadian) and slower rhythms in seizure occurrence for most of the patients with epilepsy (Karoly, Rao, Gregg, Worrell, Bernard, Cook and Baud, 2021; Baud et al., 2018; Cook, 2021) leading us closer to an answer for the first question.

Even though seizures are abrupt events, the process of ictogenesis might not be; the underlying neural activity may follow a prolonged transition between the inter-ictal and ictal states that evolve over hours to days preceding a seizure (Litt et al., 2001; Badawy et al., 2009). For almost a century, it has been known that seizure occurrence reveals temporal variability, following circadian and ultradian cycles (Karoly, Rao, Gregg, Worrell, Bernard, Cook and Baud, 2021). Recently, longer cycles have

been recognised to influence seizure timing (Baud et al., 2018). Thus, there is evidence that specific mechanisms fluctuate and affect the brain network to become epileptic in a similar oscillatory manner that might be described by a combination of circadian and multidien rhythms in a way that is unique for each subject. These time-varying processes affect not only seizure likelihood (Karoly et al., 2017), but also seizure dynamics (Schroeder et al., 2020). Consequently, variability in onset patterns (Wang et al., 2017), seizure termination, seizure duration might be due to long-term dynamic processes that reveal oscillatory behaviour. Importantly, these processes might affect the frequency, duration, pattern and nature of seizures, resulting in changes in seizure severity. Different dynamic mechanisms might generate the distinct onset patterns (Wang et al., 2017). And, more importantly, these mechanisms might reveal an oscillatory behaviour.

Advances in understanding the effect of rhythms across a range of timescales (such as circadian, multiday etc.) on ictal activity can shed light on the endogenous or exogenous factors involved in various seizure features, and could lead to novel treatments able to completely suppress seizures across the entire range of seizure syndromes. Some examples of such treatment approaches could be the use of chronotherapy (Ramgopal et al., 2013) or deep brain stimulation at appropriate times based on periods of temporal patterns (e.g. ultradian, circadian and/or multidien) associated with different seizure features.

1.2 Diagnosis and Treatment

Epilepsy involves a spectrum of syndromes, each one characterised by a combination of features that occur together and all have a common factor: recurring seizure events. This group of similar clinical characteristics and physical signs includes specific seizure patterns (seizure type(s)), the brain regions in which the seizures arose and evolved, severity of the seizures, natural history, genetic information, prognosis, etiology, factors that provoke seizures, age of onset, EEG patterns, and response to ASMs (Stafstrom and Carmant, 2015). Taking all these together, clinicians should do a precise diagnosis, in order to provide an appropriate treatment to patients and possibly control seizures.

1.2.1 Diagnosis

Diagnosis of epilepsy becomes difficult, as it involves a detailed examination of all the features related to a number of diseases and conditions (syndromes). Furthermore, most of the time clinicians rely on the history provided by the carers, as the patient most likely will not experience a seizure during the medical examination or will not be able to provide a reliable report of the seizures he/she experienced. Also, seizures can be triggered by a range of possible causes unrelated to epilepsy, such as mental or emotional events (psychogenic seizures), leading to non-epileptic seizures (Oguni, 2004) and the clinician should be able to distinguish those from the epileptic ones.

For the purpose of clinical diagnosis, the ILAE (Fisher et al., 2005, 2017) has defined epilepsy as a disease that includes one of the following conditions:

- At least two unprovoked (or reflex) seizures occurring > 24 hours apart
- One unprovoked (or reflex) seizure and a probability of further seizures similar to the general recurrence risk (at least 60%) after two unprovoked seizures, occurring over the next 10 years
- Diagnosis of an epilepsy syndrome

Despite the scientific advances on technological and medical innovations mainly over the last century, the pathophysiology and aetiology of epileptic seizures remain poorly understood. However, advanced scientific knowledge of the disease is solid enough to provide a classification scheme, even though this is constantly changing and adapting to new knowledge and understanding of epilepsy. A revised classification of seizure types is provided by the 2017 ILAE (Fisher et al., 2017). This scheme is mainly focused on three main features: the seizure onset; the degree of impaired awareness and responsiveness; the extent of muscle movement. Based on the origin of seizure in the brain, seizures can be categorised as follows (Fisher et al., 2017):

- focal-onset seizures (seizures originating in one cerebral hemisphere)
- generalised-onset seizures (seizures originating in both cerebral hemispheres)
- seizures of unknown onset

In focal seizures, the patient might be fully aware of their surrounding events and environment or may lose their consciousness during the seizure. Also, there might be short muscle spasm (myoclonic), or convulsions (clonic) amongst other symptoms. These clinical symptoms determine if the seizure is motor onset, while the absence of these signs implies non-motor onset. Non-motor seizures evolve cognitive, emotional or sensory processes etc. It is possible for focal seizures to initiate in a localised brain region in one cerebral hemisphere and propagate to both hemispheres of the brain (focal to bilateral tonic-clonic seizure). Seizures originated in both hemispheres can be motor seizures (myoclonic, tonic, clonic, tonic-clonic) or absence seizures (lose and regain consciousness during the seizure).

The presence of numerous different types of epileptic seizures and the dynamic nature of the disorder (seizures change over time within a patient, but also from patient to patient), makes the classification and the identification of an epileptic syndrome with regards to diagnosis even more challenging, especially throughout the lifespan of an individual.

1.2.2 Electroencephalogram (EEG)

The fundamental discovery of the recording of the electrical activity of the brain by Richard Caton originates back to 1875. His findings were reported in the article "The electric currents of the brain" (Caton, 1875) to the British Medical Association. Caton placed unipolar electrodes to the cerebral cortex of rabbits and amongst others, found that electrical currents tend to increase with sleep and appear to vary with flashing lights. However, it was almost 50 years later, when the first electroencephalogram (EEG) in humans was recorded by Hans Berger (Haas, 2003). In 1925, Berger described patterns derived from brain waves and one of the first rhythms he discovered was alpha rhythm (8-13 Hz) (van Putten, 2020). The publication of his observations in 1929 advanced the science of neurophysiology.

For diagnosing epilepsy, clinicians examine the patient on physical and neurological basis; these examinations might include blood test, EEG, intracranial EEG, head computed tomography (CT), brain magnetic resonance imaging (MRI), functional MRI (fMRI), positron emission tomography (PET), and single-photon emission computerized tomography (SPECT). Each one of these tests is specialised to a particular aspect

of diagnosis, for example a CT scan can provide information about the structural organisation of the brain (Oguni, 2004) or brain MRIs are used for localising the temporal lobe abnormalities (Oguni, 2004). Despite all the different modalities developed over the last years, EEG is the fundamental tool used for diagnosis, monitoring and management of seizure types, and hence for epileptic syndromes (Smith, 2005). Almost a century on, EEG is the standard tool in clinical neurology with applications ranging from diagnosing sleep disorders to pre-clinical evaluation and research on language processing (van Putten, 2020). EEG captures the electrical activity generated from millions of neurons in the brain and hence it is a useful tool for determining potential neurological deficit; in epilepsy, EEG are analysed for capturing the physiological manifestations of abnormal activity in the brain.

EEG signals can be classified into two broad categories: the surface EEG (EEG) and the intracranial EEG (iEEG).

Surface EEG records the electrical activity in the brain using electrodes that are placed on the scalp or surface of the brain. Synchronous synaptic activity to cortical pyramidal cells generates currents that are measured by the EEG signals (van Putten, 2020; Cohen, 2017). Voltages recorded at the scalp reveal a rhythmical activity (van Putten, 2020). These voltage fluctuations measured with scalp EEG range within a spectrum of frequencies; these can be infraslow (< 0.1 Hz) or higher frequencies, such as 35–80 Hz (high gamma), and > 80 Hz (high-frequency oscillations). The most commonly used limits for EEG frequency bands are: delta (1-4 Hz), theta (4-8 Hz), alpha (8-13 Hz), beta (13-30 Hz), gamma (80-150 Hz), and high gamma (80-150 Hz) (Groppe et al., 2013).

Intracranial EEG (iEEG) are EEG recordings obtained with intracranial electrodes, either as depth electrodes penetrating the brain for accessing deeper sites (e.g., hippocampus) without open brain surgery (craniotomy) known as stereoelectroencephalography (SEEG) (Khoo et al., 2020) or as subdural grids and strips known as electrocorticography (ECoG) (Fernández and Loddenkemper, 2013). Intracranial EEG are most commonly used as a complementary tool for localising the epileptogenic zone in patients with drug-resistant focal epilepsy.

Most of the research community has focused on analysing electrographic seizures and interictal epileptiform activity using interictal spikes, bursts and high frequency

oscillations. Furthermore, the relationship between seizure incidence or other seizure characteristics as observed in a clinical setting has been mainly explored using short time periods of data (often pre-ictal or interictal). However, compared to the current research, our work differs in three key aspects: 1) we focused on more global characteristics of continuous interictal EEG activity, such as frequency band power, 2) we used data over long time periods and 3) we did not focus on seizure occurrence, but rather investigated the relationship between cycles with other seizure features, such as seizure dynamics and seizure duration.

1.2.3 Treatment

The most common form of treatment is ASM. ASM do not cure epilepsy, but rather provide an effective way of suppressing or reducing seizures in some cases. However, anti-epileptic treatment medication might not be effective for some patients. Those are patients with *refractory epilepsy* and clinically are determined as the ones who do not respond to two anti-epileptic treatments based on the ILAE (Kwan et al., 2009).

A number of other options are available for patients with refractory epilepsy including surgery, dietary modifications, and neuromodulation treatments. Those treatments might control or even abolish seizures and hence improve a patient's quality of life. Amongst them, surgery seems to be promising for focal epilepsies particularly in cases of focal lesions such as tumors, arteriovenous malformations, and cortical developmental anomalies, as well as mesial temporal lobe epilepsies (MTLE) (Burneo et al., 2016). Ketogenic diet treatments have been used for almost a century (Ułamek-Kozioł et al., 2019) and proven effective in controlling seizures both in adults and children with refractory epilepsy (Martin et al., 2016; Liu et al., 2018). An alternative therapeutic approach for refractory epilepsy includes neuromodulation treatments capable of abolishing an ictal event and proved to be effective in reducing seizure frequency (Salanova et al., 2015; Bergey et al., 2015; Fisher et al., 2021). These treatments might be invasive using an implantable device and induced electrodes, such as VNS, deep brain stimulation of the anterior nucleus of the thalamus (ANT-DBS), and responsive neurostimulation (RNS) of the epileptogenic zone/s or non-invasive, such as transcutaneous VNS and transcranial stimulation (Ryvlin et al., 2021; Salanova et al., 2015; Bergey et al., 2015). Amongst them, only VNS, ANT-DBS, and RNS are currently approved treatments for

refractory focal epilepsy.

1.3 Cyclical Patterns in Epilepsy

Epilespy is a chronic disease with a dynamic nature (Lopes da Silva et al., 2003; Milton, 2010); seizures change over time in terms of their features in a patient-specific manner. One aspect of the disease's dynamic nature is reflected in the fluctuations of different timescales (Karoly, Rao, Gregg, Worrell, Bernard, Cook and Baud, 2021), while another is mirrored by abrupt and sudden changes in cortical activity manifesting as *seizures*. Recently, the availability of ultra long-term EEG recordings helped delineate the cyclical seizure patterns (Baud et al., 2018; Karoly, Goldenholz, Freestone, Moss, Grayden, Theodore and Cook, 2018; Spencer et al., 2016; Karoly, Rao, Gregg, Worrell, Bernard, Cook and Baud, 2021) that have been reported since the 19th century (Langdon-Down and Russell Brain, 1929; Griffiths and Fox, 1938). While the vast majority of research has focused on seizure occurrence oscillatory patterns (Baud et al., 2018; Mitsis et al., 2020; Karoly et al., 2017; Stirling et al., 2021) and recently modulations in seizure dynamics with artificially developed circadian and/or slower rhythms, it is unknown whether other seizure features change in a non-random, oscillatory manner.

Researchers have explored the variability of interictal features and/or their relationship with ictal features (Baud et al., 2018; Karoly, Goldenholz, Freestone, Moss, Grayden, Theodore and Cook, 2018; Mitsis et al., 2020; Gliske et al., 2018; Chen et al., 2021; Schroeder et al., 2020). Seizure diaries made it possible to capture longer rhythms of seizure occurrence as well (Karoly, Rao, Gregg, Worrell, Bernard, Cook and Baud, 2021). In this section, I will discuss the recent findings related to the cycles found in seizure features, interictal EEG features and their association.

1.3.1 Cyclical nature of seizures

Seizure frequency has been shown to change over time periodically, with cycles over multiple hours, days, months and years. Circadian patterns of seizures have been extensively studied and reported in the literature (Anderson et al., 2015; Loddenkemper, Lockley, Kaleyias and Kothare, 2011; Quigg, 2000). Additionally, subclinical seizures

(without clinical symptoms) are also reported to follow circadian patterns (Jin et al., 2017). Evidently, the prevalence of seizure cycles over longer time-periods might have a strong impact as well (Baud et al., 2018). Apart from circadian cycles, ultradian rhythms also were apparent in 98% of subjects (Spencer et al., 2016). It has been well known for years that seizures occur at a specific time of day, with a propensity for both nocturnal and diurnal cycles (Langdon-Down and Russell Brain, 1929) though diurnal seizure peaks have been found to be more prominent (Gowers, 1885). However, recent studies do not imply a specific timing in circadian seizure cycles among patients, but rather a diversity across all hours of the day (Karoly, Goldenholz, Freestone, Moss, Grayden, Theodore and Cook, 2018; Leguia et al., 2021).

Longer cycles in seizure occurrence have been extensively studied (Griffiths and Fox, 1938). In a study with seizure records over multiple years or decades, Griffiths and Fox found longer cycles of 1.5, 2 and 3.5 months. Complementary to these results, recent studies found strong weekly and longer cycles of seizure activity (Karoly, Goldenholz, Freestone, Moss, Grayden, Theodore and Cook, 2018). Monthly seizure cycles have been linked to menstrual periods (Herzog et al., 2015). However, recent studies have showed that these cycles seem to be equally present in both men and women (Karoly, Goldenholz, Freestone, Moss, Grayden, Theodore and Cook, 2018; Karoly et al., 2016; Baud et al., 2018). Additionally, studies in canine epilepsy reveal circadian, weekly and monthly cycles in seizure rate (Gregg et al., 2020). More importantly, these rhythmic patterns might relate to external factors, such as physiological processes, as they are not dependent on the anti-epileptic medication (Gregg et al., 2020). Excessively long periods of seizure occurrence emerged for three epileptic patients with one year cycle for one patient and two years cycle for the remaining two (Griffiths and Fox, 1938). For decades seizures have been linked to lunar cycles in some patients and showed to occur preferably during the full moon (Polychronopoulos et al., 2006; Leguia et al., 2021). However, studies revealed an impact of moon cycle on quality of sleep (Casiraghi et al., 2021), suggesting that seizure occurrence is likely to be affected by variations on the quality of sleep.

Beyond the cyclical patterns in seizure timing, there are other seizure characteristics that reveal variability through time within the same patient. Whether this variability can be described by cyclical patterns or not is yet an open question for most of the

seizure features if not all. A "repertoire" of seizure onset patterns has been identified electrographically (Perucca et al., 2014; Jiménez-Jiménez et al., 2015; Lagarde et al., 2016; Salami et al., 2020). Among them, the most prevalent were the low-voltage fast activity and the ultra slow wave prior to low-voltage fast activity (Lagarde et al., 2019). Some of these onset patterns have been linked to different underlying dynamic mechanisms (Wang et al., 2017). Apart from the seizure initiation patterns, researchers have studied how seizures end. There is evidence that seizures can terminate in different ways revealing two distinct patterns of bursting, synchronous termination (seizures end synchronously across the brain) and asynchronous termination (seizures end in some regions while remaining in others) (Salami et al., 2022). Even seizures of the same onset or seizure type revealed different termination patterns within the same patient (Salami et al., 2022), suggesting different mechanisms affecting the termination of seizure dynamics.

Another seizure characteristic that varies across intra- and inter-patient ictal events is the duration of seizures. It is unclear, though whether this variability is attributed to distinct dynamics, onset and termination patterns. Research has also focused on capturing the dynamic changes through time within ictal periods. These dynamic changes can be thought as a "motif" or "pathway" from onset time to termination (Burns et al., 2014; Khambhati et al., 2015). Recent work in the quantification of seizure spatio-temporal network evolutions has demonstrated that seizures with similar dynamics tend to occur closer together in time (Schroeder et al., 2020). It is shown that seizure duration has a multimodal distribution within-patients. Seizures were not accurately predicted for patients with multiple seizure clusters (Cook et al., 2013), suggesting that these seizure populations might be characterised by different pre-ictal dynamics. Short and long seizures were characterised by distinct seizure evolutions/trajectories (Cook et al., 2016; Karoly, Kuhlmann, Soudry, Grayden, Cook and Freestone, 2018), while maintaining similar onset patterns (Karoly, Kuhlmann, Soudry, Grayden, Cook and Freestone, 2018). However, other studies suggest that seizure duration might be linked to distinct seizure onsets (Liu et al., 2022) and/or seizure types (Jenssen et al., 2006; Afra et al., 2008; Dobesberger et al., 2015; Kaufmann et al., 2020). Such findings might indicate that different seizure durations might be indicative of certain seizure onset patterns or/and seizure dynamic trajectories.

Finally, the clinical manifestation of seizures is diverse within patients (Noachtar and Peters, 2009) both in time and location. Seizures with more severe clinical symptoms, such as focal to bilateral tonic-clonic seizures or seizures accompanied by post-ictal generalised EEG suppression preferably occur during sleep (Jobst et al., 2001; Lamberts et al., 2013; Peng et al., 2017) and arise according to sleep/wake or day/night cycles (Bazil and Walczak, 1997; Loddenkemper, Vendrame, Zarowski, Gregas, Alexopoulos, Wyllie and Kothare, 2011; Sinha, 2006). Nonetheless, less severe seizures, such as subclinical ones, tend to occur at specific times of day (Jin et al., 2017). Seizure timing seem to be associated with the type and location of the epileptic focus (Quigg et al., 1998; Crespel et al., 1998). Thus, seizure features reveal spatio-temporal patterns that need to be identified for designing better treatments.

1.3.2 Cycles of interictal activity

Both clinical observations (Freestone et al., 2017) and long-term iEEG monitoring (Cook et al., 2013) have revealed that seizures make up only a small part of a patient's continuous brain dynamics. For example, seizures make up less than $< 0.05\%$ of the chronic NeuroVista recordings, as demonstrated for 15 patients and up to three years of monitoring data for each one of them (Cook et al., 2013). As such, other continuous measures are needed to characterise timescales of variability in brain dynamics, as seizures alone might not reveal periodic changes in brain dynamics, especially in longer timescales. For instance, cycles over multiple timescales might be better tracked using continuous long-term interictal EEG features, including epileptic spikes or spike rate, epileptiform bursts, high frequency oscillations (HFO), functional network measures, band power in the main frequency bands and measures of cortical excitability derived from EEG. These features are biomarkers for epileptogenesis and contribute significantly in clinical practice (Engel et al., 2013; Worrell et al., 2004; Pitkänen et al., 2016).

In recent years, continuous ultra long-term EEG recordings ranging from months to years, such as NeuroVista (Cook et al., 2013; Howbert et al., 2014), NeuroPace RNS (Jarosiewicz and Morrell, 2021; Nair et al., 2020) have made it possible to capture longer oscillations in epileptic brain dynamics as mirrored in interictal biomarkers (Baud et al., 2018; Karoly et al., 2016; Maturana et al., 2020). Specifically, cyclical patterns

were prevalent in interictal spike rate (Baud et al., 2018; Karoly et al., 2016; Leguia et al., 2021; Maturana et al., 2020), network dynamics derived from EEG recordings (Kuhnert et al., 2010; Mitsis et al., 2020), cortical excitability as measured using EEG (Meisel et al., 2015; Ly et al., 2016), high frequency activity (Chen et al., 2021) and other EEG features, such as autocorrelation and variance of EEG (Maturana et al., 2020). Additionally, these interictal features have been shown to change over time within patients, such as location of high frequency oscillations (Gliske et al., 2018) and signatures of cortical excitability (Badawy et al., 2009). Thus, features of interictal iEEG are modulated by cycles at various timecsales.

1.3.3 Oscillatory behaviour in signatures of epileptic brain activity and seizure features

Existence of seizure cycles in various timescales has been extensively studied using long-term iEEG recordings. Previous work has found that seizures most preferably occurred at specific times during the day, revealing circadian (Karoly et al., 2017) and longer-term rhythms (Baud et al., 2018). These findings indicate that the epileptic brain state is possibly "activated" in an oscillatory way. This non-random pattern of seizure occurrence might inform the prediction of higher seizure risk periods (Chiang et al., 2018). Longer timescales, such as multi-day (Baud et al., 2018) and circaseptan (weekly) rhythms (Karoly, Goldenholz, Freestone, Moss, Grayden, Theodore and Cook, 2018) of interictal epileptiform activity were shown to be significant and co-modulate with seizures for most of the patients. Evidence shows that seizures tend to occur during a specific phase of these underlying rhythms of interictal epileptiform activity (Baud et al., 2018); seizures more preferably occur during the rising phase of a multidien rhythm. Aligned phases observed between circadian rhythms of seizures and interictal spikes (Karoly et al., 2016) possibly suggest that interictal epileptiform activity and seizures are modulated by common biological mechanisms characterised by cycles over a hierarchy of timescales.

We hypothesize that it is not only seizure occurrence that is influenced by the temporal patterns of the underlying interictal activity, but also other seizure features. The epileptic network is more likely to be influenced by modulatory processes, which shape

the brain dynamics during a seizure, and affect the severity of an imminent seizure. Investigating the association between various characteristics of interictal dynamics and seizure features can provide a better understanding of the seizure network as a dynamic system. More importantly, analysing the cyclical patterns that contribute to the process of epileptogenesis can lead to a better understanding of the modulatory mechanisms underlying the disease and hence provide more effective treatments. Furthermore, there is a great need for personalised forecasting which may be enhanced with established cyclical characteristics for providing more accurate predictions of various seizure features (Karoly et al., 2017; Panagiotopoulou et al., 2022) based on the patient's needs and positively impact the quality of their life. For example, it might be critical for a patient to know the type of an imminent seizure, or the duration, so as to be proactive and plan his life routine.

1.4 Methodological Approach of Measuring Cyclical Patterns in iEEG Features

1.4.1 Signal processing for iEEG

Several steps are involved in processing complex iEEG signals before performing rigorous statistical analysis. While the various steps taken in processing iEEG data may vary based on the scope of individual analyses, there are some key steps that are more commonly applied to the raw iEEG before analysing them. Intracranial electrodes are wired to recording equipment to enable the acquisition and storing of the data. Even though patients are restricted to rest in bed for prolonged periods of time throughout the implantation, wires of electrodes (when stereotaxic-EEG (sEEG) are used, which are wires of electrodes implanted in the brain without the need of craniotomy) are liable to be influenced by movement artifacts (Parvizi and Kastner, 2018). In general, in order to remove high-frequency artifacts we might use a filtering technique, such as a low-pass filter at the frequency of interest (for example 50 Hz). Low-frequency drifts can be apparent in the data and use of a high-pass filter either at 0.1 Hz or 0.5 Hz can minimise the effect of these drifts. Finally, we need to remove line noise from the iEEG recordings. In order to attenuate electrical noise, we can notch filter the raw signals at

line frequencies of 50 Hz or 60 Hz.

1.4.2 iEEG features and multiscale periodicities

In order to analyse brain activity captured from continuous EEG recordings, it is useful to disentangle the frequency representation of an EEG signal. Fourier transform can be used for extracting a frequency spectrum representation of a time series, as long as the duration of the time series analysed is stationary; a time series is stationary if some statistical moments of the data are constant, such as the mean, variance, and frequency structure that should not change over time. Importantly, the frequency structure should be time-invariant across the entire recording. In other words, stationarity can be thought of as: if we took a snapshot of a defined length of the recording, its frequency structure would be repeated throughout the entire length of the recording. Evidently, EEG signals are non-stationary data (Blanco et al., 1995; Dikanev et al., 2005), as the frequency representation of the neurophysiological activity of the brain is altered over time due to endogenous and/or exogenous processes.

The assumptions of fast fourier transform (FFT) are thus violated when using real EEG/iEEG data, and the lack of stationarity of EEG data reflects dynamic properties of the brain (Kaplan et al., 2005; Lehnertz et al., 2017). In order to overcome these problems, one can perform a sliding-window approach and long-term time-series would be divided into (non)overlapping segments/windows. The system can be denoted approximately as stationary within each segment, and thus EEG signal properties of interest (such as spectral features) can be considered time-invariant for a brief time slice of the recording, usually ranging 4 s to 1 min (e.g. segments of 10 s, 30 s etc.) (Barlow, 1985; Rieke et al., 2003; Dikanev et al., 2005; Kaplan et al., 2005; Tong et al., 2007; Kaplan, 1998; Lehnertz et al., 2021). Throughout seizures, the EEG waveforms reveal abrupt changes suggesting special attention for choosing an optimal segment length (probably small) (Jefferys, 1990). When the segment length is too short, the feature of interest might become limited if we take into account the sampling frequency (Hz) as well. A short window can lead to a low number of data points which might increase the uncertainty of the feature of interest or limit the range of frequencies that can be detected. Thus, choosing an appropriate segment length should be an interplay between accuracy of features and the approximated stationarity within the specified

segment length.

A variety of different features can be obtained from the iEEG recordings of one or multiple channels for capturing the spatio-temporal evolution of different properties, analyse the dynamics of interictal brain activity, and detect the seizure onset zone. Interictal epileptiform discharges (IEDs), such as spikes, polyspikes, and sharp waves have been associated with seizure activity and localisation of epileptogenic tissue measured as spike rate (Baud et al., 2018; Karoly et al., 2016; Conrad et al., 2020), but also in terms of their various amplitudes, curvatures, and slopes (Chavakula et al., 2013). Interictal spikes, though partially overlapping with the epileptogenic zone (EZ) forming what is known as the *irritative zone* (Rosenow, 2001), can be detected outside of the EZ as well (Bartolomei et al., 2016). HFOs have been tightly related to more accurate identification of the EZ (Jacobs et al., 2008) and are in concordance with surgical outcome (Haegelen et al., 2013; Wu et al., 2010). However, HFOs can resemble both physiological (ripples: 80-250 Hz) and pathological processes (fast HFOs or fast ripples: 250-500 Hz); physiological HFOs are apparent in normal cognitive functions, such as memory processing (Alkawadri et al., 2014; Lachner-Piza et al., 2021), while fast ripples have been identified as pathological (Urrestarazu et al., 2007; Rosenow, 2001) and have even been related solely to epileptic activity (Usui et al., 2011; Brázdil et al., 2017). However, concurrence of ripples and spikes seem to capture pathological activity rather than spikes or ripples alone (Roehri et al., 2018; Cai et al., 2021; Kramer et al., 2019). A complementary marker of abnormal electrographic activity can be defined also by obtaining the band power abnormality in various brain regions relative to a normative map of spectral characteristics across brain regions (Taylor et al., 2022; Frauscher et al., 2018; Groppe et al., 2013). Also, measures capturing functional brain networks allows for investigating interactions from different parts of the brain that likely form a network. Such measures are important for understanding the underlying network organisation in epileptic processes, such as epileptogenesis and ictogenesis (Kramer and Cash, 2012; Geier et al., 2015; Kramer et al., 2011).

Most epilepsy research has been focused on investigating the time-varying brain dynamics using short segments before (preictal state), during seizure (ictal state), after seizure (postictal state) and between seizures (interictal state). Even though researchers utilise sliding window approaches to capture how the brain changes over time, it is

still based on iEEG activity captured over only several seconds to minutes. Those approaches assume that the brain transitions from a baseline interictal state characterised by properties that are relatively stable to an abrupt event (ictal state).

However, we need to account for longer timescales when analysing brain dynamics, as different physiological and pathophysiological processes can be captured using iEEG that are entrained to cycles of multiple timescales that range from seconds to weeks. Recent advances on iEEG analysis allowed the recording of brain activity over days or weeks (Cook et al., 2013; Duun-Henriksen et al., 2020) providing the opportunity to analyse how the brain dynamics of single brain region or a network of brain regions evolve on timescales that exceed several days.

It is well known that EEG signals, among other physiological outputs, such as heart rate variability, body temperature, melatonin secretion and blood pressure are regulated by endogenous and exogenous biological rhythms (Glass, 2001) and thus exhibit rhythmical behaviour. The circadian rhythms with approximately 24 h periodicity are inherently endogenous as those are regulated by neurons from the hypothalamic suprachiasmatic nucleus (SCN) of the hypothalamus (Herzog, 2007) which acts as the *master circadian pacemaker* in mammals. However, the SCN is entrained by external (environmental) factors/stimuli, such as light condition. Circadian rhythms have been identified in spectral properties of EEG and cortical excitability obtained from humans (Scheich, 1969; Ly et al., 2016). Furthermore, an influence of ultradian rhythms has been demonstrated on EEG. Ultradian rhythms are cycles with periods shorter than 24 h (Lehnertz et al., 2021). Example ultradian rhythms include the main states of sleep, rapid eye movement (REM) and non-rapid eye movement (NREM) that alternate during sleep in cycles of 90-120 min period. Additionally, the basic rest-activity cycles are ultradian rhythms of variable periods from 20 min to a few hours occurring both in sleep and wakefulness (Kleitman, 1982). Ultradian cycles of variable periods in different frequency ranges of EEG signals have been reported in healthy individuals during wakefulness (Kaiser, 2008; Chapotot et al., 2000). Cycles with periods greater than 24 h are termed infradian cycles and can be weekly, monthly or annually. Physiological and behavioural processes, such as the menstrual cycle in females, and seasonal affective disorder are associated with infradian cycles.

Apart from circadian and ultradian timescales, pronounced fluctuations of longer

timescales have been identified in various EEG features, such as interictal epileptiform activity (Baud et al., 2018; Schroeder, Karoly, Maturana, Panagiotopoulou, Taylor, Cook and Wang, 2022; Leguia et al., 2021), functional connectivity (Gregg et al., 2020; Mitsis et al., 2020; Geier et al., 2015), high frequency oscillations (Gliske et al., 2018). Importantly, temporal cycles of multiple timescales have been linked to seizures (Baud et al., 2018; Karoly, Rao, Gregg, Worrell, Bernard, Cook and Baud, 2021; Schroeder, Karoly, Maturana, Panagiotopoulou, Taylor, Cook and Wang, 2022; Panagiotopoulou et al., 2022).

In order to extract fluctuations from interictal features over multiple timescales including long-term ranging from days to weeks, researchers have used different methods, such as continuous wavelet transform (Baud et al., 2018), auto-correlation (Mitsis et al., 2020; Karoly et al., 2016) and variants of empirical mode decomposition (EMD) (Schroeder, Karoly, Maturana, Panagiotopoulou, Taylor, Cook and Wang, 2022; Panagiotopoulou et al., 2022). In the following section, I will give a brief overview of some EMD-based methods and discuss briefly advantages and limitations over other mode decomposition methods suitable for identifying long-term fluctuations from non-stationary and non-linear data commonly used in iEEG features.

1.4.3 EMD, MEMD and their variants

Some of the most commonly used methods for representing signals in the time-frequency domain are the EMD-based methods (Huang et al., 1998; Rehman and Mandic, 2010). EMD does not require basis function for identifying band-limited modes and thus does not generate harmonics, unlike Wavelet-based approaches. The standard EMD has some limitations. First of all, in cases where we have multivariate signals, the application of EMD at the individual univariate signals results in frequency modes, where there is no alignment across the different signal dimensions. This is the so-called mode-alignment problem which can be mitigated by employing multivariate extensions of EMD, such as the bivariate-EMD (Rilling et al., 2007), trivariate EMD (Ur Rehman and Mandic, 2010), and multivariate MEMD (Rehman and Mandic, 2010). Secondly, EMD might fail to effectively decompose a multiscale signal by fully separating its inherent modes. In other words, EMD should extract an intrinsic mode function (IMF) that corresponds to a distinct frequency scale and does not overlap with frequency

ranges/limits of other IMFs. In EMD, usually the frequency components embedded in the input signal are relatively close or overlap across IMFs yielding the mode-mixing problem (Huang et al., 1998), namely an IMF containing oscillations over multiple wide scales resulting in overlapping frequency ranges covered by multiple IMFs. In order to overcome the mode-mixing problem within IMFs, a number of EMD variants have been introduced, such as ensemble EMD (EEMD) (Wu and Huang, 2009), Complete Ensemble EMD with Adaptive Noise (CEEMDAN) (Colominas et al., 2014), MEMD (Rehman and Mandic, 2010), and Noise-Assisted MEMD (Ur Rehman and Mandic, 2011). Additional developments in this area can potentially overcome most of the pitfalls of EMD-based methods (Xue et al., 2015; Deering and Kaiser, 2005; Li et al., 2015; ur Rehman and Aftab, 2019). In the following sections, we describe briefly the aforementioned EMD and its variants.

Empirical Mode Decomposition (EMD)

EMD was developed for enhancing the multiscale decomposition of a time-series complementing the time-frequency representation of signals. EMD is a data-adaptive method suitable for decomposing a non-linear and non-stationary signal into its inherent oscillatory components termed intrinsic mode functions (IMFs) (Huang et al., 1998).

Given a time series $y(n), n = 1, 2, \ldots, T$ taking values in $\mathbb{R}$ we can summarise EMD as follows:

$$y(n) = \sum_{i=1}^{L} c_i(n) + r(n), n = 1, 2, \ldots, T, \tag{1.1}$$

where $c_i(n), i = 1, 2, \ldots, L$ represents the i-th IMF, T is the number of time points and $r(n)$ is the residue signal capturing the residual information that was not captured by the mode components.

A well-behaved IMF (Mandic et al., 2013) is defined as a function that meets the following conditions:

1. The number of extrema and the number of zero-crossings should be the same or differ by one.

2. The mean value of the local minima and the local maxima envelopes should be

zero at any time point $n, n = 1, 2, \ldots, T$.

For the input signal $y(n), n = 1, 2, \ldots, T$ (Fig. 1.1a) the decomposition using EMD can be summarised by an iterative procedure named *shifting process* (Huang et al., 1998) as follows:

1. Identify the extrema values of the signal (Fig. 1.1b).
2. Obtain the upper and lower envelopes using cubic spline line for the local maxima and local minima, respectively (Fig. 1.1c & d).
3. Compute the mean between the upper and lower envelopes, $m_1(n), n = 1, 2, \ldots, T$ (Fig. 1.1e).
4. Find the first IMF by substracting the $m_1(n)$ from the input signal $y(n)$.

$$s_1(n) = y(n) - m_1(n)$$

5. Check if the $s_1(n)$ satisfies the conditions mentioned above to be designated as the first IMF.
6. If the $s_1(n)$ does not satisfy the required conditions, the shifting process is repeated using as input signal the $s_1(n)$.
7. The shifting process is replicated k times until the s_{1k} can be denoted as an IMF. The $s_{1k}(n) = c_1(n)$ can be denoted as the first IMF, which contains the shortest period component of the input signal $y(n)$.
8. Once the first component has been identified, it can be separated from the data by extracting it from the input signal $y(n)$, $y(n) - c_1(n) = r_1(n)$.
9. Then the shifting process will be iterated on $r_1(n)$.
10. Finally the signal can be expressed as a summation of L narrow-band components and a final residue as shown in equation 1.1.

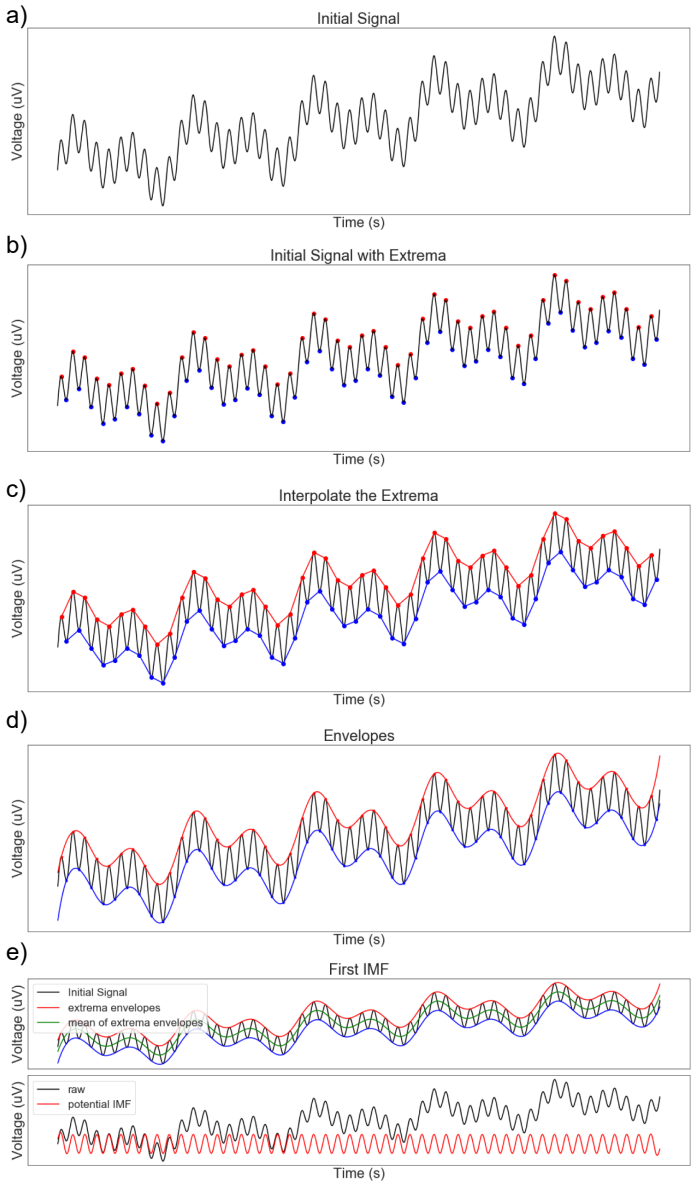

Figure 1.1 **Illustration of the EMD steps for one IMF.** Visual representation of the *shifting process* of EMD for extracting the first IMF termed IMF1 in an example univariate signal.

An illustration of the shifting process for extracting an IMF from a time series can be seen in Fig. 1.1.

The narrow-limited modes (IMFs) embedded in an example time-series can be seen

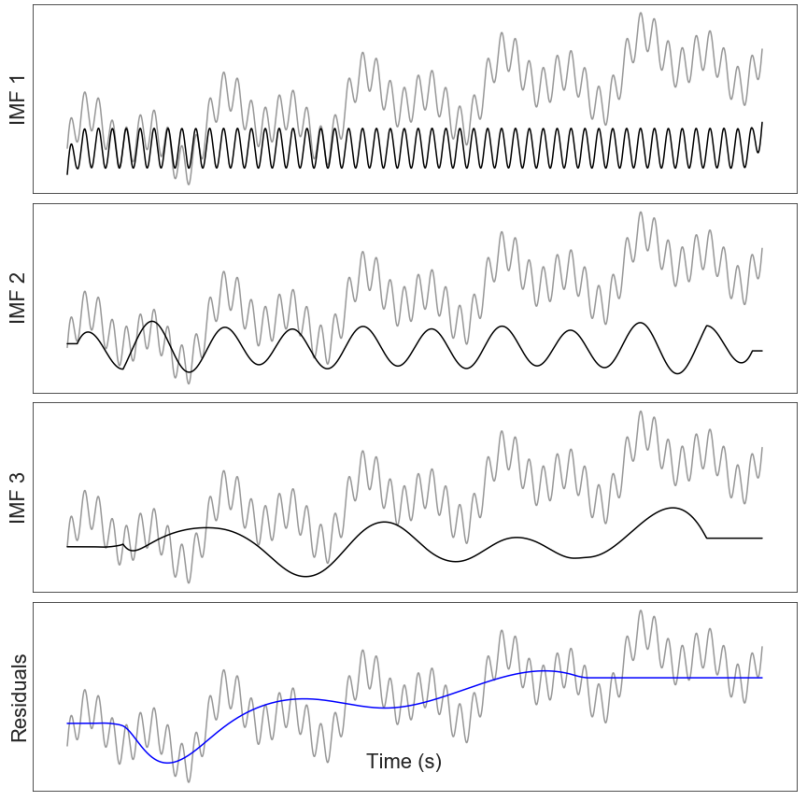

Figure 1.2 **Fluctuations (IMFs) obtained from Empirical Mode Decomposition.** Illustration of extracted IMFs as obtained from EMD in an example univariate signal.

in Fig. 1.2.

Ensemble EMD (EEMD)

Ensemble EMD is a noise-assisted data analysis suitable for alleviating the mode-mixing problem (Wu and Huang, 2009). This method is based on the idea of adding multiple, $k = 1, 2, \ldots, K$, realisations of white Gaussian noise, $W_k(n)$ to the input signal $y(n)$, so multiple EMD decompositions and averaging cancels out the noise, and the input signal is projected into distinct mode scales yielding physically meaningful modes that resemble the narrow-band frequency components of the input signal. The EEMD can be described by the following steps:

1. Generate K noise-assisted signals, $y_k(n) = y(n)+W_k(n)$ by adding white Gaussian noise to the input signal, $y(n)$. The sequences of white noise should be generated

by maintaining the standard deviation of the Gaussian process stable (Guo and Tse, 2013).

2. Apply EMD to each one of the noise-assisted signals and obtain the corresponding L IMFs, $c_{ki}(n)$, where $k = 1, \ldots, K$ denotes the number of all uniformed time-frequency spaced white noise and $i = 1, \ldots, L$ is the number of the IMFs.

$$y_k(n) = \sum_{i=1}^{L} c_{ki}(n) + r_k(n), n = 1, 2, \ldots, T. \tag{1.2}$$

3. Finally, an estimation of the ensemble IMFs, $\bar{c}_i(n)$ can be acquired by averaging the IMFs of common index. Mathematically, this can be expressed as:

$$\bar{c}_i(n) = \frac{1}{L} \sum_{k=1}^{K} c_{ki}(n) \tag{1.3}$$

$$\bar{y}(n) = \sum_{i=1}^{L} \bar{c}_i(n) + \bar{r}(n), \text{where } \bar{r}(n) \text{ is the residue signal.} \tag{1.4}$$

Complete Ensemble EMD with Adaptive Noise (CEEMDAN)

Although the EEMD method alleviates the mode-mixing problem, it leads to a higher reconstruction error of the signal as noise included in the signal is not entirely eliminated during the decomposition. Thus, Torres et al. (Torres et al., 2011) introduced Complete Ensemble EMD with Adaptive Noise (CEEMDAN) to overcome this limitation. The CEEMDAN method involves performing multiple EMD trials with different randomly generated white noise added. Finally, the outputs obtained from the decomposition trials are averaged to derive the final IMFs.

Multivariate Empirical Decomposition (MEMD)

A natural extension of the EMD algorithm and it's variants for multivariate signals is the Multivariate Mode Decomposition (MEMD) (Rehman and Mandic, 2010). This algorithm covers a more generic case of multivariate signal decomposition, where the bivariate EMD (Rilling et al., 2007) and trivariate EMD (Ur Rehman and Mandic,

2010) are special cases. The MEMD alleviates the mode-alignment problem in the standard EMD methods. In other words, in MEMD common index IMFs extracted from multiple channels are linked with the same narrow-band frequency components allowing association of modes across the dimensions of multivariate signals. In the standard EMD, the IMFs extracted from each channel might differ in number and also are not aligned, so as IMFs of the same index do not necessarily represent the same frequency band mode.

In the standard EMD method, the IMFs are obtained as local mean throughout the entire span of the signal computed by averaging the upper and lower envelopes of the signal. These envelopes are computed by interpolating the local maxima and minima of the signal. Once each IMF is acquired through these steps, it is subtracted from the initial signal and the process is repeated till a stopping criterion is met based on the properties that IMFs should fulfil. Under similar logic, the local mean, and hence the local maxima and minima should be obtained for the multivariate signals. However, these local characteristics may not have a direct definition. To obtain the local mean of the multivariate signals, several signal projections on multiple directions will be taken across m-dimensional spaces. The Hammersley sequence will be employed for generating the m-dimensional projections distributed uniformly on a $(M-1)$-sphere (Rehman and Mandic, 2010). Once, all the projections are obtained, the m-signal envelopes will be calculated by cubic spline interpolation (Rehman and Mandic, 2010); the local average of the multivariate signal will be obtained by averaging these multiple envelopes. The outline of the MEMD algorithm can be summarised in six steps:

1. A suitable Hammersley sequence is chosen for sampling on an (M-1)-sphere. (Rehman and Mandic, 2010).

2. Generate k projections of the input M-dimensional signal $\mathbf{y}(n) = (y_1(n), \ldots, y_M(n))$, along the direction $\mathbf{v}^{\theta_k} = (v_1^k, v_2^k, \ldots, v_M^k)$; each projection denoted as $p^{\theta_k}(n)$, where $n = 1, 2, \ldots, T$.

3. Find the time instants, $\mathbf{n}^{\theta_k}$ that form the maxima of all the projected signals $\mathbf{p}^{\theta_k}(n) = (p_1^{\theta_k}(n), p_2^{\theta_k}(n), \ldots, p_k^{\theta_k}(n))$.

4. Interpolate $[\mathbf{n}^{\theta_k}, \mathbf{y}(\mathbf{n}^{\theta_k})]$ for all k projections to obtain the multivariate envelopes $\mathbf{e}^{\theta_k}(n)$.

5. The envelope signals will be averaged for obtaining the local mean $\mathbf{m}(n) = \frac{1}{K}\sum_{k=1}^{K}\mathbf{e}^{\theta_k}(n)$.

6. Get the $\mathbf{d}(n) = \mathbf{v}(n) - \mathbf{m}(n)$. If $\mathbf{d}(n)$ satisfies the stopping criterion for an appropriate multivariate IMF, then the steps above should applied to $\mathbf{v}(n)-\mathbf{d}(n)$, otherwise apply them to $\mathbf{d}(n)$ (Rehman and Mandic, 2010).

Every time an IMF is obtained it is subtracted from the input signal and the process is repeated until only the residue signal remains following some stopping criteria (Rilling et al., 2003); for the multivariate case the process might yield the residue signal, when the projections do not include enough extrema, so as to construct multivariate envelopes.

Noise-Assisted MEMD (NA-MEMD)

The Noise-Assisted MEMD is a noise-assisted method that relies on the quasi-dyadic filter bank properties of MEMD on white Gaussian noise (Ur Rehman and Mandic, 2011) the same way the ensemble EMD results in IMFs that exhibit a quasi-dyadic filter bank structure. The NA-MEMD adds noise to the multivariate signal, without using multiple realisations of Gaussian noise as in the ensemble EMD. Specifically, a number of extra channels of independent white Gaussian noise are added as additional dimensions to the input multivariate signal and then MEMD is applied to this new extended multivariate signal. The IMFs associated with the white noise channels are discarded yielding a selection of the IMFs that corresponds to the input signal only. The NA-MEMD algorithm can be summarised by the following steps:

1. Generate an uncorrelated white Gaussian noise g-variate signal of the same length, $n = 1, 2, \ldots, T$, as the input signal.

2. Extend the input m-variate signal by adding the white Gaussian noise g-variate signals yielding an $(m + g)$-variate signal.

3. Apply MEMD to the new augmented signal ($(m + g)$-variate signal).

4. From the IMFs obtained from the previous step, keep only those associated with the initial input signal; discard the IMFs linked to the white Gaussian noise signals.

1.5 Research Problem, Aims and Significance

Epilepsy can be recognised as a dynamic disease, characterised by time-varying components in seizure features within each patient; diversity is captured in the timings of seizures, seizure evolution, seizure severity etc. The prevalence of circadian cycles in seizure timing has been well documented (Langdon-Down and Russell Brain, 1929; Karoly et al., 2017; Karoly, Goldenholz, Freestone, Moss, Grayden, Theodore and Cook, 2018; Gowers, 1885) and quantified as 65% (Karoly, Rao, Gregg, Worrell, Bernard, Cook and Baud, 2021) and only in recent years have a number of studies identified the importance of long-term cycles (multi-day, multi-month) (Baud et al., 2018; Karoly, Stirling, Freestone, Nurse, Maturana, Halliday, Neal, Gregg, Brinkmann, Richardson, Gerche, Grayden, D'Souza and Cook, 2021) in epilepsy. Interictal epileptic brain dynamics revealed longer cycles that are associated with seizure occurrence (Baud et al., 2018; Chen et al., 2021; Karoly, Rao, Gregg, Worrell, Bernard, Cook and Baud, 2021; Leguia et al., 2021). However, short-term cycles (e.g. ultradian with cycle period less than 24h) have been studied only in a small number of studies (Mitsis et al., 2020; Spencer et al., 2016), where authors analysed specific EEG features that capture certain pathophysiological changes in brain activity and looked only at specific seizure features (seizure occurrence, seizure onset). Additionally, whether cycles in iEEG features exhibit alterations in pathological tissue remains unclear. In this thesis, we highlight the significance of all the different timescales that appear in the epileptic brain activity. We make two hypotheses: 1) fluctuations with timescales ranging from minutes to days are associated not only with seizure occurrence, but also with other seizure features, such as the dynamics and severity of an imminent seizure; just like in seismology where multiple changes happen on the scale of minutes, hours, days or years that contribute to the burst of a seismic event and/or its magnitude, and 2) those fluctuations are diminished in epileptogenic tissue.

In that notion, I captured the continuous brain dynamics using more global measures of iEEG recordings (e.g. band power in main frequency bands) and extracted the different fluctuations over a hierarchy of timescales. Instead of looking at the seizure occurrence and its potential co-modulation with these fluctuations, I firstly analysed how seizures dynamically evolve and secondly how seizure severity change in time.

Finally, I investigated whether alterations in cycles are apparent in epileptogenic tissue compared to healthy tissue. Specifically, in my thesis I tried to address the following questions:

- Does the seizure dynamics oscillate on specific timescales?
- How do other seizure features, such as seizure severity change over time? Is seizure duration modulated by multiple cyclical patterns?
- Is the pathology associated with the alteration of cycles in brain activity?

1.6 Outline of the Structure of the Thesis

In Chapter 2, I analysed continuous iEEG recordings obtained through video-telemetry units and captured iEEG band power fluctuations over time periods that range from minutes to 12 days. Not surprisingly, all subjects exhibited circadian fluctuations in their iEEG band power, consistent with earlier research. Moreover, we observed other fluctuations of comparable magnitudes that were unique to each subject. Recently, we conducted a study to measure the varying spatio-temporal patterns of seizures in individual patients (Schroeder et al., 2020). These patterns appeared to be influenced by subject-specific circadian or longer-term fluctuations (Schroeder et al., 2020). Consequently, in this chapter, I investigated whether interictal iEEG features recorded continuously can detect such modulations over various time periods. Indeed, I found that in most subjects, the combination of fluctuations over different time scales can account for changes in seizure evolutions beyond what would be expected by chance. These findings suggest that subject-specific fluctuations in iEEG band power over minutes to days may serve as markers of seizure-modulating processes. I anticipate that future studies will link these fluctuations to their biological causes, which will be crucial for the development of innovative treatment strategies that can mitigate the clinical impact of seizures by reducing their spread, duration, or severity.

In Chapter 3, I built on work done in Chapter 2 and further investigated another seizure feature, duration of a seizure. In particular, I tested whether continuously-recorded interictal intracranial EEG (iEEG) features encapsulate signatures of modulations over different timescales and whether those are associated with seizure severity.

Seizure duration was used as an intermediate proxy of seizure severity. The duration of seizures has been found to be associated with the type of seizure, with more severe symptoms typically leading to longer durations. For instance, seizures that begin in one area of the brain and then spread to recruit additional brain areas tend to have longer durations than those that do not spread as much. This has been observed in various studies such as (Dobesberger et al., 2015; Kaufmann et al., 2020; Ferastraoaru et al., 2016). Additionally, longer seizures have been linked to extended periods of postictal suppression, which is an established indicator of seizure burden and severity, when compared to shorter seizures (Payne et al., 2018). Seizure severity is also modulated over short and long timescales, which suggests that cyclical modulators could play a role. One potential biomarker for seizure properties is cycles of interictal EEG features that appear to influence seizure evolution found in Chapter 2. In this chapter, I investigated whether seizure severity can be predicted based on interictal features using seizure duration as a proxy for severity. I analysed changes in seizure duration and their association with EEG band power fluctuation cycles within subjects. These findings suggest a relationship between interictal iEEG band power cycles and seizure duration, providing new opportunities for forecasting seizure severity in the future.

Finally, in Chapter 4, I explored whether cycles over multiple timescales are altered in pathological tissue in patients with refractory focal epilepsy. I captured ultradian and circadian cycles from time-varying band power using continuous iEEG recordings. I found that circadian and ultradian biological rhythms exist in the brain. Interestingly, when analysing the magnitude of these biological rhythms in different brain regions, we find that circadian and particularly multiple ultradian rhythms are diminished in regions that were deemed pathological. Within each patient, the level of alteration remained relatively stable over time. Further investigation of the causal mechanisms underpinning our findings is needed, and may allow for novel therapies leveraging these biological rhythms.

Chapter 2. Fluctuations in EEG Band Power at Subject-specific Timescales over Minutes to Days Explain Changes in Seizure Evolutions

Contents

2.1 Introduction

Epilepsy is a common neurological condition characterised by recurrent, unprovoked seizures (Fisher et al., 2014). It affects approximately 1% of the world's population and a third of patients experience refractory epilepsy, where seizures are not adequately controlled despite medication (Chen et al., 2018; Kwan and Brodie, 2000).

Importantly, epilepsy is not a static disorder; electrographic seizure and epileptiform activities have been shown to fluctuate over hours to years in both intensity and spatial distribution. Specifically, while seizures often share common features in the same patient (Kramer et al., 2010; Schindler et al., 2011; Schevon et al., 2012; Burns et al., 2014; Wagner et al., 2015; Truccolo et al., 2011), electrographic seizure activity may change in terms of duration (Cook et al., 2016), spatial spread (Marciani and Gotman, 1986; Karthick et al., 2018; Naftulin et al., 2018; Pensel et al., 2020), spectral properties (Alarcon et al., 1995) from one seizure to the next. Our recent work (Schroeder et al., 2020) has additionally shown that the seizure EEG spatio-temporal evolution from seizure start to seizure termination (or short: "seizure evolution") also changes from one seizure to the next in the same patient. Notably, these changes were consistent with daily (circadian) and/or longer-term fluctuations in most patients (Schroeder et al., 2020). In support of our observations, a recent study quantifying single-channel properties of seizure onset and offset also noted that different types of dynamics can be seen across different seizures in the same patient (Saggio et al., 2020). Similarly, seizure symptoms are also known to change over time. For example, focal seizures, which evolve into bilateral tonic-clonic seizures, preferentially arise from sleep (Jobst et al., 2001). Subclinical seizures (without clinical symptoms) are also reported to follow circadian patterns (Jin et al., 2017). Finally, seizure severity appears to depend on the severity of the preceding seizure in the same patient (Sunderam et al., 2007). Thus, epileptic seizures are not a fully deterministic sequence of abnormal brain activity patterns, but are clearly modulated by processes that shape the neural activity during a seizure and affect seizure severity.

However, it is unclear what these seizure-modulating processes are, and how to quantify and measure them. Given the evidence of seizure properties fluctuating over various timescales of hours to days, we hypothesise here that the seizure-modulating

processes will also fluctuate over these timescales. From existing literature, we also know that continuously recorded EEG show fluctuations over such timescales. For example, spectral properties of the EEG change from moment to moment (Oken and Chiappa, 1988) and also follow a circadian rhythm (Aeschbach et al., 1999). Global and local characteristics of the continuously recorded (interictal) functional network fluctuate over timescales from hours to days, with circadian rhythm having a particularly strong effect on these dynamics (Geier et al., 2015; Geier and Lehnertz, 2017; Mitsis et al., 2020). Interictal fluctuations related to epilepsy are also seen: HFO rates vary in location and power within each subject over time (Gliske et al., 2018). Interictal spikes also change in their location and rate over hours to days (Karoly et al., 2016; Gliske et al., 2018; Conrad et al., 2020; Baud et al., 2018; Chen et al., 2021).

In this chapter, we therefore hypothesised that fluctuations of certain features captured in continuously recorded EEG may serve as biomarkers of seizure-modulating processes. We expected these fluctuations to appear on the timescale of hours to days, and we investigated whether they can also explain how seizure evolutions change within the same patient. Previous work suggests that many interictal features, including interictal spike rate (Baud et al., 2018; Proix et al., 2021; Karoly et al., 2016, 2017) and high frequency oscillation rate (Gliske et al., 2018; Scott et al., 2021; Chen et al., 2021) may serve as biomarkers for modulatory processes. In this chapter, we investigate the full spectral range, using band power in main EEG frequency bands, to capture a complete view of brain activities. Specifically, we use clustering and dimensionality reduction to detect subject-specific spectral patterns in continuously recorded EEG. We then extract the temporal fluctuations over minutes, hour, and days in these common spectral patterns and explore whether fluctuations on different timescales are associated with how seizure evolutions change in each subject.

2.2 Methods

2.2.1 Data acquisition

We analysed open source data from subjects with drug-resistant focal epilepsy in accordance with the ethical standards set by the Newcastle University Ethics Committee

(Ref: 18818/2019). The data consist of a total of 2656 hours of long-term intracranial electroencephalography (iEEG) from 18 subjects (available at http://ieeg-swez.ethz.ch). Continuous recordings in each subject cover 24 to 128 EEG channels and vary between 2 and 12 days. More information about the data is given in Supplementary Section 2.5.1. Sampling frequency was either 512 or 1024 Hz depending on the subject. Electrodes (strip, grid, and depth) were implanted intracranially by clinicians. The onset and termination of seizures were defined electrographically in the intracranial EEG recordings by visual inspection by an epileptologist for the purpose of subsequent data analysis. The collection of the data was conducted in the Sleep-Wake-Epilepsy-Center (SWEC) at the University Hospital of Bern, Department of Neurology, as part of their presurgical evaluation programme, independently of this study (Burrello et al., 2019).

The iEEG signals were provided in already preprocessed form. Briefly, signals were median-referenced and band-pass filtered from $0.5 - 120$ Hz using a 4^{th} order Butterworth filter (forward and backward). Seizure onset and termination times were determined by a board-certified epileptologist. Channels with artifacts were also identified and excluded by the same epileptologist. These steps were all conducted independently of this study and resulted in the publicly available data and annotations. All subjects formally consented to their iEEG data being used for research purposes (Burrello et al., 2019).

2.2.2 iEEG preprocessing

We performed additional preprocessing steps to extract iEEG band power from five main frequency bands (Fig. 2.1a). For each recording channel, the signal was divided into 30 s epochs (Fig. 2.1b). For each epoch, the band power was computed for the following frequency bands: $\delta: \ 1-4$ Hz, $\theta: \ 4-8$ Hz, $\alpha: \ 8-13$ Hz, $\beta: \ 13-30$ Hz and $\gamma: \ 30-80$ Hz. Band power across the five main frequency bands was estimated using Welch's method for every 30 s epoch, with 3 s sliding window without overlap between consecutive windows. This estimation yielded a time-varying band power, with each time point corresponding to the mean power within a 30 s window. The band power values were aggregated into band-specific matrices with dimensions #channels $\times$ #epochs. Then, these matrices were log transformed and standardised across all epochs and channels within a frequency band. To enable subsequent analysis steps, we also

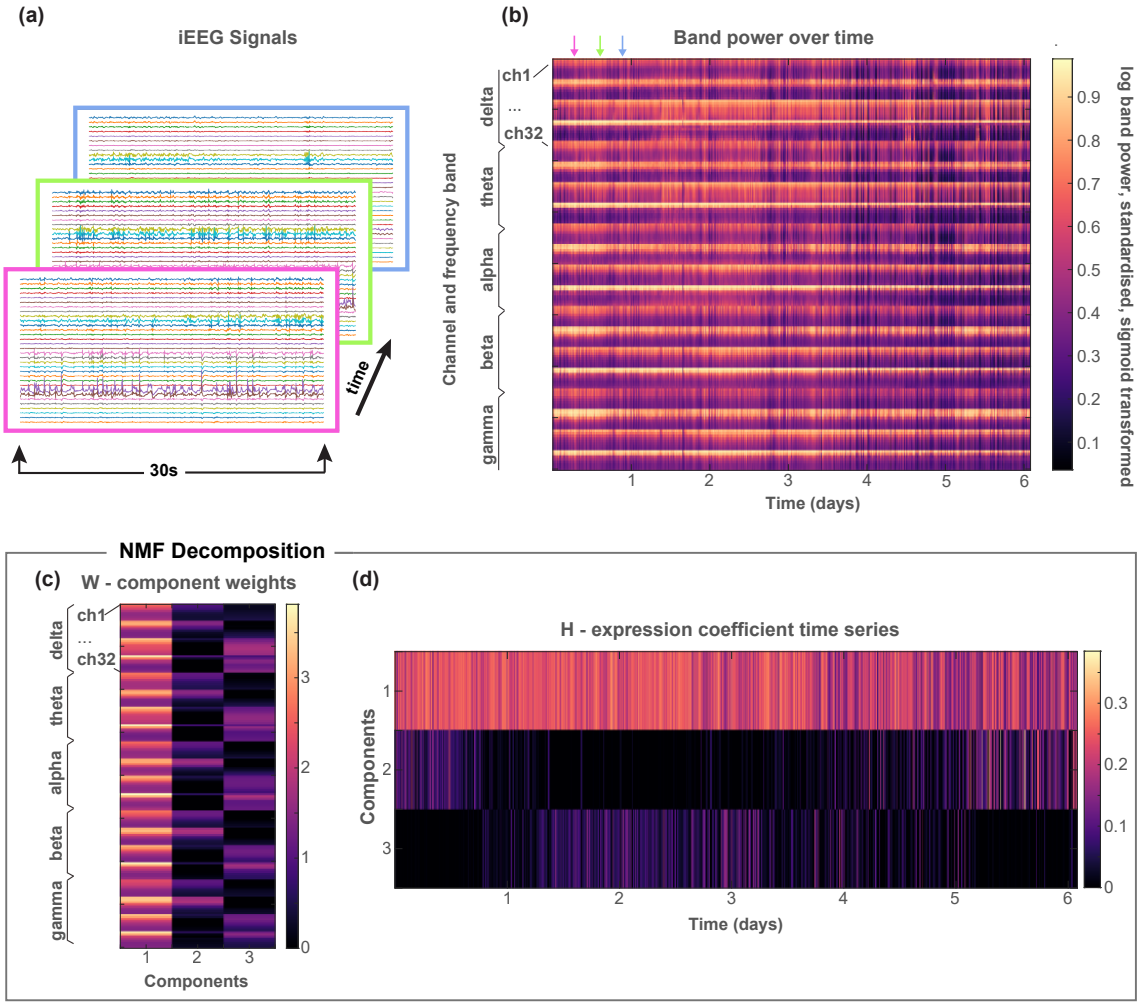

Figure 2.1 **Workflow of data preprocessing; calculation of band power in 30 s epochs and subsequent dimensionality reduction to detect subject-specific spectral patterns**. (a) The multi-channel continuous iEEG recording was divided into 30 s non-overlapping epochs. (b) The standardised, log and sigmoid transformed band power. (c)&(d) NMF (dimensionality reduction) of the band power matrix results in the decomposition $W \times H$. (c) The matrix W contains the basis vectors, each of which had $5 \times \#channels$ weights that represents a pattern of frequency across all channels and frequency bands. (d) The coefficients matrix H captures the contribution of each frequency pattern (basis vector) to each time window.

Sigmoid transformed ($S(x) = [1+\exp(-x)]^{-1}$) the standardised data to ensure positive entries between 0 and 1. For each subject, we then concatenated the matrices from all

frequency bands yielding a single (5 × #channels) × #epochs (henceforth defined as $n \times T$; Fig. 2.1b). We will refer to this matrix as the data matrix X throughout the paper.

Note that we did not exclude seizure epochs from the construction of the data matrix, as seizures only represent a few epochs in the context of the continuous recording. Our downstream analysis (with empirical mode decomposition) is robust to "noise" of this type, and we show in Supplementary Section 2.5.8 that this choice does not affect our main results. Note also that our measure of how seizure evolutions change over time (in Section 2.2.11) (Schroeder et al., 2020) was based on functional network activity of the seizure, whilst we used band power features to measure fluctuations of the continuous EEG. Therefore, the fluctuations of the continuous EEG were not trivially related to variability in seizure evolutions (also shown in Supplementary Section 2.5.3).

2.2.3 Non-Negative Matrix Factorization for dimensionality reduction

As the data matrix X for each subject is high-dimensional with redundant information (e.g. in different channels), we applied a dimensionality reduction step on X using Non-Negative Matrix Factorization (NMF) (Lee and Seung, 1999). NMF provides a low-rank approximation to a non-negative input matrix $X \in \mathbb{R}_+^{n \times T}$ as the product of two non-negative matrices, $W \in \mathbb{R}_+^{n \times k}$ and $H \in \mathbb{R}_+^{k \times T}$, such that $X \approx W \times H \equiv X'$, given an integer k. Specifically, we applied the non-negative singular value decomposition (SVD) with low-rank correction (NNSVD-LRC) (Atif et al., 2019), which is a method of low-rank approximation using an NMF initialisation approach based on SVD.

In this way, we decomposed each subject's band power data matrix X into W and H matrices (Fig. 2.1c-d). Every column of matrix W corresponded to a single NMF component and formed a basis vector or feature weight with n elements. Each row of H represented how a single NMF component evolves over time across all T time epochs. We also refer to a single row of H as the NMF-expression coefficient time series. This dimensionality reduction step not only compressed the data matrix X into a few relevant dimensions, but can also be understood as a data-driven pattern detection, or (soft) clustering of recurrent spectral patterns in the continuously recorded EEG. For example, Fig. 2.1 shows that the band power in each channel at a particular time window could be (approximately) described as a weighted sum of three patterns (given by the three

basis vectors in W). The weights were given as the expression coefficients (in H) at each time point. This data-driven spectral pattern detection essentially provided us with a comprehensive view of the EEG in each subject, without the need to pre-define specific patterns of interest, which may not acknowledge subject-specific variations in these spectral patterns.

To determine the optimal number of representative NMF components, k, for each subject, we performed NNSVD-LRC for $k = 3, 4, \ldots, 15$. For each value of k, we obtained the matrices W and H. Using these matrices, we calculated the relative reconstruction errors

$$\sum_{n,T} |X - X'|/(n \times T),$$

as well as the quantity

$$c = max\{max(|Corr(W)|), max(|Corr(H)|)\}$$

for each k, where $max(|Corr(W)|)$ represents the maximum absolute correlation among all column pairs of W, and $max(|Corr(H)|$ represents the maximum absolute correlation among all row pairs of H. The latter represents the strongest correlation or anticorrelation between NMF components in terms of their feature weights W and their expression coefficient time series H. In this way, redundant information, particularly in H, was excluded whilst preserving the important spatio-temporal patterns for the next processing steps. A distinct number of NMF components, k, was selected for each subject. This was the k yielding the smallest correlation between the NMF components that had a relative reconstruction error smaller than 5%.

After determining the optimal choice of k, we obtained two matrices for each subject, W and H. To reiterate, the matrix W consists of the basis vectors, while H is a multivariate time series with dimensions equal to $k \times T$ (= the number of NMF components $\times$ the total number of epochs).

2.2.4 Extracting fluctuations in interictal band power using MEMD

To investigate fluctuations in band power on different timescales, we analysed the matrix H using Empirical Mode Decomposition (EMD) (Huang et al., 1998, 2003). It is

well known that EEG signals are non-stationary processes characterised by time-varying features (Kaplan et al., 2005; Fingelkurts and Fingelkurts, 2001). EMD is a popular data-adaptive method to detect non-stationary and non-rhythmic fluctuations on different timescales. Compared to Fourier and Wavelet-based approaches, EMD does not assume any particular basis function or local stationarity. EMD also does not require detrended time series and does not make assumptions about trends or timescales of trends. It has the advantage of fully decomposing the signal into the full range of timescales of fluctuations; their point-wise summation fully reconstructs the original signal. As the nature of these band power fluctuations is unknown and most likely not stationary, we opted for a data-driven method that makes as few assumptions as possible.

EMD decomposes an input signal $Y(t)$, into M finite narrow-band fluctuations, known as intrinsic mode functions (IMFs), based on the local extrema of the signal: $Y(t) = \sum_{i=1}^{M} \mathrm{IMF}_i(t) + r(t)$, where $r(t)$ is the residue signal (Huang et al., 1998). The IMFs additionally satisfy the properties that make the Hilbert-transform well-defined and therefore naturally yield instantaneous frequency and phases for each IMF.

However, local extrema are not directly applicable to multivariate time series signals (Rehman and Mandic, 2010), as we have in the H matrix. Therefore, we used an extension of the EMD to multi-dimensional space, called the Multivariate Empirical Mode Decomposition (MEMD) (Rehman and Mandic, 2010). In MEMD, multiple projections of the multivariate signal are generated along different directions in n-dimensional spaces; the multidimensional envelope of the signal is then obtained by interpolating across the different envelopes of these projections (Rehman and Mandic, 2010). An additional advantage of this method is that it yields the same number of IMFs across the different dimensions of the multivariate signal, and preserves fluctuations of similar frequency across the different dimensions within each of the IMFs (mode-alignment) (Rehman and Mandic, 2010).

For the purpose of this analysis, we used MEMD to decompose the NMF-expression coefficient time series, H, into a number of multi-dimensional oscillatory modes. Therefore, the matrix H can be represented by the sum of M multi-dimensional IMF signals, where the dimension for each IMF is equal to k (i.e. the number of rows of the matrix H, which corresponds to the number of NMF components). To clarify, we can

think of all IMFs in a specific dimension as the decomposition of the corresponding NMF-expression coefficient time series. Thus, $\text{IMF}_{i,j}$ refers to the j-th dimension of the i-th IMF timescale. The j-th NMF-expression coefficient time series $H_j = Y_j(t)$ can be written as $Y_j(t) = \sum_{i=1}^{M} \text{IMF}_{i,j}(t) + r_j(t)$. This equation applies to every NMF component $j = 1, \ldots, k$.

2.2.5 Extracting time-varying characteristics from band power fluctuations (IMFs) using Hilbert Spectral Analysis

To obtain a time-frequency representation of the oscillatory modes (IMFs), and hence derive their time-varying characteristics (instantaneous frequency, phase, and amplitude), we applied a Hilbert-transform on each dimension of the IMF (following classical analysis methods for EMD) (Huang et al., 1998, 2003; Huang, 2014).

For any (real-valued) univariate signal $u(t)$, we can define its Hilbert transform as:

$$H(u)(t) = \frac{1}{\pi} P \int_{-\infty}^{+\infty} \frac{u(\tau)}{t - \tau} d\tau, \tag{2.1}$$

where P represents the Cauchy principal value for any function $u(t) \in L^P$ class (Huang et al., 1998).

The analytical signal $v(t)$ obtained from the Hilbert transform can be expressed as:

$$v(t) = u(t) + iH(u)(t) = a(t)e^{i\theta(t)}, \tag{2.2}$$

where

$$a(t) = \sqrt{u(t)^2 + H(u)(t)^2} \tag{2.3}$$

and

$$\theta(t) = \tan^{-1}\left(\frac{H(u)(t)}{u(t)}\right) \tag{2.4}$$

where $a(t)$ and $\theta(t)$ are the instantaneous amplitude and instantaneous phase, respectively.

The instantaneous frequency, $f(t)$, can then be calculated as follows:

$$f(t) = \frac{d\theta(t)}{dt}. \tag{2.5}$$

The application of EMD along with Hilbert transform leads to the so-called Hilbert-Huang transform. Through the Hilbert spectral analysis, each IMF's instantaneous frequency can be represented as functions of time. The result is a frequency-time distribution of signal amplitude (or energy using the squared values of amplitude, $a^2(t)$), designated as Hilbert amplitude spectrum or Hilbert spectrum (or Hilbert energy spectrum if energy is used instead of amplitude), $H(f, t)$.

For each univariate IMF signal, we can obtain the Hilbert energy spectrum as a function of instantaneous frequency and time mathematically using the following formula:

$$H(f,t) = \begin{cases} a^2(t), & f = f(t) \\ 0, & \text{otherwise.} \end{cases} \tag{2.6}$$

For visualisation purposes we will display the inverse of the instantaneous frequency, i.e. the instantaneous period length, also termed 'cycle length' in the following.

The Hilbert-Huang marginal spectrum $h(f)$ of the original signal $u(t)$ can then be defined as the total energy distributed across the frequency space within a time period $[0, T]$. Mathematically, this definition can be expressed as shown below:

$$h(f) = \int_0^T H(f,t)dt. \tag{2.7}$$

By using Equations 3.6 and 3.7 we can obtain the Hilbert-Huang marginal spectrum for a univariate IMF signal. However, the application of the multivariate EMD results in multivariate IMF signals. In order to compute the Hilbert-Huang marginal spectrum of each multivariate IMF signal across all dimensions, we simply averaged over the dimensions $H_i(f, t)$ across $i = 1, \ldots, k$ dimensions:

$$\bar{H}(f,t) = \frac{\sum_{i=1}^{k} H_i(f,t)}{k}. \tag{2.8}$$

The corresponding marginal spectrum $\bar{h}(f)$ was then similarly defined as:

$$\bar{h}(f) = \int_0^T \bar{H}(f,t)dt. \tag{2.9}$$

For numerical computations, we discretised time t to compute the integrals as sums. Figure 2.2 shows the marginal Hilbert-Huang spectra for different multivariate IMFs in an example subject.

2.2.6 Peak fluctuation frequency in each IMF

Within each subject, each IMF was characterised by a peak fluctuation frequency (measured in cycles/day here). It was determined as the frequency with the highest power based on the marginal Hilbert-Huang spectrum over all frequencies, $\bar{h}(f)$.

2.2.7 Finding a circadian IMF

We will later focus one part of our analysis on IMFs that fluctuate on the timescale of 24 hours (1 cycle/day). To detect those IMFs, we found IMF(s) with a peak fluctuation frequency of 1 cycle/day. If two IMFs were found (i.e. both displayed a peak frequency at around 1 cycle/day), then the circadian IMF was determined to be the IMF with the higher power. This case only occurred in one subject.

2.2.8 Relative contribution of iEEG main frequency bands in different IMFs

To understand how much each of the iEEG frequency bands and channels contributed to a certain IMF, we first determined how much each dimension of the IMF contributed to the overall power of the IMF. To this end, we first obtained the mean power E_{ij} in each dimension j of every i-th IMF signal:

$$E_{ij} = \frac{\sum_{t=0}^{T} a_{ij}(t)^2}{T}, \tag{2.10}$$

where T is, as before, the number of time epochs, and $a_{ij}(t)$ is the instantaneous amplitude for the j-th dimension of i-th IMF signal at time point t. One of the main properties of MEMD is that multivariate signals are decomposed into multivariate IMF

signals of the same dimensions, where all dimensions within an IMF share fluctuations of the same timescale (Lv et al., 2016). Hence, focusing on the mean power over time of each dimension within an IMF is a good indication of the power on a particular timescale. The relative contribution of each j-th dimension to the i-th IMF (or relative power) was then defined as:

$$R_{ij} = \frac{E_{ij}}{\sum_{j=1}^{k} E_{ij}}, \tag{2.11}$$

with k indicating the number of dimensions.

Using the relative contribution of each dimension as weights, we can then form the weighted sum of all dimensions in terms of contributions of iEEG main frequency bands. By summing channel contributions for each iEEG main frequency band (see Fig. 2.3b&c for an example subject), we obtained a matrix of dimensions (# main frequency bands = 5) $\times$ (# dimensions = k). This matrix was then multiplied with the weight indicating the contribution of each dimension to yield a vector (of length # main frequency bands = 5) representing the contribution of each main frequency band to a particular IMF for each subject (Fig. 2.3d).

2.2.9 Different band power fluctuations reveal spatial heterogeneity within iEEG main frequency band

To determine whether all recording channels contribute homogeneously to an IMF in a particular frequency band, we used a measure that quantifies sparsity of a distribution: the *Gini index* (Hurley and Rickard, 2009). Given a vector $\boldsymbol{x} = (x_1, x_2, \ldots, x_N)$ sorted in ascending order such that $x_1 < x_2 < \cdots < x_N$, the Gini index can be derived using the following formula:

$$G(\boldsymbol{x}) = 1 - 2\sum_{i=1}^{N} \frac{x_i}{\|\boldsymbol{x}\|_1} \left(\frac{N - i + \frac{1}{2}}{N} \right). \tag{2.12}$$

It can range from 0 to 1, with values closer to 0 indicating low sparsity (homogeneity) and values closer to 1 corresponding to higher sparsity (heterogeneity).

We derived the Gini index for each IMF across different channels within each main frequency band. In other words, for each IMF, we first computed the contribution C_i to

each i-th IMF as the product of the relative power (eqn. 2.11) and the weights matrix: $C_i = \sum_j R_{ij} \times W_j$, with i indexing the IMF number, and j indexing its dimension. Specifically, W_j is the j-th column of the W matrix from the NMF decomposition (Fig. 2.1c), whereas R_{ij} is a scalar representing the relative power of the j-th dimension to the i-th IMF (see 2.2.8). The resulting C_i is a vector of length #frequency bands $(= 5) \times$ #channels, i.e. the same length as W_j. As we are interested in the distribution of each C_i across channels for each frequency band, we applied the Gini index to each frequency band separately in each C_i, yielding one Gini index per frequency band and IMF.

2.2.10 Seizure distance in terms of a particular band power fluctuation (IMF)

For each subject, we quantified the difference between pairs of seizures in terms of each IMF. This measure (which we subsequently term the "IMF distance") thus quantifies how different two seizures are to each other in terms of a particular fluctuation of the band power. To obtain this difference, we first computed the product $W \times \mathrm{IMF}_i(t)$, where $\mathrm{IMF}_i(t)$ is the multi-dimensional i-th IMF ($k \times T$ matrix). The product yields the matrices X'_{IMF_i} for all $i = 1, \ldots, M$ timescales. X'_{IMF_i} reconstructs the i-th IMF in the original space of all channels and frequency bands. For each X'_{IMF_i}, we computed a distance matrix based on the multivariate Euclidean distance of IMF values for each pair of seizures: $D_i(a, b) = ||X'_{\mathrm{IMF}_i}(t_a) - X'_{\mathrm{IMF}_i}(t_b)||$, where t_a and t_b are the time epochs of the seizure pair's onset. Therefore, we obtained M IMF seizure distance matrices per subject, each representing the pairwise seizure distance for a specific IMF.

Note that any seizure-induced changes in the band power will only be present in a few epochs (as we use 30 s long epochs). Therefore, the seizures are considered to only influence the fastest IMFs (highest-frequency fluctuations), while they have little effect on the slower IMFs. Supplementary Section 2.5.8 additionally shows that our main results were reproduced by using the IMF seizure distances obtained from one epoch before the seizure onset epoch ($t_a - 1$ and $t_b - 1$).

2.2.11 Quantifying differences in seizure evolutions using seizure dissimilarity

To quantify how seizures themselves change over time in terms of the seizure EEG evolutions, in our previous work we introduced a quantitative measure of how dissimilar two seizures are within a subject (Schroeder et al., 2020). Briefly, each epileptic seizure in a subject was analysed in terms of its evolution through the space of functional network dynamics (using exactly the same pipeline as (Schroeder et al., 2020)). Each pair of seizures was then compared to each other using dynamic time warping (Sakoe and Chiba, 1978), allowing us to recognise seizures with shared evolutions (or parts of evolutions), even if the seizures evolved at different rates. The average distance between the warped seizures was then taken as the dissimilarity measure. As such, for each subject, we obtained a "seizure dissimilarity" matrix, which captures the pairwise dissimilarity between the subject's seizure evolutions.

2.2.12 Association between seizure dissimilarity and IMF seizure distance

Finally, we related how seizure evolutions changed over time (quantified using seizure dissimilarity) with fluctuations seen in the continuously recorded iEEG (quantified using IMF seizure distances). In subjects with at least six recorded seizures, we investigated whether IMF seizure distances were associated with seizure dissimilarity. For every subject, we used a linear regression framework, where the seizure dissimilarity was the response variable and the IMF seizure distances were the explanatory variables. The observations were the entries of the seizure dissimilarity matrix and IMF seizure distance matrix. As each matrix was symmetric, we only used the upper/lower triangular elements. We also included the EMD residue signal distances, and temporal distances of seizures (how far apart in time each pair of seizures occurred) as additional explanatory variables. The responses, as well as the explanatory variables, were standardised individually before fitting the model.

We performed a variable selection step for our analysis, as the number of explanatory variables (i.e. $M + 2$) was relatively large. We used LASSO (Least Absolute Shrinkage

and Selection Operator) (Tibshirani, 1996), which is a sparse shrinkage method. Linear regression coefficients were calculated based on least squares, subject to the L_1 penalty. The LASSO also accounted for any collinearity issues between variables. As we were interested in detecting positive relationships between the response variable (as these were distances) and the explanatory variables, we used a constrained positive LASSO; that is, coefficients were constrained to be non-negative. For the LASSO, the tuning parameter λ was selected using a 10-fold cross validation method from a range of values $\lambda = 10^{-3}, 10^{-2.95} \ldots, 10^{1.95}, 10^{2}$ (see Supplementary Fig. 2.12).

After selecting a small number of explanatory variables, an ordinary least squares regression was performed for each subject to obtain R^2 and 95% confidence intervals for the coefficients.

2.2.13 Statistical analysis

To assess whether the level of explanatory power of the best model selected for each subject has occurred by chance, we performed two separate tests of statistical significance for the adjusted R^2. Both tests yielded very similar results and are are shown in Supplementary Section 2.5.4.

In the first test, we randomly selected seizure onset times by generating a sample from the uniform distribution on the interval $(0, T)$ over 500 iterations. The size of the sample was equal to the number of annotated seizures for each iteration. Then, keeping the randomly picked seizure onset times unsorted, we obtained for each one of them new IMF seizure distance matrices and performed the LASSO and linear regression, as described in the previous section, leaving the response variable unchanged. Finally, we calculated the adjusted R^2 for each iteration. Across all iterations, the adjusted R^2 values were used to estimate the distribution of the test statistic used in the permutation test. P-values were then calculated as the percentage of adjusted R^2 values that were larger in the permutation distribution. Statistical significance was determined based on a significance level of 5%.

In the second test, we permuted the order of the seizures without permuting the seizure timing over 500 iterations. We then performed the LASSO and subsequent steps as in the first test.

2.2.14 Data and code availability

The long-term iEEG recordings for all subjects are available at http://ieeg-swez.ethz.ch/ under the section "Long-term Dataset and Algorithms" (Burrello et al., 2019).

Initial signal processing was performed using Matlab version 2019a and Matlab's built-in functions. NMF and MEMD were implemented using the following publicly available functions:

- **Non-negative matrix factorization** was conducted using the `NNSVD-LRC` function from `https://sites.google.com/site/nicolasgillis/code` (Atif et al., 2019).
- **Multivariate empirical mode decomposition** was applied using code from `http://www.commsp.ee.ic.ac.uk/~mandic/research/emd.htm` (Rehman and Mandic, 2010).

For the remainder of the analysis and the construction of all figures we used Python version 3.5. Either standard functions obtained from published libraries supported by Python were used or custom code written in Python. The main functions used in the analysis are listed below:

- **Hilbert transform**: `scipy.signal.hilbert`
- **LASSO**: `sklearn.linear_model.Lasso`
- **k-fold cross-validation**: `sklearn.model_selection.kFold`
- **Multiple Linear Regression**: `statsmodels.api.ols`

Our analysis code and data (post processing) can be found at `https://dx.doi.org/10.5281/zenodo.5798022`.

2.3 Results

We analysed fluctuations in band power for 18 subjects with focal epilepsy. We investigated whether fluctuations on specific timescales were driven by particular iEEG frequency bands or spatially localised activity. We then explored whether these temporal fluctuations were associated with how seizures change within subjects.

2.3.1 iEEG band power patterns fluctuate on different timescales

After extracting band power in the main frequency bands ($\delta, \theta, \alpha, \beta, \gamma$) in 30 s non-overlapping sliding windows for each iEEG channel (Fig. 2.1a,b), we performed dimensionality reduction using a non-negative matrix factorisation (NMF) approach. NMF effectively grouped channels and frequency bands to form components that represent specific band power patterns. Weights for channels and frequency bands in each component are shown as columns in matrix W, Fig. 2.1c. The expression coefficients of these components at each time point was then given by the H matrix, which essentially yielded a time series for each component (Fig. 2.1d). The weight represented a subject-specific pattern of EEG band power activity across channels, and the strength of expression of this pattern at any given time point was given by the expression coefficients. In short, the set of coefficient time series (rows in H) indicated the fluctuations of subject-specific EEG spectral patterns over time.

For each subject, we then used Multivariate Empirical Mode Decomposition (MEMD) to determine the different fluctuations on different timescales for each NMF coefficient time series. Figure 2.2a shows the MEMD results for a single NMF component in example subject ID06, yielding 15 Intrinsic Mode Functions (IMFs) and a residue signal. Faster IMFs (e.g., IMF1, 2 and 3) are often thought to contain noise, but might also reflect genuine fluctuations in the initial signal, such as cyclic alternating pattern (Parrino et al., 2014). For simplicity, we retained all IMFs for the subsequent main results and refer the reader to Supplementary Section 2.5.7 for a more detailed analysis of noisy IMFs based on permutation tests.

Using the instantaneous frequency and amplitude through the Hilbert transform, we obtained the marginal spectral densities of each IMF in each dimension. Figure 2.2b shows the marginal spectral densities averaged across all dimensions for each IMF (blue lines) for example subject ID06. Some distinct peaks are seen especially in the slower IMFs, e.g. IMF13 (at cycle length of $\approx$ 1 day), IMF14 (at cycle length of $\approx$ 3.3 days), IMF9 (cycle length $\approx$ 3 hours), IMF8 (cycle length $\approx$ 1.6 hours), etc. Note that both EMD and MEMD essentially act as dyadic filter banks (Wu and Huang, 2004; Flandrin et al., 2004; Ur Rehman and Mandic, 2011); thus, the dyadic pattern seen in the faster IMFs is not surprising. Supplementary Section 2.5.7 shows the marginal spectral densities corrected for potential noise fluctuations.

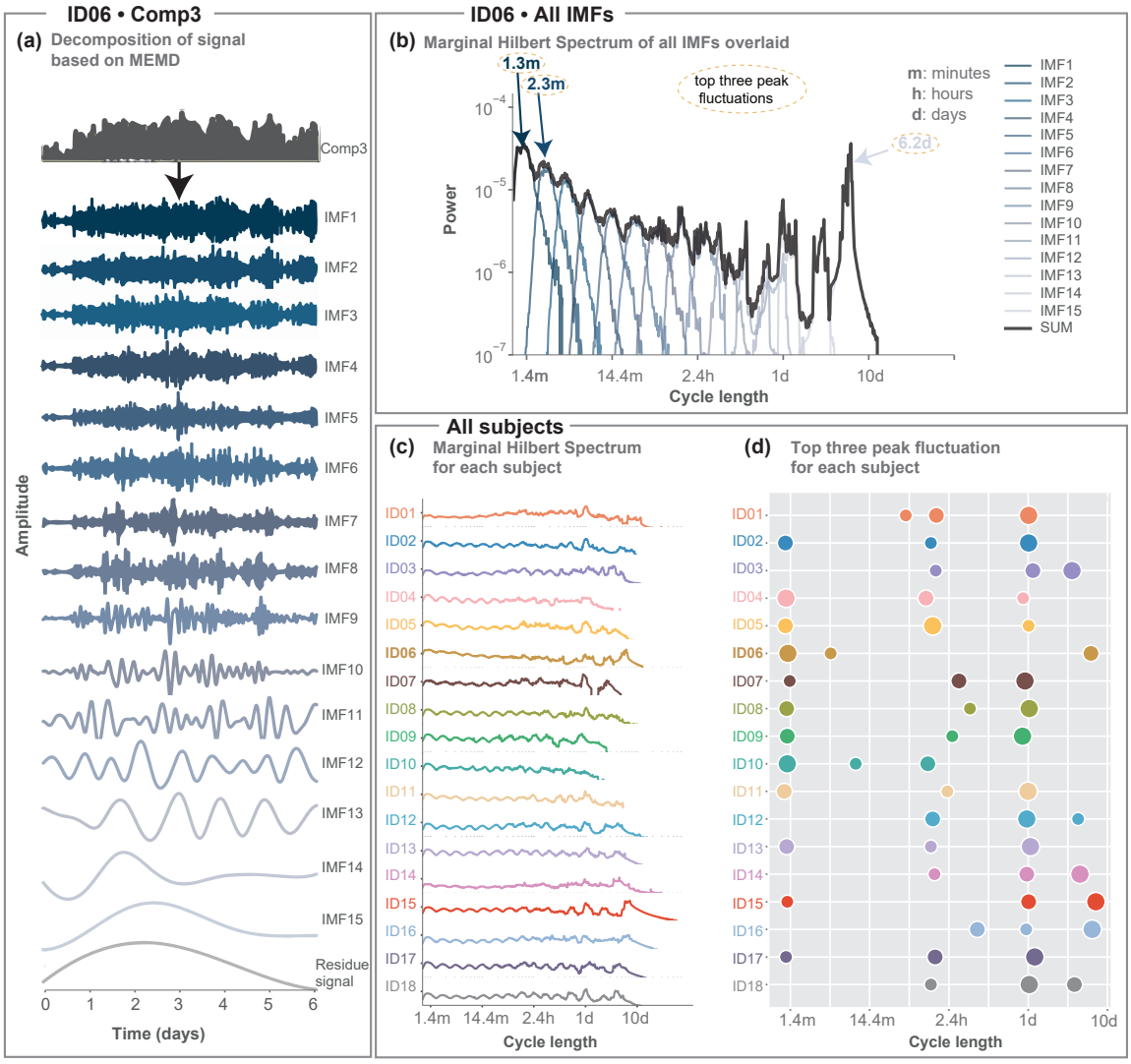

Figure 2.2 **MEMD detects fluctuations on different timescales for each subject.** (a) MEMD yields 16 IMFs in example subject ID06. Only one dimension of the IMF (corresponding to the first NMF component) is shown for simplicity. IMFs are presented in ascending order (fastest to slowest, top to bottom). The last trace is the residue signal. (b) Marginal Hilbert spectrum for all IMFs aggregated across all dimensions in example subject ID06. The black line represents the Marginal Hilbert frequency spectrum across all IMFs. The x-axis shows the instantaneous period length (inverse of instantaneous frequency), which we also termed 'cycle length'. Top three peak fluctuations are indicated with arrows. (c) Marginal Hilbert frequency spectrum across all IMFs for each subject. (d) Bubble plot of peak fluctuations for the three highest power densities according to the Marginal Hilbert frequency spectrum across all IMFs for each subject. The size of the bubbles indicates the first, second and third peak in descending order.

As expected from previous literature (Baud et al., 2018; Karoly et al., 2016), we found that all subjects displayed circadian band power fluctuations (Fig. 2.2c). The presence of these circadian fluctuations helps validate our approach for extracting relevant timescales in interictal fluctuations. Meanwhile, fluctuations on other timescales were more subject-specific in cycle length. For 10 out of 18 subjects (ID01, ID02, ID07, ID08, ID09, ID11, ID12, ID13, ID17 and ID18) the circadian fluctuation had the highest density (Fig. 2.2d). For six subjects (ID03, ID04, ID05, ID14, ID15 and ID16) the circadian fluctuation was slightly lower in density, as the highest density was seen in slower or faster IMFs. For two subjects (ID06 and ID10) the circadian fluctuation did not feature in the top three highest densities, but a peak at one cycle per day can still be observed in ID06 (Fig. 2.2c).

2.3.2 All iEEG frequency bands contribute to the circadian IMF

Following the observation of a circadian fluctuation in all subjects, we assessed the contribution of each iEEG frequency band to the circadian IMF. We first determined the circadian IMF, which was IMF 13 in example subject ID06 (Fig. 2.3a). We then calculated the relative power in each dimension of the IMF, each of which corresponded to an NMF component. For example, in subject ID06, the majority of its power (54%) was concentrated in dimension 1 (Fig. 2.3a). We also noted that the circadian fluctuation did not follow the same phase in all dimensions of the IMF, potentially indicating the presence of multiple processes fluctuating on a circadian timescale. Since we are interested in the overall contribution of each frequency band to the circadian cycle, we decided to assess the contribution of different frequency bands over all dimensions next.

From the dimensionality reduction step, we had already obtained the weights across all iEEG frequency bands and channels (matrix W, see Fig. 2.3b). For each NMF component, we computed the weight of each frequency band by summing the weights of that frequency band across all channels (Fig. 2.3c). Finally, a sum weighted by the relative power in the IMF over all dimensions was obtained representing the relative contribution of each frequency band to the IMF. For most subjects, δ band power contribution was slightly higher compared to the other frequency bands for the circadian IMF. However, other frequency bands also contributed to the circadian IMF in most subjects (Fig. 2.3d).

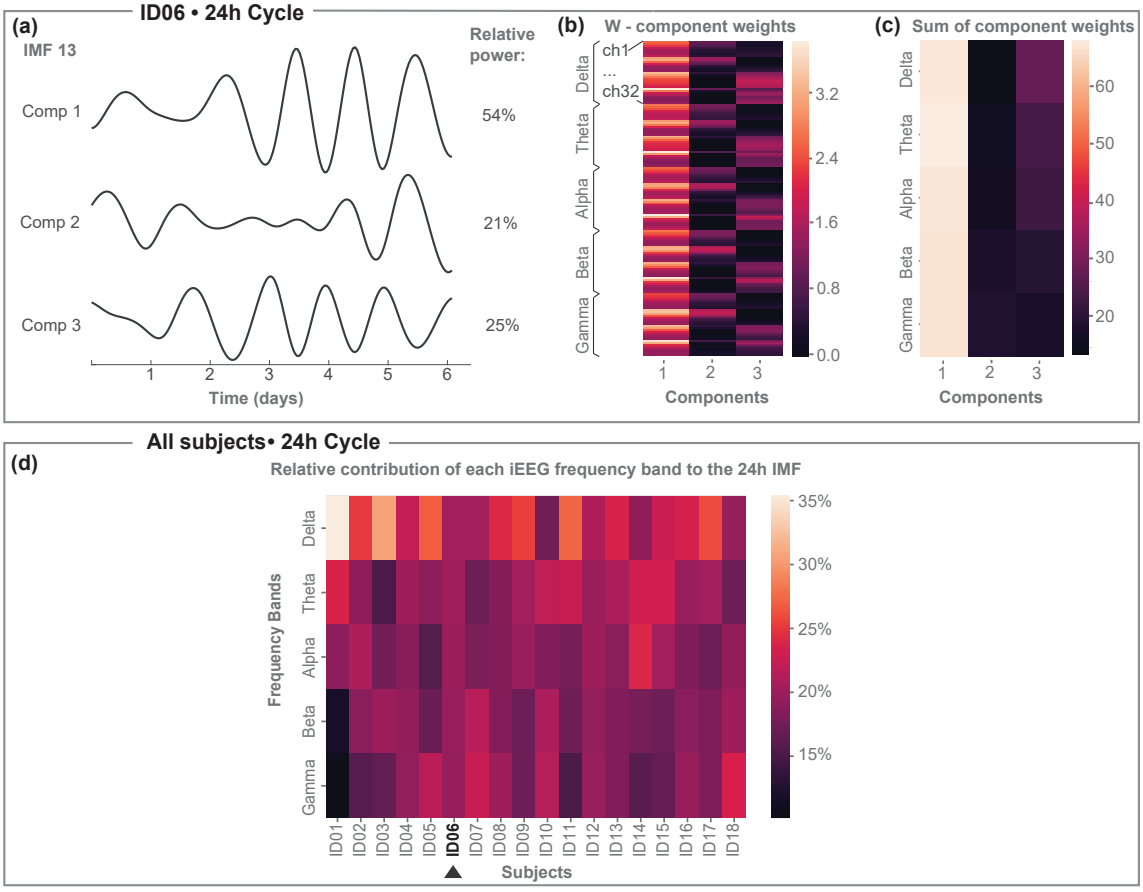

Figure 2.3 **Contribution of iEEG main frequency bands to the circadian IMF.** (a) IMF 13 in example subject ID06 shows circadian fluctuations across all three dimensions, each of which corresponds to an NMF component. Dimension 1 shows the highest relative power in this IMF. (b) W component weight matrix (same as Fig. 2.1c). (c) The sum of the component weights across all channels within each frequency band. (d) Contribution of each iEEG frequency band to the circadian IMF across all subjects obtained by forming the sum over the matrix in (c) weighted by the relative power in (a). To be able to compare subjects to each other, each column here has been normalised to form a percentage contribution.

2.3.3 Subsets of channels contribute to multidien band power fluctuations

Within each frequency band we also investigated the contribution of each channel to an IMF. Specifically, we investigated whether the contributions were heterogeneous across channels. We used the Gini index as a measure of spatial heterogeneity, where 0

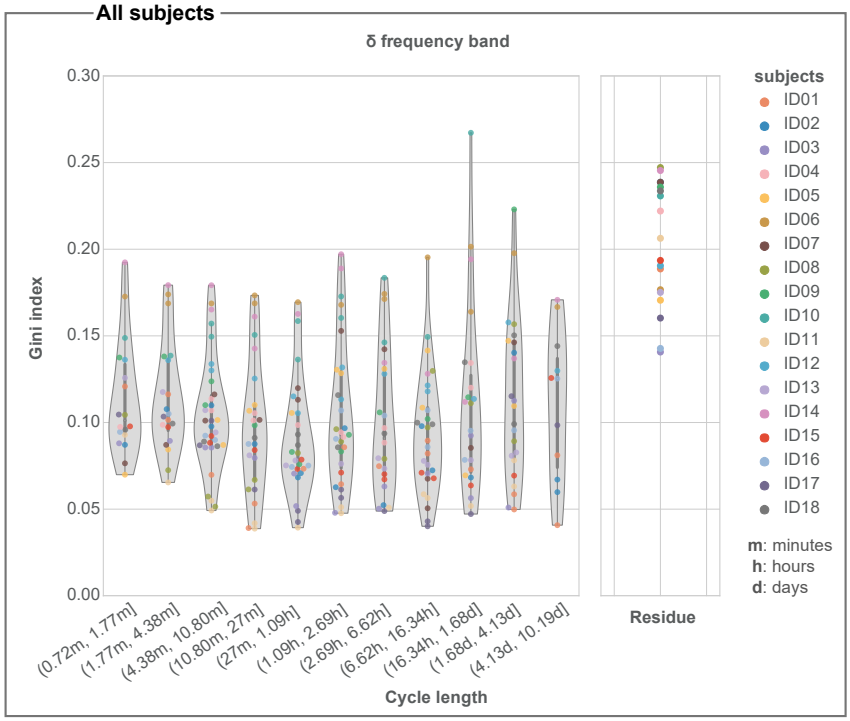

Figure 2.4 **Gini index of IMFs for the δ frequency band across all subjects.** Across all subjects, we grouped IMFs based on their peak IMF cycle length and show the distribution of the corresponding Gini indices as a violin plot with enclosed box plot. The thick grey bar represents the inter-quartile range. For visualisation, we converted the peak frequency to cycle length (x-axis). The residue is shown separately.

(1) indicates a completely homogeneous (heterogeneous) channel contribution for each IMF. Figure 2.4 shows the distribution of Gini indices of all IMFs in the δ band across all subjects, where IMFs are grouped by the IMF peak frequency. Results for other iEEG main frequency bands are similar and shown in Supplementary Fig. 2.11. Overall, the Gini indices are low for all IMFs, indicating that IMFs are not driven by a small group of channels. However, there is a clear tendency for long-term trends to display a higher Gini index, indicating that a subsets of channels may contribute more to those.

2.3.4 Band power IMF fluctuations are associated with seizure dissimilarity in most subjects

As the final part of our analysis, we investigated whether these fluctuations on different timescales influenced, or modulated, changes in seizure evolutions over time in individual subjects. Particularly, we previously showed that seizure network evolutions change over time in every subject, and that these changes could be explained by hypothetical circadian or longer timescale modulators (Schroeder et al., 2020). Hence, we explored whether the subject-specific fluctuations represented by the IMFs were associated with changes in seizure evolutions.

For each IMF in each subject, we first determined their corresponding seizure IMF Euclidean distance matrix (Fig. 2.5a,b). For example, in subject ID06's IMF6, we calculated the Euclidean distance of every time point to the time point of the first seizure (Fig. 2.5a) across all dimensions. By reading out all the Euclidean distances to all the other seizure time points, we obtained the first row of the seizure IMF Euclidean distance matrix (Fig. 2.5b). The same process was repeated for all other seizures in this subject. This distance matrix had dimensions of number of seizures by number of seizures and represented how different the IMF state was for each seizure pair.

By using the same techniques as in (Schroeder et al., 2020), we obtained a seizure dissimilarity matrix, which expressed the dissimilarity of each pair of seizure evolutions through the space of network dynamics (Fig. 2.5c,d). The seizure dissimilarity matrix thus quantified how much each pair of seizures differed within a subject. By relating the set of seizure dissimilarities to the corresponding set of IMF Euclidean distance, we investigated whether there was an association between changes in seizure evolutions and interictal band power fluctuations (Fig. 2.5e).

To generalise this approach to all IMFs in a subject, we fitted a multiple linear regression model, where the sets of seizure IMF distances (derived from different IMFs) were explanatory variables and the seizure dissimilarity was the response variable (Fig. 2.6a). We also included the EMD residue signal and temporal distance between seizures (i.e. how far apart in time each seizure pair occurred) as explanatory variables to model fluctuations of longer timescales than the recording time. The observations were pairs of seizures. After LASSO variable selection and linear regression, the estimated regression

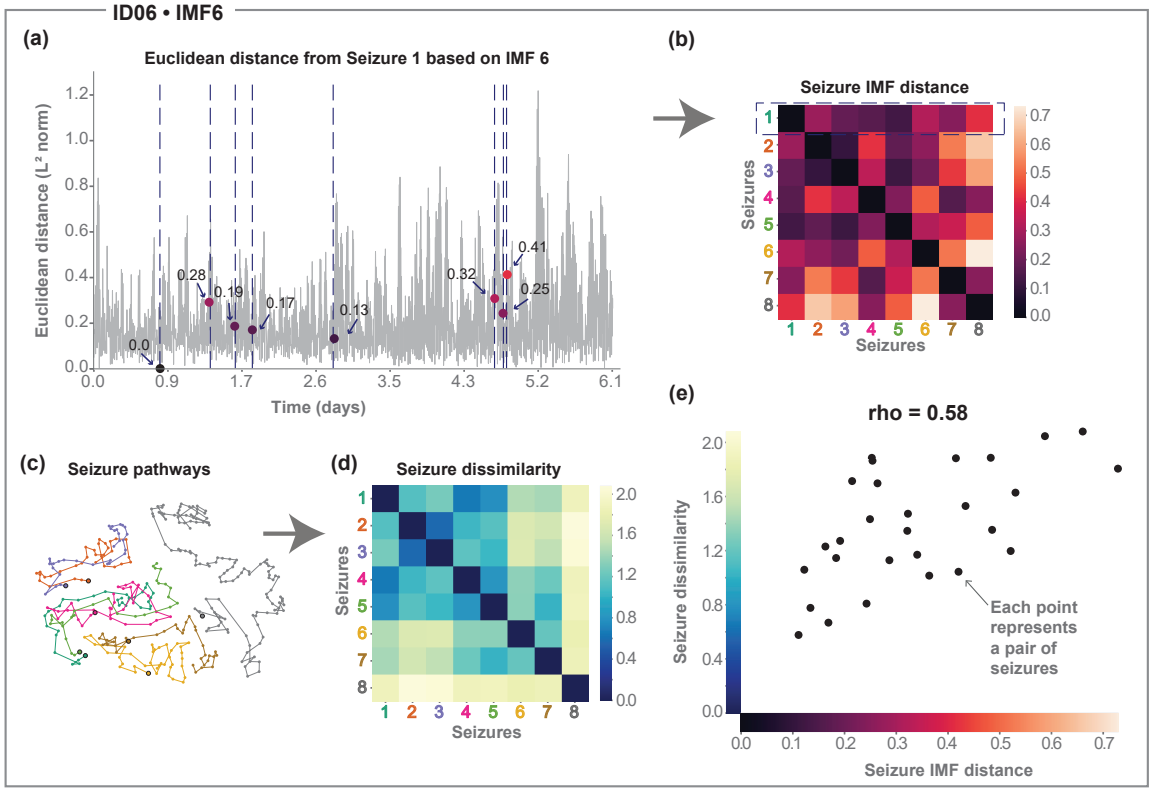

Figure 2.5 **Relating seizure dissimilarity and IMF seizure distance.** Throughout the figure we use example subject ID06 and IMF6. (a) Euclidean distance of all time points to the first seizure in terms of IMF6. Blue dashed vertical lines indicate seizure timing. Dots mark the value of the IMF distance to the first seizure and colours of dots correspond to the colour scale in (b). (b) Seizure IMF distance matrix for IMF6. The first row is a representation of the data in (a). (c) Visualising seizure evolutions as pathways (see Supplementary Section 2.5.2 and (Schroeder et al., 2020)). Seizures are displayed with distinct colours to distinguish seizure events. The starting points of seizures are marked with a black outline circle. In this projection, parts of seizures with similar network evolutions tend to be placed closer together, and seizures with similar evolutions will therefore approximately overlap (e.g., orange and purple pathways). (d) Seizure dissimilarity matrix, capturing the differences in seizure evolutions over time between each pair of seizures. (e) Scatter plot of seizure dissimilarity and the seizure IMF distance (Spearman's correlation, $\rho = 0.58$).

coefficients for example subject ID06 are shown in Fig. 2.6c. For this particular subject, the strongest explanatory effect (as measured by the standardised regression coefficients, also know as beta-weights) was seen in the EMD residue signal followed by some faster IMFs (IMF [**Cycle length**]: IMF3 [**4 min**], IMF4 [**7.5 min**], IMF5 [**15 min**]

and IMF6 [**26 min**]). According to the model, 67.42% of the variability in seizure dissimilarities was explained by explanatory variables (i.e. adjusted $R^2 = 0.6742$).

Across subjects, we fitted the multiple linear regression model only for subjects with at least six seizures, resulting in eight subjects with analysed seizure evolutions. Out of our cohort of eight subjects, six had an adjusted R^2 around or above 0.6 (Fig. 2.6d). Suppl. Fig. 2.9 additionally shows that the adjusted R^2 values would have not occurred by chance in any subject except for ID10. For six out of eight subjects, circadian IMFs were also part of the explanatory variables (Fig. 2.6d). Ultradian IMFs also tended to remain as explanatory variables in the models for all subjects. Temporal distance between seizures remained as an explanatory variable in three subjects, and the residue signal also remained as an explanatory variable in three additional subjects. Overall, a subject-specific combination of different fluctuations provided a good explanation of seizure variability in most subjects.

Note that band power fluctuations are not expected to trivially correlate with how seizures change, as (i) the seizure network evolution changes are detected on a finer timescale (seconds) using a functional network measure of the time series rather than a spectral property; (ii) seizure onset network patterns (as measured by functional networks) are also expected to differ substantially from pre-ictal network patterns (Shah et al., 2019); (iii) the impact of seizures on the band power fluctuation are most likely to be limited to one or few 30 s windows and hence also likely to be limited to the fastest IMF only. In Suppl. Section 2.5.3 we show that the band power without being decomposed into different timescales does not explain how seizures change, indicating that our results did not arise from trivial associations between seizure evolutions and their corresponding interictal periods. In Suppl. Section 2.5.8 we also reproduced our results using the pre-ictal (one 30 s window ahead of the seizure) band power fluctuations, which were not impacted by seizure evolutions.

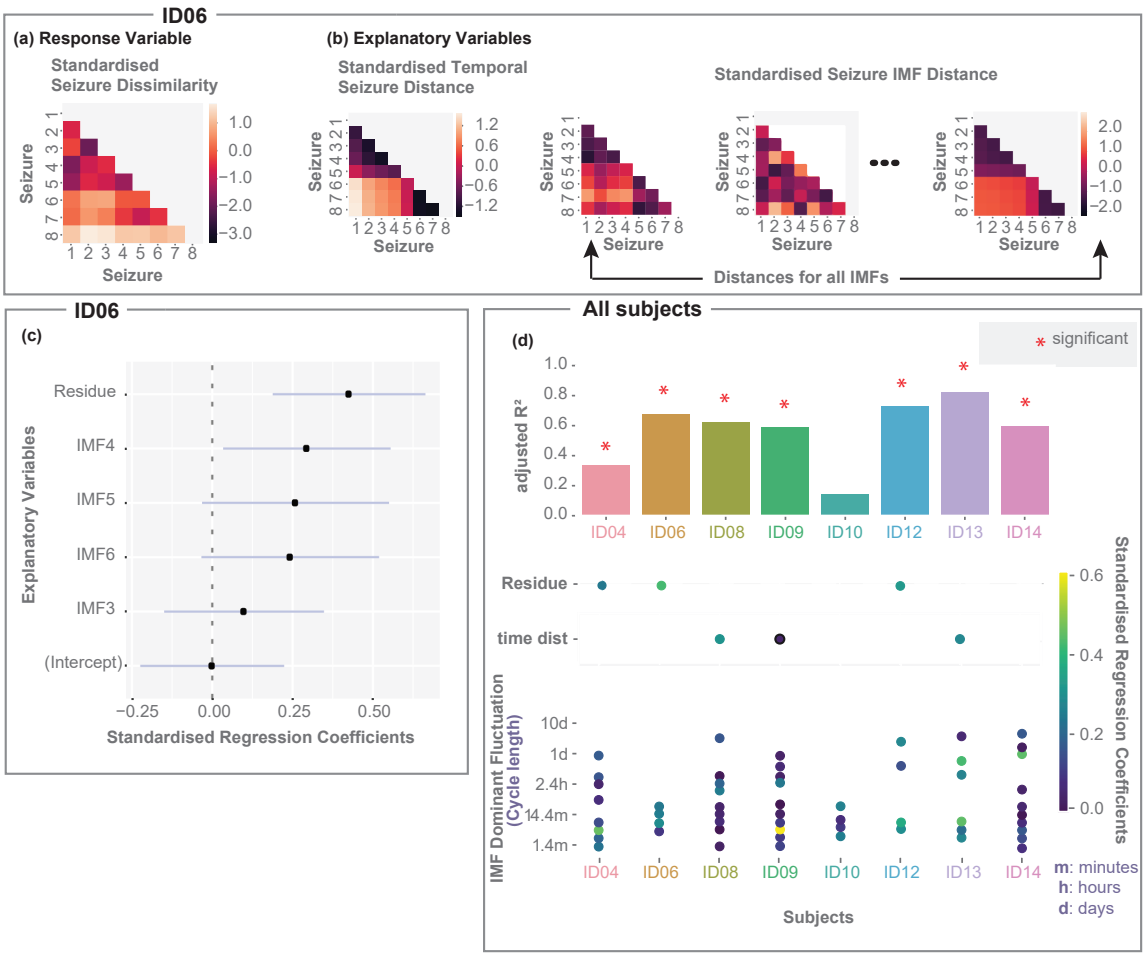

Figure 2.6 **A combination of IMF seizure distances on different timescales can explain seizure dissimilarity in most subjects in a multiple regression model.** (a) Standardised seizure dissimilarity matrix (response variable). Only the lower triangle of the symmetric matrix is shown, where each entry serves as an observation. (b) Explanatory variables: The matrix on the left shows the standardised temporal seizure distance. Each entry corresponds to the absolute time difference between seizures. The remaining matrices are standardised seizure IMF distance matrices. (c) Coefficient estimates (black dots), based on ordinary least squares regression for subject ID06, with lines indicating 95% confidence intervals. Only five explanatory variables were left after performing variable selection based on constrained LASSO. (d) Summary across subjects based on Ordinary Least Squares (OLS) models with explanatory variables obtained by the constrained LASSO. Top: Bar chart of the adjusted R^2. Red stars indicate p-values ≤ 0.05. Bottom: Scatter plot indicating the OLS coefficient estimates for the residue, temporal distance (when these variables remained in the model), together with explanatory IMFs and their corresponding IMF peak frequency for each subject. For visualisation, we converted the peak frequency to cycle length.

2.4 Discussion

In this chapter, we analysed fluctuations in subject-specific iEEG band power patterns over time and found that these patterns fluctuate over a wide range of timescales (from minutes to days), including a strong circadian fluctuation in most patients. A subject-specific combination of these fluctuations provided a good explanation (adjusted $R^2 >= 0.6$) for how seizure EEG spatio-temporal evolutions change from one seizure to the next within the same subject. Based on these findings, we suggest that band power fluctuations in continuously recorded EEG may be a marker of modulators of seizure activity.

Fluctuations on various timescales of the continuous EEG have been reported in several studies using iEEG recordings. The prevalence of a strong circadian rhythm in EEG patterns has long been known (Scheich, 1969; Spencer et al., 2016; Smyk and van Luijtelaar, 2020; Cummings et al., 2000). Weaker ultradian (more than 1 cycle per day) rhythms have been reported in long-term EEG band power (Kaiser, 2008; Chapotot et al., 2000) and functional connectivity (Mitsis et al., 2020). Subject-specific multidien (multi-day, i.e. less than 1 cycle per day) rhythms have also been detected in, for example, the rate of interictal epileptiform activity (Baud et al., 2018; Karoly et al., 2016), and the variance and autocorrelation of EEG signals (Maturana et al., 2020). In agreement, we observed the circadian cycle in all subjects and additional fluctuations on ultradian and multidien timescales that were subject-specific.

These fluctuations of EEG features on different timescales most likely reflect biological processes. However, the mapping from EEG biomarkers to underlying time-varying processes is incomplete. Various hypotheses exist regarding the interpretation of these EEG fluctuations (Bernard, 2021; Karoly, Rao, Gregg, Worrell, Bernard, Cook and Baud, 2021; Rao et al., 2021), and their possible drivers (Badawy et al., 2012; Meisel et al., 2015; Karoly, Rao, Gregg, Worrell, Bernard, Cook and Baud, 2021; Payne et al., 2021; Rakers et al., 2017) include hormonal and metabolic cycles, changes in antiepileptic medications, and external influences such as the weather. In this work, we therefore took a subject-specific data-driven approach that allowed us to detect any prominent fluctuations, regardless of their subject-specific source. Future work will explore a wider range of EEG biomarkers and elucidate the exact mapping between different fluctua-

tions and the underlying physiological or pathological processes.

Additionally, we make two observations about band power fluctuations on different timescales. First, we saw that different frequency bands appeared to contribute a similar amount to the circadian fluctuation of iEEG band power, although subtle subject-specific patterns of contribution are also noted. However, our analysis was performed across all dimensions of our data. The different dimensions of the IMF can display phase and amplitude differences (see e.g. Fig. 2.3a), indicating that different circadian fluctuations (with different phases) exist in each subject, as has been reported before (Aeschbach et al., 1999). Future work may wish to investigate the frequency contributions to different dimensions of IMFs and also relate those IMFs to other physiological variables such as body temperature or plasma melatonin (Aeschbach et al., 1999).

The second observation is that slower fluctuations (multi-day fluctuations, and slow trends) tended to result from changes in subsets of channels, whereas faster (circadian and ultradian) fluctuations tended to arise as a more equal contribution from all channels. A limitation in our analysis is that iEEG provides limited spatial coverage and the electrode layout is patient-specific, making it difficult to compare patterns of band power fluctuations across subjects. To fully uncover the spatial and frequency band contributions to each dimension of each IMF, we suggest that future work should consider the spatial location of iEEG channels and perform an iterative combination of dimensionality reduction and empirical mode decomposition to find components and their contributions for each IMF. From a clinical perspective, information on the spatial coverage and location of the electrodes would further allow us to investigate the overlap of the location of these temporal fluctuations with the epileptogenic zone in focal epilepsies.

We applied empirical mode decomposition (EMD) to derive band power fluctuations on different timescales. EMD is a popular data-driven adaptive method with applications on a broad range of scientific topics, such as geology (Battista et al., 2007), hydrology (Hu and Si, 2013), and neuroscience (Huang et al., 2013; Rojas et al., 2013) amongst many others. It is suitable for extracting fluctuations on different timescales without assumptions of local stationarity, linearity, or specific basis functions, and for these reasons preferable for our application. Since EMD does not require a ba-

sis function to identify different timescales of fluctuations, it also does not generate harmonics (as in Fourier or Wavelet-type approaches) of fluctuations, making the decomposed cycles easier to interpret. However, EMD also has some limitations. Most notably, the IMFs' timescales of fluctuations may overlap, which is known as 'mode mixing' (Ur Rehman and Mandic, 2011). EMD may also struggle to distinguish two distinct fluctuations that have very similar periods, and they may be merged into one IMF. Ongoing developments (Xue et al., 2015; Deering and Kaiser, 2005; Li et al., 2015) in this area may overcome these limitations. Future work should explore how to capture non-stationary (Kaplan et al., 2005), non-linear (Stam, 2005), and potentially hierarchical (Vidaurre et al., 2017) time-varying properties of the continuously recorded EEG.

Our main goal was to investigate whether there is an association between variability in seizure evolutions and fluctuations in long-term iEEG band power. Changes in seizure evolutions can be quantitatively described using seizure dissimilarity, which captures how different any pair of seizures are in a given subject in terms of their seizure network evolutions (Schroeder et al., 2020). Previous work has also shown that fluctuations in seizure evolutions were well-explained by processes incorporating Gaussian noise, circadian, and/or slower timescales of changes in most subjects (Schroeder et al., 2020). In agreement with this work, we found that circadian or multidien fluctuations contributed strongly in most subjects in explaining seizure dissimilarity. In three subjects (ID04, ID06, ID12), the residue signal also contributed to the explanation, indicating that fluctuations on longer periods than the recording durations also played a role. Interestingly, we also found many faster (ultradian) fluctuations as explanatory variables in most subjects. These fluctuations could be contributing explanatory power through what previously was modelled as noise (Schroeder et al., 2020). However, there may also be a true biological fluctuation underpinning the explanation; faster fluctuations in the EEG have also been reported, for example in the cyclic alternating pattern (Parrino et al., 2014). With larger datasets using more seizures recorded over a longer period, future work should investigate ultradian contributions carefully and assess whether noise would perform as well as the cumulative ultradian contributions.

While fluctuations in long-term iEEG band power can explain seizure dissimilarity fairly well, this association should not be interpreted as causal evidence. The observed

band power fluctuations can be understood as signatures of multiple biological processes, which could directly dictate seizure evolutions or be co-modulated by the same upstream processes as the seizure evolutions. Our data cannot distinguish these cases. Additional fluctuations that are not captured by iEEG band power may also explain changes in seizure evolutions, and a more detailed analysis of the exact fluctuations and the differences in specific seizure features may be more informative. Interestingly, band power fluctuations did not account for all the seizure variability in most subjects. The highest adjusted R^2 was around 0.8 and the unexplained variability based on the models suggests that there are additional factors, or possibly a level of stochasticity, that impact seizure evolutions. Nevertheless, to make our findings clinically useful, for example as a predictive model of upcoming seizure evolutions or seizure severity, neither causality nor completeness of the predictors is required. Our results indicate that a predictive model of seizure evolutions is possible with continuously recorded features such as iEEG band power, and this model should achieve good predictive performance in the majority of subjects.

To improve predictive performance, other factors could be considered in future, e.g. the anti-epileptic drug (AED) level at any given time or additional EEG features. Specifically, it is well-known that AED changes and withdrawal can change the severity and evolutions of seizures. For example, bilateral tonic-clonic seizures are more prevalent when AED levels are reduced (Pensel et al., 2020). AEDs have further been shown to impact inter- and peri-ictal brain activity (Badawy et al., 2009; Meisel et al., 2015), making it an important feature to consider. In this study, we did not incorporate information regarding drug doses, but future studies may wish to investigate how AED levels impact iEEG band power (Arzy et al., 2010), in combination with their potential explanatory power for seizure evolution changes. However, it is unlikely that AEDs are the sole driver of changing seizure characteristics, such as seizure occurrence (Karoly, Freestone, Eden, Stirling, Li, Vianna, Maturana, D'Souza, Cook, Richardson, Brinkmann and Nurse, 2021) and seizure evolution (Schroeder et al., 2020). Notably, prior studies on canine epilepsy showed that various seizure cycles (circadian, weekly and monthly) exist even in the absence of anti-epileptic medication (Gregg et al., 2020). In future work, incorporating personalised medication records could unravel the behaviour of seizure rhythms with respect to changes in drugs and/or doses. Any multi-

way association between continuously recorded brain activity, seizure evolutions, and treatments (such as AEDs) has the potential to introduce entirely new treatment strategies. If, for example, particular interictal EEG signatures predict more severe seizures, and these signatures are also influenced by AED dose, then one can hypothesise that responsively adapting AED dose according to these interictal signatures might decrease seizure severity. If this hypothesis can be verified, then on-demand drug-delivery systems programmed to respond to patient-specific interictal signatures could become the next generation of epilepsy treatments (Carney et al., 2014; Manganaro et al., 2017; Ramgopal et al., 2013).

In a more general context, our work is another contribution to the wider literature of explaining ictal features from interictal EEG features or hypothesised circadian/multidien rhythms. For example, studies have established that there is often a subject-specific relationship between fluctuations of interictal EEG features and the timing of ictal events (Baud et al., 2018; Karoly et al., 2016; Mitsis et al., 2020; Maturana et al., 2020; Leguia et al., 2021). Interestingly, we found no evidence of an association between band power fluctuations of the interictal EEG and seizure occurrence (data not shown). Seizures were not more likely to occur during particular phases of particular IMFs in most subjects in our data set. This finding is in agreement with a previous study (Mitsis et al., 2020) that reported functional network fluctuations, rather than band power fluctuations, to be more predictive of seizure timing. Future work should investigate temporal fluctuations in a range of EEG features, such as band power (Cummings et al., 2000), functional connectivity (Mitsis et al., 2020), high frequency oscillations (Gliske et al., 2018), variance, and autocorrelation (Maturana et al., 2020). Apart from seizure timing, our work has shown that band power fluctuations on different timescales also explain changes in seizure evolutions. Future work should explore this avenue further to illuminate the exact processes and timescales that modulate or dictate the various aspects of a seizure.

Finally, our study contributes to the growing literature of alternative treatment approaches in epilepsy that predict and react to the temporal changes of the disease. Most prominently, predicting when seizures happen has been an active and re-invigorated area of research for many years (Karoly et al., 2017; Cook et al., 2013; Freestone et al., 2017; Stirling et al., 2021). Our work further contributes to being able to predict seizure dy-

namics and evolutions and thus also seizure severity and symptoms. Additionally, the aforementioned (slow) fluctuations in EEG features we and others investigate may also serve as biomarkers that can track treatment response, and therefore open the gateway to on-demand treatment options (Karoly, Rao, Gregg, Worrell, Bernard, Cook and Baud, 2021; Bernard, 2021; Carney et al., 2014; Leite Góes Gitai et al., 2019; Potruch et al., 2020; Ramgopal et al., 2013). The association we investigated between how seizures change and slow fluctuations in EEG features therefore serves as a vital link to make the leap between treatment outcome (improved seizure symptoms/severity) and the given intervention that can be tracked with slow fluctuations in EEG features.

In conclusion, fluctuating interictal EEG features may not only correlate with clinical seizure timing, but also with seizure evolutions on multidien, circadian, and ultradian timescales. In the future, it may be possible to use these temporal patterns of EEG fluctuations to predict seizure evolutions. Prediction of various seizure features, including seizure evolution and seizure severity is a critical unmet need for people with epilepsy. If successful, this improved forecasting approach would open up new opportunities for therapeutics and maximising quality of life.

2.5 Supplementary

2.5.1 Subject data information

Subject	Duration in hours	Duration in days	Number of seizures	Mean seizure duration (minutes)
ID01	293	12	2	10.030
ID02	235	10	2	1.468
ID03	158	7	4	1.078
ID04	41	2	14	0.699
ID05	109	5	4	0.278
ID06	146	6	8	0.765
ID07	69	3	4	1.159
ID08	144	6	70	0.366
ID09	41	2	27	0.706
ID10	42	2	17	1.181
ID11	212	9	2	1.526
ID12	191	8	9	2.441
ID13	104	4	7	1.717
ID14	161	7	60	0.430
ID15	196	8	2	1.576
ID16	177	7	5	3.174
ID17	130	5	2	1.632
ID18	205	9	5	3.319
Total	2656	111	244	
Average				1.864

Table 2.1 For each subject the following information is provided: **Duration in hours:** duration of iEEG recordings in hours. **Duration in days:** duration of iEEG recordings in days. **Number of seizures:** number of subject's seizures annotated. **Mean seizure duration:** mean seizure duration across all annotated seizures in minutes.

2.5.2 Visualising seizure dissimilarity

The iEEG traces of all seizures for subject ID06 are shown in Suppl. Fig. 2.7 a for visual comparison of the different seizures and the quantified seizure evolution differences displayed as trajectories (Suppl. Fig. 2.7b) along with the dissimilarity values

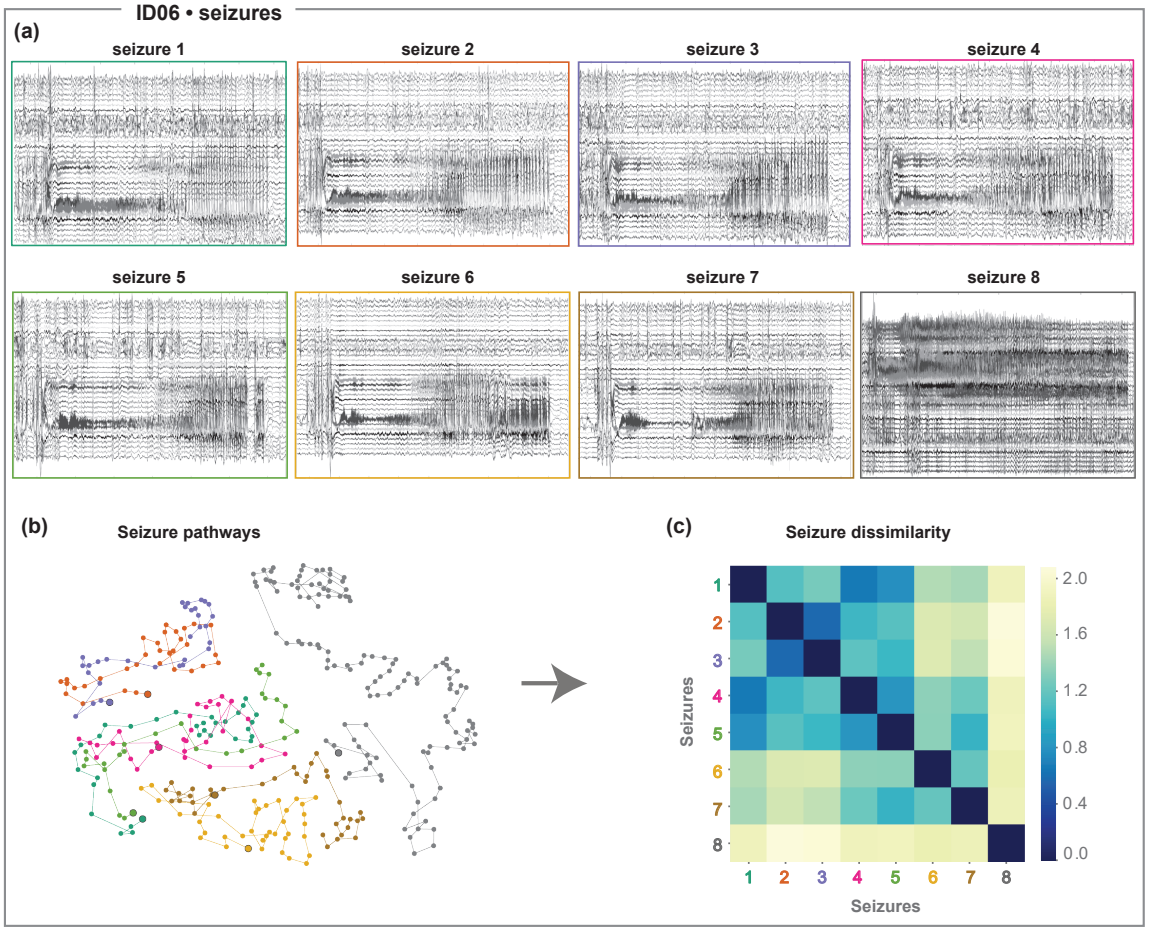

Figure 2.7 **Seizure dissimilarity matrix for example subject ID06.** (a) Seizure iEEG traces are shown in the top panel of the figure. (b) Functional network evolution of all seizures projected into 2D space using multi-dimensional scaling (MDS) for visualisation of seizure pathways (see (Schroeder et al., 2020) for details). Similar seizures tend to be placed closer together in this projection. Seizures are displayed with distinct colours to distinguish seizure events. The starting points of seizures are marked with a black outline circle. (c) Seizure dissimilarity matrix, capturing the differences in seizure pathways between each pair of seizures.

(Suppl. Fig. 2.7c) for each pair of seizures. The bottom panel of the figure is similar to Fig. 2.5a,b.

2.5.3 Association between seizure dissimilarity and seizure band power distance

Here, we want to demonstrate that the band power signal itself does not explain how seizure pathways change, or at least not as well as specific fluctuations of bandpower on particular timescales (as we presented in the main results). To this end, we associated each subject's pathway dissimilarity matrix with differences in the raw band power signal (termed band power distance from now on).

In order to explore whether band power distance explains seizure dissimilarity, we applied a linear regression framework. We implemented two models: (i) using the seizure onset time window and (ii) using the time window just before the seizure onset (onset window - 1).

For consistency with the main part of our analysis (see Fig. 2.5a,b) and to allow comparison with findings in Fig. 2.6, a pairwise band power distance was obtained as the euclidean distance from the data matrix X shown in Fig. 2.1b. In other words, the band power distance is the euclidean distance between two time windows in terms of their band power in all frequency bands and channels.

As can be seen in Suppl. Fig. 2.8, the low values of adjusted R^2 across all subjects indicate the band power signal itself does not explain how seizures change over time. Instead the decomposition of the band power signal into fluctuations of particular timescales is crucial, and only some of these timescales contribute explanatory power, as we have shown in Fig. 2.6.

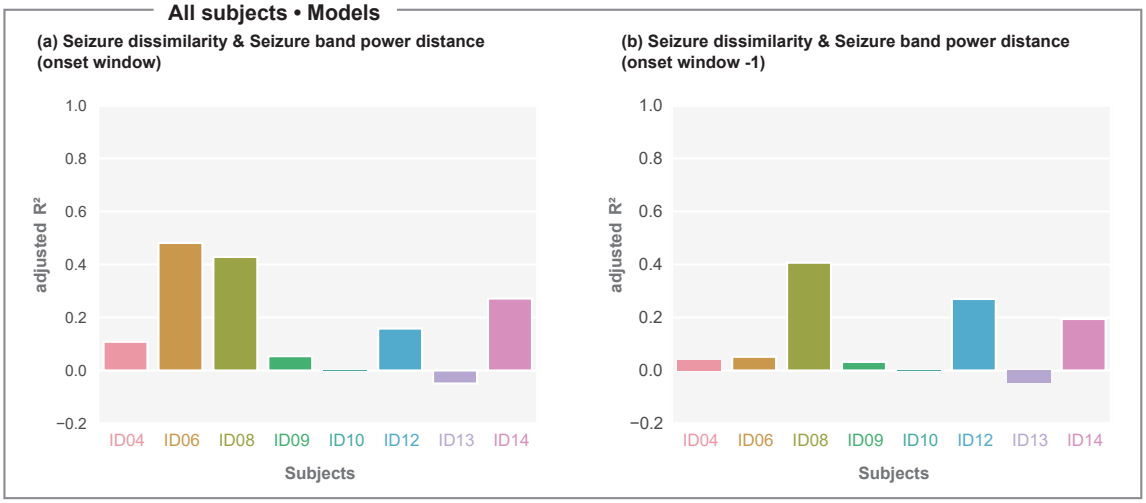

Figure 2.8 **Relating seizure dissimilarity with seizure band power distance.** (a) and (b) Summary across subjects represented with bar charts of the adjusted R^2 values obtained from the linear models using the onset window (Left plot: (a)) and the onset window -1 (Right plot: (b)).

2.5.4 Tests for statistical significance in model R^2

Randomly shifted onset times

We randomly shifted seizure onset times to test whether the multiple linear regression model R^2 values would have occurred by chance. Adjusted R^2 values for 500 iterations, along with the actual adjusted R^2 are shown in Suppl. Fig. 2.9.

Randomly permuted onset times

Similarly to the analysis described in the previous section, we additionally performed a permutation test. In each permutation iteration, we first randomly permuted the order of the seizures (but not their timing). Then, we obtained new IMF seizure distance matrices and performed the LASSO and linear regression, exactly as described in Section 2.2.12, leaving the response variable unchanged. Finally, we calculated the adjusted R^2 for each iteration (see Suppl. Fig. 2.10). Statistical significance was determined based on a significance level of 5%. Again, the aforementioned steps were performed for all subjects with at least six recorded seizures. Significance levels were

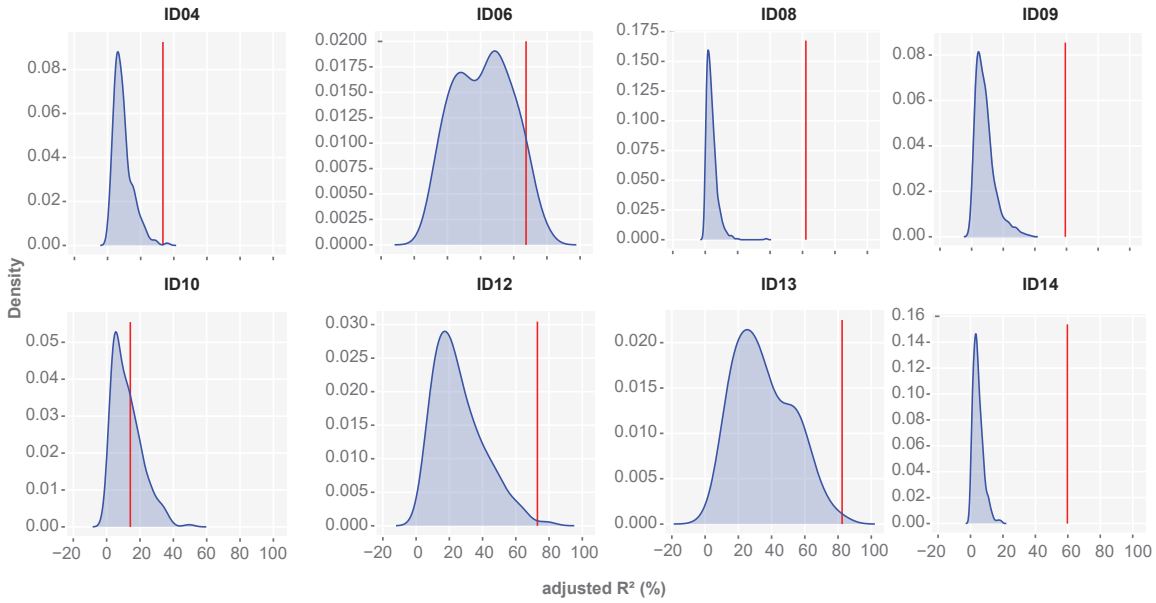

Figure 2.9 **Distribution of the adjusted R^2 values using random seizure timings, after implementing the positive LASSO and OLS regression model for each subject.** The seizure dissimilarity matrix was used as response variable, while the seizure IMF distance matrices for the random seizure times and the seizure temporal distance were included in the model as explanatory variables. The vertical red line represents the adjusted R^2 for the same analysis performed on the original seizure onset times (see Section 2.2.12 and Fig. 2.6d).

similar for all tested subjects as in the previous section.

2.5.5 Gini index for frequency bands θ, α, β and γ

As described in Section 2.2.9, we obtained the Gini index for the frequency bands: θ, α, β and γ (see Suppl. Fig. 2.11) in the same way as for δ band (Fig. 2.4).

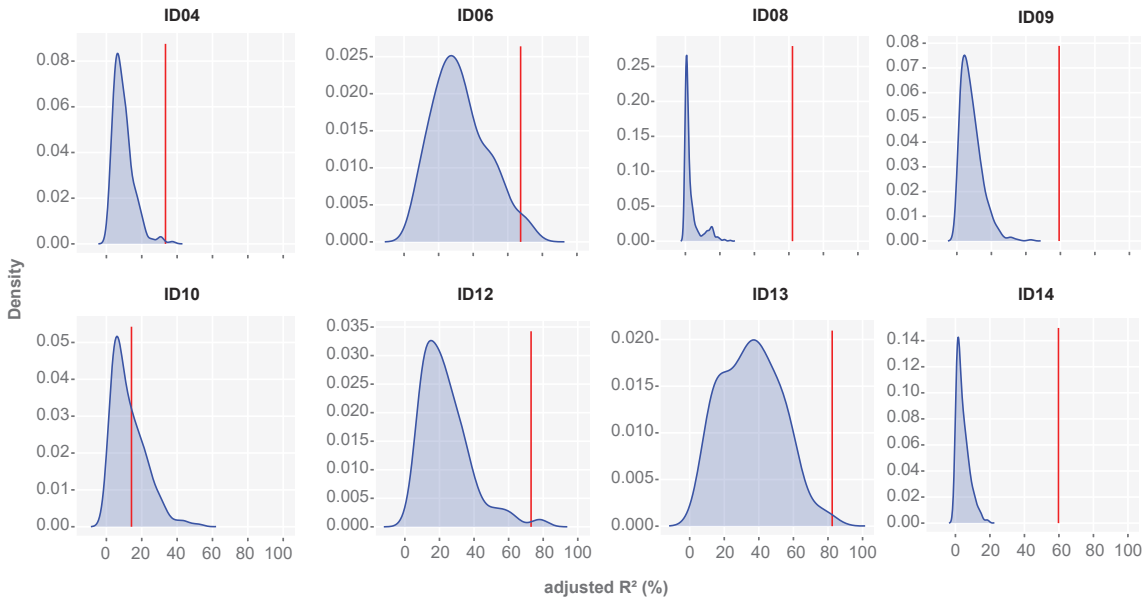

Figure 2.10 **Distribution of the adjusted R^2 values using permuted seizure orders.** The seizure dissimilarity matrix was used as response variable, while the seizure IMF distance matrices for the random seizures and the seizure temporal distance were included in the model as explanatory variables. The vertical red line represents the adjusted R^2 for the same analysis performed on the original seizure order (see Section 2.2.12 and Fig. 2.6d).

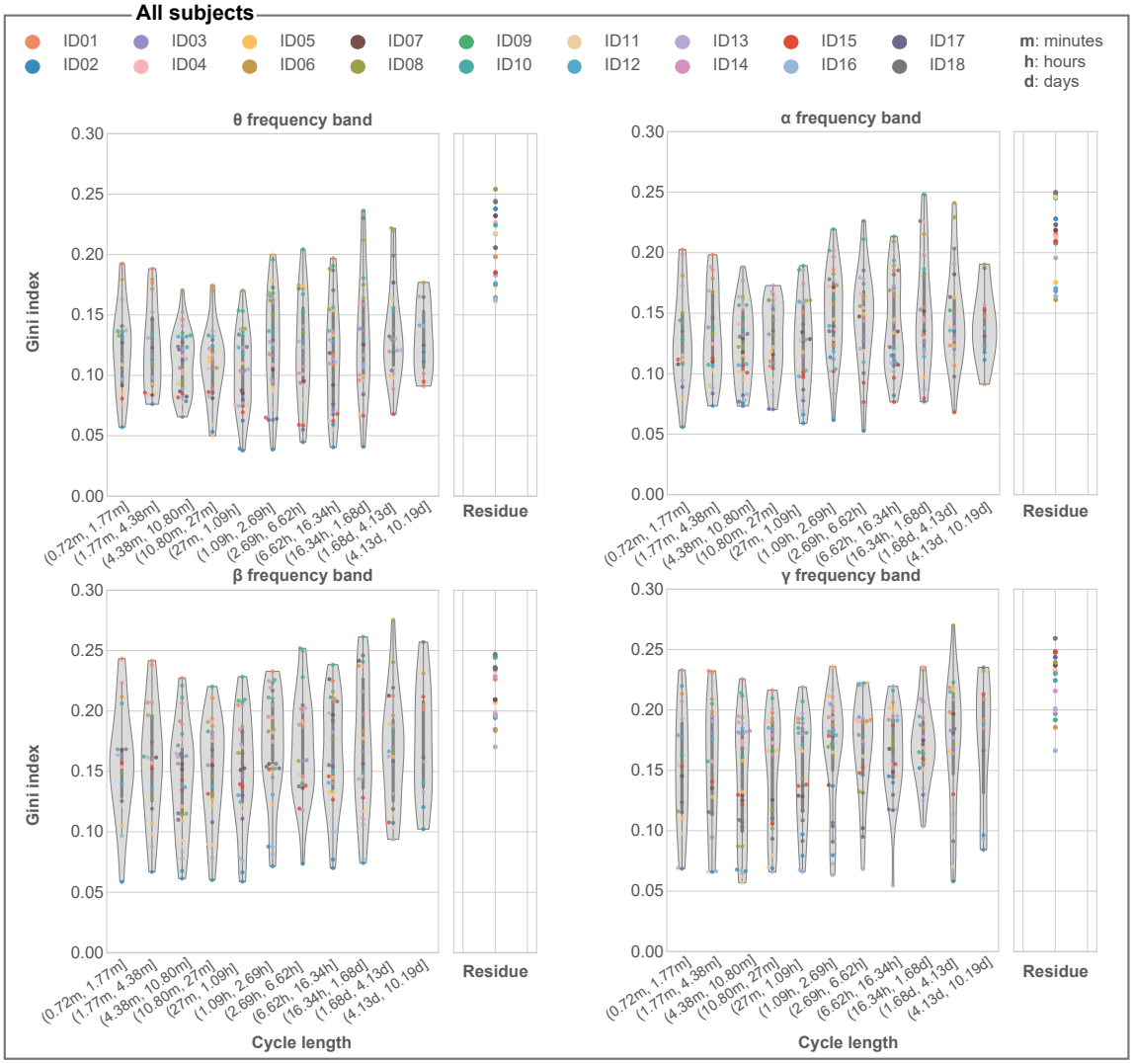

Figure 2.11 **Supporting Gini Index results for the θ, α, β and γ frequency bands across all subjects.** Equivalent figure to Fig. 2.4

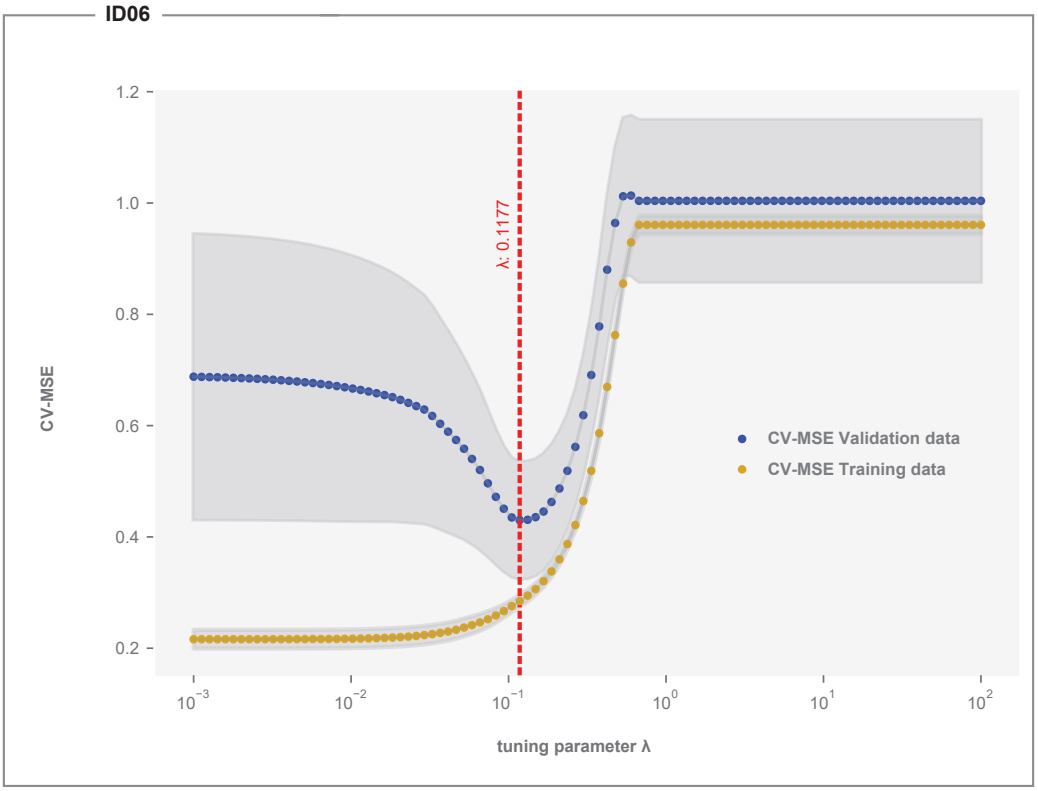

Figure 2.12 **Cross-validation MSEs for the application of positive LASSO regression for example subject ID06.** For each value of the tuning parameter λ, the CV-MSEs across the 10 folds are displayed in blue along with error bars which cover the mean plus or minus one standard error. Training MSE is displayed in yellow. The red vertical line represents the selected λ value that corresponds to the minimum Cross-Validation MSE for the validated data set.

2.5.6 Choice of tuning parameter λ for LASSO

Supplementary Figures 2.12 and 2.13 are complementary plots supporting the intermediate steps of the analysis described in Section 2.2.12. We implemented a 10-fold cross validation for choosing the best λ parameter in LASSO. We chose a λ that minimised the Cross-Validation Mean Square Error (CV-MSE) for the validated data set. The CV-MSE error for the training data set is also presented in Suppl. Fig. 2.12 for reference for one example subject, ID06.

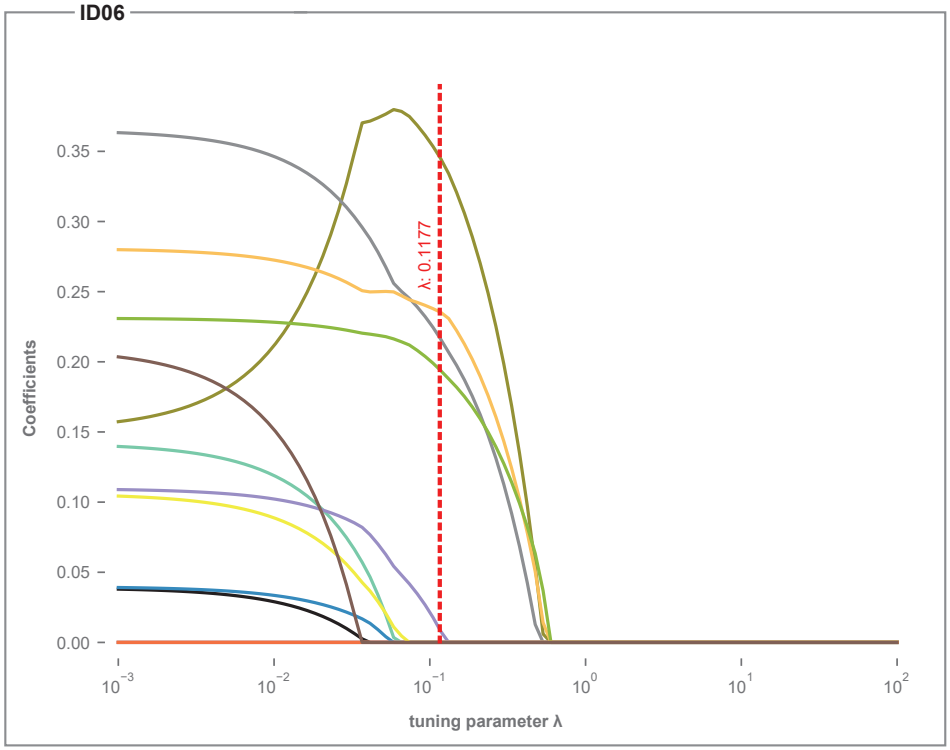

Figure 2.13 **The effect of the tuning parameter λ on positive LASSO regression coefficients for subject ID06.** Each line represents the regression coefficient estimate for each explanatory variable. The red vertical line corresponds to the λ parameter selected based on 10-fold cross validation approach.

2.5.7 Determining which IMF fluctuations overlap with noise

In order to evaluate whether each of the IMFs is a good representation of fluctuations present in the data, we implemented an empirical analysis based on permutation resampling of the original time series (H expression coefficients). We used this nullmodel to produce distributions of IMF fluctuation frequencies that would be expected from noise. In our nullmodel, we assumed a permuted time series (permuting time points in H) to represent noise, i.e. we preserve the distribution of the values in the time series, but the temporal fluctuations are destroyed through the permutation.

We randomly shuffled the columns (timing) of the H matrix over 50 iterations and performed the MEMD analysis for each iteration. Then, for each IMF, in each iteration, we estimated the 2D distribution of the instantaneous frequency, and instantaneous amplitude (across all time points). We formed the average distribution across all iterations. We repeated the same analysis for the original (non-shuffled) data, for each IMF. Therefore we can calculate overlap in the distributions (between original and shuffled data).

We used a 2D grid of (frequency, amplitude) with 800 frequency bin between 10^{-3} and 10^{4} in logarithmic scale, and 400 amplitude bins between 10^{-4} and 10^{0} in logarithmic scale (logarithmic scales of base 10 were used). In each (frequency, amplitude) bin, where the original signal overlapped with the permuted signal, the corresponding data points were labelled as overlapping with noise. These points can subsequently be removed from the calculation of the marginal Hilbert-Huang spectra for the original signal. These newly obtained marginal Hilbert-Huang spectra, excluding data points overlapping with noise, are shown in red in Suppl. Figures 2.14 and 2.15.

In Supplementary Figures 2.14 and 2.15, we can clearly see that many frequencies of fluctuations in IMF1-3 are overlapping with noise in most subjects. The slower IMFs do not appear to be affected (as noise-IMF tend to decrease in amplitude for slower IMFs). While we could discard faster IMFs as noise due to the overlap, it is worth noting that these faster IMFs could carry some true fluctuation that is simply on the same timescale and of the same amplitude as the noise. This would be impossible to distinguish here, and therefore we present all results on all IMFs in the main text and will present supporting results with the faster IMFs removed in Suppl. Section 2.5.8.

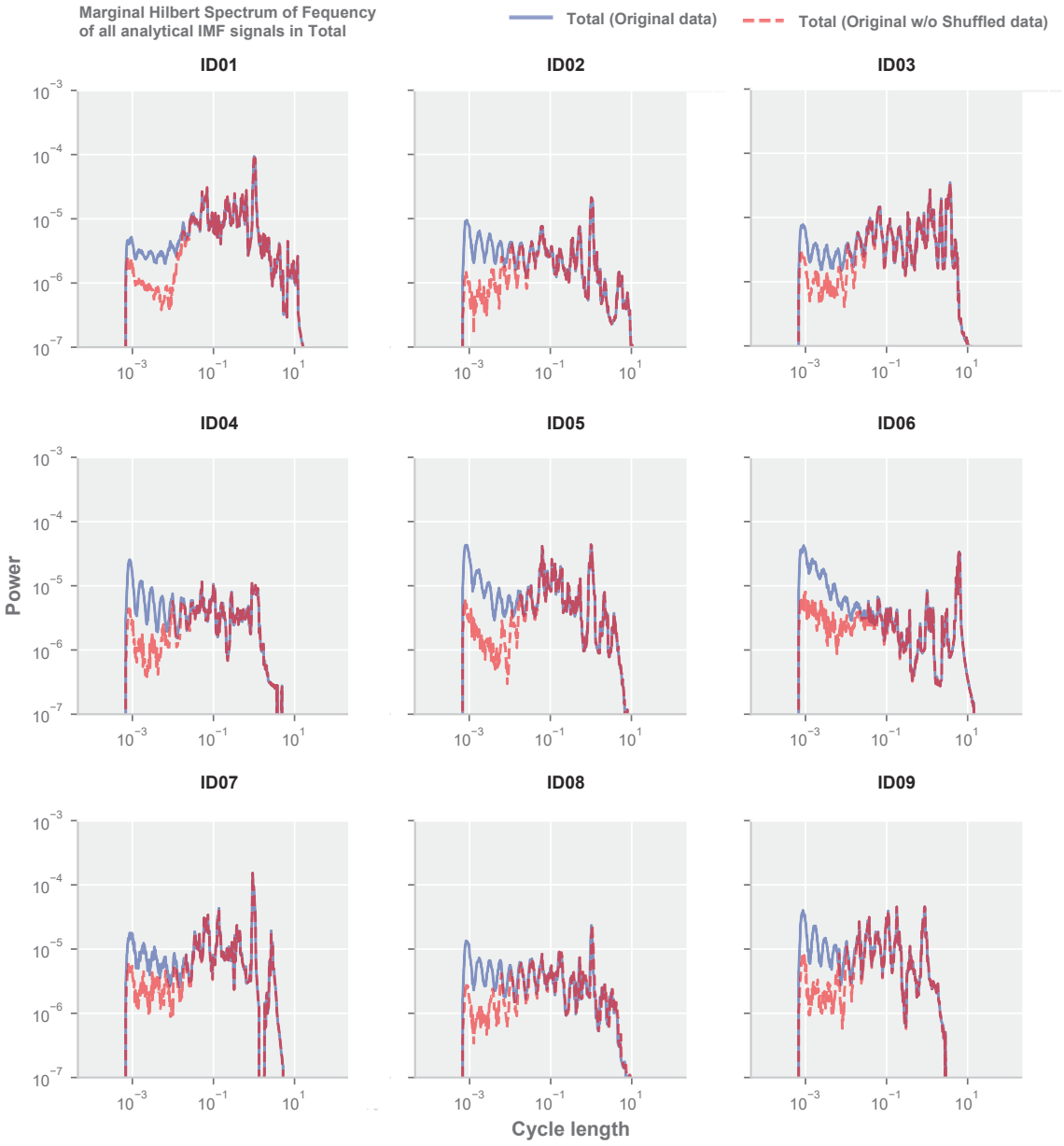

Figure 2.14 **Marginal Hilbert Spectrum for capturing the noisy IMF signals for subjects ID01-ID09.** Marginal Hilbert spectrum of frequency for all analytical IMF signals across all dimensions for both the original data (blue line) and after excluding frequency-amplitude data points overlapping with noise (red line). Each panel corresponds to one subject.

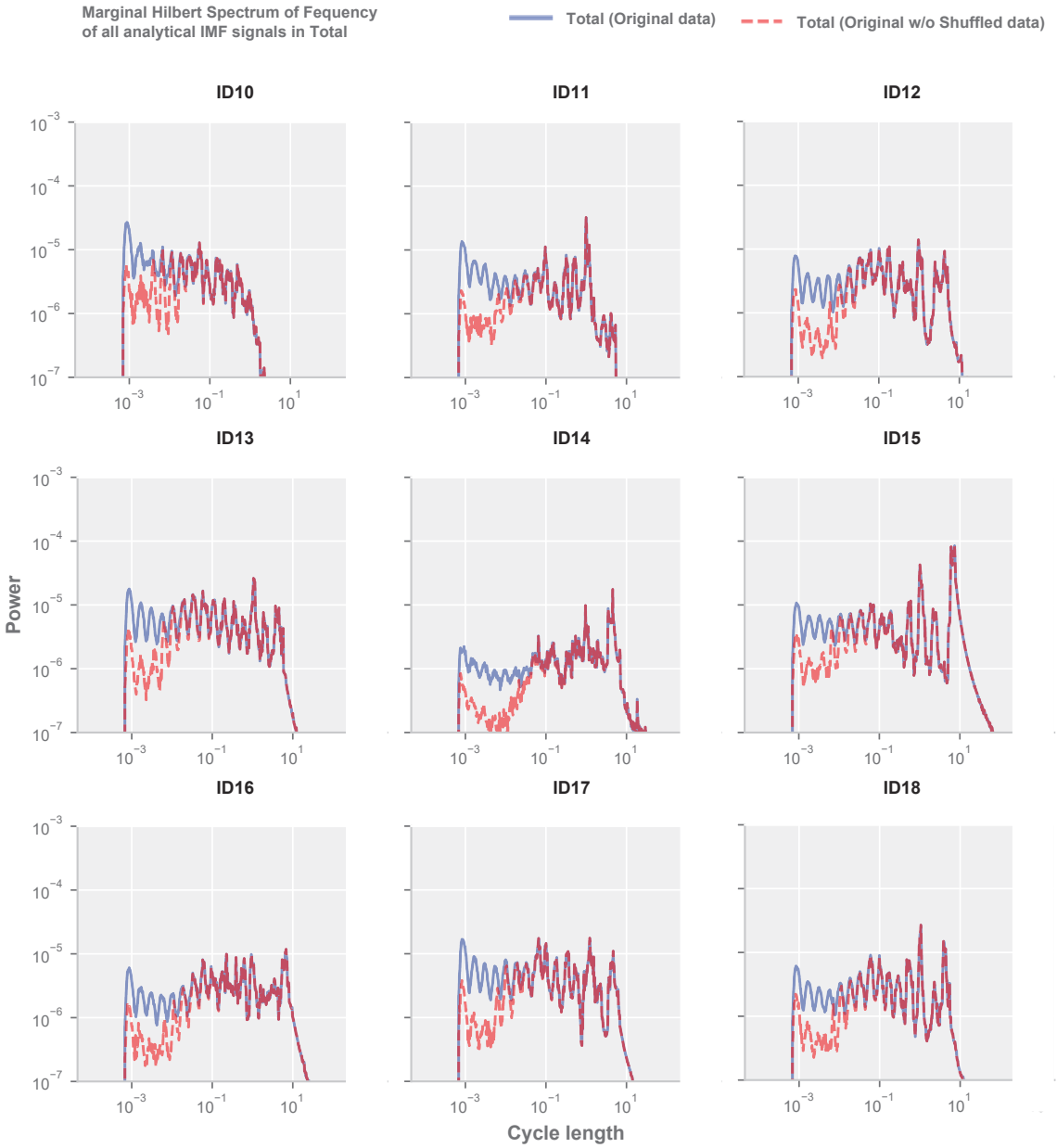

Figure 2.15 **Marginal Hilbert Spectrum for capturing the noisy IMF signals for subjects ID10-ID18.** Continued: Marginal Hilbert spectrum of frequency for all analytical IMF signals across all dimensions for both the original data (blue line) and after excluding frequency-amplitude data points overlapping with noise (red line). Each panel corresponds to one subject.

2.5.8 Alternative models for explaining the diversity in within-subject seizure evolutions

We tested additional models to see how well they explain seizure variability, using the same framework as is described in Section 2.2.12.

Association between seizure dissimilarity and IMF seizure distance based on the time window before the seizure

To further validate our model in terms of the time window chosen for obtaining the seizure IMF distances, we performed an additional analysis using one time window before the window containing the seizure onset (termed onset window-1). The reasoning is that the IMF distances obtained in this manner cannot contain any seizure-related changes in band power. As can be seen in Suppl. Fig. 2.16a and in the first two columns of the Suppl. Table 2.2, the adjusted R^2, as well as the coefficient estimates and the IMF components remaining in the model for each subject are in agreement with the model shown in Fig. 2.6d. Thus, both models perform similarly, indicating that the IMF distance results are robust towards changing a single window.

Association between seizure dissimilarity & IMF seizure distance excluding noise

We further performed the regression analysis in Section 2.2.12 excluding the first three IMFs, which could represent noise (Suppl. Section 2.5.7). As can be seen in Suppl. Fig. 2.16, the adjusted R^2 values for the majority of subjects were comparable for the two models (albeit generally slightly lower). Only for subject ID09, the adjusted R^2 was dramatically lower for the model without the first three IMFs (see Supplementary Table 2.2 and Suppl. Fig. 2.16b). Note also our Discussion on the role of the faster IMFs.

We also observed that the IMFs and corresponding coefficients were substantially different in ID04, ID09, and ID10 between the two models. This is not surprising given that both ID04 and ID10 had a low adjusted R^2 in the first place, and ID09 had a low adjusted R^2 in the model without the first IMFs. In summary, we conclude that the first three IMFs do not contribute substantially to explaining seizure dissimilarities

in most subjects. However, in some subjects, faster IMFs may play a strong role in explaining seizure dissimilarities.

subjects	**Seizure dissimilarity & IMF Seizure distance Adjusted R^2**		
	onset window	**onset window -1**	**onset window w/o noise**
ID04	0.3343	0.1545	0.0347
ID06	0.6742	0.5755	0.6787
ID08	0.6207	0.6279	0.6201
ID09	0.5927	0.5601	0.1865
ID10	0.1419	0.1949	0.0608
ID12	0.7299	0.6489	0.6529
ID13	0.8243	0.8060	0.7197
ID14	0.5973	0.5834	0.5306

Table 2.2 **Adjusted R^2 values for additional models.** Adjusted R^2 values for the models described in Section 2.2.12 and Supplementary Section 2.5.8 for each subject with at least six recorded seizures.

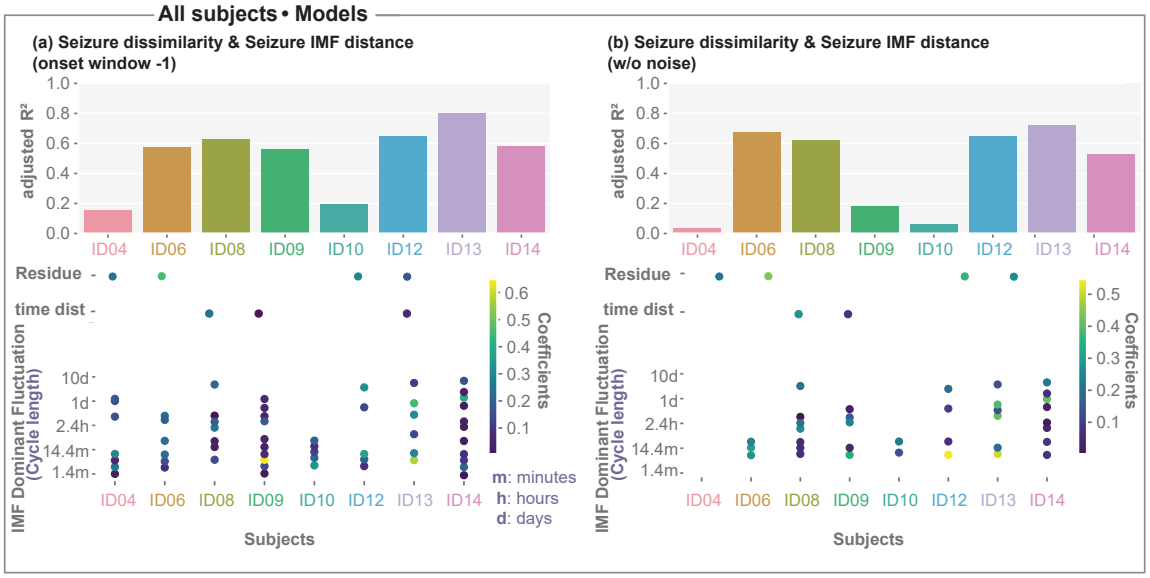

Figure 2.16 **Alternative models for explaining seizure variability within subjects**. (a) and (b) Summary across subjects based on OLS models with explanatory variables obtained by the constrained LASSO using similar representation as in Fig.2.6d for the models described in Supplementary Section 2.5.8. Top: Bar chart of the adjusted R^2. Bottom: Dot plot indicating the OLS coefficient estimates for the residue or time distance (when this variable remained in the model) together with OLS coefficient estimates at the corresponding value of IMF peak frequency for each subject. For visualisation, we converted the peak frequency to cycle length.

Chapter 3. Seizure Duration is Associated with Multiple Timescales in Interictal iEEG Band Power

Contents

3.1 Introduction

Seizure severity plays an important role in evaluating therapies for people with epilepsy by identifying which treatments reduce severity. Importantly as the severity of seizures naturally fluctuates over time (Lamberts et al., 2013; Jobst et al., 2001; Peng et al., 2017; Gascoigne et al., 2023), characterising or forecasting severity in real-time could improve treatment protocols or open new treatment avenues. Although multiple tools have been developed to retrospectively quantify seizure severity in individual people with epilepsy (Cramer and French, 2001; Todorova et al., 2013; Baker et al., 1991, 1998; Duncan and Sander, 1991; Gascoigne et al., 2023; Pattnaik et al., 2022), there is no established way to forecast seizure severity.

Forecasting seizure severity is challenging since seizure properties change over time within individual people with epilepsy (Karoly, Rao, Gregg, Worrell, Bernard, Cook and Baud, 2021; Schroeder et al., 2020; Panagiotopoulou et al., 2022). For example, onset locations (Gliske et al., 2018), propagation patterns (Karthick et al., 2018), network evolutions (Schroeder et al., 2020; Panagiotopoulou et al., 2022; Mitsis et al., 2020), durations (Cook et al., 2016; Schroeder, Chowdhury, Cook, Diehl, Duncan, Karoly, Taylor and Wang, 2022), onset times (Karoly, Rao, Gregg, Worrell, Bernard, Cook and Baud, 2021; Baud et al., 2018), and patterns of electrographic epileptiform activity (Ilyas et al., 2022) can differ from one seizure to the next. Importantly, seizures with more severe symptoms, such as focal to bilateral tonic clonic (FTBTC) seizures, are more likely to occur at certain times during sleep/wake or day/night cycles (Bazil and Walczak, 1997; Loddenkemper, Vendrame, Zarowski, Gregas, Alexopoulos, Wyllie and Kothare, 2011; Sinha, 2006; Lamberts et al., 2013; Jobst et al., 2001; Peng et al., 2017). These findings suggest that seizure properties, including severity, are modulated over short (minutes, hours, and days) and long (weeks, months, and years) timescales (Karoly, Rao, Gregg, Worrell, Bernard, Cook and Baud, 2021; Schroeder et al., 2020; Baud et al., 2018). Previous studies have not systematically investigated potential cyclical modulators of seizure severity.

Cycles in interictal activity could be a biomarker of severity-modulating cycles. Interictal iEEG markers showed prominent cyclical patterns over circadian (Panagiotopoulou et al., 2022; Mitsis et al., 2020; Karoly et al., 2016, 2017; Karoly, Golden-

holz, Freestone, Moss, Grayden, Theodore and Cook, 2018; Spencer et al., 2016; Karoly, Rao, Gregg, Worrell, Bernard, Cook and Baud, 2021) and multi-day (Baud et al., 2018, 2019; Karoly et al., 2016; Karoly, Rao, Gregg, Worrell, Bernard, Cook and Baud, 2021) timescales that appear to influence seizure properties, such as seizure evolution (Panagiotopoulou et al., 2022; Schroeder et al., 2020). It is likely that interictal EEG features and seizures are modulated by common biological factors that cyclically fluctuate over different timescales. As such, cycles of interictal features are a potential biomarker for seizure properties.

In this chapter, we investigate whether seizure severity can be predicted based on interictal features. We use seizure duration as a proxy for seizure severity due to association of seizure duration with clinical seizure types and severity symptoms (Dobesberger et al., 2015; Jenssen et al., 2006; Afra et al., 2008; Kim et al., 2011; Kaufmann et al., 2020; Ferastraoaru et al., 2016). We analysed changes in seizure duration, and their association with EEG band power fluctuation cycles within subjects. We first examined the association between seizure duration and each band power cycle using correlation metrics. We then assessed the relationship between seizure duration and a combination of band power cycles using a multiple regression framework. Our results demonstrate the relationship between interictal iEEG band power cycles and seizure duration which could provide new opportunities for forecasting seizure severity in the future.

3.2 Methods

3.2.1 Patient cohort and data acquisition

For this study, we analysed iEEG data collected during the presurgical evaluation from 20 adult subjects with refractory focal epilepsy. We used subjects with at least 15 annotated seizures. Data were obtained from the University College London Hospital (UCLH) (13 subjects), the NHS Greater Glasgow and Clyde center (GGC) (three subjects), as well as the Sleep-Wake-Epilepsy-Center (SWEC) at the University Hospital of Bern, Department of Neurology (four subjects) (available at http://ieeg-swez.ethz.ch) (Burrello et al., 2019). For all subjects, seizures were annotated by clinicians, independently of this study. Seizure durations were measured in seconds, and for analysis

converted into log seizure duration using the natural logarithm (Schroeder, Chowdhury, Cook, Diehl, Duncan, Karoly, Taylor and Wang, 2022; Cook et al., 2016). Demographic details are given in Supplementary Table 3.1.

3.2.2 iEEG preprocessing and band power computation

The iEEG signals from the SWEC cohort were provided in already preprocessed form. Briefly, signals were median-referenced and band-pass filtered from $0.5-120$ Hz using a 4^{th} order Butterworth filter (forward and backward). Channels with artifacts were also identified and excluded by the same epileptologist. These steps were all conducted independently of this study and resulted in the publicly available data and annotations (Burrello et al., 2019).

For the UCLH and GGC cohorts, we applied similar pre-processing steps before computing the iEEG features of interest. We divided each subject's long-term iEEG data into 30 s non-overlapping time segments. All channels in each time segment were re-referenced to a common average references. Within each time segment channels that appeared to have outlier amplitude ranges were denoted as noisy and disregarded from the common average calculation. To remove power line noise, each time segment was notch filtered at 50 Hz and 100 Hz. Finally, segments were band-pass filtered from $0.5-120$ Hz (UCLH cohort) or $0.5-110$ Hz (GGC Cohort) using a 4^{th} order zero-phase Butterworth filter (second order forward and backward filter applied).

For each subject within the SWEC, UCLH, and GGC cohorts, we processed their entire iEEG recording. We extracted iEEG band power from 30 s non-overlapping iEEG segments in five main frequency bands ($\delta:\ 1-4$ Hz, $\theta:\ 4-8$ Hz, $\alpha:\ 8-13$ Hz, $\beta:\ 13-30$ Hz and $\gamma:\ 30-80$ Hz) based on Welch's method with 3 s non-overlapping windows. Missing data were tolerated if one contiguous at least 15 s long segment was available. If missing data were present for one time segment, we applied all processing steps and computed the band power to the non-missing part of this segment.

For each frequency band, extracted continuous band power values were log transformed (natural logarithm), standardised and summarised across all channels by their median. This step resulted in a matrix A for each subject with five rows (number of frequency bands) and number of columns equal to the total number of 30 s time segments in the entire recording. Missing data in A were imputed (see Supplementary

Section 3.5.1) to enable extraction of band power cycles on different timescales in the data. Imputed data were not used for later analysis as seizure data were not available in missing periods.

3.2.3 Delineating iEEG band power cycles using MEMD

To extract oscillatory modes embedded in band power, we applied a signal decomposition method called Empirical Mode Decomposition (EMD) (Huang et al., 1998, 2003) that does not require any assumption about stationarity or signal outputs from a linear process. EMD captures a finite number, M of narrow-band modes, known as intrinsic mode functions (IMFs), based on the local minima and maxima of the signal. Here the input signal is represented by $Y(t) = \sum_{i=1}^{M} \text{IMF}_i(t) + r(t)$, where $r(t)$ is the residue signal (Huang et al., 1998). The IMFs are limited to a narrow-band frequency and have a local mean of zero, therefore satisfying the properties needed for Hilbert-transform. Hilbert analysis can be applied to each IMF yielded instantaneous phase (see Supplementary Section 3.5.3). As our input matrix A was multidimensional, we applied a multivariate version of EMD, which results in multidimensional IMFs that have the same five dimensions as A (see Supplementary Section 3.5.2). Following the same logic as in the univariate case of EMD (MEMD), each mutlidimensional IMF will reflect a frequency-range related mode across all dimensions (frequency bands).

Cycles refer to oscillations with a very narrow band frequency representation, whereas fluctuations indicate signals with more variability in their frequency. IMFs are usually narrow-band signals, but due to challenges in the signal, mode mixing may occur in some instances and multiple frequencies may be present. Nevertheless, we will use the term "cycle" refer to the IMF obtained from MEMD in following, to be more consistent with previous literature investigating long-term phenomena in interictal iEEG.

3.2.4 Statistical analysis

To test if any band power cycle phase (circular variable) is correlated with seizure duration (linear variable), we first performed Mardia's linear-circular correlation (Mardia, 1976). This results in a correlation coefficient bounded between zero (no relationship) and one (perfect relationship). P-values are calculated from randomisation tests (see

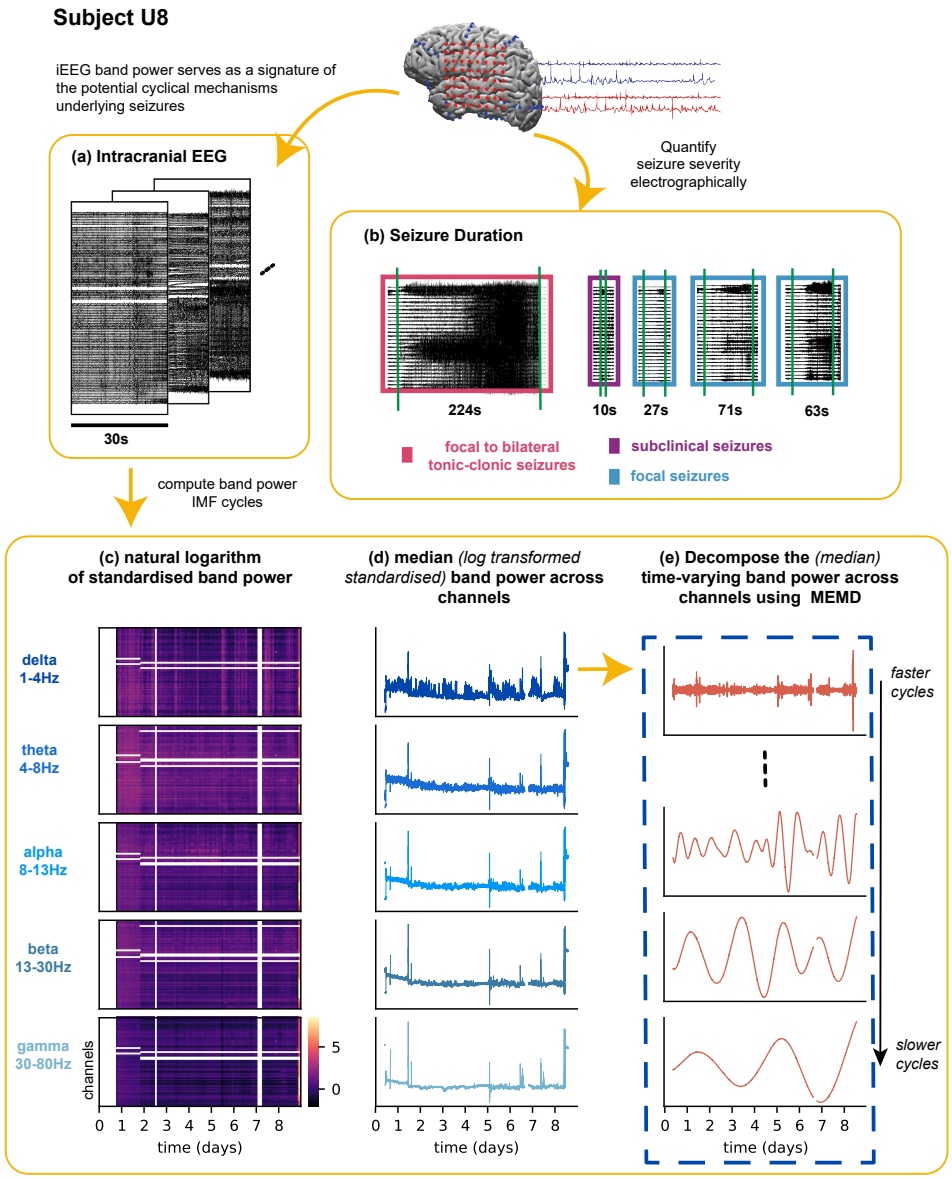

Figure 3.1 **Quantifying band power cycles and seizure duration**. (a) Traces of iEEG recordings across channels. Each one corresponds to 30 s of recording. (b) Traces of iEEG recordings for five example seizures with their duration displayed. More severe seizures, such as focal to bilateral tonic-clonic seizures tend to last longer, in comparison with less severe seizures, such as focal or subclinical seizures. (c) Heatmaps of the natural logarithm of (standardised) band power values across channels for each one of the five main frequency bands used in the analysis. (d) Line plots of the median (log transformed standardised) band power across channels against time. Each line plot depicts one frequency band and is coloured accordingly. (e) Visualisation of some example cycles of the delta frequency median band power as extracted using Multivariate Mode Decomposition (MEMD).

Supplementary Section 3.5.5). FDR correction (see Supplementary Section 3.5.10) was applied to all p-values across all individuals and tests; the significance level was set to 5%.

To test if a combination of band power cycles are able to explain seizure duration, we applied Linear-circular regression (see Supplementary Section 3.5.6). We applied a model selection process (see Supplementary Section 3.5.7). Model performance was assessed using root-mean-squared-error (RMSE) and adjusted R^2 as model performance metrics. A range of models were tested in the selection process, including all band power cycles (all IMFs) in the delta, theta, alpha, beta and gamma band individually, as well as the strongest cycles embedded in the signals (cycles with very high power across all dimensions (frequency bands) – we term the resultant models as "peak" models. Finally, we tested if the variable selection and regression process for the selected model could have yielded a high performance by chance using a permutation test (see Supplementary Section 3.5.9 for details). The significance level was set to 5%.

3.3 Results

3.3.1 Association of seizure duration and individual band power cycles

For each subject, we first determined any association between the seizure duration and the phase of each band power cycle at which the seizure occurred using the rank linear-circular correlation D_n (Mardia, 1976). In example patient U10, Fig. 3.2a and b illustrate a moderate correlation ($D_n = 0.40$, $p = 0.0093$) between the seizure duration and a gamma band power cycle (7.4h characteristic cycle period). Longer seizures tended to occur during the falling phase of the cycle (Fig. 3.2a and b). Fig. 3.2c shows the correlations between the seizure duration and the phases of gamma band power cycles across subjects. Overall, there are some weak to moderate correlations with some stronger ones appearing for two subjects (ID10 and U5).

Across subjects, we mostly found weak to moderate correlations between the seizure duration and the phases of individual band power cycles for every frequency band (see Supplementary Fig. 3.7).

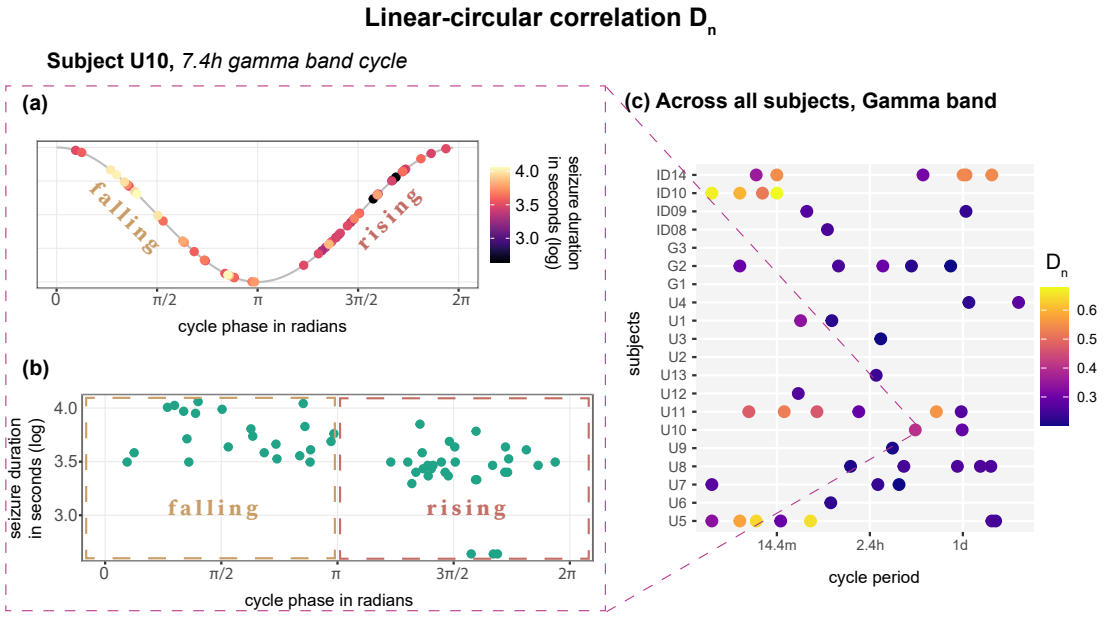

Figure 3.2 **Example associations of seizure duration with phases of band power cycles**. (a) Representation of the phase of the 7.4h gamma band power cycle $[0, 2\pi]$. The curve illustrates the falling and rising phase of the band power cycle. Each point represents one seizure that occurred at the corresponding phase of the band power cycle and are coloured by seizure duration in seconds (log). (b) Alternative, scatter plot representation of the same data as in (a): seizure duration shown against phases of the band power cycle. (c) Dot plot of the Mardia's rank correlation between the seizure duration and the phases of the band power cycles across all subjects. Weak associations ($D_n \leq 0.2$) are not shown for clarity of visualisation.

3.3.2 Seizure duration is modulated by cycles on multiple timescales

We further investigated whether seizure duration is more strongly associated with a combination of two or more band power cycles, as individual cycles only showed weak to moderate associations (Fig. 3.2c and Suppl. Fig. 3.7). To uncover such associations, we applied a circular-linear model selection and regression (see Supplementary section 3.5.6). Fig. 3.3 illustrates the selected model for an example subject, U4. This model had the best fit on the data with an adjusted R^2 of 82% (Fig. 3.3a). The performance of this model can be seen in Fig. 3.3b, where the predicted seizure durations based on band power cycles were close to the actual seizure duration values. Fig. 3.3c illustrates how much each band power cycle contributed to the seizure duration predictions based

on the final model.

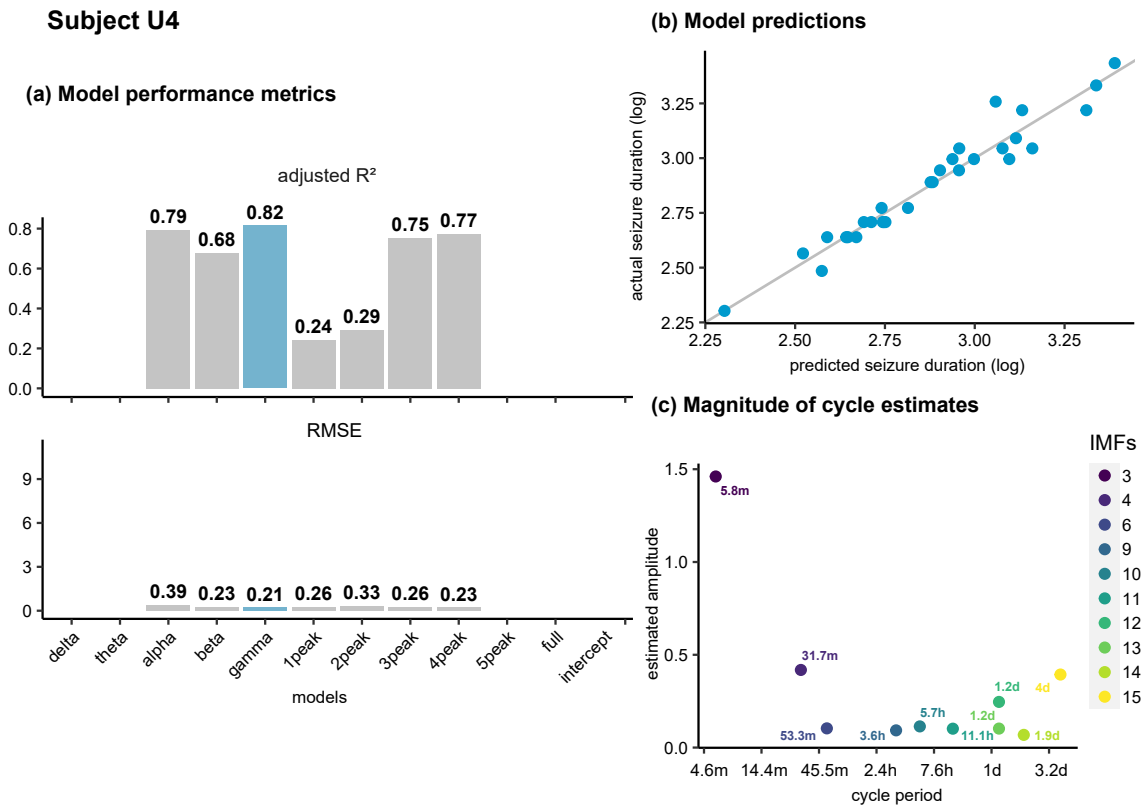

Figure 3.3 **Illustration of the final selected model for one example subject**. (a) Bar plots representing the performance of the different models evaluated for this example subject. The top plot shows the adjusted R^2, while the bottom plot shows the root-mean-squared-error (RMSE) as obtained from the Leave-one-out-cross-validation (LOOCV). The non-grey coloured bars indicate the selected model, while all the other models are displayed with grey colour. Performance metrics for models that were not valid are not shown. (b) Scatter plots depicting the estimated quantities obtained from the model against the actual seizure duration (natural logarithm) in this patient. (c) Band power cycle importance as expressed by its estimated amplitude/magnitude (see Supplementary section 3.5.6) for the corresponding cycle included in the model plotted against their corresponding cycle period (days/cycle).

Across subjects, we found 70% of the subject-specific models had an adjusted R^2 over 60% (Fig. 3.4a). From these models, around 80% were deemed to be above chance-level (p-value <= 0.05) based on permutation tests (see Fig. 3.4a, Supplementary Fig. 3.13). The intercept model performed better compared to all the models in only one sub-

ject (U12), indicating that this subject's variability in seizure duration was not well-predicted by band power cycles. Overall, these models could explain more than 60% of the variability captured in seizure duration for those subjects.

Different band power cycles of various timescales contributed in seizure duration variability in the selected models (Fig. 3.4b). Timescales less than 1 day contributed to the seizure duration diversity in all 19 subjects. For subjects U9 and ID10 the circadian cycle was not apparent. Thus, circadian band power cycle was detected and included in the models in 17 subjects out of 19. In 11 out of these 17 subjects the circadian rhythm contributed in the selected models. For four subjects, slower cycles with cycle period 2 or 4 days were included in the modeling process (subject (period of slower cycle in days): ID14 (2 days), U4 (4 days), U8 (2 days) and U5 (2.3 days)) (see Supplementary section 3.5.4), those appeared to have cycles with periods longer than one day in the selected models.

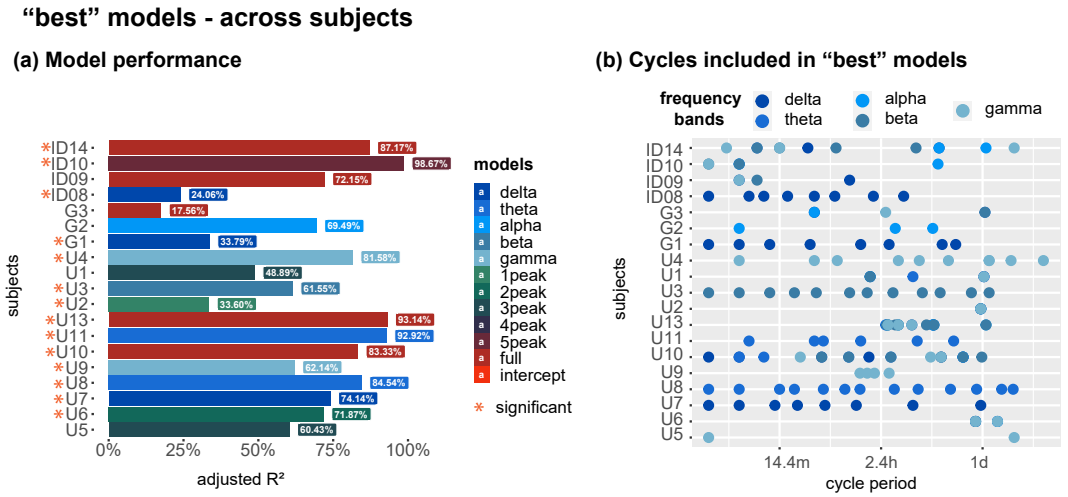

Figure 3.4 **Selected models across subjects**. (a) Barplot of the adjusted R^2 as obtained from the selected model for each subject. The significance is indicated with a red asterisk as determined by a permutation test for the adjusted R^2 (see Supplementary Fig. 3.13). (b) Dot plot illustrating the cycle period of the variables selected in the final model for each subject. Colours depict the frequency band associated with these band power cycles.

3.4 Discussion

A combination of cycles in interictal band power can explain the variability in seizure severity, as measured by seizure duration, within individual subjects. We found that a range of timescales provided explanatory power, including faster cycles (cycle period < 1 day), circadian cycles (cycle period $= 1$ day) and some slower cycles (cycle period > 1 day). It is likely that a combination of oscillatory mechanisms, each with distinct cycle period, shapes how seizure severity changes over time. The incorporation of these findings into therapeutic interventions, such as chronotherapy (Carney et al., 2014; Ramgopal et al., 2013) may mitigate seizure severity.

Even though a combination of different band power cycles could explain seizure duration, this relationship should not be interpreted as a causal effect. Each band power cycle is most likely a reflection of an underlying modulatory process. It is not surprising that a combination of different timescales predicts seizure duration, as multiple mechanisms (Panagiotopoulou et al., 2022; Schroeder et al., 2020) appear to modulate features such as seizure occurrence (Karoly, Rao, Gregg, Worrell, Bernard, Cook and Baud, 2021; Bernard and Nehlig, 2021) and seizure duration (Schroeder, Chowdhury, Cook, Diehl, Duncan, Karoly, Taylor and Wang, 2022).

The nature of these modulatory processes is still elusive, although their timescales may provide some insights. Circadian cycles might be due to molecular oscillations (Bernard, 2021) or may be linked to the sleep-wake cycle (Jin et al., 2020). Shorter timescales might be related to blood concentrations of metabolites, as glucose and ketone bodies fluctuate in timescales ranging from minutes to hours (Verbeek et al., 2016; Simeone et al., 2018). These metabolic substances have also been linked to neural hyperexcitability (Simeone et al., 2018). Thus, cycles in iEEG markers such as band power could serve as biomarkers for oscillatory mechanisms that influence brain dynamics; these mechanisms might in turn modulate the initiation, severity, and/or termination of seizures.

Although we found many associations between band power cycles and seizure duration, we were unable to explain duration variability in a small number of individuals. Incorporation of longer cycles (than the ones captured in our data) into the models might contribute to the unexplained variability of seizure duration. However, the lack

of ultra long-term iEEG recordings (several weeks or months) limited our analysis to multiday cycles up to four days (see Supplementary Figures 3.5 and 3.6). In previous studies, cycles over a span of 5.5-33 days (Baud et al., 2018) have been associated with seizure occurrence. Additionally, multi-month cycles have been associated with changes in features of seizure evolutions (Schroeder, Karoly, Maturana, Panagiotopoulou, Taylor, Cook and Wang, 2022). Another explanation is some level of random variability (stochasticity) on seizure duration (Lopes da Silva et al., 2003; Suffczynski et al., 2006); this stochastic element cannot be predicted. Lastly, other non-rhythmic factors could contribute to variable seizure duration. For example, environmental and physiological factors (Payne et al., 2021) have been shown to affect seizure occurrence. Anti-seizure drug withdrawal could be another contributing factor (Kirby et al., 2020; Spencer et al., 1981; Zhou et al., 2002; Duy et al., 2020). These external and internal factors might also impact other seizure characteristics, such as seizure duration and severity. A model that quantifies these factors may achieve better predictive performance of the seizure duration.

In this study, we analysed a broad spectrum of spectral properties of brain activity represented by a time-varying band power. We focused on the temporal changes by using the median band power across channels, providing an overview of the possible time-scales of modulatory cycles. However, variability of seizure severity might be linked to specific brain regions where band power cycles have a unique signature. For example, more severe seizures, such as FTBTC seizures have been linked to subcortical areas, such as the thalamus (Caciagli et al., 2020). Future work may therefore benefit from including spatial information from iEEG or other modalities.

Another limitation is that we used seizure duration as a proxy for seizure severity. Even though seizure duration has been linked to seizure types (Kaufmann et al., 2020), postictal activity (Payne et al., 2018), and SUDEP (Ochoa-Urrea et al., 2021), it does not encapsulate all aspects of seizure severity. Various other aspects of seizure severity could be quantified electrographically, such as the strength and extent of spread of ictal activity, as well as the duration of post-ictal suppression (Gascoigne et al., 2023). Additionally, other physiological markers of seizure severity have been used in previous studies (Gascoigne et al., 2023). As with seizure duration, individual markers of seizure severity can be associated with band power cycles using our approach (Supplementary

Fig. 3.14 shows one example). However, combining different severity markers may lead to a more representative overall measure of severity for better evaluating its temporal cyclical patterns. Identifying potential endogenous mechanisms (physiological and cognitive) or/and external factors that fluctuate on similar periodicities might unravel the physiological drivers of variable seizure severity.

Finally, we were limited to a relatively short recording period of a few days, possibly missing longer cycles. The number of seizures in each patient was also relatively low, and we therefore did not attempt testing the performance of a prospective predictor. Although we could show statistically that our association was above chance-level, future work should test whether prospective prediction is feasible.

In conclusion, we have observed that seizure severity can be explained by a range of cycles on different timescales captured in time-varying iEEG band power. We conclude that prospective predictions may be possible in future with longer recordings, possibly including other modalities. Our results provide evidence for multiple modulatory cycles on different timescales that impact seizures and their severity, which future work may investigate further. Ultimately, a better understanding of the seizure modulating processes will enable the development of novel treatment strategies that could minimise seizure severity and therefore the clinical impact of seizures.

3.5 Supplementary

3.5.1 Imputation of missing data

To allow subsequent steps of analysis, we imputed any missing data in the band power matrix A before extracting the cycles on different timescales in the data. Missing values were later placed at the corresponding entries in the data for the final output (i.e. we are not using imputed data for our final analysis). For each frequency band, we identified all the missing blocks of the band power and further imputed them. For missing blocks of size equal to one, we used the mean of one value before and after the missing block. For missing blocks of size greater than one, we first identified the segments of equal length with the missing block, before and after the missing block. In cases where the missing blocks were at the start of the recording or the preceding segment was lower in size than the missing block, we applied imputation using just the segment following the missing block. We linearly interpolated the data of missing blocks using the mean of the surrounding segments. The final imputed values were the interpolated ones with Gaussian noise of mean zero and standard deviation, the 60% of the standard deviation of the surrounding segments. If there were missing data apparent in the surrounding segments, those were ignored.

3.5.2 Capturing oscillatory modes using MEMD

In order to extract oscillatory modes embedded in band power, we applied a signal decomposition method called EMD (Huang et al., 1998, 2003). EMD does not require any assumption about stationary or linear characteristics of the signal; EEG signals are non-stationary processes influenced by complex non-linear dynamics (Kaplan et al., 2005; Fingelkurts and Fingelkurts, 2001; Lehnertz et al., 2017). EMD captures a finite number, M of narrow-band modes from an input signal $Y(t)$, known as intrinsic mode functions (IMFs), based on the local minima and maxima of the signal: $Y(t) = \sum_{i=1}^{M} \text{IMF}_i(t) + r(t)$, where $r(t)$ is the residue signal (Huang et al., 1998). The IMFs correspond to a limited-band frequency and have a local mean of zero, satisfying the properties needed for Hilbert-transform to be well-defined. Thus, Hilbert analysis can be applied to each IMF yielding instantaneous characteristics of the signals, such

as amplitude, frequency and phases.

Therefore, in order to obtain a time-frequency representation of the oscillatory modes (IMFs), and hence derive their time-varying characteristics (instantaneous frequency, phase, and amplitude), we applied a Hilbert-transform on each dimension of the IMF (following Hilbert Spectral Analysis methods for EMD) (Huang et al., 1998, 2003; Huang, 2014).

However, in order to decompose multivariate signals (in our case band power across frequency bands) we used an extension of the EMD to multi-dimensional space, called the Multivariate Empirical Mode Decomposition (MEMD) (Rehman and Mandic, 2010); local extrema can not be applied to multidimensional data (Rehman and Mandic, 2010). In MEMD, multiple projections of the multivariate signal are generated along different directions in n-dimensional spaces; the multidimensional envelope of the signal is then obtained by integrating across the different envelopes over all these projections (Rehman and Mandic, 2010; Rilling et al., 2007). This method yields the same number of oscillatory modes (IMFs) across the different dimensions of the multivariate signal. Also, each oscillatory mode across dimensions corresponds to the same narrow-band mode (frequency) (mode-alignment) (Rehman and Mandic, 2010).

3.5.3 Representation of marginal Hilbert spectrum for IMF signals

A suitable representation of the energy or power of a non-stationary and/or non-linear signal across the full range of frequency designated as marginal Hilbert spectrum and can be obtained using Hilbert Spectral Analysis. This should not be misinterpreted as Power Spectral Density (PSD) representation of a stationary signal extracted using Fourier Transform. In a PSD, peak values in power at certain frequencies indicate a cos or sin wave to be pronounced and contribute to the signal throughout the whole time span. However, pronounced values of energy or power within the marginal Hilbert spectrum indicate that there is a greater likelihood to be a pronounced sin or cos component prevalent within the signal spread locally in time (Huang et al., 1998). In order to calculate the marginal Hilbert spectrum, firstly we apply the Hilbert transform (Huang et al., 1998, 2003; Huang, 2014) to each univariate signal (dimension of IMF cycles) for deriving their time-varying characteristics (instantaneous frequency, phase, and amplitude).

For any (real-valued) univariate signal $u(t)$, we can derive its Hilbert transform as:

$$H(u)(t) = \frac{1}{\pi} P \int_{-\infty}^{+\infty} \frac{u(\tau)}{t-\tau} d\tau, \tag{3.1}$$

where P represents the Cauchy principal value for any function $u(t) \in L^P$ class (Huang et al., 1998).

The analytical signal $v(t)$ obtained from the Hilbert transform can be expressed as:

$$v(t) = u(t) + iH(u)(t) = a(t)e^{i\theta(t)}, \tag{3.2}$$

where

$$a(t) = \sqrt{u(t)^2 + H(u)(t)^2} \tag{3.3}$$

and

$$\theta(t) = \tan^{-1}\left(\frac{H(u)(t)}{u(t)}\right) \tag{3.4}$$

where $a(t)$ and $\theta(t)$ are the instantaneous amplitude and instantaneous phase, respectively.

The instantaneous frequency, $f(t)$, can then be calculated as follows:

$$f(t) = \frac{d\theta(t)}{dt}. \tag{3.5}$$

Through the Hilbert spectral analysis, each IMF's instantaneous frequency can be represented as functions of time. Thus, an energy-frequency-time distribution can be obtained for each IMF signal named as the Hilbert energy spectrum or Hilbert spectrum.

For each univariate IMF signal, we can obtain the Hilbert spectrum (the squared value of the amplitude) as a function of instantaneous frequency and time using the following equation:

$$H(f,t) = \begin{cases} a^2(t), & f = f(t) \\ 0, & \text{otherwise.} \end{cases} \tag{3.6}$$

For better clarity through visualisations, we will display the inverse of the instantaneous frequency, i.e. the instantaneous cycle period.

Taking into consideration a well-defined Hilbert spectrum $H(f,t)$, we can then ob-

tain the marginal Hilbert spectrum $h(f)$ of the signal $u(t)$. $h(f)$ is the total energy distributed across the frequency space within a time span of $[0, T]$. Mathematically, this is defined as:

$$h(f) = \int_0^T H(f,t)dt. \tag{3.7}$$

In order to obtain a Hilbert spectrum representation for multivariate signals based on equation 3.6, we simply averaged over the dimensions $H_i(f,t)$ across $i = 1, \ldots, k$ dimensions:

$$\bar{H}(f,t) = \frac{\sum_{i=1}^{k} H_i(f,t)}{k}. \tag{3.8}$$

Then, equation 3.7 is applicable for obtaining the marginal Hilbert spectrum for a univariate IMF signal. Because in our case we have multivariate IMF signals we will compute the marginal Hilbert spectrum of each multivariate IMF signal across all dimensions. In order to do that we are going to integrate over the full time span the averaged Hilbert spectrum across all dimensions, $\bar{H}(f,t)$.

This can be expressed as:

$$\bar{h}(f) = \int_0^T \bar{H}(f,t)dt. \tag{3.9}$$

For numerical computations, we discretised time t to compute the integrals as sums. For each multivariate IMF signal, a marginal Hilbert (energy) spectrum was obtained. For defining which frequency of the initial signal is representative from each IMF, we identified the dominant frequency as the frequency with the global maximum energy value within the marginal Hilbert (energy) spectrum representation. Then, each IMF signal is characterised by a pair of (energy/power, frequency) and this can be visualised for each subject as can be seen in Supplementary Figures 3.5 and 3.6.

3.5.4 Choice of band power cycles for further analysis

In order to select appropriate IMF signals for further analysis, we used the cycle period (inverse of frequency) along with the power for each IMF (Supplementary Figures 3.5 and 3.6). Cycles lower or equal to the circadian cycle if apparent (cycle period ≤ 1

day/cycle) were included in the analysis. Cycles greater than 1 day/cycle were included in the analysis, if their cycle period was at least $\frac{1}{3}$ of the total recording indicating that this cycle is more stable and we are more confident that this cycle is embedded within the signal as we do not rely on observing one cycle only, but at least three cycles within the full recording. Thus, in most of the cases the last three or more slowest band power cycles including the band power residue were extracted from the overall analysis. Finally, the fastest band power cycle (named IMF1) was not included in the analysis as it often captures noise from the raw signal.

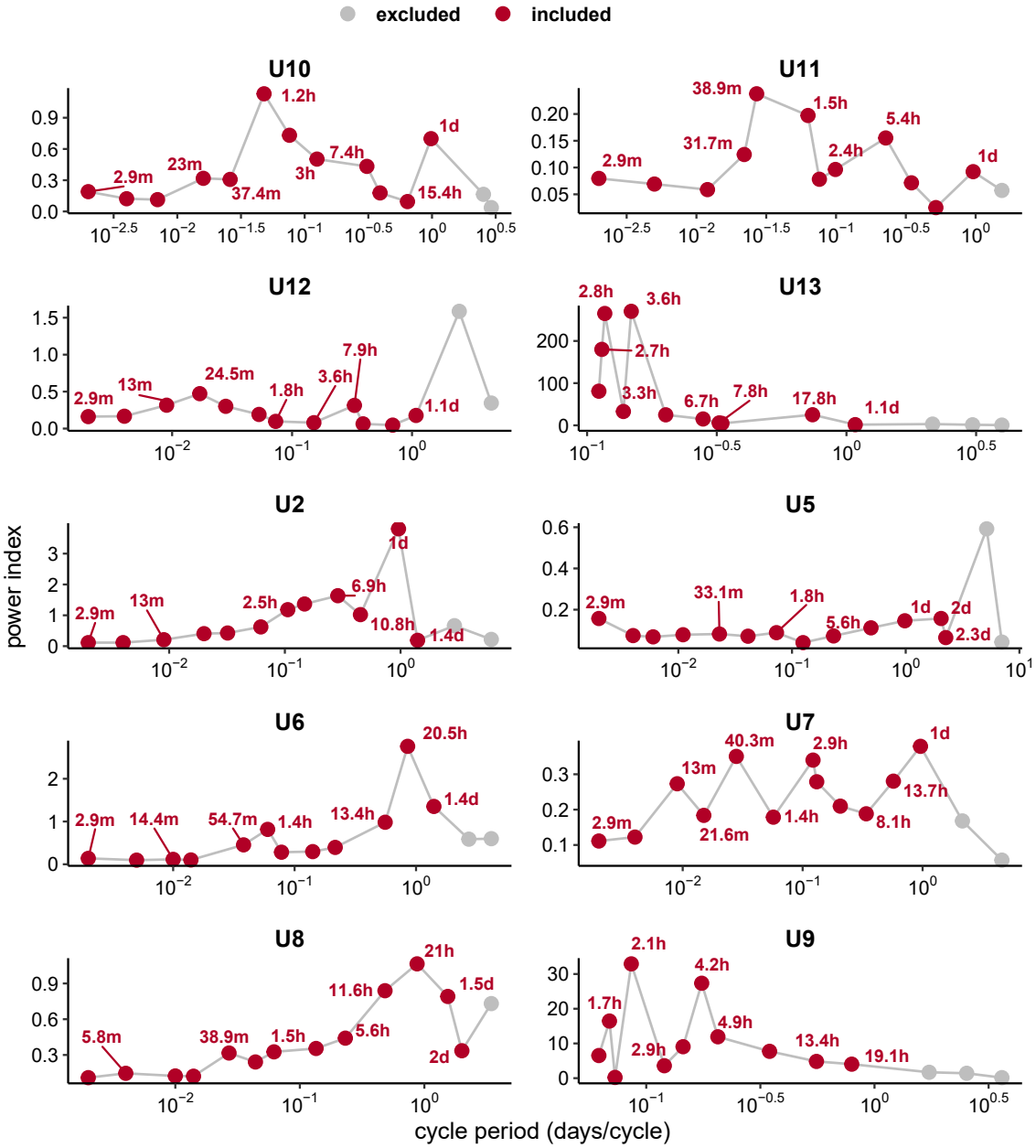

Figure 3.5 **Characteristic cycle period and energy for the band power IMF cycles as obtained from MEMD**. Each plot corresponds to each subject and represents the power for each cycle period (days/cycle) of all band power IMF cycles. Red coloured circles indicate cycles that were included in the analysis, while grey coloured ones are the ones excluded. The band power IMF1 cycle as well as the band power residue are excluded from each subject's plot. Only selected labels are shown in the graph for better clarity and visualisation.

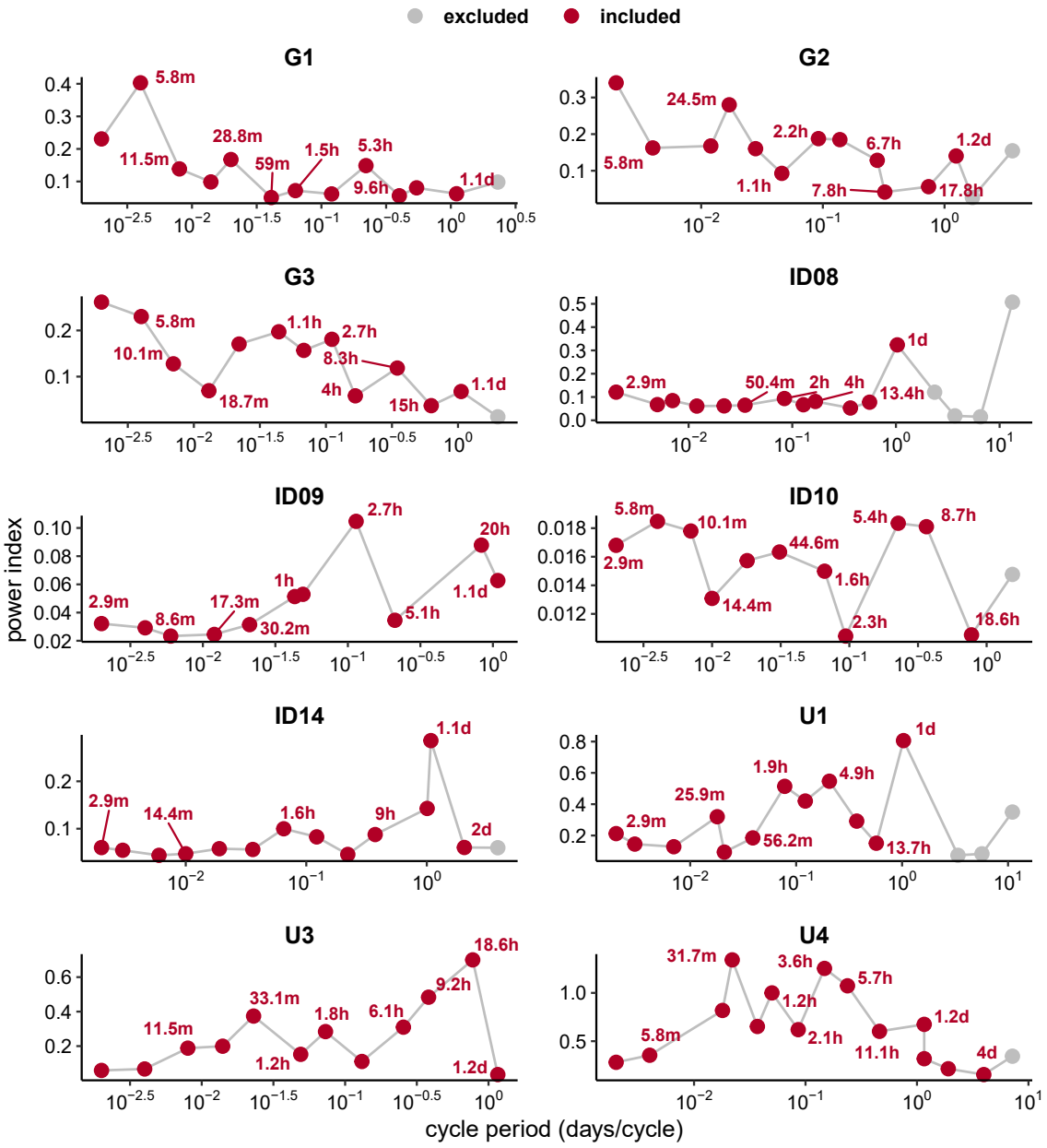

Figure 3.6 **Characteristic cycle period and energy for the band power IMF cycles as obtained from MEMD**. Equivalent figure to Fig. 3.5

3.5.5 Linear-circular correlation between the phase of band power cycles and severity measure – a univariate measure

For each patient, we compared the seizure duration for every seizure to the patient's band power cycles; for each mode within each frequency band (dimension), we found

the mode phases of seizures based on the associated onset times and further correlated those with seizure duration. Mode phases are angular data and thus common correlation metrics, such as Pearson or Spearman's rank correlation coefficients are not appropriate. To determine the association between seizure duration (linear variable) and mode phase in a frequency band (circular variable) we computed Mardia's non-parametric Linear-Circular Correlation coefficient which measures association using ranks (Mardia, 1976). This is a non-parametric measure, which means that it does not assume any form of underlying distribution for both the linear and circular variables. It can be thought of as the equivalent to Spearman's rank correlation coefficient between a linear and a circular random variable.

Mardia's rank correlation coefficient

A measure of association between two random variables X and Φ, where X is a linear variable on $(-\infty, +\infty)$ and Φ a circular variable on $[0, 2\pi)$ was proposed by Mardia (Mardia, 1976) where the random sample, $(x_i, \phi_i), i = 1, 2, \ldots, n$, of observations on (X, Φ) are re-arranged by their ranks; x_i and ϕ_i are arranged by the ranks i and r_i, respectively. The observations of the linear variable are first reordered from smallest to largest, so as $x_1 \leq \cdots \leq x_n$ and assigned a corresponding rank, i, based on the associated index $i = 1, \ldots, n$. For the circular observations ϕ_i, then a circular ranked variable m_i can be defined as:

$$m_i = \frac{2\pi(r_i)}{n}, \tag{3.10}$$

where $\{r_i, i = 1, \ldots, n\}$ represent the circular ranks and n is the sample size of the linear-circular pairs of observations, (x_i, ϕ_i). Then, Mardia's rank correlation coefficient is defined as:

$$U_n = \frac{24(T_C^2 + T_S^2)}{n^2(n+1)} \sim \mathrm{X}_2^2 \text{ for n} \to \infty, \tag{3.11}$$

where X_2^2 is the X^2 distribution with 2 degrees of freedom and

$$\begin{aligned} T_C &= \sum_{i=1}^{n} x_i cos(m_i) \\ T_S &= \sum_{i=1}^{n} x_i sin(m_i). \end{aligned} \tag{3.12}$$

Higher values of U_n indicate stronger association. Also, U_n is invariant under a change of origin for the linear variable, X or under rotations of the circular variable, Φ.

However, for reporting the correlation we used a scaled measure of the U_n termed D_n. This is because the U_n does not scale within $[0, 1]$, as the common R^2 values. Thus, using a suitable transformation function, a_n, we can obtain a scaled version of the Mardia's rank correlation coefficient within the range $[0, 1]$ as follows:

$$D_n = a_n(T_c^2 + T_S^2), \tag{3.13}$$

where if n is even,

$$a_n = \frac{1}{1 + 5cot^2(\frac{\pi}{n}) + 4cot^4(\frac{\pi}{n})}, \tag{3.14}$$

whereas if n is odd,

$$a_n = \frac{2sin^4(\frac{\pi}{n})}{(1 + cos(\frac{\pi}{n}))^3}. \tag{3.15}$$

Randomisation test

For large n, U_n under independence follows approximately the X^2 on two degrees of freedom if X and Φ have continuous distributions. Significance of the independence can be established using the $U_n^* = (T_C^2 + T_S^2)$ measure of association (Pandolfo, 2015) based on a randomisation test. We use U_n^* as it is less computationally intensive. For the randomisation test, we randomly obtain the circular ranking and further define the circular ranked variable m_i which is paired randomly with the linear ranks i. The U_n^* measure was obtained for $1,000$ random selected linear and circular ranking to form a null distribution. The p-value of the observed U_n^* measure was the percentage of times a U_n^* measure of association obtained from the random selected ranking was greater or equal to the observed correlation coefficient, U_n^*.

Linear-circular correlation between seizure duration and the phase of band power cycles

To determine the association between the seizure duration and the phase of each band power cycle at which the seizure occurred we performed the rank linear-circular correlation D_n (Mardia, 1976) for each subject. Supplementary Fig. 3.7 shows the correlations between the seizure duration and the phases of band power cycles in each frequency band across subjects. Overall, there are some weak to moderate correlations across all frequency bands.

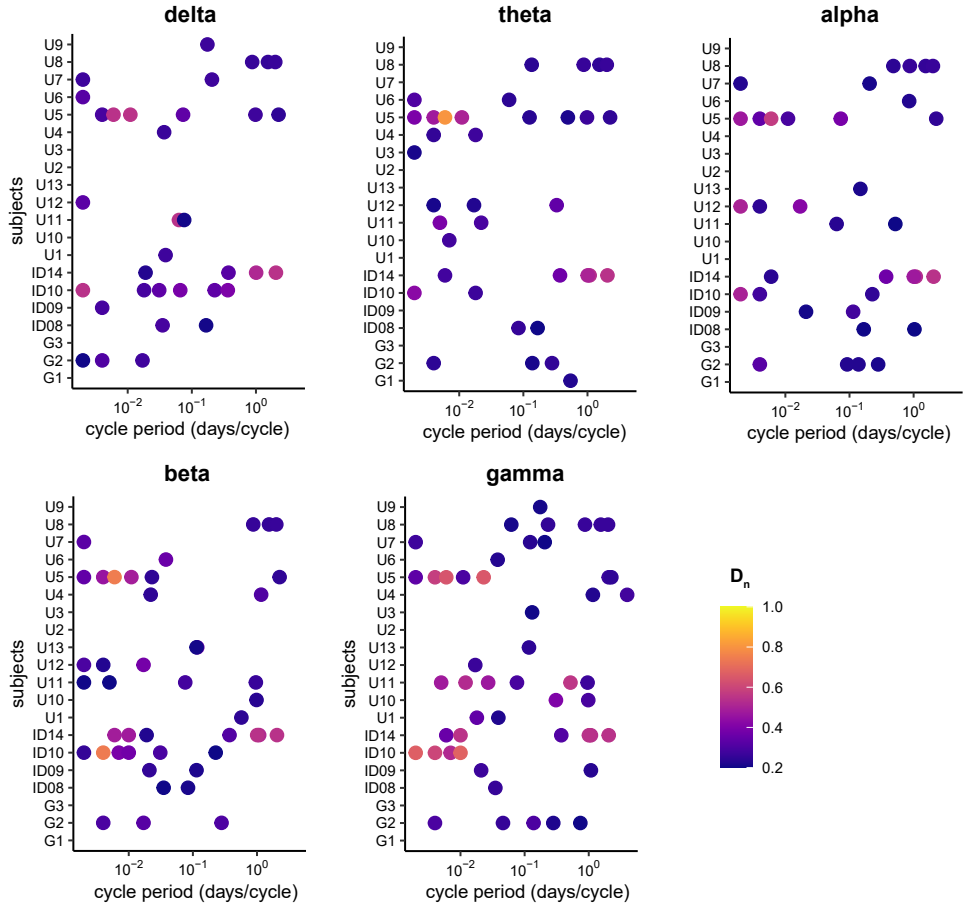

Figure 3.7 **Associations of seizure duration with phases of band power cycles**. Dot plots of the Mardia's rank correlation between the seizure duration and the phases of the band power cycles across all subjects. Each dot plot represents one main frequency band. Band power cycles from weak associations ($D_n \leq 0.2$) are not shown for clarity of visualisation.

3.5.6 Modeling seizure duration using linear-circular regression

Linear-circular regression for cylindrical data

For modelling the relationship between a linear response variable, Y_t, and a circular random variable ϕ_t, $t = 1, 2, \ldots, n$ we used the following cosine regression (Mardia, 1976; Pewsey and García-Portugués, 2021):

$$Y_t = \mu + \beta cos(\phi_t - \phi_0) + \epsilon_t \tag{3.16}$$

The n represents the total number of seizures, $\phi_.$ is the instantaneous phase for the specific IMF cycle, $Y_.$ is the linear response of interest (here, the log seizure duration) and ϕ_0 is the so-called acrophase angle. This is the phase of the corresponding IMF cycle where seizure occurrence reached its peak in the corresponding IMF cycle, as the sample of phases for every IMF cycle was chosen based on the onset times.

The above cosine formula can be rewritten as:

$$Y_t = \mu + \gamma cos(\phi_t) + \delta sin(\phi_t) + \epsilon_t \tag{3.17}$$

This regression can be thought of as a multiple linear regression of Y on $(cos(\phi_t), sin(\phi_t))$.

Extending this regression from the univariate case to the multivariate case by using multiple (K) IMF cycles, this can then be written as (Mardia and Jupp, 1999):

$$Y_t = \mu + \sum_{k=1}^{K} \beta_k cos(\phi_t^k - \phi_0^k) + \epsilon_t \tag{3.18}$$

Finally, the above cosine equation can be rewritten as:

$$Y_t = \mu + \sum_{k=1}^{K} \gamma_k cos(\phi_t^k) + \sum_{k=1}^{K} \delta_k sin(\phi_t^k) + \epsilon_t \tag{3.19}$$

In all the different forms of the cosine model, μ is the expected mean value of the linear response variable Y. $\beta_k = \sqrt{\gamma_k^2 + \delta_k^2}$ is the magnitude of contribution of the k-th IMF cycle.

Equation 3.19 can be fitted based on data using a multiple regression framework yielding estimates for γ_k, and δ_k, for each k-th IMF cycle. Subsequently, we can thus ob-

tain the magnitude of contribution by each k-th IMF through β_k. Previous study (Proix et al., 2021) has used a similar approach for including cycles of multiple timescales into a linear generalised regression model. Proix et al. obtained cycles from interictal spike rate data using wavelet analysis, in order to predict whether a seizure will occur or not. So the response variable was binary as opposed to our study, where the response can take values in $\mathbb{R}$.

3.5.7 Forming models for seizure duration

We wanted to investigate the relationship of seizure duration with combinations of band power IMFs extracted from the MEMD. We fitted 12 models per subject, each with a different selection of explanatory variables. The 12 models can be grouped into four categories, the "frequency band models" (five models) (Fig.3.8), the "peak models" (five models) (see Fig.3.9), the full (all explanatory variables) and the intercept (without any explanatory variables) models.

The band power cycles from a given frequency band formed the explanatory variables for the corresponding "frequency band model" (Suppl. Fig. 3.8). Note that all cycles corresponding to the cycle periods that selected for further analysis (see Supplementary section 3.5.4) were identified within each frequency band and included in the corresponding "frequency band model". Fig. 3.8f illustrates the characteristic power and cycle period of cycles included in each of the "frequency band models" for an example subject, U8. For each one of the five "peak models", we used the band power cycles across all frequency bands that appeared to have more prominent amplitudes (Suppl. Figures 3.5 and 3.6). Starting from the "peak 1" model that contains the band power cycles (across all frequency bands) with the highest power, we then constructed the "peak 2" model by adding the two most prominent band power cycles across all frequency bands, and sequentially formed the remaining "peak models" (Suppl. Fig. 3.9). Finally, we formed the full model and the intercept one. The former included all the band power cycles across all frequency bands as independent variables, while the latter had no variables, just the intercept term.

Initially, we performed a variable selection step for our analysis, as the number of explanatory variables was relatively large compared to the sample size for all models except the intercept one. We used group-LASSO (Yuan and Lin, 2006; Breheny and

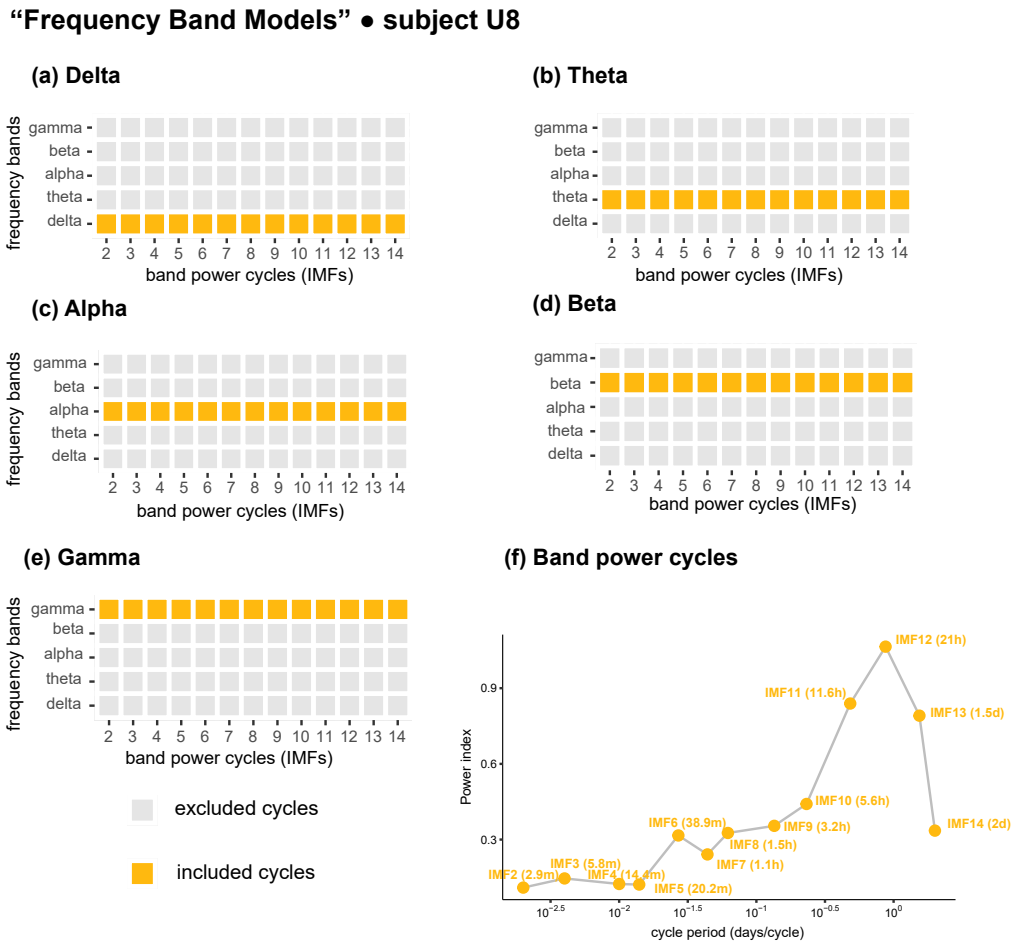

Figure 3.8 **Illustration of "frequency band" models in an example subject**. (a-e) Heatmaps of all the different band power cycles for all frequency bands. The rows depict the frequency bands and the columns the spectrum of the narrow-band band power cycles selected for further analysis (see Suppl. Section 3.5.4). Cells coloured with yellow indicate the corresponding variables used in each "frequency band" model. (f) Characteristic power and cycle period (days/cycle) of cycles included in each of the frequency band models with text displaying the band power cycle (IMF) and the characteristic cycle period in parenthesis.

Huang, 2015), which is a sparse shrinkage method and formed groups of the $sin()$ and $cos()$ terms for each band power cycle involved in the model. For the LASSO, the tuning parameter λ was selected using a 10-fold cross validation method from a range of values $\lambda = 10^{-3}, 10^{-2.92} \ldots, 10^{4.92}, 10^{5}$.

After selecting a small number of explanatory variables, a linear-circular regression

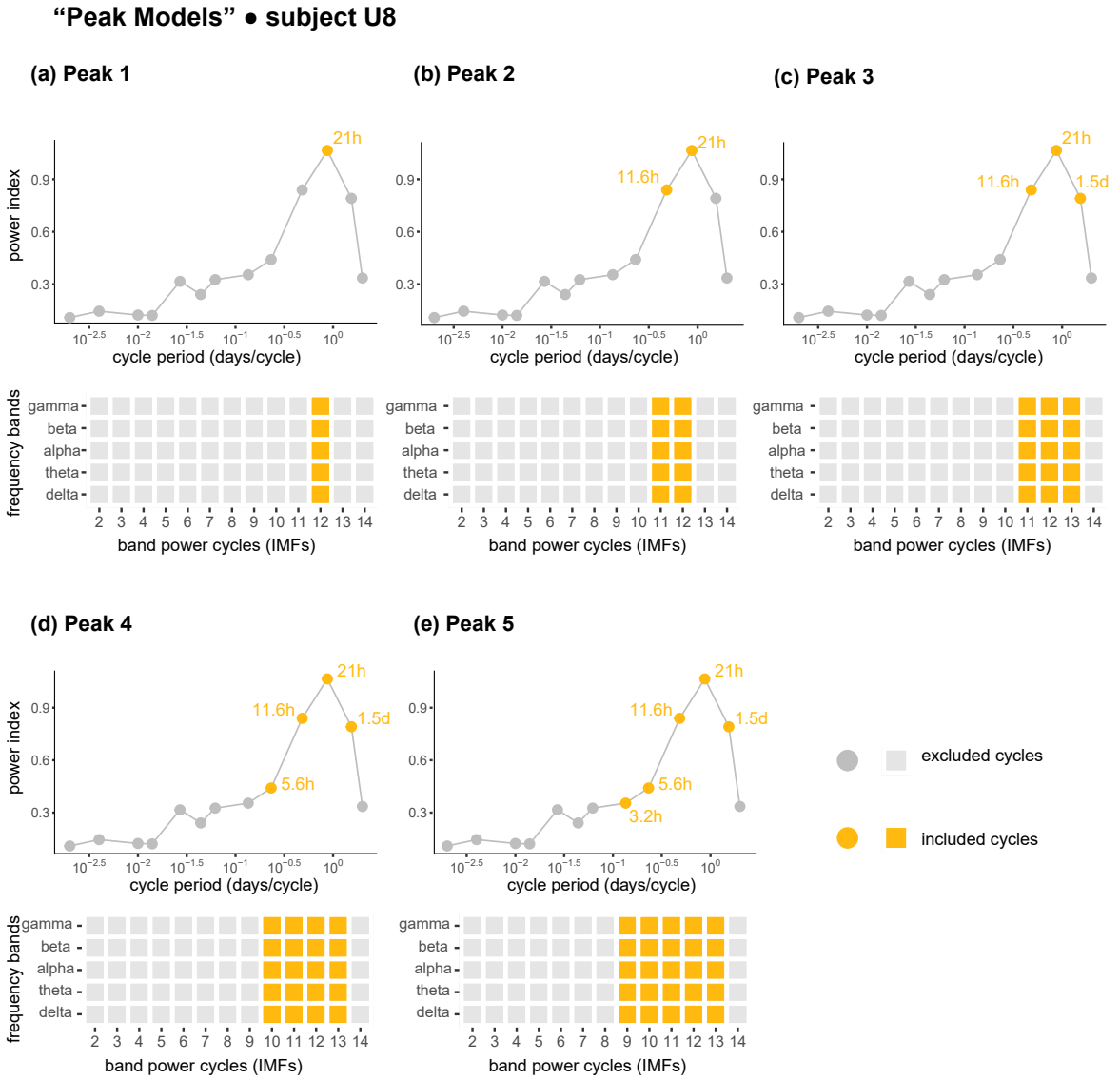

Figure 3.9 **Illustration of "Peak" models in an example subject**. (a-e) Within each panel, the top plots show the characteristic power and cycle period (days/cycle) of all band power cycles selected for further analysis (see Supplementary Section 3.5.4) represented by circle dots for an example subject. Circle dots coloured in yellow depict the band power cycles included in the corresponding "peak" models with text displaying their characteristic cycle period. The bottom plots are a visual representation of all band power cycles across all frequency bands that share the same cycle period. Variables included in the corresponding "peak" models are coloured with yellow.

was performed for each subject. We obtained adjusted R^2 as a model performance metric. A LOOCV was also performed as an additional metric for assessing model performance. Both performance metrics were used to select the "best" model. The adjusted R^2 was used to assess how well the model can explain the variability observed in seizure duration, while the LOOCV was taken into account for accurately estimating the out-of-sample error (overfitting) (Burman, 1989; Arlot and Celisse, 2010).

For choosing the best model, we first identified the model with $RMSE_0, RMSE_0 = \min(RMSE)$, as well as the one with max(adjusted R^2). If these two models matched, then the final selected model was determined (see Supplementary Fig. 3.10 Case 2). In cases where the model with $\min(RMSE)$ did not have the max(adjusted R^2) (see Supplementary Fig. 3.10 Case 1), we computed the absolute percentage difference of the RMSE corresponding to all models with the $RMSE_0$, $RMSE_{diff} = abs(RMSE - RMSE_0)/RMSE_0) * 100\%$ (see Supplementary Fig. 3.10 c and f). If there was a model with higher adjusted R^2 and $\%RMSE_{diff} < 20\%$, then this was selected as "best". In cases where the $RMSE_0$ corresponded to the "intercept" model, then this was chosen as "best" model (this occurred only in one subject, U12).

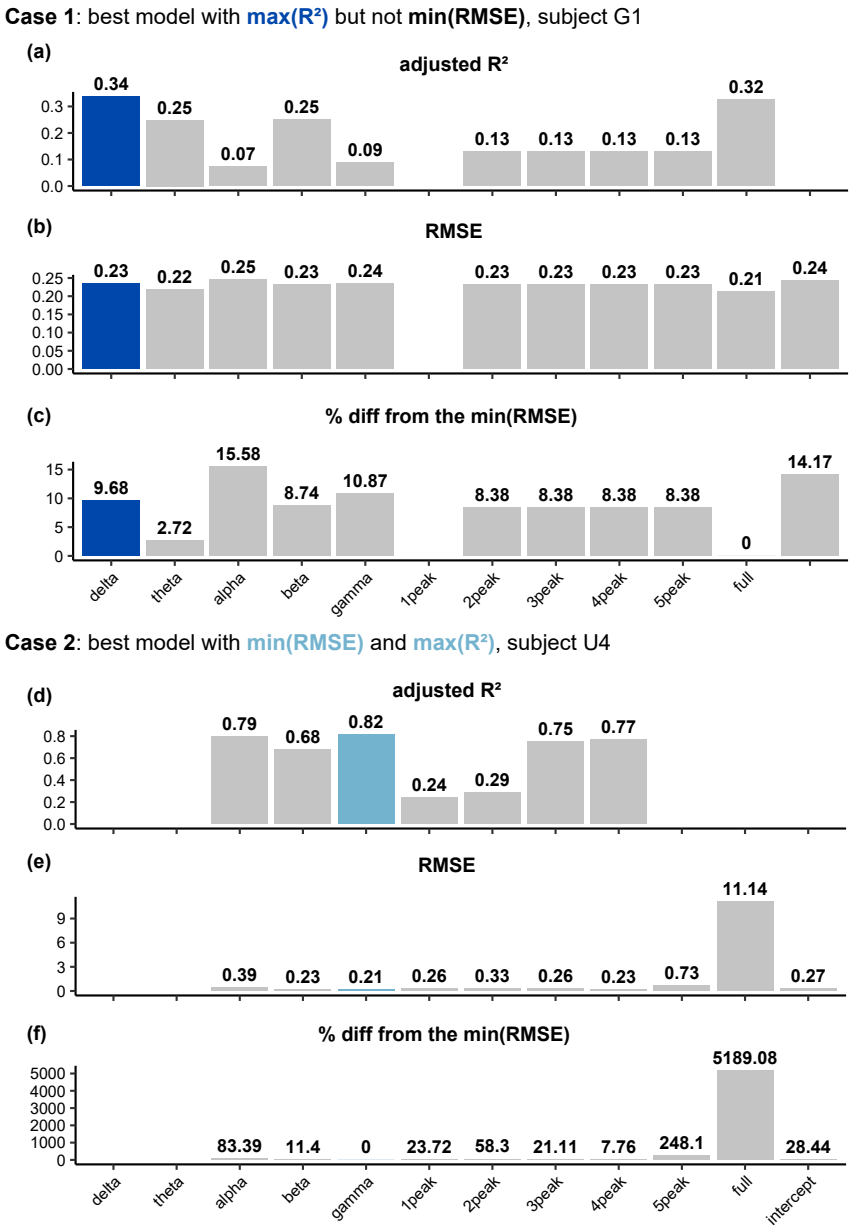

Figure 3.10 **Selection of the "best" model in two example subjects**. (a-c) Representation of model selection in an example subject, where the model with min(RMSE) obtained from the LOOCV did not correspond to the model with max(R^2). (d-f) Illustration of model selection in an example subject, where the "best" model had min(RMSE) obtained from the LOOCV and max(R^2). (a,d) Bar plots of the adjusted R^2 obtained across all models for two example subjects. Non-grey coloured bars indicate the final selected model. (b,e) Bar plots of the RMSE obtained from the LOOCV. (c,f) Bar plots representing the %absolute difference between the RMSE of each model with the min(RMSE).

3.5.8 Performance of the "best" model based on its predictive accuracy

For each subject, we performed a circular-linear model selection and regression (see Supplementary Section 3.5.6). The performance of each subject's "best" model can be seen in Suppl. Figures 3.11 and 3.12, where the predicted seizure durations based on band power cycles were plotted against the actual seizure duration values.

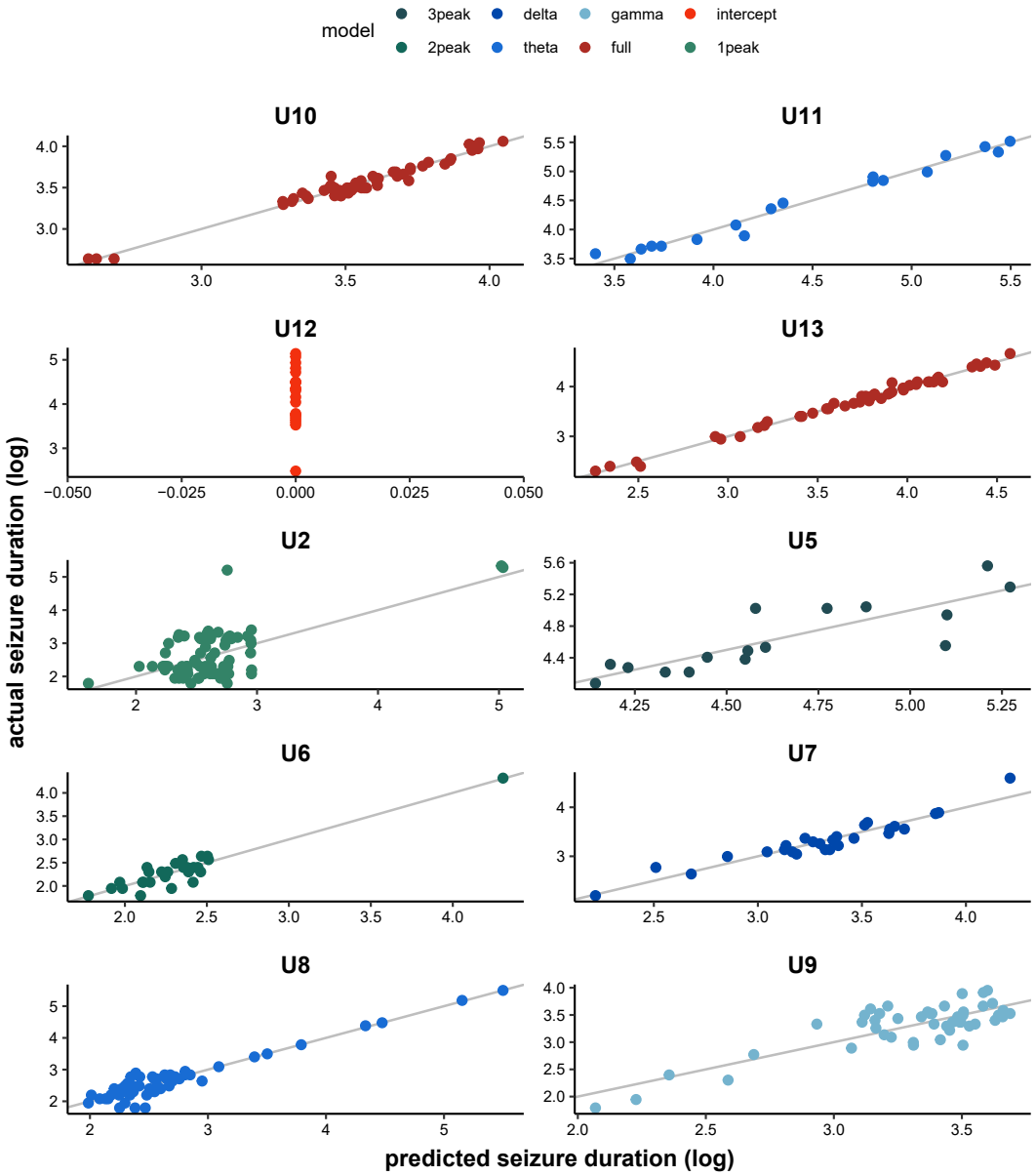

Figure 3.11 **Actual against fitted values across all subjects**. Scatterplots of the actual against the predicted values for seizure duration (log scale) for each subject as obtained from the final "best" models.

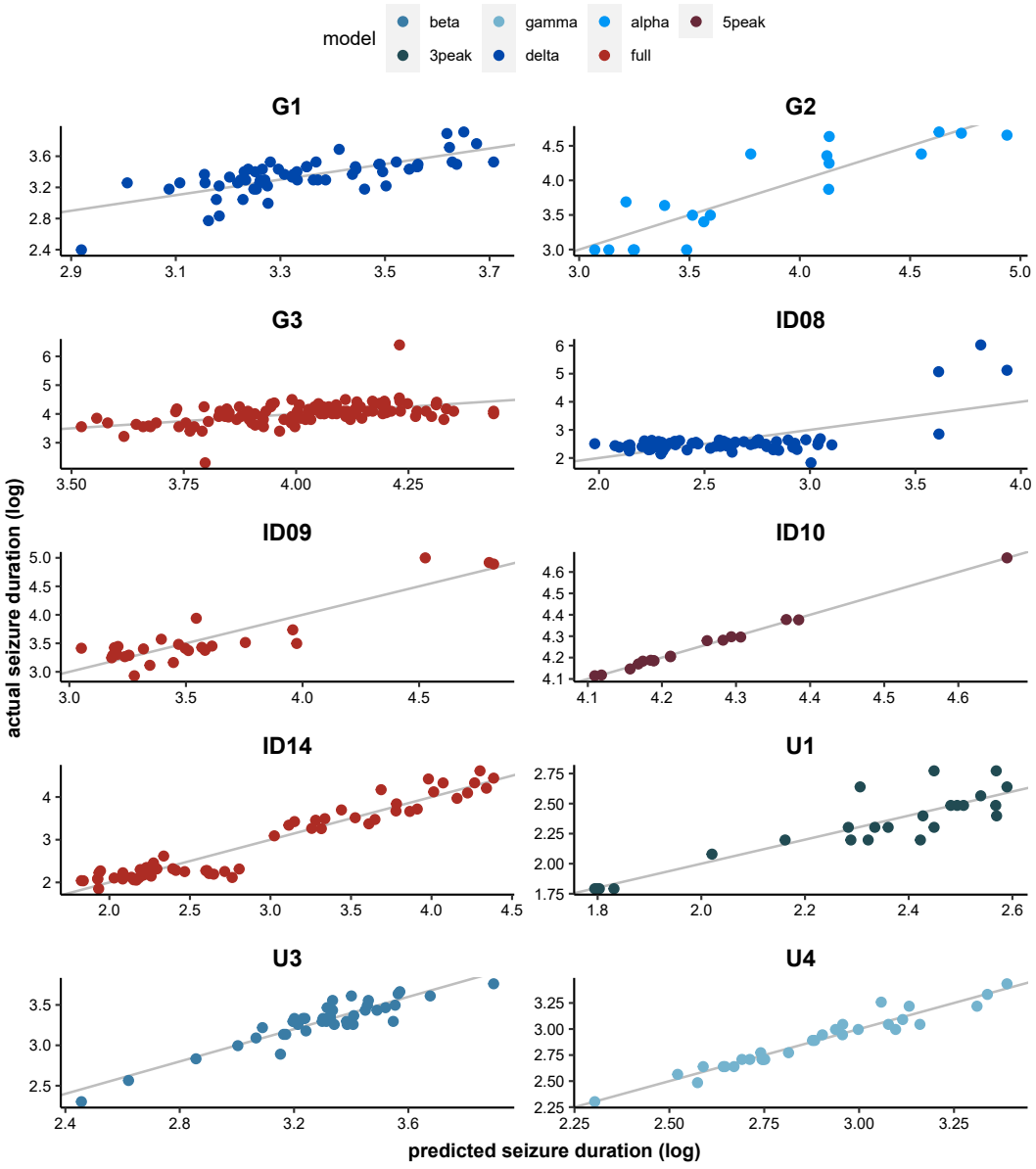

Figure 3.12 **Actual against fitted values across all subjects**. Equivalent to Fig. 3.11

3.5.9 Performance of the "best" models based on permutation tests

To assess the performance of the "best" models we performed a permutation test. In each permutation iteration, we first randomly permuted the order of the seizures by randomly shuffling the response variable (seizure duration). Then, using the band power

cycles from the selected model, we applied group-LASSO and circular-linear regression including only those variables (keeping them unchanged). Finally, we calculated the adjusted R^2 for each iteration. We repeated this procedure as many times as the number of permutations, which we selected as 500. Statistical significance was determined based on a significance level of 5%.

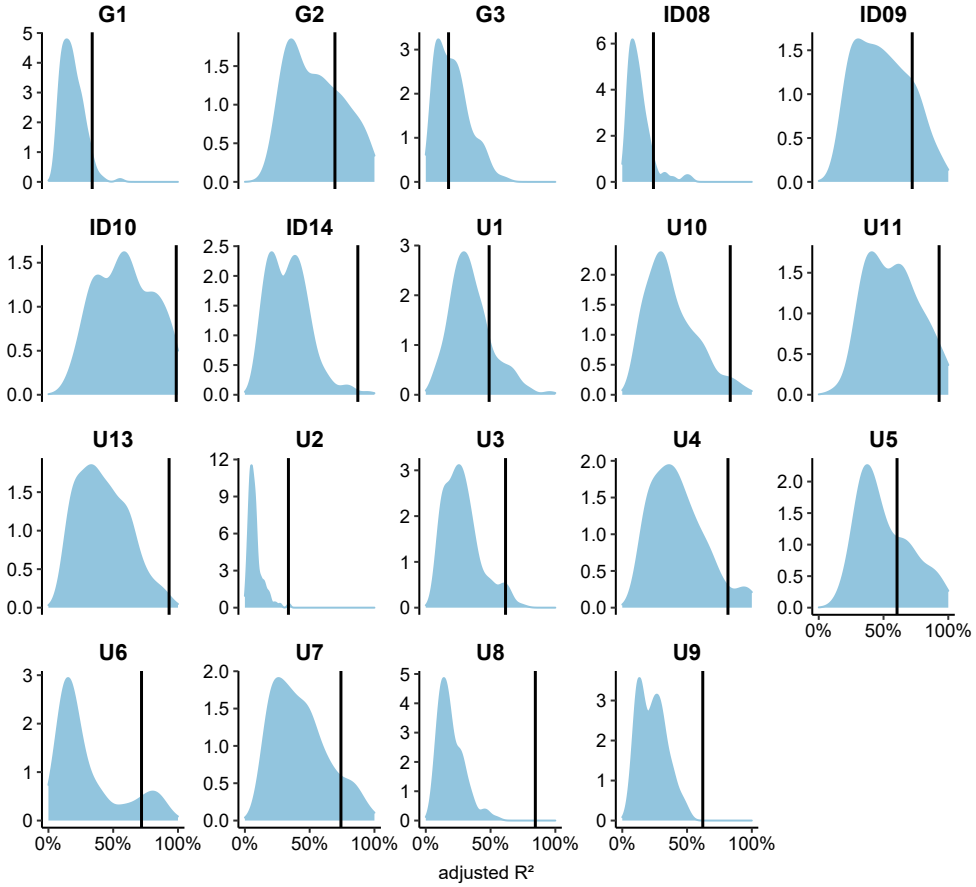

Figure 3.13 **Distribution of the adjusted R^2 values using permuted seizure orders.** The seizure duration was used as response variable, while the band power cycles were included in the model as explanatory variables. The vertical black line represents the adjusted R^2 for the same analysis performed on the original seizure order (see Suppl. Sections 3.5.6 and 3.5.7).

3.5.10 Correction for multiple comparisons

We adjusted all p-values using the Benjamini-Hochberg false discovery rate FDR correction for multiple comparisons (Benjamini and Hochberg, 1995). FDR correction was applied for all statistical tests across all subjects (except permutation tests). The significance of Mardia's rank correlation was assessed using randomization tests as described in Supplementary Section 3.5.5 yielding uncorrected p-values. After applying FDR correction, the significance level was set to 5%.

3.5.11 Statistical analysis for other severity measures

To assess whether band power cycles were associated with other markers of severity, we performed all steps of the analysis for an example severity marker (Gascoigne et al., 2023). Specifically, we used one of the "peak" markers, the top delta, calculated as described previously (Gascoigne et al., 2023). Briefly, this marker encapsulates the maximum level of activity in delta band power during a seizure. Within each subject, seizures with pre-ictal period less or equal to 120 s were excluded from this analysis (Suppl. Table 3.1). Suppl. Fig. 3.14a shows that 10 out of 18 subjects had an adjusted R^2 >= 60%. A combination of band power cycles of different timescales could explain the variability in seizure severity, as measured from this peak marker (Suppl. Fig. 3.14b). For two subjects, the intercept model performed better compared to all the models, indicating that this subject's variability in top-delta marker was not well-predicted by band power cycles. Those subjects are not included in the Suppl. Fig. 3.14.

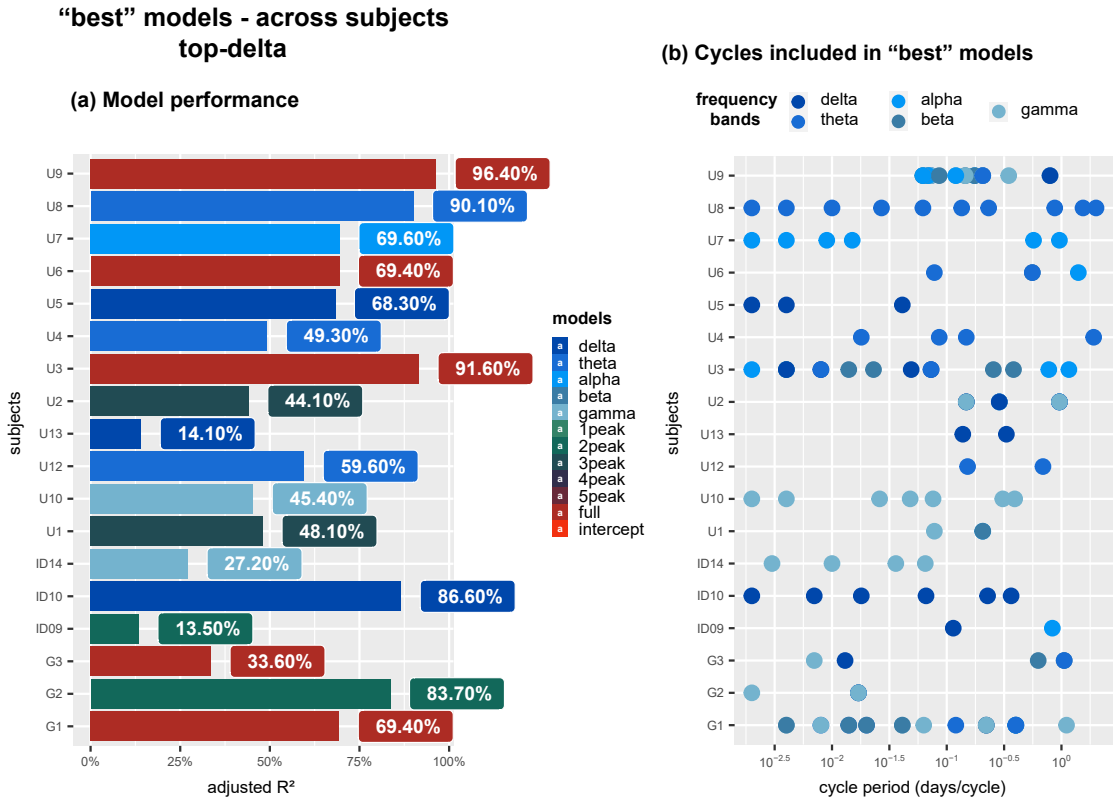

Figure 3.14 **Selected models for one peak marker of severity across subjects**. (a) Barplot of the adjusted R^2 as obtained from the selected model for each subject. (b) Dot plot illustrating the cycle period of the variables selected in the final model for each subject. Colours depict the frequency band associated with these band power cycles.

Subject	*Cohort*	*Age (yrs)*	*Sex*	*Hemisphere (Lobe)*	*Total recording time*	*# seizures analysed for seizure duration*	*# seizures analysed for top-delta marker of severity*
ID08	SWEC	-	-	-	6d	70	15
ID09	SWEC	-	-	-	2d	27	27
ID10	SWEC	-	-	-	2d	17	17
ID14	SWEC	-	-	-	7d	60	54
U1	UCLH	35	M	L (OP)	7d 1h	24	17
U2	UCLH	43	F	L (FP	7d 2h	79	79
U3	UCLH	28	F	R (OP)	1d 19h	41	41
U4	UCLH	28	M	L (T)	12d 5h	30	30
U5	UCLH	21	F	R (T)	8d 21h	16	16
U6	UCLH	26	M	R (F)	6d 2h	27	27
U7	UCLH	43	F	R (TOP)	7d 22h	27	27
U8	UCLH	27	F	L (F)	8d	59	26
U9	UCLH	39	M	L (P)	5d 22h	48	44
U10	UCLH	28	M	R (P)	5d 5h	54	54
U11	UCLH	24	F	R (T)	2d 19h	18	18
U12	UCLH	26	M	R (T)	5d 7h	21	21
U13	UCLH	32	M	L (T)	6d 7h	47	47
G1	GGC	37	M	L (TOP)	3d 19h	60	60
G2	GGC	35	F	L (T)	3d 20h	19	19
G3	GGC	28	M	L (TP)	3d 15h	110	110

Cohort
SWEC = Sleep-Wake-Epilepsy-Center
UCLH = University College London Hospital
GGC = NHS Greater Glasgow and Clyde center

Sex
M = male
F = female

Lobe
T = temporal
F = frontal
P = parietal
O = occipital
IH = interhemispheric

Hemisphere
L = left
R = right
B = bilateral

Dash indicates no available information

Table 3.1 **Demographic and Clinical Information for EMU subjects.** No metadata information for SWEC cohort. Information provided from the clinical reports for UCLH and GGC cohorts. **Subject**: Patient identifier. **Hospital**: hospital where the presurgical assessment, intracranial EEG monitoring and cortical stimulation) took place. **Age**: age, in years, at the time of the presurgical evaluation (this differs from the age of onset). **Hemisphere (Lobe)**: the hemisphere (lobe) where the onset of seizures lies on based on clinical findings. **Total recording time**: total duration of the iEEG implantation (the total recording time was computed based on the edf files available). **# seizures analysed for seizure duration**: number of seizures analysed for each patient based on the criteria used in this study when seizure duration was the variable of interest (response variable). **# seizures analysed for top-delta marker of severity**: number of seizures analysed for each patient based on the criteria used in this study when top-delta marker of severity was the variable of interest (response variable).

Chapter 4. Diminished Circadian and Ultradian Rhythms in Pathological Brain Tissue in Humans in Vivo

Contents

4.1 Introduction

Biological rhythms play a crucial role in regulating various physiological and behavioural processes in the brain and peripheral organs. Such processes can be the sleep-wake cycle (Wulff et al., 2009), core body temperature (Coiffard et al., 2021), blood pressure (Agarwal, 2010), metabolic processes (Serin and Acar Tek, 2019), immune responses (Keller et al., 2009) and neural activity/brain function (Colwell, 2011; Yang et al., 2022). Evidently, alterations of the internal biological rhythms have adverse effects on human health (Bass and Lazar, 2016; Roenneberg and Merrow, 2016) and elevate the likelihood of developing chronic diseases, including cardiovascular diseases (Vetter et al., 2016; Manohar et al., 2017), metabolic diseases (Davies et al., 2014; Bell et al., 2013; Buxton et al., 2012), cancer (Savvidis and Koutsilieris, 2012) and neurological disorders (Leng et al., 2019; Fifel and Videnovic, 2020; Yalýn et al., 2006; Khan et al., 2018; Badawy et al., 2006; Li et al., 2017; Matos et al., 2018). Delineating the link of biological rhythms and disease can lead to novel therapies.

One open question is whether pathology is associated with the alteration of biological rhythms in neurological disorders. There is some evidence that individuals suffering from neurological disorders often exhibit indications of alterations of their circadian rhythms, as manifested from behavioural and biological markers of the circadian internal clock, such as night shift work, travel across time zones, exposure to light-dark cycles, sleep disturbances, changes in cortisol or melatonin expressions, cortical excitability and others. Also, dynamic connectivity related to brain function in shorter timescales has been shown to be altered in patients with epilepsy (Tauste Campo et al., 2018). At the molecular level, dysregulation is observed in the expression of clock genes (Li et al., 2017; Matos et al., 2018; Wallace et al., 2018; Cermakian et al., 2011; Cai et al., 2010; Breen et al., 2014; Ding et al., 2011). Interestingly, in patients with drug-refractory temporal lobe epilepsy, the expression of the CLOCK gene was found to be reduced in resected epileptogenic tissue compared to healthy tissue (Wu et al., 2021). Also, disturbances in sleep and changes in amplitude or phase of melatonin rhythms have been associated with several neurodevelopmental disorders (Philipsen et al., 2006; Jin et al., 2018) and with epilepsy (Yalýn et al., 2006; Molina-Carballo et al., 1994) and might even contribute to more severe symptoms of the disease (Kothare and Zarowski, 2011; van Eeghen et al.,

2011; Bonilla-Jaime et al., 2021; Rybak et al., 2007). Dysfunctions in other hormones, such as changes in cortisol levels have been associated with various diseases (Baird et al., 2012; van Campen et al., 2016; Pritchard III, 1991; Den Heijer et al., 2018); for example cortisol levels have been associated with different types of epilepsy (van Campen et al., 2016; Pritchard III, 1991; Den Heijer et al., 2018). Furthermore, cortical excitability, which is regulated by circadian patterns (Ly et al., 2016) has been shown to be increased during wakefulness following sleep deprivation in patients with focal or generalised epilepsy with spatial changes related to epilepsy syndrome (Badawy et al., 2006). As such, alterations on biological rhythms over specific timescales need to be investigated in the pathological brain to understand how those affect the brain and link them to possible modulatory processes contributing to the development of the disorders.

One way we can capture biological rhythms in the brain is through long-term electroencephalographic (EEG) recording. Brain activity fluctuates over a wide range of timescales spanning from milliseconds to several hours, which is evident on EEG (Aeschbach et al., 1999; Geier and Lehnertz, 2017; Geier et al., 2015; Mitsis et al., 2020; Panagiotopoulou et al., 2022; Lehnertz et al., 2021), and might reflect a spectrum of physiological and pathophysiological functions. States of alertness and sleep deprivation have been linked to frequency-specific changes in brain activity as captured by EEG (Strijkstra et al., 2003; Drapeau and Carrier, 2004; Meisel et al., 2017). Circadian regulation of cortical excitability is associated with changes in measures of awake state (EEG theta power) and cognitive performance (Ly et al., 2016). Furthermore, seizures occur in divergent circadian patterns, depending on the type of epilepsy (etiology) (Loddenkemper, Vendrame, Zarowski, Gregas, Alexopoulos, Wyllie and Kothare, 2011), the location of seizure onset (Durazzo et al., 2008; Hofstra et al., 2009; Karafin et al., 2010; Loddenkemper, Vendrame, Zarowski, Gregas, Alexopoulos, Wyllie and Kothare, 2011), the semiology of seizures (seizure types) (Ramgopal, Shah, Zarowski, Vendrame, Gregas, Alexopoulos, Loddenkemper and Kothare, 2012; Loddenkemper, Vendrame, Zarowski, Gregas, Alexopoulos, Wyllie and Kothare, 2011; Hofstra et al., 2009) and age (Ramgopal, Shah, Zarowski, Vendrame, Gregas, Alexopoulos, Loddenkemper and Kothare, 2012; Ramgopal, Vendrame, Shah, Gregas, Zarowski, Rotenberg, Alexopoulos, Wyllie, Kothare and Loddenkemper, 2012). Notably, complementary to the circadian rhythms, there are other rhythms, such as ultradian rhythms that manifest in vari-

ous brain activities, including neuronal firing rates, sleep arousals, sleep spindles, and seizures (Leopold et al., 2003; Staba et al., 2014; Steriade et al., 1993). Ultradian rhythms with period length from 90 minutes to approximately 110 minutes or even longer in EEG might signify repeated cycling of the basic rest-activity states (Kleitman, 1982; Shannahoff-Khalsa, 1991) during wakefulness or alternating periods of distinct sleep stages; rapid eye movement (REM) and non-rapid eye movement (NREM) sleep (Lubin et al., 1973; Aeschbach and Borbély, 1993; Dement and Kleitman, 1957). Neurotransmitters and neuromodulators released in different regions of the brain follow ultradian rhythms and are involved in different brain functions, such as brain arousal (Blum et al., 2014), central blood pressure (Philippu, 1988) and might be negatively correlated with rhythmic patterns of similar periodicities in theta and delta waves in EEG (Philippu, 2019). However, alterations in rhythms of brain activity characteristics over longer brain recordings have not been explored.

In this work, we first identify circadian and ultradian fluctuations in a brain activity feature (band power) using long-term intracranial EEG from patients with focal refractory epilepsy. We further explore the magnitude of those rhythms in different brain regions aiming to compare pathological and healthy tissue. To this aim, we found that circadian and ultradian rhythms were diminished in pathological tissue compared to healthy tissue. Finally, we explored whether this effect of alteration in circadian and ultradian rhythms remains stable throughout time. Even though there is some within-patient variability in the level of alteration, we show that diminished rhythms are consistent throughout time.

4.2 Methods

4.2.1 Preprocessing of long-term iEEG recordings

We analysed long-term iEEG recordings from 39 subjects with refractory focal epilepsy from the University College London Hospital (UCLH) (Table 4.1). For each subject we processed their entire iEEG recordings. Firstly, we divided each subject's iEEG data into 30 s non-overlapping, consecutive time segments. All channels in each time segment were re-referenced to a common average reference. In each time segment,

we excluded any noisy channels (with outlier amplitude ranges) from the computed common average. To remove power line noise, each time segment was notch filtered at 50 Hz. Finally, segments were band-pass filtered from $0.5 - 80$ Hz using a 4^{th} order zero-phase Butterworth filter (second order forward and backward filter applied) and further downsampled to 200 Hz. Missing data were not tolerated in any time segment and denoted as missing for the downstream analysis.

We then calculated the iEEG band power for each 30 s time segment for all channels. We extracted iEEG band power from 30 s non-overlapping iEEG segments in five frequency bands ($\delta: \ 1-4$ Hz, $\theta: \ 4-8$ Hz, $\alpha: \ 8-13$ Hz, $\beta: \ 13-30$ Hz and $\gamma: \ 30-47.5$ Hz, $52.5-57.5$ Hz, $62.5-77.5$ Hz) using Welch's method with 3 s non-overlapping windows. In detail, for each channel in every 2 s window we calculated the power spectral density (PSD) and used Simpson's rule to obtain the band power values which then averaged over all time windows within a 30 s segment to get the final band power values. In order to remove electrical noise, we selected custom range limits for the gamma frequency band. We log_{10}-transformed and normalised the band power values to sum to one for each 30 s segment yielding a relative log_{10} band power for each frequency band. Thus, for each subject we obtained a relative log_{10} band power series of values across the entire recording for all channels and frequency bands.

In order to map the relative log band power values obtained for each channel to region of interest (ROI) level, we averaged over the relative log band power of all electrodes included in each ROI. Thus, for each subject we had the relative log band power at the ROI level for each frequency band.

In the majority of subjects iEEG recordings had missing data in time-varying relative log band power values that we imputed (Suppl. Section 4.5.1) to enable extraction of cycles and their time-varying characteristics, such as instantaneous frequency and amplitude. Imputed data were not used for subsequent analysis.

4.2.2 Extracting dominant band power cycles using bandpass filter

To extract cycles of various timescales from the relative log band power, we performed a 4^{th} order zero-phase Butterworth filter (second order forward and backward filter applied). Within each subject, we extracted ultradian cycles across different period lengths (1h-3h, 3h-6h, 6h-9h, 9h-12h, 12h-19h). Finally, we denoted a circadian cycle

	ILAE1	**ILAE>1**	**Test statistic**
N (%)	16(41%)	23(59%)	
Age (mean,SD)	29.7 (4.3)	31.8 (9.5)	p=0.41, t=-0.84
Sex (M,F)	7,9	11,12	p=0.80, χ^2=0.06
Temporal, extratemporal	8,8	11,12	p=0.89, χ^2=0.02
Side (Left, Right)	10,6	13,10	p=0.71, χ^2=0.14
Num contacts (mean, sd)	76.9 (27.5)	63.3 (22.8)	p=0.1, t=1.68
Recording Duration in hours (mean, sd)	122.9 (56.1)	123.1 (43.9)	p=0.99, t=-0.01

Table 4.1 Summary of UCLH patient data.

with period length of 19h-1.3d.

4.2.3 MRI processing for identifying regions and resected tissue

To map electrode coordinates to brain regions we used similar methods as described previously (Taylor et al., 2022). In brief, we assigned electrodes to one of 128 regions from the Lausanne scale60 atlas (Hagmann et al., 2008). We used FreeSurfer to generate volumetric parcellations of each patient's pre-operative MRI (Hagmann et al., 2008; Fischl, 2012). Each electrode contact was assigned to the closest grey matter volumetric region within 5 mm. If the closest grey matter region was >5mm away then the contact was excluded from further analysis.

To identify which regions were later resected, we used previously described methods (Taylor et al., 2018, 2022). We registered post-operative MRI to the pre-operative MRI and manually delineated the resection cavity. This manual delineation accounted for post-operative brain shift and sagging into the resection cavity. Electrode contacts within 5mm of the resection were assigned as resected. Regions with >25% of their electrode contacts removed were considered as resected for downstream analysis.

4.2.4 Computing AUC for band power cycles in pathological tissue

In order to quantify the strength of each band power cycle at the ROI level for each subject, we computed the average power of each cycle obtained from the bandpass filter. Thus, for each subject and band power cycle we obtained the mean power for

all ROIs. In order to compare the strength of each cycle (in terms of power) between pathological and healthy tissue, we computed the area under the curve (AUC). AUC can be defined as a quantification which reveals the level of distinction between ROIs classified as pathological and healthy with respect to the band power. AUC values higher than 0.5 resemble diminished band power cycles in pathological tissue, while AUC lower than 0.5 indicate diminished band power cycles in spared ROIs and finally AUC = 0.5 indicates a random discrimination between pathological and healthy tissue.

Within each subject, pathological tissue was determined in two ways: 1) as the resected regions; those were the ROIs that were later surgically resected and 2) as the regions where seizures originated, which formed the seizure onset zone (SOZ) as determined by clinician's reports during the presurgical evaluation. The healthy tissue was categorised either as regions that were spared or as non-seizure onset zone (non-SOZ) regions.

4.3 Results

4.3.1 Diminished circadian cycles in pathological tissue

Fig. 4.1a shows the circadian cycle obtained for each ROI in one example, subject 95, along with the corresponding average power of the cycle. It is evident that the magnitude of the circadian cycle as represented by the average power of the cycle tends to be lower in brain regions labeled as SOZ. This is depicted by the high AUC value (Fig. 4.1b and c), suggesting diminished circadian cycle in pathological tissue (SOZ) compared to healthy tissue (non-SOZ) for this example subject. We further investigated the expression of the circadian cycle across all subjects (38 subjects in total, where the SOZ information was determined) in each frequency band.

Across subjects, the AUC values were overall higher than 0.5 (p-value = 0.003, one-sided Wilcoxon signed rank test) with median AUC of 0.618 (Fig. 4.1d), implying diminished circadian cycle in SOZ as expressed by the average power values of the cycle in the delta frequency band. As can be seen in Fig. 4.1e, similar observations hold for the circadian cycle obtained for all frequency bands (theta: p-value = 0.013, alpha: p-value = 0.002, beta: p-value = 4e-05, gamma: p-value = 0.0005, one-sided Wilcoxon

signed rank test).

We then investigated the magnitude of the circadian cycle between resected and spared regions within each subject for all frequency bands. As the surgically resected brain areas were available, we used the entire cohort for this analysis (39 subjects). Fig. 4.2a shows the distribution of the AUC values between resected and spared across subjects for the beta frequency band. Overall, the AUC values are greater than 0.5 (p-value = 3e-05, one-sided Wilcoxon signed rank test), with high median AUC of 0.705 (Fig. 4.2a). As can be seen in Fig. 4.2b, for all frequency bands, except gamma band, the AUC values tend to be higher than 0.5, indicating that the circadian cycle is strongly expressed in non-SOZ as opposed to SOZ in all subjects in most frequency bands (delta: p-value = 0.008, theta: p-value = 0.03, alpha: p-value = 0.004, gamma: p-value = 0.15, one-sided Wilcoxon signed rank test).

4.3.2 Ultradian rhythms of various timescales are diminished in pathological tissue

We next investigated the expression of ultradian cycles in pathological tissue (either SOZ or surgically resected tissue) as opposed to healthy tissue in our cohort. Analysis involved the SOZ included 38 subjects, while analysis involving resected information included the entire cohort of 39 subjects.

Fig. 4.3a shows the distribution of AUC values obtained between SOZ and non-SOZ across subjects for the delta band. Within the delta band, AUC values were higher than 0.5 for all ultradian cycles (1h-3h: p-value = 1e-05, 3h-6h: p-value = 4e-05, 6h-9h: p-value = 4e-05, 9h-12h: p-value = 7e-05, 12h-19h: p-value = 0.001, one-sided Wilcoxon signed rank test). Faster ultradian cycles have a high median AUC (1h-3h: 0.71, 3h-6h: 0.70, 6h-9h: 0.72) and slower ones displayed moderate to high AUC values (9h-12h: 0.65, 12h-19h: 0.60). Thus, in all subjects ultradian cycles are diminished in SOZ compared to healthy tissue in the delta frequency band. AUC values greater than 0.5 are apparent in all ultradian cycles and frequency bands, except the fastest ultradian cycle with period length of 12h-19h in theta band (Fig. 4.3b).

Fig. 4.4a illustrates the distribution of AUC values for the beta band, representing the relationship between resected and spared brain regions across subjects. It is

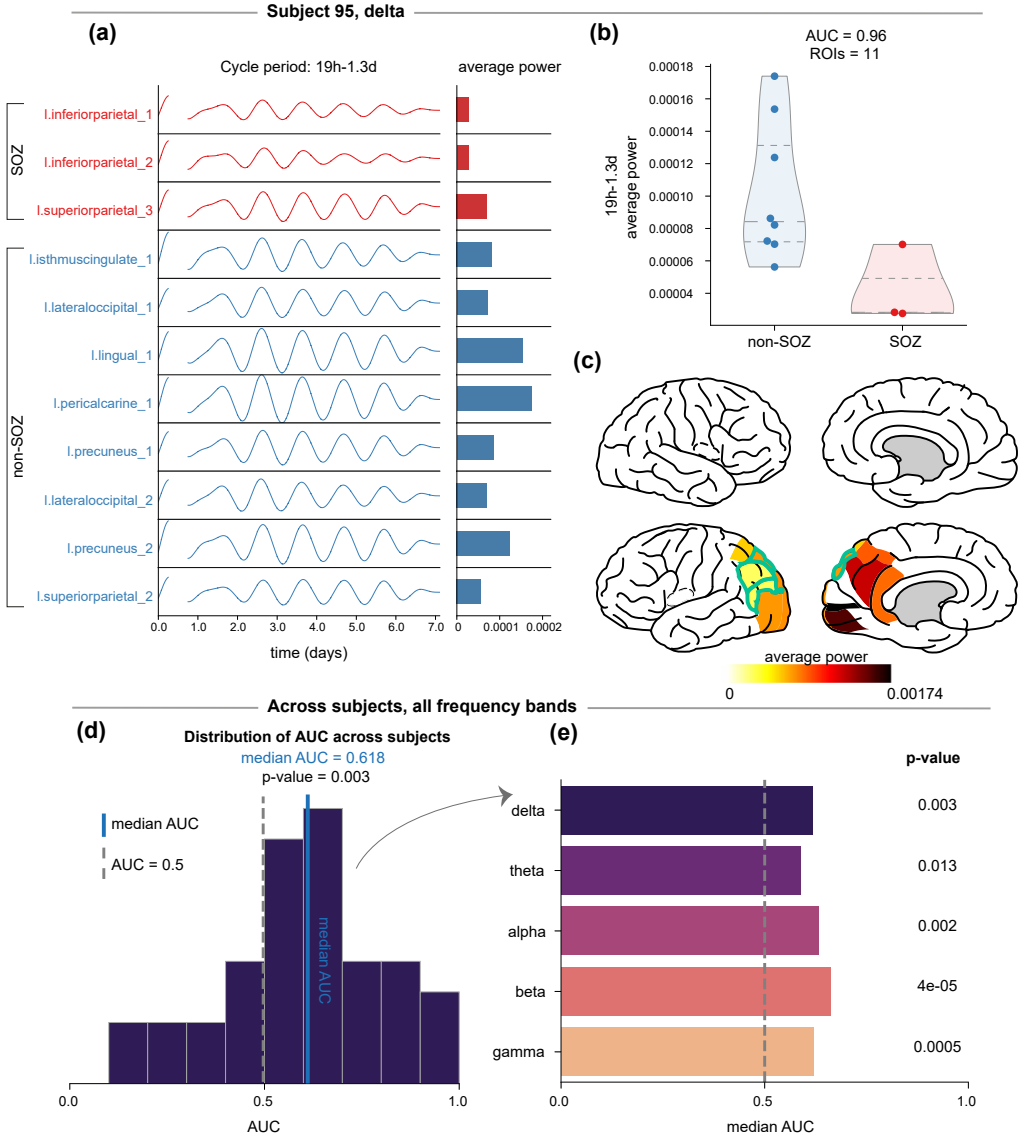

Figure 4.1 **AUC values between SOZ and non-SOZ indicate diminished circadian cycle for each frequency band.** a-c) Example subject 95: a) The circadian cycles across time as obtained using bandpass filter for each ROI. The colours depict tissue within SOZ (red) and outside the SOZ (blue). b-c) Average power of subject's prominent cycles for regions within and outside the SOZ. The power values are shown as b) distributions for SOZ and non-SOZ tissue and c) presented on brain surface from side views (Scholtens et al., 2021). The SOZ is outlined with cyan color. d-e) All subjects: d) Distribution of AUC values across all subjects for the circadian cycle for delta frequency band. The median AUC is shown with a blue vertical line. e) Median AUC values for circadian cycle for all frequency bands. P-values are shown for testing the hypothesis that AUC is equal to 0.5 against the alternative hypothesis that AUC is higher than 0.5 (one-sided Wilcoxon signed rank test) across subjects within each frequency band.

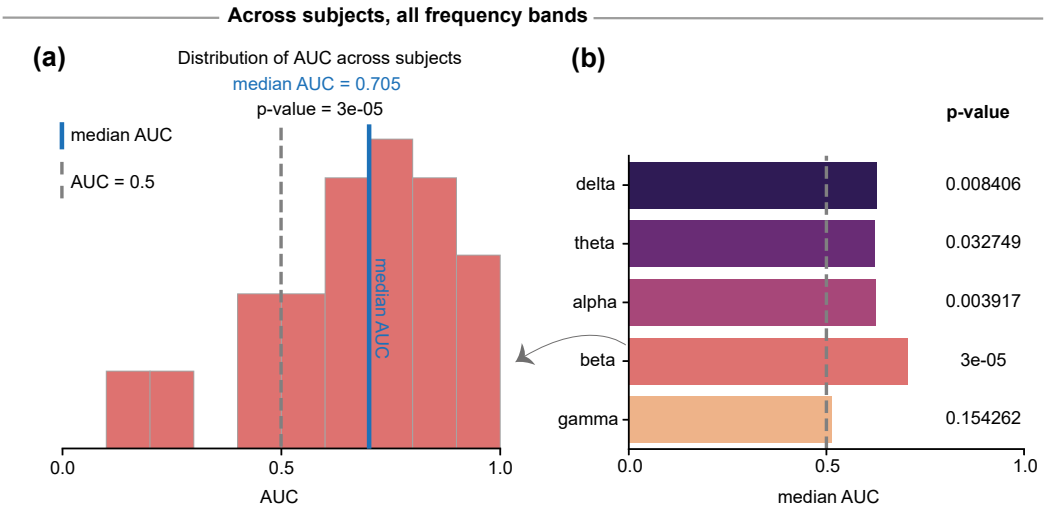

Figure 4.2 **AUC values between resected and spared tissue indicate diminished circadian cycle for some frequency bands.** a-b) All subjects: a) Distribution of AUC values across all subjects for the circadian cycle for beta frequency band. The median AUC is shown with a blue vertical line. e) Median AUC values for circadian cycle for all frequency bands. P-values are shown for testing the hypothesis that AUC is equal to 0.5 against the alternative hypothesis that AUC is higher than 0.5 (one-sided Wilcoxon signed rank test) across subjects within each frequency band.

observed that within the beta band, all ultradian cycles exhibited AUC values higher than 0.5. Statistical analysis using a one-sided Wilcoxon signed rank test confirms the significance of these findings for each cycle (1h-3h: p = 5e-05, 3h-6h: p = 0.0, 6h-9h: p = 6e-05, 9h-12h: p = 0.00015, 12h-19h: p = 0.0001). The median AUC for all ultradian cycles (1h-3h: 0.69, 3h-6h: 0.72, 6h-9h: 0.74, 9h-12h: 0.71, 12h-19h: 0.71) was relatively high. Therefore, in the beta band, resected areas demonstrate reduced ultradian cycles as expressed by the average power of the cycle compared to healthy tissue across all subjects. Except for some ultradian cycles in specific theta band (slowest ultradian cycles) and all cycles in gamma band, AUC values greater than 0.5 were observed in most ultradian cycles and frequency bands (Fig. 4.4b).

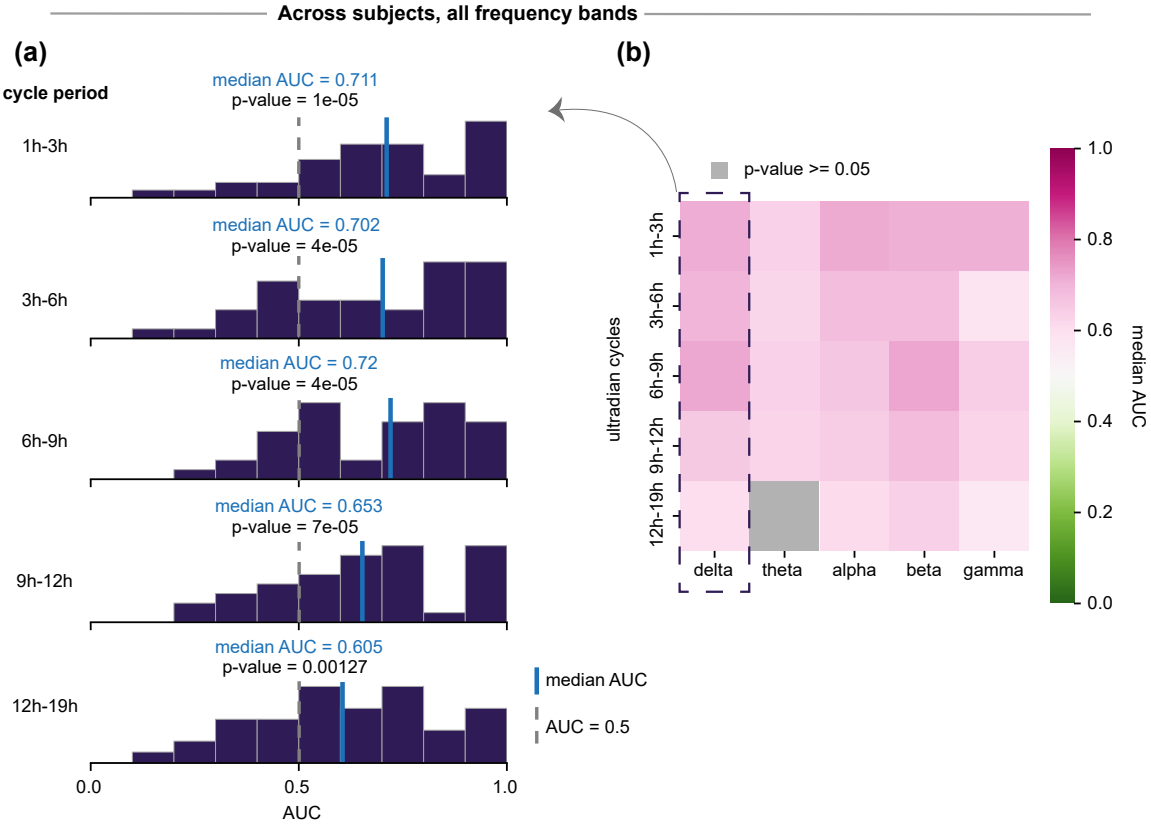

Figure 4.3 **AUC values between SOZ and non-SOZ indicate diminished ultradian cycles for some frequency bands.** a-b) All subjects: a) Distribution of AUC values across all subjects for ultradian cycles for delta frequency band. Each plot corresponds to an ultradian timescale. The median AUC is shown with a grey vertical line. b) Heatmap representing the median AUC values across ultradian cycles and frequency bands. P-values are shown for testing the hypothesis that AUC is equal to 0.5 against the alternative hypothesis that AUC is higher than 0.5 (one-sided Wilcoxon signed rank test) across subjects within each frequency band. Non-grey coloured squares depict cycles with AUC values higher than 0.5 based on the one-sided Wilcoxon signed rank test (p-value < 0.05) across subjects, while grey squares denote AUC values with p-value $>= 0.05$ (we cannot reject the null hypothesis H_0: AUC $= 0.5$).

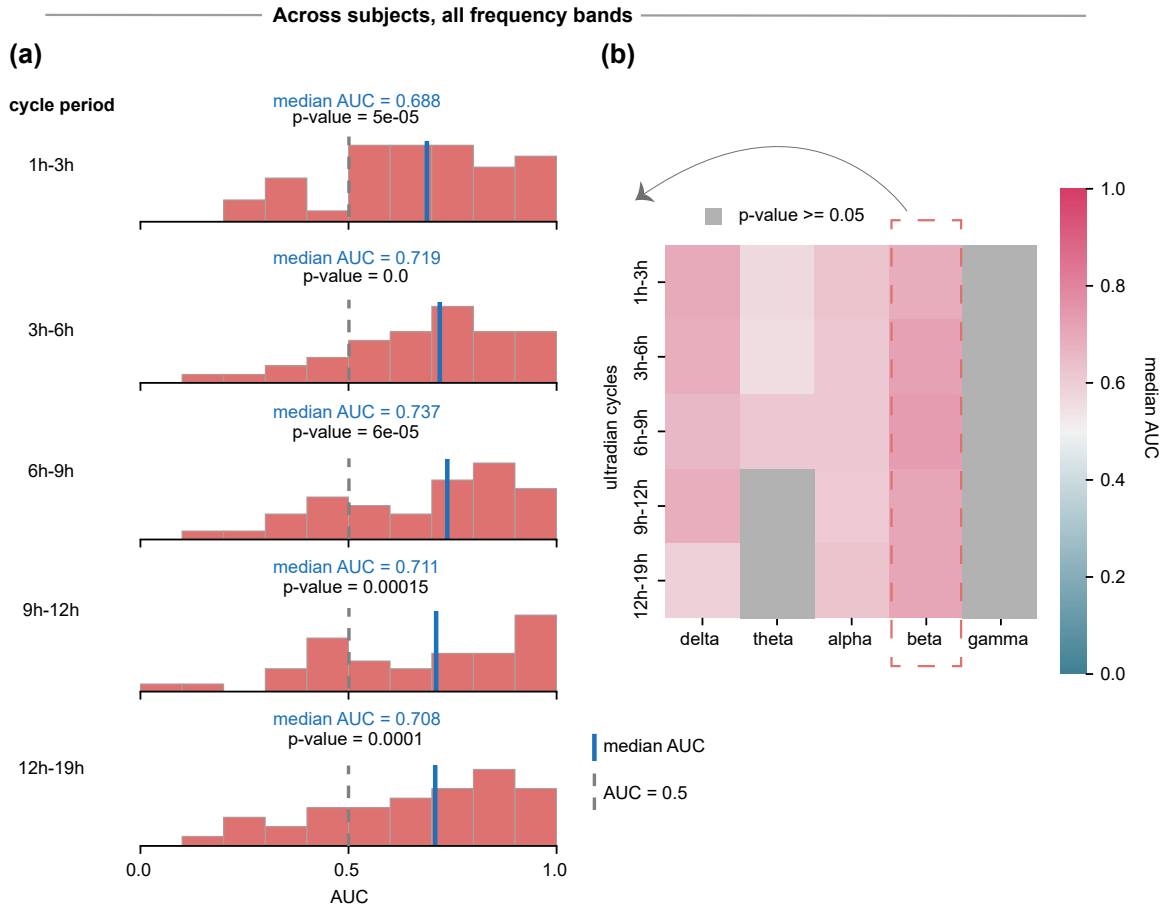

Figure 4.4 **AUC values between resected and spared tissue indicate diminished ultradian cycles for some frequency bands.** a-b) All subjects: a) Distribution of AUC values across all subjects for ultradian cycles for beta frequency band. Each plot corresponds to an ultradian timescale. The median AUC is shown with a grey vertical line. b) Heatmap representing the median AUC values across ultradian cycles and frequency bands. P-values are shown for testing the hypothesis that AUC is equal to 0.5 against the alternative hypothesis that AUC is higher than 0.5 (one-sided Wilcoxon signed rank test) across subjects within each frequency band. Non-grey colored squares depict cycles with AUC values higher than 0.5 based on the one-sided Wilcoxon signed rank test (p-value < 0.05) across subjects, while grey squares denote AUC values with p-value $>= 0.05$ (we cannot reject the null hypothesis H_0: AUC $= 0.5$).

4.3.3 Diminished rhythms are persistent in time

Finally, we investigated the variability of AUC values obtained between the SOZ and non-SOZ in 38 subjects (38 out of 39 subjects). Fig. 4.5a shows the power of the circadian cycle in the beta band across all ROIs in an example subject, 95. A representation of the circadian cycles of all ROIs is shown in Fig. 4.5b demonstrating a lower magnitude of the cycle in SOZ (red lines) as opposed to non-SOZ (blue lines). Then, to delineate how stable the AUC is across time, we first computed the time-varying AUC (Fig. 4.5c) using the power values (Fig. 4.5a) between the ROIs that contributed in SOZ and non-SOZ and further obtained its rolling median using window equal to the 1.5 * cycle period (1.5 days for the circadian cycle). As can be seen in Fig. 4.5d, the AUC was relatively stable around a high AUC of approx. 0.87, suggesting that the diminished effect of circadian cycle is persistent in time and less variable. This is evident also visually by the distribution of AUC values (obtained from the rolling median AUC), where values tend to concentrate around a particular value (Fig. 4.5e).

Fig. 4.6a shows the distribution of AUC values as obtained from the rolling median AUC across time for the 38 subjects. Overall, for most subjects the distributions exhibited a unimodal pattern, characterized by AUC values concentrated around a specific value.

To quantify the stability of the level of alteration in cycles, we computed the percentage of time segments with AUC greater than 0.5 (Fig. 4.6b) within each subject; high percentage indicates that the corresponding cycle is consistently diminished in SOZ. Fig. 4.6b shows the distribution of the percentage of time segments with AUC greater than 0.5 across subjects for ultradian and circadian cycles and frequency bands. Overall, all distributions are right skewed indicating that diminished cycles are relatively consistent in time in all frequency bands.

4.3.4 Relation to patients' metadata

There are multiple factors that may influence the cycles observed in patients with brain disorders, as well as the presence and extent of alterations in brain activity cycles. One such factor could be the duration of the disease. We examined the correlation between the degree of cycle alterations and the duration of epilepsy, and we found

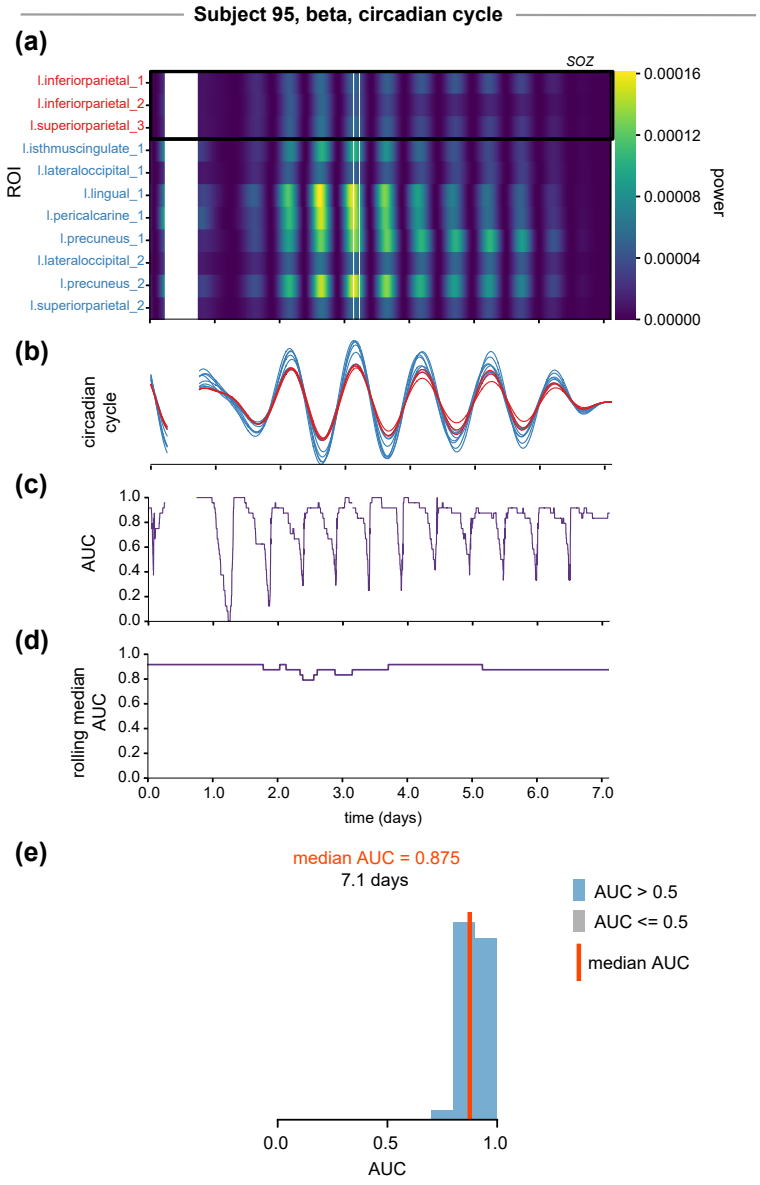

Figure 4.5 **Time-varying AUC between soz and non-SOZ for the circadian cycle in beta frequency band in an example subject**. a) Heatmap of the power of the circadian cycle throughout the patient's iEEG recording in each ROI for the beta frequency band. Each cell represents the power of the circadian cycle in the corresponding ROI and 30 s time segment. ROI names with red/blue color denote SOZ/non-SOZ. ROIs labeled as SOZ are outlined with a black box. b) A representation of the circadian cycle obtained using bandpass filter for each ROI; Red lines correspond to SOZ areas, while blue ones depict non-SOZ areas. c) Time-varying AUC for the circadian cycle computed between SOZ and non-SOZ ROIs. d) A rolling median of the time-varying AUC of the circadian cycle obtained using as window 1.5 * cycle period = $1.5d$. e) A histogram of the rolling median AUC, with median value marked with a vertical orange line.

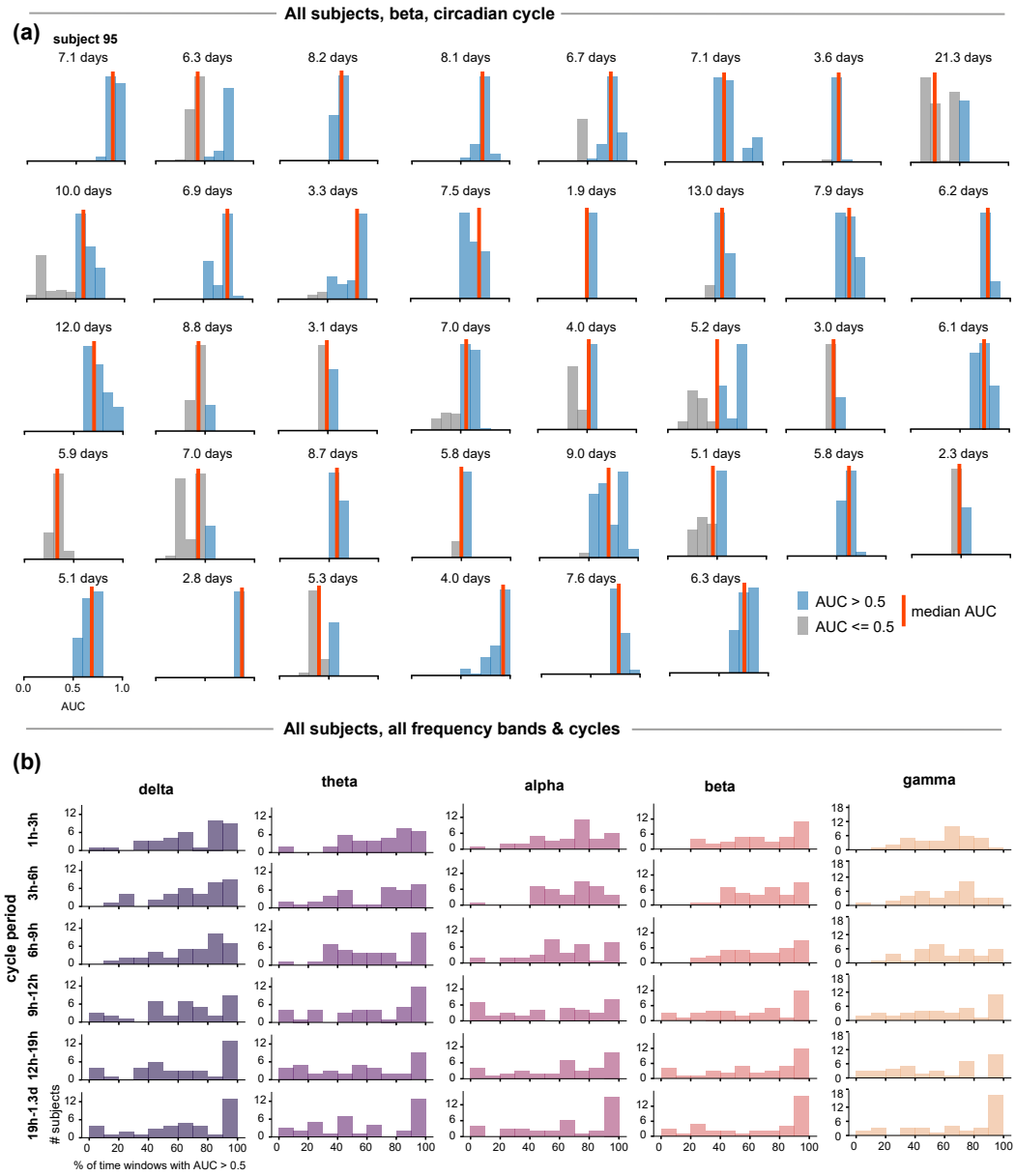

Figure 4.6 **AUC variability across subjects captured by rolling median for all frequency bands and cycles**. a) Distribution of AUC computed between SOZ and non-SOZ areas in each patient's iEEG recording for the circadian cycle in beta frequency band. Similar representation for example subject 95 is shown in Fig. 4.5e. Within each histogram, bars are coloured with blue for AUC values greater than 0.5 and grey for values lower than or equal to 0.5. Median AUC is marked with a vertical orange color line. b) Representation of the percentage of time windows with AUC > 0.5 across subjects for each frequency band and cycle. Each plot is a histogram of the % of time segments with AUC > 0.5 across subjects in the corresponding cycle and frequency band. The height of the bars within each histogram corresponds to the number of subjects.

varied low-level associations in most cycles without a consistent direction across all cases (Suppl. Fig. 4.11). When we analyzed the relationship between the magnitude of cycles in pathological brain regions and the duration of epilepsy, we identified a weak to moderate positive association in certain cycles and frequency bands (Suppl. Fig. 4.11). It is possible that specific cycles over distinct timescales have been partially restored with the passage of time and are more pronounced in pathological areas. As the disease progresses, structural and functional deficits might impact specific cycles at different stages throughout its course. Moreover, our results would provide more meaningful insights if this analysis were to be replicated on a larger cohort of patients with varying durations of epilepsy.

Other factors, such as age and gender, may also contribute to potential changes in cycles. For example, it is well established that circadian cycles exhibit alterations as we age (Chen et al., 2016; Cornelissen and Otsuka, 2017). It might be possible that the effect of alteration might also change with age. In our cohort, we observed reductions in cycles at the ultradian and circadian timescales that were similar between men and women (Suppl. Fig. 4.14), suggesting that altered cycles in patients with epilepsy may not be attributed to gender-related hormonal mechanisms. However, it is still plausible that cycles of different timescales exhibit variations between males and females, although some alterations may be shared across both genders. Regarding age, we found a weak to moderate negative correlation between the degree of cycle alterations and age across most cycles and frequency bands. Additionally, we identified a positive association between the magnitude of cycles in pathological tissue and age in specific cycles and frequency bands (Suppl. Fig. 4.10). To obtain more robust results, future research should investigate further the association between alterations in cycles and gender or age with using a larger cohort of patients capturing a wider age range.

4.4 Discussion

We analysed cycles in subject-specific interictal relative band power patterns over time using intracranial continuous EEG recordings and found that biological rhythms exist in the brain on a range of timescales, from hours (ultradian) to days (infradian). Notably, when analysing the magnitude of these biological rhythms in various brain regions,

we found diminished circadian and ultradian rhythms in regions that were identified as pathological, suggesting that the expression of cycles is altered in brain regions linked to the pathology. Furthermore, we have shown that this effect remains relatively consistent over time, indicating that it is not a transient state. Instead, it may serve as an indicator of pathological brain activity.

These findings hold potential implications for clinical practice, particularly in the diagnosis of brain disorders. Our study has demonstrated the association between biological rhythms and pathology, and importantly, we have observed the persistence of diminished cycles over time in patients with focal refractory epilepsy. This temporal stability of diminished cycles could serve as an effective diagnostic marker for epilepsy, indicating both the presence of pathological brain activity and the consistency of this trait. We further observed a consistent diminished effect in cycles across various epilepsy etiologies (pathologies) (Suppl. Fig. 4.13) or epilepsy syndromes (Suppl. Fig. 4.8). These findings suggest that diminished ultradian and circadian cycles could serve as a potential diagnostic marker for focal epilepsy, irrespective of the underlying pathology or specific pathological brain area. However, it is important to note that replicating this analysis with a larger sample size in specific pathologies would provide more concrete results. Additionally, further exploration is required to determine whether this trait can be utilised for localising the epileptogenic tissue. When comparing our quantification of cycle alterations (AUC) between patients who are seizure-free and those who are not, we did not observe substantial differences between the two surgical groups (Suppl. Fig. 4.7), suggesting that diminished cycles were apparent in all subjects in our cohort. Diminished cycles might therefore be a sensitive, but not specific, marker of pathology, and not necessarily epileptogenic pathology.

Our results do not imply a causal relationship between altered cycles and pathology, but rather support an association between the two in epilepsy. However, identifying a causal connection between altered cycles and pathology remains a challenge. Recent studies have suggested that disorganised circadian rhythms may directly contribute to promoting seizures, particularly in absence epilepsy (Smyk and van Luijtelaar, 2020). Additionally, in individuals with Parkinson's disease, sleep-wake disturbances often precede the onset of motor or cognitive symptoms (Rothman and Mattson, 2012). Future research should focus on exploring the causal relationship between disruptions of

biological rhythms and brain disorders through experimental approaches. For example, conducting laboratory experiments in humans where the natural sleep-wake and melatonin rhythms are intentionally disturbed can help assess the impact of circadian rhythm on clinical symptoms associated with brain disorders. Understanding the causal relationship between altered biological rhythms and brain disorders is crucial for identifying the underlying mechanisms contributing to the manifestation or progression of these disorders. Moreover, if a causal link is established, these temporal patterns can potentially serve as effective diagnostic markers for the diseases.

Even though identifying a causal relationship might enhance altered biological rhythms as a potential diagnostic marker, evidence for a bidirectional relationship between the two cannot be disregarded. The relationship between altered biological rhythms and neurological disorders is primarily bidirectional. On one hand, neurological disorders such as epilepsy, Parkinson's disease, and Alzheimer's disease can disrupt the normal functioning of biological rhythms, including sleep-wake cycles, circadian rhythms, and other physiological oscillations. These disruptions can manifest as sleep disturbances (Bonilla-Jaime et al., 2021; Moran et al., 2005; Rothman and Mattson, 2012), abnormal hormone secretion (van Campen et al., 2016; Pritchard III, 1991; Den Heijer et al., 2018; Videnovic and Zee, 2015), and impairments in various brain and body functions (Benca et al., 2009). On the other hand, disrupted biological rhythms themselves can contribute to the development or exacerbation of neurological disorders. Irregular sleep patterns, for example, have been associated with increased susceptibility to more severe seizures in epilepsy patients (Bonilla-Jaime et al., 2021) and can worsen cognitive impairments in individuals with Alzheimer's disease (Moran et al., 2005). Therefore, unravelling the bidirectional relationship between altered biological rhythms and neurological disorders is crucial for developing effective treatment strategies and improving the well-being of individuals affected by brain disorders.

We found diminished cycles in pathological tissue, and whether chronotherapeutics can be effective treatments for brain disorders remains an open question. Alternative forms of chronotherapeutics may target directly altered biological rhythms by resetting them to their normal rhythmicity. One potential method is the utilisation of phototherapy, which has been widely employed to reset the circadian rhythm in both the central pacemaker and peripheral organs (Gronfier et al., 2007; Cuesta et al., 2017).

This form of therapy has shown effectiveness in improving sleep disturbances and rest-activity alterations associated with neurodegenerative disorders, such as Alzheimer's (Yamadera et al., 2000) and Parkinson's (Martino et al., 2018) diseases alleviating associated symptoms. The realignment of circadian clocks can also be achieved through hormone supplementation, such as melatonin, for various brain disorders (Sánchez-Barceló et al., 2011). In the case of epilepsy, melatonin administration may potentially reduce the severity of seizures due to its anticonvulsant properties (Molina-Carballo et al., 2007). Additionally, external behavioural adaptations such as exercise have been reported to affect the circadian pacemaker, and thus help individuals adjust to a normal sleep-wake schedules (Barger et al., 2004). Lastly, time-dependent neurostimulation delivery systems can be utilised for certain brain disorders (Jonsdottir et al., 2004). For example, in epilepsy (Bergey et al., 2015) a targeted localised neurostimulation can be applied specifically at the pathological tissue during nighttime or daytime depending on whether the seizures are nocturnal or diurnal. This approach aims to prevent disturbances in the sleep-wake cycle and gradually restore the circadian clock. Therefore, chronotherapeutics that focus on rectifying dysfunction in biological rhythms may be a promising avenue for treatment of various brain disorders, including epilepsy.

One limitation of our work is the lack of information regarding the doses of anti-epileptic medication administered. In this chapter, we examined individuals diagnosed with refractory focal epilepsy who underwent various treatments with anti-epileptic drugs as part of their pre-surgical evaluation. Information about the exact timing and dose of anti-epileptic drugs was not available for further analysis. Previous studies on canine epilepsy have indicated that changes in anti-epileptic medication do not drive the various seizure cycles observed, including circadian, weekly, and monthly patterns (Gregg et al., 2020). However, it has also been demonstrated that decreased medication dose increases the likelihood of seizures. More severe seizures, like focal seizures that progress into bilateral tonic-clonic seizures, become more prevalent when the dose of antiepileptic drugs is reduced (Pensel et al., 2020). Future research should explore the relationship between the timing of drug administration and cycles, aiming to optimise the differential dosing of drugs to alleviate the effect in biological rhythms associated with anti-epileptic drugs leading to more effective time-adaptive interventions for patients with brain disorders.

In summary, our research has demonstrated that pathological tissue reveals diminished circadian and ultradian cycles, as observed through interictal relative band power in subject-specific intracranial continuous EEG recordings. This outcome suggests a connection between altered cycles and the presence of pathology. Importantly, this alteration in cycles remains consistent over time, indicating that it may not be a temporary state that could be attributed to irregular biological rhythms associated with specific changes in brain activity. Instead, it could potentially serve as an indicator of pathology. Recognising the association between altered endogenous cycles could pave the way for the development of diagnostic tools or alternative therapies capable of restoring normal intra-body rhythms in patients with brain disorders such as epilepsy.

4.5 Supplementary

4.5.1 Imputation of missing data

To facilitate further analysis, we employed imputation techniques to fill any gaps in the relative log band power of each ROI before proceeding with cycle extraction at various timescales. However, we did not utilise imputed data for the final analysis. We identified missing blocks within each frequency band and imputed them accordingly. If a missing block had a size equal to one, we replaced it with the mean of the value before and after the block. For missing blocks larger than one, we identified the surrounding segments of equal length before and after the block. When the preceding segment was smaller than the missing block or the missing blocks were at the start of the recording, we used only the following segment for imputation. We interpolated the data of missing blocks using the mean of the adjacent segments and added Gaussian noise with a mean of zero and standard deviation of 60% of the standard deviation of the surrounding segments. Any missing data present in the adjacent segments was disregarded. The final values used for analysis were the interpolated ones with added Gaussian noise.

4.5.2 Relation to patients' metadata

For the subsequent analysis in the following sections we used AUC values determined as level of distinguishability of cycle between SOZ and non-SOZ in terms of the average power of the cycle (see Section 4.2.4). As information about SOZ was not available for one subject, the total number of subjects included was 38.

Distribution of AUC by surgical outcome

We investigated whether the diminished effect of any cycle can localise epileptogenic tissue by identifying whether the AUC can distinguish patients by their surgical outcome (Fig. 4.7). For each cycle and frequency band, the distributions of AUC between seizure free and not seizure free patients was similar, except for the 6h-9h ultradian cycle in alpha band (p-value = 0.02, two-sided Wilcoxon rank-sum test).

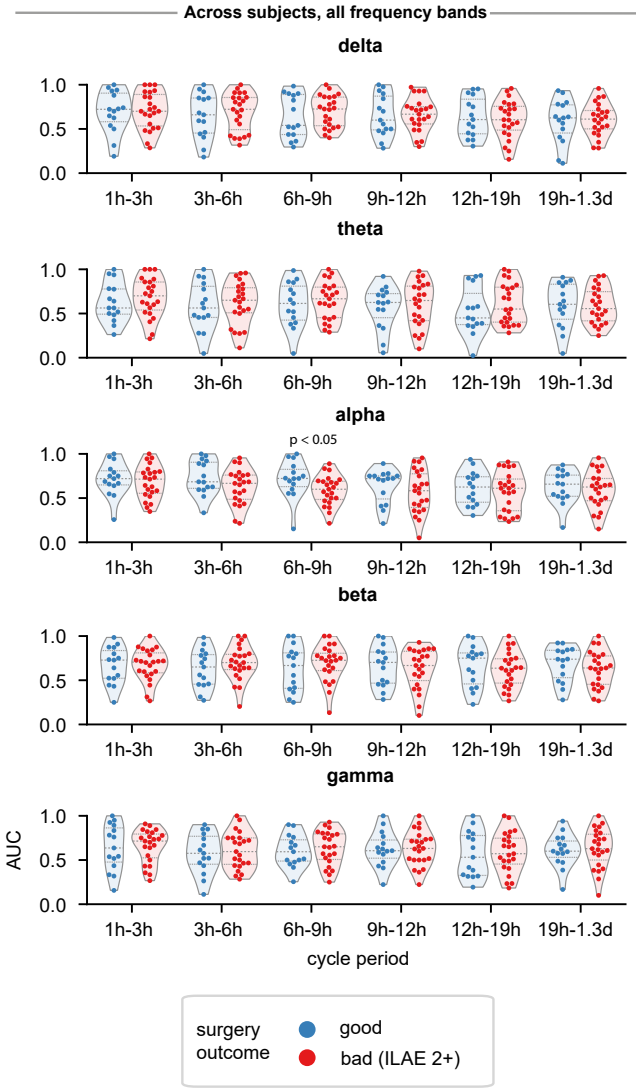

Figure 4.7 **Distribution of AUC values by surgical outcome.** Comparison of AUC distributions between seizure free (good; ILAE1) and not seizure free (bad; ILAE2-5) after surgery for each frequency band and cycle. Each plot corresponds to a frequency band and the AUC distributions are shown as violin plots comparing the good and bad outcome patients are shown for each cycle. Within each violin plot, the dashed lines represent the quartiles of the corresponding AUC distribution.

Distribution of AUC values by epilepsy syndrome

In order to evaluate whether the diminished effect of ultradian and circadian cycles is not a characteristic of a specific epilepsy syndrome, but rather a pattern in cycles

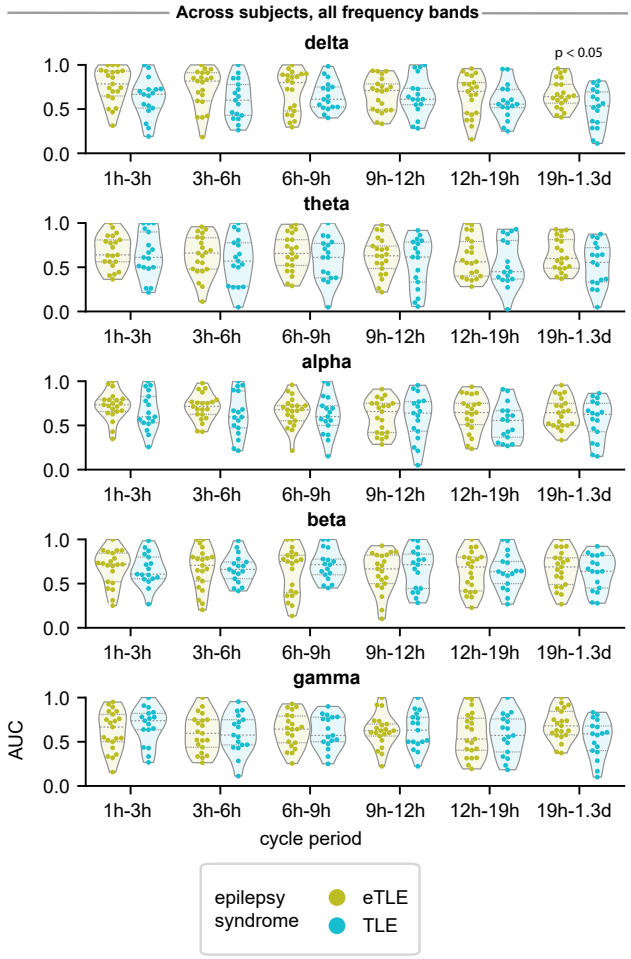

Figure 4.8 **Distribution of AUC values by epilepsy syndrome.** Comparison of AUC distributions between eTLE and TLE patients for each frequency band and cycle. Each plot corresponds to a frequency band and the AUC distributions are shown as violin plots comparing the eTLE and TLE patients for each cycle. Within each violin plot, the dashed lines represent the quartiles of the corresponding AUC distribution.

across all patients with focal epilepsy, we compared the distributions of AUC values between temporal lobe epilepsy (TLE) and extra temporal lobe epilepsy (eTLE) patients (Fig. 4.8). TLE and eTLE patients did not differ in terms of the diminished affect in SOZ for any cycle and frequency band, except for the circadian cycle in delta band (p-value = 0.04, two-sided Wilcoxon rank-sum test).

Association between AUC values and age

To investigate the potential relationship between the degree of reduced cycles and the age of patients, we measured the correlation between the AUC and age for each cycle and frequency band across all participants.

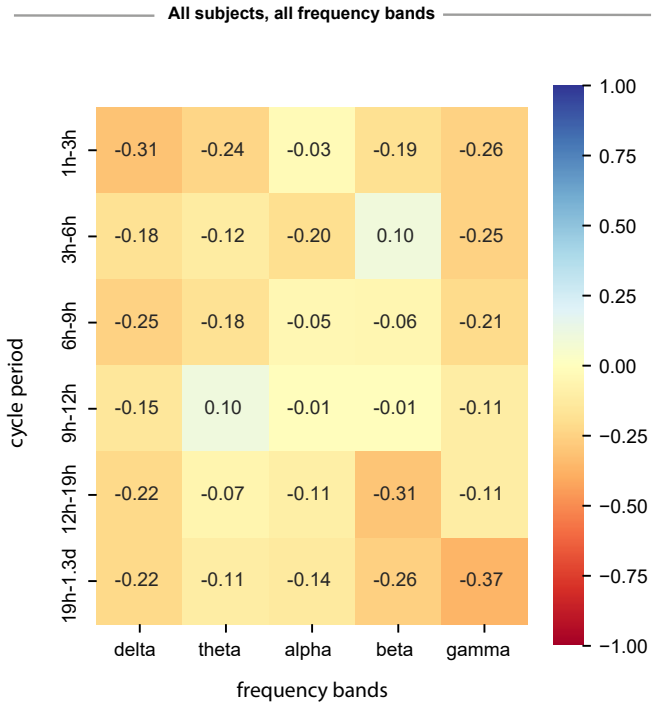

Figure 4.9 **Association between AUC and age.** Heatmap representing the Pearson's correlation coefficient between AUC and age across all subjects for all cycles and frequency bands. Each entry corresponds to one cycle and frequency band.

Figure 4.9 presents the Pearson's correlation coefficient between AUC and age, encompassing all cycles and frequency bands. In general, we observed a weak to moderate negative correlation between AUC and age across most cycles and frequency bands. This suggests that the extent of diminished cycles may be less prominent in older individuals.

Association between power of cycles in SOZ and age

To assess the relationship between the intensity of cycles in the pathological regions of the brain and the age of patients, we measured the correlation between the average power and age across all individuals. This analysis was conducted for each cycle and frequency range within the SOZ.

Figure 4.10 **Association between power of cycles in SOZ and age.** Heatmap illustrating the Pearson's correlation coefficient between the average cycle power in the SOZ and age, encompassing all participants in all cycles and frequency bands. Each cell within the heatmap corresponds to a specific cycle and frequency band combination.

The correlation between the average power of cycles in the SOZ and age is depicted in Figure 4.10 using Pearson's correlation coefficient. The findings indicate that, on the whole, there is a weak to moderate positive correlation between the power of cycles in the SOZ and age across most cycles and frequency bands. This suggests that the magnitude of cycles in the SOZ tends to increase with age in certain frequency bands, such as theta, beta, and gamma bands for ultradian cycles spanning 1 to 3 hours and 3 to 6 hours, as well as in the alpha band for cycles spanning 9 to 12 hours and 12 to

19 hours.

Association between AUC and duration of epilepsy

To investigate the potential relationship between the degree of weakened cycles and the duration of epilepsy in patients, we measured the correlation between the AUC and epilepsy duration for each cycle and frequency band across all participants.

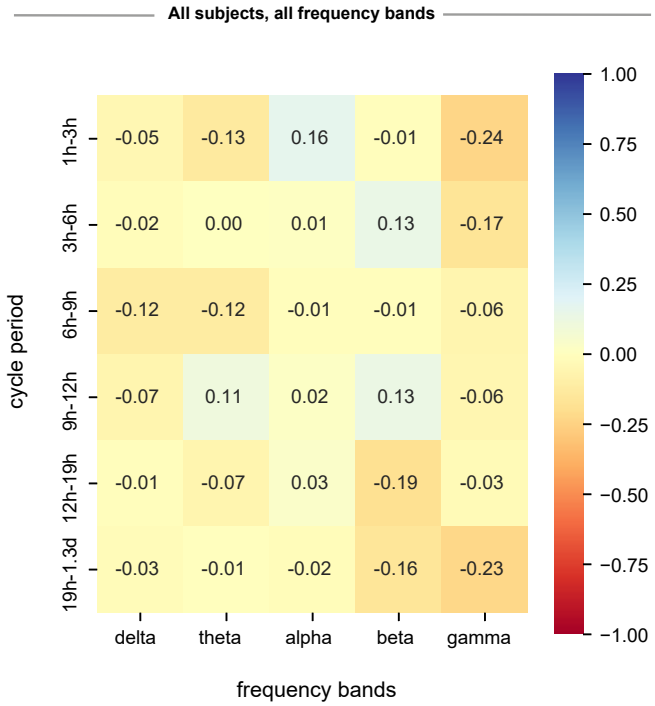

Figure 4.11 **Association between AUC and duration of epilepsy.** Heatmap displaying the Pearson's correlation coefficient between the AUC and the duration of epilepsy for all cycles and frequency bands across all subjects. Each entry in the heatmap corresponds to a specific cycle and frequency band combination.

Fig. 4.11 presents the Pearson's correlation coefficient between AUC and epilepsy duration, encompassing all cycles and frequency bands. In general, we observed a weak to moderate positive or negative correlation between AUC and epilepsy duration across most cycles and frequency bands. This suggests that the extent of diminished cycles may be less or more prominent in specific cycles and frequency bands as the disease progresses.

Association between power of cycles in SOZ and duration of epilepsy

To assess the relationship between the magnitude of cycles in the pathological regions of the brain and the duration of epilepsy in patients, we measured the correlation between the average power and epilepsy duration across all individuals. This analysis was conducted for each cycle and frequency band within the SOZ.

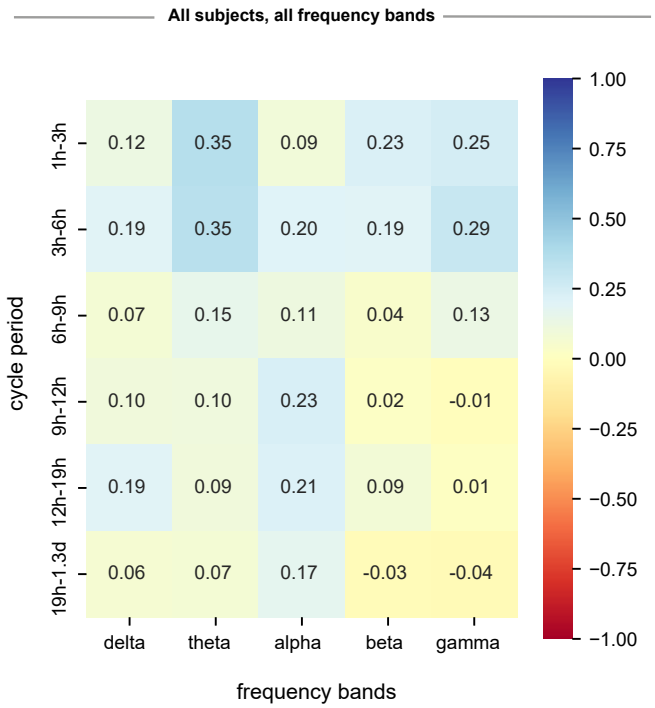

Figure 4.12 **Association between power in SOZ and duration of epilepsy.** Heatmap representing the Pearson's correlation coefficient between the average cycle power in SOZ and the duration of epilepsy, including all participants in all cycles and frequency bands. Each cell in the heatmap corresponds to a specific combination of cycle and frequency band.

The correlation between the average power of cycles in the SOZ and duration of epilepsy is depicted in Fig. 4.12 using Pearson's correlation coefficient. Overall, we observed a weak to moderate positive correlation between the power of cycles in the SOZ and the duration of epilepsy across most cycles and frequency bands. This suggests that the magnitude of cycles in the SOZ tends to increases as epilepsy progresses, especially in ultradian cycles in specific frequency bands. The circadian cycle depicted a weak positive correlation only in the alpha band.

Distribution of AUC by pathology

To evaluate the degree of diminished cycles among patient groups with different pathological conditions, we examined the distribution of AUC between these groups. These findings were derived from the evaluation of postoperative tissue samples.

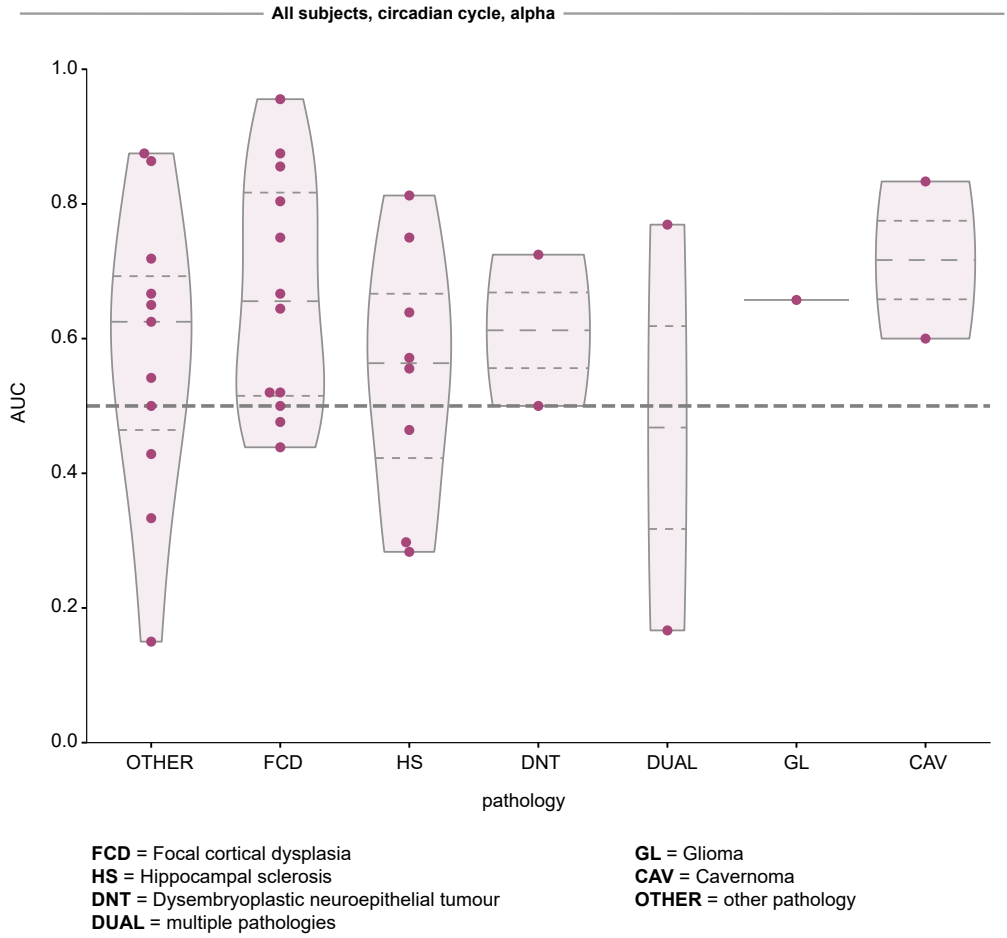

Figure 4.13 **Distribution of AUC by pathology.** Distributions of AUC for groups of patients associated with different pathological post-operative findings for the circadian cycle in alpha band. Within each violin plot, the dots correspond to the AUC value of one subject and the dashed lines represent the quartiles of the corresponding AUC distribution.

Fig. 4.13 illustrates the AUC distribution for patients with different pathology findings for the circadian cycle in the alpha band. Overall, the AUC is greater than 0.5 for all subjects, regardless of the etiology of their epilepsy. However, it should be noted that

for certain pathological findings, the sample size was insufficient to draw any conclusive results. Similar observations were made across all cycles and frequency bands.

Distribution of AUC values by gender

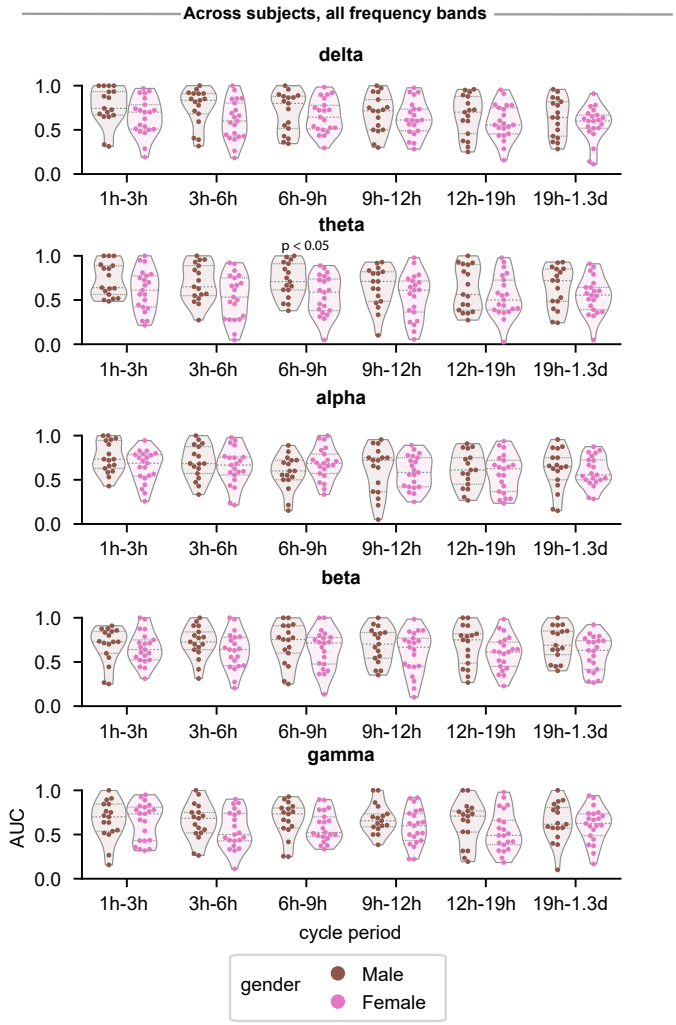

Figure 4.14 **Distribution of AUC values by gender.** Comparison of AUC distributions between male and female patients for each frequency band and cycle. Each plot corresponds a frequency band and the AUC distributions comparing the male and female patients are shown as violin plots for each cycle. Within each violin plot, the dashed lines represent the quartiles of the corresponding AUC distribution.

To determine whether the diminished effect of ultradian and circadian cycles differs

by gender, we compared the AUC distributions between men and women (Fig. 4.14). The distributions of AUC values were similar between men and women for all cycles and frequency bands, except the 6h-9h ultradian cycle in theta band (p-value = 0.02, two-sided Wilcoxon rank-sum test).

Chapter 5. Discussion

Contents

5.1 Contributions of This Thesis

Epilepsy is recognised as a dynamic disease, where both seizure susceptibility and seizure characteristics themselves change over time. Specifically, we recently quantified the variable electrographic spatio-temporal seizure evolutions that exist within individual patients (Schroeder et al., 2020). This variability appears to follow subject-specific circadian, or longer, timescale modulations. Furthermore, other seizure features, such as seizure severity, exhibit temporal changes; seizure severity change from one seizure to the next within individual people with epilepsy (Lamberts et al., 2013; Jobst et al., 2001; Peng et al., 2017; Gascoigne et al., 2023). It is unclear if and how seizure evolutions and seizure severity are modulated over multiple (longer) timescales. Characterising variability in seizure evolutions and severity over time could lead to tailored treatments. It is therefore important to know whether continuously-recorded interictal iEEG features can capture signatures of these modulations over different timescales.

Importantly, changes in brain activity captured by continuous iEEG recordings might reflect biological rhythms in brain function. A variety of intra-body physiological and behavioural functions are entrained to endogenous and exogenous rhythms, from ultradian to circadian. While a variety of neurological disorders, such as epilepsy (Li et al., 2017; Matos et al., 2018; Wallace et al., 2018) have been linked to the dysfunction of those biological rhythms (Logan and McClung, 2019), it is unclear whether the rhythmicity is functionally diminished in pathological tissue in patients with epilepsy.

In this thesis, I first explored the temporal variability of seizure evolutions and seizure severity using continuous iEEG recordings (Chapters 2 & 3). Then, I investigated whether temporal patterns obtained from iEEG features exhibit alterations in pathological tissue compared to healthy tissue (Chapter 4). Taking all this together, I addressed the following open questions:

1. How do seizure dynamics change over time? Does variability in seizure dynamics evolve in multiple timescales?

2. How do other seizure features, such as seizure severity, evolve over time? Does seizure severity reveal a rhythmic organisation?

3. Is the pathology associated with the alteration of cycles in brain activity?

In Chapter 2, I analysed continuous intracranial electroencephalographic (iEEG) recordings from video-telemetry units and found fluctuations in iEEG band power over timescales ranging from minutes up to 12 days. As expected and in agreement with previous studies (Karoly, Rao, Gregg, Worrell, Bernard, Cook and Baud, 2021), I found that all subjects show a circadian fluctuation in their iEEG band power. I additionally found other fluctuations of similar magnitude on subject-specific timescales. Importantly, I found that a combination of these fluctuations on different timescales can explain changes in seizure evolutions in most subjects above chance level. These results suggest that subject-specific fluctuations in iEEG band power over timescales of minutes to days may serve as markers of seizure modulating processes.

In Chapter 3, I analysed iEEG recordings of at least one day obtained from patients with focal refractory epilepsy. I identified cycles on timescales of hours to days embedded in long-term iEEG band power and associated them with seizure severity, which I approximated using seizure duration. In order to quantify these associations, I created linear-circular statistical models of seizure duration that incorporated different band power cycles within each subject. In most subjects, seizure duration was weakly to moderately correlated with individual band power cycles. Combinations of multiple band power cycles significantly explained most of the variability in seizure duration. Specifically, we found 70% of the models had a higher than 60% adjusted R^2 across all subjects. From these models, around 80% were deemed to be above chance-level (p-value ≤ 0.05) based on permutation tests. Models included cycles of ultradian, circadian and slower timescales in a subject-specific manner. These results suggest that seizure severity, as measured by seizure duration, may be modulated over timescales of minutes to days by subject-specific cycles in interictal iEEG signal properties. Thus, these cycles likely serve as markers of seizure modulating processes.

In Chapter 4, I used intracranial continuous EEG recordings over multiple days in patients with focal refractory epilepsy and demonstrated that biological rhythms on circadian and ultradian timescales exist in the brain. Interestingly, when analysing the magnitude of these biological rhythms in different brain regions, I found that circadian and particularly multiple ultradian rhythms are diminished in regions that were deemed pathological. Within each patient, the level of alteration remained relatively stable over time. These findings suggest that brain pathology alters biological rhythms on circa-

dian and ultradian timescales, and this alteration is likely to be a trait of pathological activity, and not a transient state.

Overall, in this thesis, I have identified ultradian, circadian and slower fluctuations captured in interictal iEEG features by analysing the entire length of iEEG recordings from patients with refractory focal epilepsy. Importantly, when analysing the association between those fluctuations and seizure features, such as seizure evolutions (Chapter 2) and severity (Chapter 3), I demonstrated that variability in these features can be explained by a combination of multiscale fluctuations in a subject-specific manner. Finally, I evaluated that those fluctuations have different characteristics in brain regions that are linked to the pathology (Chapter 4). The outcomes of this work provide some evidence that not only seizure occurrence, but also other seizure features follow multiscale temporal fluctuations, suggesting that seizures and their characteristics are modulated by time-varying processes. These modulatory processes might include physiological and behavioural factors that are reflected in biological rhythms. Thus, the findings in Chapter 4, diminished ultradian and circadian fluctuations in epileptogenic tissue, contribute further to a better understanding of the characteristics of those fluctuations across different brain regions, both pathological and healthy. For the remaining chapter, I will discuss limitations of the current work, and various recommendations for future research.

5.2 Learning the Temporal Structure of Epilepsy using Traits from Diverse Physiological Systems

Cycles obtained from interictal iEEG features have been associated with seizure features, such as seizure occurrence (Baud et al., 2018; Karoly et al., 2016) and seizure evolutions (Schroeder, Karoly, Maturana, Panagiotopoulou, Taylor, Cook and Wang, 2022). Our work contributes also to this growing field with evidence of cyclical patterns related to seizure network evolutions and seizure duration (Chapters 2 & 3). However, other modalities might be adequate for capturing cycles of similar timescales. Such cycles have been identified from physiological signals of autonomic nervous system function (heart rate variability) (Karoly, Stirling, Freestone, Nurse, Maturana, Halliday, Neal, Gregg, Brinkmann, Richardson, Gerche, Grayden, D'Souza and Cook, 2021;

Gregg et al., 2023), electrodermal activity (Gregg et al., 2023), and body temperature (Gregg et al., 2023) have been linked to seizure occurrence. Studies have indicated a correlation between epilepsy and alterations in autonomic activity measured using heart rate variability which mirrors how the autonomic nervous system affects the heart (Opherk et al., 2002; Nei et al., 2000). Furthermore, sleep deprivation (Shouse et al., 1996), and stress (Haut et al., 2003; Temkin and Davis, 1984) might be triggering factors for ictogenesis.

Importantly, various potential indicators of physiological rhythms, such as heart rate, sleep quality metrics, body temperature, blood oxygen levels, electrodermal activity, and weather conditions (Gregg et al., 2023; Dumanis et al., 2017) can be easily obtained using wearable devices and mobile apps for an extended period of time (even for years) giving the opportunity to investigate a wide spectrum of timescales ranging from seconds to years. The cyclical patterns of these measurements can be potential biomarkers of several seizure features, such as seizure occurrence, seizure spread, seizure evolutions and seizure severity.

Apart from currently available wearable biosensors, future work could explore a number of sensors, such as sweat-sampling sensors capable for monitoring hormonal and metabolic factors (Gualandi et al., 2016; Kim et al., 2015). Such factors linked to epilepsy might be melatonin (Hofstra and de Weerd, 2009), cortisol (van Campen et al., 2016), reproductive hormones (Herzog et al., 1997), glucose (Schauwecker, 2012), and others (Brinkmann et al., 2021; Aminoff et al., 1984). Those measurements can be available through non-invasive wearable devices using sweat-sampling sensors (Martín et al., 2017) capable of capturing cyclical characteristics over days or weeks from long-term recording. Using those measurements we can utilise statistical models or machine learning approaches (Nasseri et al., 2021) in real-time for forecasting an impending seizure or different seizure properties, such as duration or severity of an imminent seizure.

5.3 Incorporating Spatial Information

Obtaining details about the spatial coverage and positioning of the electrodes would provide valuable insights from a clinical standpoint, as it would enable us to explore the

correlation between the location of temporal fluctuations and the epileptogenic zone in focal epilepsies. Our results (Chapter 2) indicated that different frequency bands play a comparable role in the circadian fluctuation of iEEG band power, with some subject-specific patterns also observed. Nonetheless, it is worth noting that we conducted our analysis across all dimensions of our data. Moreover, we found that slower fluctuations (multi-day fluctuations and slow trends) tended to be the result of changes in specific subsets of channels, whereas faster (circadian and ultradian) fluctuations were more evenly distributed across all channels. However, our study was limited in terms of spatial coverage of iEEG and the patient-specific electrode layout, which make it challenging to compare band power fluctuation patterns across individuals. Future research should consider the spatial location of iEEG channels and employ an iterative combination of dimensionality reduction and empirical mode decomposition to identify components and their contributions for each IMF in each dimension.

Establishing a potential association between the temporal patterns arising from specific brain regions and seizure features, such as seizure evolutions and severity, may inform novel treatment strategies. For example, identifying temporal patterns of seizure severity in various brain areas within individual subjects could lead to the specific biological drivers of these detected fluctuations and may aid new treatments that minimise seizure severity. Spatial patterns of various iEEG features, such as iEEG band power (Panagiotopoulou et al., 2022), high frequency activity (Gliske et al., 2018), and interictal spike rate (Conrad et al., 2020) change over time. Interestingly, band power changes have been associated with seizure spread in areas outside of the seizure focus, suggesting a widespread activity might manifest more severe seizures, such as secondarily generalised ones (Naftulin et al., 2018). Cortical areas such as frontal and temporal lobe have been associated with the phenomenon of seizure clustering (Ferastraoaru et al., 2016), yielding to more severe seizure manifestations, as seizure clusters are associated with an increased risk of prolonged seizures, status epilepticus (Haut et al., 2005), and/or postictal morbidity, such as psychosis (Rose et al., 2003). Interestingly, seizure clustering reveals a predisposition on distinct circadian cycles/signatures between frontal and temporal lobe seizures, as it occurs at different times between the two sites (Pavlova et al., 2012). Future work can extend further our work in seizure evolutions (Chapter 3) and severity (Chapter 4) by disentangling the spatio-temporal representation of cycles

embedded in interictal iEEG features in order to identify oscillatory activity of specific brain regions that could explain variability in seizure severity.

Spatial information of cycles in brain activity can also be useful for localising the pathology. Identifying irregular patterns in cycles of various timescales might help in localising the pathological tissue. One idea would be to explore cycles over multiple timescales captured in iEEG band power from brain regions that form healthy tissue from a large cohort of subjects constructing a normative map of the band power cycles. Then, capturing the changes on those cycles in brain regions classified as epileptogenic compared to this normative map (Bernabei et al., 2022; Taylor et al., 2022; Groppe et al., 2013) would help us better identify brain areas with abnormal activity. It might be that different cycles exhibit abnormal signatures in different brain regions and those differences may be quantified as changes in various properties of the cycle, such as alterations in phase, amplitude and duration. In Chapter 4, we touched on this idea by looking at the extent of alteration in various cycles (mostly ultradian and circadian) as expressed in terms of power obtained from pathological tissue, either later surgically resected tissue or brain areas identified by clinicians as seizure onset zone. Future work can further investigate constructing normative maps that describe cyclical properties of brain activity in healthy tissue as those can be quantified using continuous long-term EEG features, such as band power and network measures.

5.4 Importance of Ultradian cycles

It is important to note that the presence of ultradian cycles in physiology and epilepsy might imply a link between biological driver(s) and seizure-modulating processes. Ultradian cycles are important in various biological processes, including cycling of sleep states, the basic rest-activity cycles occurring both in sleep and wakefulness (Kleitman, 1982), and brain activity in healthy individuals during wakefulness (Kaiser, 2008; Chapotot et al., 2000). In this thesis, I found ultradian cycles associated with seizure evolutions (Chapter 2) and durations (Chapter 3), as well as the pathology (Chapter 4). There is a critical need to better understand the role of ultradian cycles in seizure modulating processes, as this will enable the development of novel treatment strategies that could minimise the seizure spread, duration, or severity and therefore the clinical

impact of seizures.

Identifying the exact biological factors underlying ictogenesis and epileptogenesis involves a combination of different data collection and experimental techniques. One idea would be to collect simultaneously EEG and actigraphy data from individuals with epilepsy outside of the clinic. EEG data might be suitable for that purpose, as they can be collected for extended periods of time while the patient is engaging in their daily activities. Likewise, actigraphy data, which involves wearing a device that records movement and activity, can provide information about temporal patterns during sleep and activity levels in a non-clinic environment. Investigating the association between ultradian cycles in sleep and wakefulness and seizure features might lead to identification of the exact physiological processes that trigger a seizure or contribute to more severe symptoms. Future work is needed for linking ultradian cycles to their biological driver(s).

5.5 Chronobiology and Epilepsy

Epileptic seizures exhibit patterns that are not random and likely follow multiscale fluctuations, such as ultradian, circadian and multidien rhythms which may be related to day/night cycles, wakefulness and sleep (Shouse et al., 1996; Jin et al., 2020), time of day, and internal biological clocks (Hofstra and de Weerd, 2008, 2009). These patterns, (Langdon-Down and Russell Brain, 1929; Gowers, 1885; Karoly, Rao, Gregg, Worrell, Bernard, Cook and Baud, 2021; Baud et al., 2018) and importantly their significance in the treatment of seizures, have been identified for several decades (Ramgopal et al., 2013). Recently, better methods of characterising day and nighttime patterns of different epilepsy types have become available, and it is now possible to distinguish between external regulators, such as time of day and internal markers, such as intra-body biological rhythms. Improved ways to quantify and record not only seizure timing, but also other varying seizure properties, such as seizure spread, severity, duration, and identify internal clocks are needed for advancing this area of research. Understanding a person's propensity to seize at certain times and importantly capturing the severity associated with their seizure may allow us to develop personalised profiles of seizure features that could guide treatment.

Medications may be adjusted in time for a number of treatment strategies in patients with epilepsy. For example, vagus nerve (Fisher et al., 2021), deep brain or cortical stimulation (Lin and Wang, 2017), and meal timing of diet treatments (i.e. ketogenic diet) (Fenoglio-Simeone et al., 2009). Treating seizures by the clock falls under the area of chronobiology and has been termed chrono-epileptology (Loddenkemper, 2012). Chrono-epileptology has the potential not just to facilitate the modification of treatments during periods of heightened seizure susceptibility by adjusting the dose level based on the propensity of specific seizure type or severity to specific times of day (Guilhoto et al., 2011; Yegnanarayan et al., 2006), but also enable the adjustment of "zeitgebers" – external cues (e.g. temperature or blue light) that regulate the body's internal clock (Re et al., 2020). Future research will need to explore additional epilepsy biomarkers, the role of sleep, the interaction with different seizure type or severity, and whether resetting internal clocks can advance our understanding of epileptogenesis and hence effectively treating epilepsy.

5.6 Limitations for Future Work

5.6.1 Antiepileptic seizure medication

Patients included in the thesis suffered from refractory epilepsy and hence received a number of different drugs during treatment, as part of the pre-surgical evaluation. In the analyses conducted for all research chapters (Chapters 2, 3 & 4), I did not incorporate information regarding drug doses, as medication records were not available. Notably, prior studies on canine epilepsy showed that various seizure cycles (circadian, weekly and monthly) are not driven by the changes in anti-epileptic medication (Gregg et al., 2020; Schroeder et al., 2020). It is likely that the various periodicities of seizure activity might not be induced by changes in anti-seizure drug doses, but rather influenced by endogenous time-varying factors. However, it has been shown that changes in medication increase seizure likelihood; focal seizures which evolve into tonic-clonic seizures become more prevalent when antiepileptic drugs are reduced (Pensel et al., 2020). Also, medication affects cortical excitability (Kimiskidis et al., 2006; Cantello et al., 2006) and increasing cortical excitability might be related to higher seizure risk (Meisel et al.,

2015) and also contributes to seizure spread (Badawy et al., 2009). Sleep also modulates cortical excitability (Usami et al., 2015) and sleep has been linked to epilepsy (Jin et al., 2020). In future work, incorporating personalised medication records could unravel the behaviour of rhythms in seizure features with respect to the changes in drugs and/or doses. It might be that a change in medication dose has an impact on other biological mechanisms that are reflected in certain characteristics of rhythms.

5.6.2 Approaches for capturing multiscale fluctuations in time series

In Chapters 2 and 3, I derived band power fluctuations on different timescales using EMD. It is a data-adaptive and empirical method capable of extracting fluctuations on different timescales without relying on assumptions of local stationarity, linearity, or specific basis functions, and for these reasons it is preferable for our application. EMD has been widely applied in a range of scientific topics, such as geology (Battista et al., 2007), hydrology (Hu and Si, 2013), and neuroscience (Huang et al., 2013; Rojas et al., 2013) amongst many others. EMD is capable of identifying different timescales of fluctuations, without pre-determined basis functions. It also does not generate harmonics (as in Fourier or Wavelet-type approaches) of fluctuations, making the decomposed cycles easier to interpret. However, EMD also has some limitations. Most notably, the IMFs' timescales of fluctuations may overlap, which is known as 'mode mixing' (Ur Rehman and Mandic, 2011). EMD may also struggle to distinguish two distinct fluctuations that have very similar periods, and they may be merged into one IMF. Ongoing developments (Xue et al., 2015; Deering and Kaiser, 2005; Li et al., 2015) in this area may overcome these limitations. Future work should explore how to capture non-stationary (Kaplan et al., 2005), non-linear (Stam, 2005), and potentially hierarchical (Vidaurre et al., 2017) time-varying properties of the continuously recorded EEG.

5.6.3 Seizure severity as a multifactorial entity

In Chapter 4, I used seizure duration as a proxy for seizure severity. Duration of a seizure has been also used in other studies as a measure of severity (Gascoigne et al., 2023; Beniczky et al., 2020). Interestingly, seizure duration has been linked to seizure

types (Dobesberger et al., 2015; Jenssen et al., 2006; Afra et al., 2008; Kim et al., 2011): seizure types with more severe symptoms tend to last longer. For example, seizures that start in one area on one side of the brain (focal) and spread across the brain, recruiting additional brain areas (bilateral tonic-clonic) tend to have longer duration compared to those that do not spread further (Dobesberger et al., 2015; Kaufmann et al., 2020; Ferastraoaru et al., 2016). Longer seizures have also been associated with extensive periods of postictal suppression (an undisputed marker of seizure burden and severity) compared to short seizures (Payne et al., 2018). Thus, seizure duration might be an intermediate proxy of seizure severity.

Even though seizure duration is used as an intermediate proxy of seizure severity (Chapter 4), there are multiple aspects contributing to the extent to which a seizure is more severe or not that are not captured by seizure duration alone. A number of physiological markers of seizure severity (Gascoigne et al., 2023) can be associated with temporal patterns in band power. Future research may perform a methodological approach suitable for detecting interactions between multivariate datasets, such as Canonical correlation analysis (CCA) (Zhuang et al., 2020). One dataset can include all the measures of seizure severity and the other will consist of cycles over multiple timescales. Then, applying CCA one can identify the exact cycles each severity marker is associated with.

5.7 Conclusion

In focal epilepsy, there is a need for understanding the mechanisms underlying epilepsy and seizures for developing more effective treatments for patients that do not respond to anti-epileptic medication and are not eligible for surgery. Even though cycles in seizure timing have been studied for years (Griffiths and Fox, 1938; Langdon-Down and Russell Brain, 1929), it is only recently there has been growing evidence of cycles in brain dynamics (Baud et al., 2019; Leguia et al., 2021; Gliske et al., 2018; Proix et al., 2021) and further investigation into their relationship (Karoly, Goldenholz, Freestone, Moss, Grayden, Theodore and Cook, 2018; Baud et al., 2018; Leguia et al., 2021; Karoly, Rao, Gregg, Worrell, Bernard, Cook and Baud, 2021). Importantly, clues for cycles in other seizure features have just started to emerge (Schroeder et al., 2020; Gascoigne

et al., 2023), but the full range of cycles (timescales) and their association with temporal changes in brain activity is still an active area of research. Additionally, the link between biological drivers and temporal changes in brain activity needs further investigation. My work contributes to the growing literature of alternative treatment approaches in epilepsy that predict and react to the temporal changes of the disease. This new era of chronobiology in epilepsy has been termed chrono-epileptology (Loddenkemper, 2012) and is not only limited to adapting the timing of neurostimulation or drug dose administration based on the propensity of seizure type or severity, but also enabling the re-entrainment of the body's internal clocks.

Predicting when seizures happen has been an active and re-invigorated area of research for many years (Karoly et al., 2017; Cook et al., 2013; Freestone et al., 2017; Stirling et al., 2021). My work further contributes to being able to predict seizure dynamics, evolutions, seizure severity and symptoms. Additionally, the fluctuations in EEG features we and others investigate may also serve as biomarkers that can track treatment response, and therefore enable on-demand treatment options (Karoly, Rao, Gregg, Worrell, Bernard, Cook and Baud, 2021; Bernard, 2021; Carney et al., 2014; Leite Góes Gitai et al., 2019; Potruch et al., 2020; Ramgopal et al., 2013). The association I investigated between how seizures change and fluctuations in EEG features therefore serves as a crucial link to bridge the gap between treatment outcome (improved seizure symptoms/severity) and the given intervention that can be tracked with fluctuations in EEG features. Furthermore, my work provides a first step in understanding the link between altered biological rhythms and pathology. I found diminished cycles in pathological tissue, and this finding enhances the research towards a pillar of chrono-epileptology, the one that focuses on restoring biological rhythms to their normal rhythmicity as an effective treatment.

References

Aeschbach, D. and Borbély, A. A. (1993). All-night dynamics of the human sleep EEG, *Journal of Sleep Research* **2**(2): 70–81.

Aeschbach, D., Matthews, J. R., Postolache, T. T., Jackson, M. A., Giesen, H. A. and Wehr, T. A. (1999). Two circadian rhythms in the human electroencephalogram during wakefulness, *American Journal of Physiology-Regulatory, Integrative and Comparative Physiology* **277**(6): R1771–R1779.

Afra, P., Jouny, C. C. and Bergey, G. K. (2008). Duration of complex partial seizures: An intracranial EEG study, *Epilepsia* **49**(4): 677–684.

Agarwal, R. (2010). Regulation of circadian blood pressure – from mice to astronauts, *Current opinion in nephrology and hypertension* **19**(1): 51–58.

Alarcon, G., Binnie, C. D., Elwes, R. D. C. and Polkey, C. E. (1995). Power spectrum and intracranial EEG patterns at seizure onset in partial epilepsy, *Electroencephalography and Clinical Neurophysiology* **94**(5): 326–337.

Alkawadri, R., Gaspard, N., Goncharova, I. I., Spencer, D. D., Gerrard, J. L., Zaveri, H., Duckrow, R. B., Blumenfeld, H. and Hirsch, L. J. (2014). The spatial and signal characteristics of physiologic high frequency oscillations, *Epilepsia* **55**(12): 1986–1995.

Aminoff, M. J., Simon, R. P. and Wiedemann, E. (1984). The hormonal responses to generalized tonic-clonic seizures, *Brain* **107**(2): 569–578.

Anderson, C. T., Tcheng, T. K., Sun, F. T. and Morrell, M. J. (2015). Day-night patterns of epileptiform activity in 65 patients with long-term ambulatory electrocorticography, *Journal of Clinical Neurophysiology: Official Publication of the American Electroencephalographic Society* **32**(5): 406–412.

Arlot, S. and Celisse, A. (2010). A survey of cross-validation procedures for model selection, *Statistics Surveys* **4**(none).

Arzy, S., Allali, G., Brunet, D., Michel, C. M., Kaplan, P. W. and Seeck, M. (2010). Antiepileptic drugs modify power of high EEG frequencies and their neural generators, *European Journal of Neurology* **17**(10): 1308–1312.

Atif, S. M., Qazi, S. and Gillis, N. (2019). Improved SVD-based initialization for nonnegative matrix factorization using low-rank correction, *Pattern Recognition Letters* **122**: 53–59.

Badawy, R. A. B., Curatolo, J. M., Newton, M., Berkovic, S. F. and Macdonell, R. A. L. (2007). Changes in cortical excitability differentiate generalized and focal epilepsy, *Annals of Neurology* **61**(4): 324–331.

Badawy, R. A. B., Freestone, D. R., Lai, A. and Cook, M. J. (2012). Epilepsy: Everchanging states of cortical excitability, *Neuroscience* **222**: 89–99.

Badawy, R., Curatolo, J. M., Newton, M., Berkovic, S. F. and Macdonell, R. A. (2006). Sleep deprivation increases cortical excitability in epilepsy: Syndrome-specific effects, *Neurology* **67**(6): 1018–1022.

Badawy, R., Macdonell, R., Jackson, G. and Berkovic, S. (2009). The peri-ictal state: Cortical excitability changes within 24 h of a seizure, *Brain* **132**(4): 1013–1021.

Baird, A. L., Coogan, A. N., Siddiqui, A., Donev, R. M. and Thome, J. (2012). Adult attention-deficit hyperactivity disorder is associated with alterations in circadian rhythms at the behavioural, endocrine and molecular levels, *Molecular Psychiatry* **17**(10): 988–995.

Baker, G. A., Smith, D. F., Dewey, M., Morrow, J., Crawford, P. M. and Chadwick, D. W. (1991). The development of a seizure severity scale as an outcome measure in epilepsy, *Epilepsy Research* **8**(3): 245–251.

Baker, G. A., Smith, D. F., Jacoby, A., Hayes, J. A. and Chadwick, D. W. (1998). Liverpool seizure severity scale revisited, *Seizure* **7**(3): 201–205.

Barger, L. K., Wright, K. P., Hughes, R. J. and Czeisler, C. A. (2004). Daily exercise facilitates phase delays of circadian melatonin rhythm in very dim light, *American Journal of Physiology-Regulatory, Integrative and Comparative Physiology* **286**(6): R1077–R1084.

Barlow, J. S. (1985). Methods of analysis of nonstationary EEGs, with emphasis on segmentation techniques: A comparative review, *Journal of Clinical Neurophysiology* **2**(3): 267–304.

Bartolomei, F., Trébuchon, A., Bonini, F., Lambert, I., Gavaret, M., Woodman, M., Giusiano, B., Wendling, F. and Bénar, C. (2016). What is the concordance between the seizure onset zone and the irritative zone? A SEEG quantified study, *Clinical Neurophysiology* **127**(2): 1157–1162.

Bass, J. and Lazar, M. A. (2016). Circadian time signatures of fitness and disease, *Science (New York)* **354**(6315): 994–999.

Battista, B. M., Knapp, C., McGee, T. and Goebel, V. (2007). Application of the empirical mode decomposition and Hilbert-Huang transform to seismic reflection data, *Geophysics* **72**(2): H29–H37.

Baud, M. O., Ghestem, A., Benoliel, J. J., Becker, C. and Bernard, C. (2019). Endogenous multidien rhythm of epilepsy in rats, *Experimental Neurology* **315**: 82–87.

Baud, M. O., Kleen, J. K., Mirro, E. A., Andrechak, J. C., King-Stephens, D., Chang, E. F. and Rao, V. R. (2018). Multi-day rhythms modulate seizure risk in epilepsy, *Nature Communications* **9**(1): 1–10.

Bazil, C. W. and Walczak, T. S. (1997). Effects of sleep and sleep stage on epileptic and nonepileptic seizures, *Epilepsia* **38**(1): 56–62.

Bell, L. N., Kilkus, J. M., Booth, J. N., Bromley, L. E., Imperial, J. G. and Penev, P. D. (2013). Effects of sleep restriction on the human plasma metabolome, *Physiology & Behavior* **122**: 25–31.

Ben-Menachem, E. (2002). Vagus-nerve stimulation for the treatment of epilepsy, *The Lancet Neurology* **1**(8): 477–482.

Benca, R., Duncan, M. J., Frank, E., McClung, C., Nelson, R. J. and Vicentic, A. (2009). Biological rhythms, higher brain function, and behavior: Gaps, opportunities, and challenges, *Brain Research Reviews* **62**(1): 57–70.

Beniczky, S., Arbune, A. A., Jeppesen, J. and Ryvlin, P. (2020). Biomarkers of seizure severity derived from wearable devices, *Epilepsia* **61**(S1): S61–S66.

Benjamini, Y. and Hochberg, Y. (1995). Controlling the false discovery rate: A practical and powerful approach to multiple testing, *Journal of the Royal Statistical Society: Series B (Methodological)* **57**(1): 289–300.

Bergey, G. K., Morrell, M. J., Mizrahi, E. M., Goldman, A., King-Stephens, D., Nair, D., Srinivasan, S., Jobst, B., Gross, R. E., Shields, D. C., Barkley, G., Salanova, V., Olejniczak, P., Cole, A., Cash, S. S., Noe, K., Wharen, R., Worrell, G., Murro, A. M., Edwards, J., Duchowny, M., Spencer, D., Smith, M., Geller, E., Gwinn, R., Skidmore, C., Eisenschenk, S., Berg, M., Heck, C., Van Ness, P., Fountain, N., Rutecki, P., Massey, A., O'Donovan, C., Labar, D., Duckrow, R. B., Hirsch, L. J., Courtney, T., Sun, F. T. and Seale, C. G. (2015). Long-term treatment with responsive brain stimulation in adults with refractory partial seizures, *Neurology* **84**(8): 810–817.

Bernabei, J. M., Sinha, N., Arnold, T. C., Conrad, E., Ong, I., Pattnaik, A. R., Stein, J. M., Shinohara, R. T., Lucas, T. H., Bassett, D. S., Davis, K. A. and Litt, B. (2022). Normative intracranial EEG maps epileptogenic tissues in focal epilepsy, *Brain* **145**(6): 1949–1961.

Bernard, C. (2021). Circadian/multidien Molecular Oscillations and Rhythmicity of Epilepsy (MORE), *Epilepsia* **62**(1): S49–S68.

Bernard, C. and Nehlig, A. (2021). Seizures: About the right time to explore their mechanisms, *Epilepsia* **62**(S1): S1–S1.

Blanco, S., Garcia, H., Quiroga, R., Romanelli, L. and Rosso, O. (1995). Stationarity of the EEG series, *IEEE Engineering in Medicine and Biology Magazine* **14**(4): 395–399.

Blum, I. D., Zhu, L., Moquin, L., Kokoeva, M. V., Gratton, A., Giros, B. and Storch, K. F. (2014). A highly tunable dopaminergic oscillator generates ultradian rhythms of behavioral arousal, *eLife* **3**: e05105.

Bonilla-Jaime, H., Zeleke, H., Rojas, A. and Espinosa-Garcia, C. (2021). Sleep disruption worsens seizures: Neuroinflammation as a potential mechanistic link, *International Journal of Molecular Sciences* **22**(22): 12531.

Brázdil, M., Pail, M., Halámek, J., Plešinger, F., Cimbálník, J., Roman, R., Klimeš, P., Daniel, P., Chrastina, J., Brichtová, E., Rektor, I., Worrell, G. A. and Jurák, P. (2017). Very high-frequency oscillations: Novel biomarkers of the epileptogenic zone: VHF Oscillations in epilepsy, *Annals of Neurology* **82**(2): 299–310.

Breen, D. P., Vuono, R., Nawarathna, U., Fisher, K., Shneerson, J. M., Reddy, A. B. and Barker, R. A. (2014). Sleep and circadian rhythm regulation in early parkinson disease, *JAMA Neurology* **71**(5): 589.

Breheny, P. and Huang, J. (2015). Group descent algorithms for nonconvex penalized linear and logistic regression models with grouped predictors, *Statistics and Computing* **25**(2): 173–187.

Brinkmann, B. H., Karoly, P. J., Nurse, E. S., Dumanis, S. B., Nasseri, M., Viana, P. F., Schulze-Bonhage, A., Freestone, D. R., Worrell, G., Richardson, M. P. and Cook, M. J. (2021). Seizure diaries and forecasting with wearables: Epilepsy monitoring outside the clinic, *Frontiers in Neurology* **12**.

Burman, PRABIR. (1989). A comparative study of ordinary cross-validation, v-fold cross-validation and the repeated learning-testing methods, *Biometrika* **76**(3): 503–514.

Burneo, J. G., Shariff, S. Z., Liu, K., Leonard, S., Saposnik, G. and Garg, A. X. (2016). Disparities in surgery among patients with intractable epilepsy in a universal health system, *Neurology* **86**(1): 72–78.

Burns, S. P., Santaniello, S., Yaffe, R. B., Jouny, C. C., Crone, N. E., Bergey, G. K., Anderson, W. S. and Sarma, S. V. (2014). Network dynamics of the brain and

influence of the epileptic seizure onset zone, *Proceedings of the National Academy of Sciences* **111**(49): E5321–E5330.

Burrello, A., Cavigelli, L., Schindler, K., Benini, L. and Rahimi, A. (2019). Laelaps: An energy-efficient seizure detection algorithm from long-term human iEEG recordings without false alarms, *2019 Design, Automation & Test in Europe Conference & Exhibition (DATE)*, IEEE, Florence, Italy, pp. 752–757.

Buxton, O. M., Cain, S. W., O'Connor, S. P., Porter, J. H., Duffy, J. F., Wang, W., Czeisler, C. A. and Shea, S. A. (2012). Adverse metabolic consequences in humans of prolonged sleep restriction combined with circadian disruption, *Science Translational Medicine* **4**(129).

Caciagli, L., Allen, L. A., He, X., Trimmel, K., Vos, S. B., Centeno, M., Galovic, M., Sidhu, M. K., Thompson, P. J., Bassett, D. S., Winston, G. P., Duncan, J. S., Koepp, M. J. and Sperling, M. R. (2020). Thalamus and focal to bilateral seizures, *Neurology* **95**(17): e2427–e2441.

Cai, Y., Liu, S., Sothern, R. B., Xu, S. and Chan, P. (2010). Expression of clock genes *Per1* and *Bmal1* in total leukocytes in health and Parkinson's disease: Clock genes in PD, *European Journal of Neurology* **17**(4): 550–554.

Cai, Z., Sohrabpour, A., Jiang, H., Ye, S., Joseph, B., Brinkmann, B. H., Worrell, G. A. and He, B. (2021). Noninvasive high-frequency oscillations riding spikes delineates epileptogenic sources, *Proceedings of the National Academy of Sciences* **118**(17): e2011130118.

Cantello, R., Civardi, C., Varrasi, C., Vicentini, R., Cecchin, M., Boccagni, C. and Monaco, F. (2006). Excitability of the human epileptic cortex after chronic valproate: A reappraisal, *Brain Research* **1099**(1): 160–166.

Carney, P., Stanley, D. and Talathi, S. (2014). Chronotherapy in the treatment of epilepsy, *ChronoPhysiology and Therapy* **4**: 109–123.

Casiraghi, L., Spiousas, I., Dunster, G. P., McGlothlen, K., Fernández-Duque, E., Valeggia, C. and de la Iglesia, H. O. (2021). Moonstruck sleep: Synchronization of human sleep with the moon cycle under field conditions, *Science Advances*

7(5): eabe0465.

Caton, R. (1875). The electric currents of the brain.

Cermakian, N., Waddington Lamont, E., Boudreau, P. and Boivin, D. B. (2011). Circadian clock gene expression in brain regions of Alzheimer 's disease patients and control subjects, *Journal of Biological Rhythms* **26**(2): 160–170.

Chapotot, F., Jouny, C., Muzet, A., Buguet, A. and Brandenberger, G. (2000). High frequency waking EEG: Reflection of a slow ultradian rhythm in daytime arousal, *NeuroReport* **11**(10): 2223–2227.

Chavakula, V., Sánchez Fernández, I., Peters, J. M., Popli, G., Bosl, W., Rakhade, S., Rotenberg, A. and Loddenkemper, T. (2013). Automated quantification of spikes, *Epilepsy & Behavior* **26**(2): 143–152.

Chen, C.-Y., Logan, R. W., Ma, T., Lewis, D. A., Tseng, G. C., Sibille, E. and McClung, C. A. (2016). Effects of aging on circadian patterns of gene expression in the human prefrontal cortex, *Proceedings of the National Academy of Sciences* **113**(1): 206–211.

Chen, Z., Brodie, M. J., Liew, D. and Kwan, P. (2018). Treatment outcomes in patients with newly diagnosed epilepsy treated with established and new antiepileptic drugs: A 30-year longitudinal cohort study, *JAMA neurology* **75**(3): 279–286.

Chen, Z., Grayden, D. B., Burkitt, A. N., Seneviratne, U., D'Souza, W. J., French, C., Karoly, P. J., Dell, K., Leyde, K., Cook, M. J. and Maturana, M. I. (2021). Spatiotemporal patterns of high-frequency activity (80–170 Hz) in long-term intracranial EEG, *Neurology* **96**(7): e1070–e1081.

Chiang, S., Vannucci, M., Goldenholz, D. M., Moss, R. and Stern, J. M. (2018). Epilepsy as a dynamic disease: A Bayesian model for differentiating seizure risk from natural variability, *Epilepsia Open* **3**(2): 236–246.

Cohen, M. X. (2017). Where does EEG come from and what does it mean?, *Trends in Neurosciences* **40**(4): 208–218.

Coiffard, B., Diallo, A. B., Mezouar, S., Leone, M. and Mege, J.-L. (2021). A tangled threesome: Circadian rhythm, body temperature variations, and the immune system, *Biology* **10**(1): 65.

Colominas, M. A., Schlotthauer, G. and Torres, M. E. (2014). Improved complete ensemble EMD: A suitable tool for biomedical signal processing, *Biomedical Signal Processing and Control* **14**: 19–29.

Colwell, C. S. (2011). Linking neural activity and molecular oscillations in the SCN, *Nature Reviews Neuroscience* **12**(10): 553–569.

Conrad, E. C., Tomlinson, S. B., Wong, J. N., Oechsel, K. F., Shinohara, R. T., Litt, B., Davis, K. A. and Marsh, E. D. (2020). Spatial distribution of interictal spikes fluctuates over time and localizes seizure onset, *Brain* **143**(2): 554–569.

Cook, M. J. (2021). Advancing seizure forecasting from cyclical activity data, *The Lancet Neurology* **20**(2): 86–87.

Cook, M. J., Karoly, P. J., Freestone, D. R., Himes, D., Leyde, K., Berkovic, S., O'Brien, T., Grayden, D. B. and Boston, R. (2016). Human focal seizures are characterized by populations of fixed duration and interval, *Epilepsia* **57**(3): 359–368.

Cook, M. J., O'Brien, T. J., Berkovic, S. F., Murphy, M., Morokoff, A., Fabinyi, G., D'Souza, W., Yerra, R., Archer, J., Litewka, L., Hosking, S., Lightfoot, P., Ruedebusch, V., Sheffield, W. D., Snyder, D., Leyde, K. and Himes, D. (2013). Prediction of seizure likelihood with a long-term, implanted seizure advisory system in patients with drug-resistant epilepsy: A first-in-man study, *The Lancet Neurology* **12**(6): 563–571.

Cornelissen, G. and Otsuka, K. (2017). Chronobiology of aging: A mini-review, *Gerontology* **63**(2): 118–128.

Cramer, J. A. and French, J. (2001). Quantitative assessment of seizure severity for clinical trials: A review of approaches to seizure components, *Epilepsia* **42**(1): 119–129.

Crespel, A., Baldy-Moulinier, M. and Coubes, P. (1998). The relationship between sleep and epilepsy in frontal and temporal lobe epilepsies: Practical and physiopathologic considerations, *Epilepsia* **39**(2): 150–157.

Cuesta, M., Boudreau, P., Cermakian, N. and Boivin, D. B. (2017). Rapid resetting of human peripheral clocks by phototherapy during simulated night shift work, *Scientific Reports* **7**(1): 16310.

Cummings, L., Dane, A., Rhodes, J., Lynch, P. and Hughes, A. M. (2000). Diurnal variation in the quantitative EEG in healthy adult volunteers, *British Journal of Clinical Pharmacology* **50**(1): 21–26.

Davies, S. K., Ang, J. E., Revell, V. L., Holmes, B., Mann, A., Robertson, F. P., Cui, N., Middleton, B., Ackermann, K., Kayser, M., Thumser, A. E., Raynaud, F. I. and Skene, D. J. (2014). Effect of sleep deprivation on the human metabolome, *Proceedings of the National Academy of Sciences* **111**(29): 10761–10766.

de Tisi, J., Bell, G. S., Peacock, J. L., McEvoy, A. W., Harkness, W. F., Sander, J. W. and Duncan, J. S. (2011). The long-term outcome of adult epilepsy surgery, patterns of seizure remission, and relapse: A cohort study, *The Lancet* **378**(9800): 1388–1395.

Deering, R. and Kaiser, J. (2005). The use of a masking signal to improve empirical mode decomposition, *Proceedings. (ICASSP '05). IEEE International Conference on Acoustics, Speech, and Signal Processing, 2005.*, Vol. 4, pp. iv/485–iv/488 Vol. 4.

Dement, W. and Kleitman, N. (1957). Cyclic variations in EEG during sleep and their relation to eye movements, body motility, and dreaming, *Electroencephalography and Clinical Neurophysiology* **9**(4): 673–690.

Den Heijer, J. M., Otte, W. M., Van Diessen, E., Van Campen, J. S., Lorraine Hompe, E., Jansen, F. E., Joels, M., Braun, K. P. J., Sander, J. W. and Zijlmans, M. (2018). The relation between cortisol and functional connectivity in people with and without stress-sensitive epilepsy, *Epilepsia* **59**(1): 179–189.

Devinsky, O. and Lai, G. (2008). Spirituality and religion in epilepsy, *Epilepsy & Behavior* **12**(4): 636–643.

Dikanev, T., Smirnov, D., Wennberg, R., Velazquez, J. P. and Bezruchko, B. (2005). EEG nonstationarity during intracranially recorded seizures: Statistical and dynamical analysis, *Clinical Neurophysiology* **116**(8): 1796–1807.

Ding, H., Liu, S., Yuan, Y., Lin, Q., Chan, P. and Cai, Y. (2011). Decreased expression of Bmal2 in patients with Parkinson's disease, *Neuroscience Letters* **499**(3): 186–188.

Dobesberger, J., Ristić, A. J., Walser, G., Kuchukhidze, G., Unterberger, I., Höfler, J., Amann, E. and Trinka, E. (2015). Duration of focal complex, secondarily generalized tonic–clonic, and primarily generalized tonic–clonic seizures — A video-EEG analysis, *Epilepsy & Behavior* **49**: 111–117.

Drapeau, C. and Carrier, J. (2004). Fluctuation of waking electroencephalogram and subjective alertness during a 25-hour sleep-deprivation episode in young and middle-aged subjects, *Sleep* **27**(1): 55–60.

Dumanis, S. B., French, J. A., Bernard, C., Worrell, G. A. and Fureman, B. E. (2017). Seizure forecasting from idea to reality. Outcomes of the my seizure gauge epilepsy innovation institute workshop, *eNeuro* **4**(6).

Duncan, J. S. and Sander, J. W. (1991). The Chalfont seizure severity scale., *Journal of Neurology, Neurosurgery & Psychiatry* **54**(10): 873–876.

Durazzo, T. S., Spencer, S. S., Duckrow, R. B., Novotny, E. J., Spencer, D. D. and Zaveri, H. P. (2008). Temporal distributions of seizure occurrence from various epileptogenic regions, *Neurology* **70**(15): 1265–1271.

Duun-Henriksen, J., Baud, M., Richardson, M. P., Cook, M., Kouvas, G., Heasman, J. M., Friedman, D., Peltola, J., Zibrandtsen, I. C. and Kjaer, T. W. (2020). A new era in electroencephalographic monitoring? Subscalp devices for ultra–long-term recordings, *Epilepsia* **61**(9): 1805–1817.

Duy, P. Q., Krauss, G. L., Crone, N. E., Ma, M. and Johnson, E. L. (2020). Antiepileptic drug withdrawal and seizure severity in the epilepsy monitoring unit, *Epilepsy & Behavior* **109**: 107128.

Engel, J., Pitkänen, A., Loeb, J. A., Dudek, F. E., Bertram, E. H., Cole, A. J., Moshé, S. L., Wiebe, S., Fureman, B. E., Jensen, F. E., Mody, I., Nehlig, A. and Vezzani, A. (2013). Epilepsy biomarkers, *Epilepsia* **54**(0 4): 61–69.

Fenoglio-Simeone, K. A., Wilke, J. C., Milligan, H. L., Allen, C. N., Rho, J. M. and Maganti, R. K. (2009). Ketogenic diet treatment abolishes seizure periodicity and improves diurnal rhythmicity in epileptic Kcna1-null mice, *Epilepsia* **50**(9): 2027–2034.

Ferastraoaru, V., Schulze-Bonhage, A., Lipton, R. B., Dümpelmann, M., Legatt, A. D., Blumberg, J. and Haut, S. R. (2016). Termination of seizure clusters is related to the duration of focal seizures, *Epilepsia* **57**(6): 889–895.

Fernández, I. S. and Loddenkemper, T. (2013). Electrocorticography for seizure foci mapping in epilepsy surgery, *Journal of Clinical Neurophysiology* **30**(6): 554–570.

Fifel, K. and Videnovic, A. (2020). Circadian alterations in patients with neurodegenerative diseases: Neuropathological basis of underlying network mechanisms, *Neurobiology of Disease* **144**: 105029.

Fingelkurts, A. A. and Fingelkurts, A. A. (2001). Operational architectonics of the human brain biopotential field: Towards solving the mind-brain problem, *Brain and Mind* **2**(3): 261–296.

Fischl, B. (2012). FreeSurfer, *NeuroImage* **62**(2): 774–781.

Fisher, B., DesMarteau, J. A., Koontz, E. H., Wilks, S. J. and Melamed, S. E. (2021). Responsive vagus nerve stimulation for drug resistant epilepsy: A review of new features and practical guidance for advanced practice providers, *Frontiers in Neurology* **11**: 610379.

Fisher, R. S., Acevedo, C., Arzimanoglou, A., Bogacz, A., Cross, J. H., Elger, C. E., Engel, J., Forsgren, L., French, J. A., Glynn, M., Hesdorffer, D. C., Lee, B. I., Mathern, G. W., Moshé, S. L., Perucca, E., Scheffer, I. E., Tomson, T., Watanabe, M. and Wiebe, S. (2014). ILAE official report: A practical clinical definition of epilepsy, *Epilepsia* **55**(4): 475–482.

Fisher, R. S., Boas, W. v. E., Blume, W., Elger, C., Genton, P., Lee, P. and Engel, J. (2005). Epileptic seizures and epilepsy: Definitions proposed by the International League Against Epilepsy (ILAE) and the International Bureau for Epilepsy (IBE), *Epilepsia* **46**(4): 470–472.

Fisher, R. S., Cross, J. H., French, J. A., Higurashi, N., Hirsch, E., Jansen, F. E., Lagae, L., Moshé, S. L., Peltola, J., Perez, E. R., Scheffer, I. E. and Zuberi, S. M. (2017). Operational classification of seizure types by the International League Against Epilepsy: Position paper of the ILAE commission for classification and terminology, *Epilepsia* **58**(4): 522–530.

Flandrin, P., Rilling, G. and Goncalves, P. (2004). Empirical mode decomposition as a filter bank, *IEEE Signal Processing Letters* **11**(2): 112–114.

Frauscher, B., Von Ellenrieder, N., Zelmann, R., Doležalová, I., Minotti, L., Olivier, A., Hall, J., Hoffmann, D., Nguyen, D. K., Kahane, P., Dubeau, F. and Gotman, J. (2018). Atlas of the normal intracranial electroencephalogram: Neurophysiological awake activity in different cortical areas, *Brain* **141**(4): 1130–1144.

Freestone, D. R., Karoly, P. J. and Cook, M. J. (2017). A forward-looking review of seizure prediction:, *Current Opinion in Neurology* **30**(2): 167–173.

Gascoigne, S. J., Waldmann, L., Schroeder, G. M., Panagiotopoulou, M., Blickwedel, J., Chowdhury, F., Cronie, A., Diehl, B., Duncan, J. S., Falconer, J., Faulder, R., Guan, Y., Leach, V., Livingstone, S., Papasavvas, C., Thomas, R. H., Wilson, K., Taylor, P. N. and Wang, Y. (2023). A library of quantitative markers of seizure severity, *Epilepsia* p. epi.17525.

Geier, C. and Lehnertz, K. (2017). Long-term variability of importance of brain regions in evolving epileptic brain networks, *Chaos: An Interdisciplinary Journal of Nonlinear Science* **27**(4): 043112.

Geier, C., Lehnertz, K. and Bialonski, S. (2015). Time-dependent degree-degree correlations in epileptic brain networks: From assortative to dissortative mixing, *Frontiers in Human Neuroscience* **9**: 462.

Glass, L. (2001). Synchronization and rhythmic processes in physiology, *Nature* **410**(6825): 277–284.

Gliske, S. V., Irwin, Z. T., Chestek, C., Hegeman, G. L., Brinkmann, B., Sagher, O., Garton, H. J. L., Worrell, G. A. and Stacey, W. C. (2018). Variability in the location of high frequency oscillations during prolonged intracranial EEG recordings, *Nature Communications* **9**(1): 2155.

Gowers, W. R. (1885). Epilepsy and other chronic convulsive diseases: Their causes, symptoms & treatment.

Gregg, N. M., Nasseri, M., Kremen, V., Patterson, E. E., Sturges, B. K., Denison, T. J., Brinkmann, B. H. and Worrell, G. A. (2020). Circadian and multiday seizure periodicities, and seizure clusters in canine epilepsy, *Brain Communications* **2**(1).

Gregg, N. M., Pal Attia, T., Nasseri, M., Joseph, B., Karoly, P., Cui, J., Stirling, R. E., Viana, P. F., Richner, T. J., Nurse, E. S., Schulze-Bonhage, A., Cook, M. J., Worrell, G. A., Richardson, M. P., Freestone, D. R. and Brinkmann, B. H. (2023). Seizure occurrence is linked to multiday cycles in diverse physiological signals, *Epilepsia* p. epi.17607.

Griffiths, G. M. and Fox, J. T. (1938). Rhythm in epilepsy, *The Lancet* **232**(5999): 409–416.

Gronfier, C., Wright, K. P., Kronauer, R. E. and Czeisler, C. A. (2007). Entrainment of the human circadian pacemaker to longer-than-24-h days, *Proceedings of the National Academy of Sciences* **104**(21): 9081–9086.

Groppe, D. M., Bickel, S., Keller, C. J., Jain, S. K., Hwang, S. T., Harden, C. and Mehta, A. D. (2013). Dominant frequencies of resting human brain activity as measured by the electrocorticogram, *NeuroImage* **79**: 223–233.

Gualandi, I., Marzocchi, M., Achilli, A., Cavedale, D., Bonfiglio, A. and Fraboni, B. (2016). Textile organic electrochemical transistors as a platform for wearable biosensors, *Scientific Reports* **6**(1): 33637.

Guilhoto, L., Loddenkemper, T., Vendrame, M., Bergin, A., Bourgeois, B. and Kothare, S. (2011). Higher evening antiepileptic drug dose for nocturnal and early-morning seizures, *Epilepsy & Behavior* **20**(2): 334–337.

Guo, W. and Tse, P. W. (2013). A novel signal compression method based on optimal ensemble empirical mode decomposition for bearing vibration signals, *Journal of Sound and Vibration* **332**(2): 423–441.

Haas, L. F. (2003). Hans Berger (1873–1941), Richard Caton (1842–1926), and electroencephalography, *Journal of Neurology, Neurosurgery & Psychiatry* **74**(1): 9–9.

Haegelen, C., Perucca, P., Châtillon, C.-E., Andrade-Valença, L., Zelmann, R., Jacobs, J., Collins, D. L., Dubeau, F., Olivier, A. and Gotman, J. (2013). High-frequency oscillations, extent of surgical resection, and surgical outcome in drug-resistant focal epilepsy, *Epilepsia* **54**(5): 848–857.

Hagmann, P., Cammoun, L., Gigandet, X., Meuli, R., Honey, C. J., Wedeen, V. J. and Sporns, O. (2008). Mapping the structural core of human cerebral cortex, *PLoS Biology* **6**(7): e159.

Haut, S. R., Shinnar, S. and Moshé, S. L. (2005). Seizure clustering: Risks and outcomes, *Epilepsia* **46**(1): 146–149.

Haut, S. R., Vouyiouklis, M. and Shinnar, S. (2003). Stress and epilepsy: A patient perception survey, *Epilepsy & Behavior* **4**(5): 511–514.

Herzog, A. G., Fowler, K. M., Sperling, M. R. and Massaro, J. M. (2015). Distribution of seizures across the menstrual cycle in women with epilepsy, *Epilepsia* **56**(5): e58–e62.

Herzog, A. G., Klein, P. and Rand, B. J. (1997). Three patterns of catamenial epilepsy, *Epilepsia* **38**(10): 1082–1088.

Herzog, E. D. (2007). Neurons and networks in daily rhythms, *Nature Reviews Neuroscience* **8**(10): 790–802.

Hofstra, W. A. and de Weerd, A. W. (2008). How to assess circadian rhythm in humans: A review of literature, *Epilepsy & Behavior* **13**(3): 438–444.

Hofstra, W. A. and de Weerd, A. W. (2009). The circadian rhythm and its interaction with human epilepsy: A review of literature, *Sleep Medicine Reviews* **13**(6): 413–420.

Hofstra, W. A., Grootemarsink, B. E., Dieker, R., van der Palen, J. and de Weerd, A. W. (2009). Temporal distribution of clinical seizures over the 24-h day: A retrospective observational study in a tertiary epilepsy clinic, *Epilepsia* **50**(9): 2019–2026.

Howbert, J. J., Patterson, E. E., Stead, S. M., Brinkmann, B., Vasoli, V., Crepeau, D., Vite, C. H., Sturges, B., Ruedebusch, V., Mavoori, J., Leyde, K., Sheffield, W. D., Litt, B. and Worrell, G. A. (2014). Forecasting seizures in dogs with naturally occurring epilepsy, *PLOS ONE* **9**(1): e81920.

Hu, W. and Si, B. C. (2013). Soil water prediction based on its scale-specific control using multivariate empirical mode decomposition, *Geoderma* **193–194**: 180–188.

Huang, J. R., Fan, S. Z., Abbod, M. F., Jen, K. K., Wu, J. F. and Shieh, J. S. (2013). Application of multivariate empirical mode decomposition and sample entropy in EEG signals via artificial neural networks for interpreting depth of anesthesia, *Entropy* **15**(9): 3325–3339.

Huang, N. E. (2014). *Hilbert-Huang Transform and Its Applications*, World Scientific.

Huang, N. E., Shen, Z., Long, S. R., Wu, M. C., Shih, H. H., Zheng, Q., Yen, N.-C., Tung, C. C. and Liu, H. H. (1998). The empirical mode decomposition and the Hilbert spectrum for nonlinear and non-stationary time series analysis, *Proceedings of the Royal Society of London. Series A: Mathematical, Physical and Engineering Sciences* **454**(1971): 903–995.

Huang, N. E., Wu, M.-L. C., Long, S. R., Shen, S. S., Qu, W., Gloersen, P. and Fan, K. L. (2003). A confidence limit for the empirical mode decomposition and Hilbert spectral analysis, *Proceedings of the Royal Society of London. Series A: Mathematical, Physical and Engineering Sciences* **459**(2037): 2317–2345.

Hurley, N. and Rickard, S. (2009). Comparing measures of sparsity, *IEEE Transactions on Information Theory* **55**(10): 4723–4741.

Ilyas, A., Toth, E., Chaitanya, G., Riley, K. and Pati, S. (2022). Ictal high-frequency activity in limbic thalamic nuclei varies with electrographic seizure-onset patterns in temporal lobe epilepsy, *Clinical Neurophysiology* **137**: 183–192.

Jacobs, J., LeVan, P., Chander, R., Hall, J., Dubeau, F. and Gotman, J. (2008). Interictal high-frequency oscillations (80-500 Hz) are an indicator of seizure onset areas independent of spikes in the human epileptic brain, *Epilepsia* **49**(11): 1893–1907.

Jacoby, A. (2002). Stigma, epilepsy, and quality of life, *Epilepsy & Behavior* **3**(6): 10–20.

Janmohamed, M., Brodie, M. J. and Kwan, P. (2020). Pharmacoresistance – Epidemiology, mechanisms, and impact on epilepsy treatment, *Neuropharmacology* **168**: 107790.

Jarosiewicz, B. and Morrell, M. (2021). The RNS System: Brain-responsive neurostimulation for the treatment of epilepsy, *Expert Review of Medical Devices* **18**(2): 129–138.

Jefferys, J. (1990). Basic mechanisms of focal epilepsies, *Experimental Physiology* **75**(2): 127–162.

Jenssen, S., Gracely, E. J. and Sperling, M. R. (2006). How long do most seizures last? A systematic comparison of seizures recorded in the epilepsy monitoring unit, *Epilepsia* **47**(9): 1499–1503.

Jiménez-Jiménez, D., Nekkare, R., Flores, L., Chatzidimou, K., Bodi, I., Honavar, M., Mullatti, N., Elwes, R. D. C., Selway, R. P., Valentín, A. and Alarcón, G. (2015). Prognostic value of intracranial seizure onset patterns for surgical outcome of the treatment of epilepsy, *Clinical Neurophysiology* **126**(2): 257–267.

Jin, B., Aung, T., Geng, Y. and Wang, S. (2020). Epilepsy and its interaction with sleep and circadian rhythm, *Frontiers in Neurology* **11**: 327.

Jin, B., Wang, S., Yang, L., Shen, C., Ding, Y., Guo, Y., Wang, Z., Zhu, J., Wang, S. and Ding, M. (2017). Prevalence and predictors of subclinical seizures during scalp video-EEG monitoring in patients with epilepsy, *International Journal of Neuroscience* **127**(8): 651–658.

Jin, Y., Choi, J., Won, J. and Hong, Y. (2018). The relationship between autism spectrum disorder and melatonin during fetal development, *Molecules* **23**(1): 198.

Jobst, B. C., Williamson, P. D., Neuschwander, T. B., Darcey, T. M., Thadani, V. M. and Roberts, D. W. (2001). Secondarily generalized seizures in mesial temporal epilepsy: Clinical characteristics, lateralizing signs, and association with sleep-wake cycle, *Epilepsia* **42**(10): 1279–1287.

Jonsdottir, S., Bouma, A., Sergeant, J. A. and Scherder, E. J. (2004). Effects of Transcutaneous Electrical Nerve Stimulation (TENS) on cognition, behavior, and the rest-activity rhythm in children with attention deficit hyperactivity disorder, combined type, *Neurorehabilitation and Neural Repair* **18**(4): 212–221.

Kaiser, D. A. (2008). Ultradian and circadian effects in electroencephalography activity, *Biofeedback* **36**(4): 148.

Kaplan, A. I. (1998). The nonstability of the EEG: a methodological and experimental analysis, *Uspekhi Fiziologicheskikh Nauk* **29**(3): 35–55.

Kaplan, A. Y., Fingelkurts, A. A., Fingelkurts, A. A., Borisov, S. V. and Darkhovsky, B. S. (2005). Nonstationary nature of the brain activity as revealed by EEG/MEG: Methodological, practical and conceptual challenges, *Signal Processing* **85**(11): 2190–2212.

Karafin, M., St. Louis, E. K., Zimmerman, M. B., Sparks, J. D. and Granner, M. A. (2010). Bimodal ultradian seizure periodicity in human mesial temporal lobe epilepsy, *Seizure* **19**(6): 347–351.

Karoly, P. J., Freestone, D. R., Boston, R., Grayden, D. B., Himes, D., Leyde, K., Seneviratne, U., Berkovic, S., O'Brien, T. and Cook, M. J. (2016). Interictal spikes and epileptic seizures: Their relationship and underlying rhythmicity, *Brain*

139(4): 1066–1078.

Karoly, P. J., Freestone, D. R., Eden, D., Stirling, R. E., Li, L., Vianna, P. F., Maturana, M. I., D'Souza, W. J., Cook, M. J., Richardson, M. P., Brinkmann, B. H. and Nurse, E. S. (2021). Epileptic seizure cycles: Six common clinical misconceptions, *Frontiers in Neurology* **12**.

Karoly, P. J., Goldenholz, D. M., Freestone, D. R., Moss, R. E., Grayden, D. B., Theodore, W. H. and Cook, M. J. (2018). Circadian and circaseptan rhythms in human epilepsy: A retrospective cohort study, *The Lancet Neurology* **17**(11): 977–985.

Karoly, P. J., Kuhlmann, L., Soudry, D., Grayden, D. B., Cook, M. J. and Freestone, D. R. (2018). Seizure pathways: A model-based investigation, *PLOS Computational Biology* **14**(10): e1006403.

Karoly, P. J., Rao, V. R., Gregg, N. M., Worrell, G. A., Bernard, C., Cook, M. J. and Baud, M. O. (2021). Cycles in epilepsy, *Nature Reviews Neurology* **17**(5): 267–284.

Karoly, P. J., Stirling, R. E., Freestone, D. R., Nurse, E. S., Maturana, M. I., Halliday, A. J., Neal, A., Gregg, N. M., Brinkmann, B. H., Richardson, M. P., Gerche, A. L., Grayden, D. B., D'Souza, W. and Cook, M. J. (2021). Multiday cycles of heart rate are associated with seizure likelihood: An observational cohort study, *eBioMedicine* **72**.

Karoly, P. J., Ung, H., Grayden, D. B., Kuhlmann, L., Leyde, K., Cook, M. J. and Freestone, D. R. (2017). The circadian profile of epilepsy improves seizure forecasting, *Brain* **140**(8): 2169–2182.

Karthick, P. A., Tanaka, H., Khoo, H. M. and Gotman, J. (2018). Prediction of secondary generalization from a focal onset seizure in intracerebral EEG, *Clinical Neurophysiology* **129**(5): 1030–1040.

Kaufmann, E., Seethaler, M., Lauseker, M., Fan, M., Vollmar, C., Noachtar, S. and Rémi, J. (2020). Who seizes longest? Impact of clinical and demographic factors, *Epilepsia* **61**(7): 1376–1385.

Keller, M., Mazuch, J., Abraham, U., Eom, G. D., Herzog, E. D., Volk, H.-D., Kramer, A. and Maier, B. (2009). A circadian clock in macrophages controls inflammatory immune responses, *Proceedings of the National Academy of Sciences* **106**(50): 21407–21412.

Khambhati, A. N., Davis, K. A., Oommen, B. S., Chen, S. H., Lucas, T. H., Litt, B. and Bassett, D. S. (2015). Dynamic network drivers of seizure generation, propagation and termination in human neocortical epilepsy, *PLOS Computational Biology* **11**(12): e1004608.

Khan, S., Nobili, L., Khatami, R., Loddenkemper, T., Cajochen, C., Dijk, D.-J. and Eriksson, S. H. (2018). Circadian rhythm and epilepsy, *The Lancet Neurology* **17**(12): 1098–1108.

Khoo, H. M., Hall, J. A., Dubeau, F., Tani, N., Oshino, S., Fujita, Y., Gotman, J. and Kishima, H. (2020). Technical aspects of SEEG and its interpretation in the delineation of the epileptogenic zone, *Neurologia medico-chirurgica* **60**(12): 565–580.

Kim, D., Cho, J. W., Lee, J., Joo, E. Y., Hong, S. C., Hong, S. B. and Seo, D. W. (2011). Seizure duration determined by subdural electrode recordings in adult patients with intractable focal epilepsy, *Journal of Epilepsy Research* **1**(2): 57–64.

Kim, J., Imani, S., De Araujo, W. R., Warchall, J., Valdés-Ramírez, G., Paixão, T. R., Mercier, P. P. and Wang, J. (2015). Wearable salivary uric acid mouthguard biosensor with integrated wireless electronics, *Biosensors and Bioelectronics* **74**: 1061–1068.

Kimiskidis, V. K., Papagiannopoulos, S., Kazis, D. A., Sotirakoglou, K., Vasiliadis, G., Zara, F., Kazis, A. and Mills, K. R. (2006). Lorazepam-induced effects on silent period and corticomotor excitability, *Experimental Brain Research* **173**(4): 603–611.

Kirby, J., Leach, V. M., Brockington, A., Patsalos, P., Reuber, M. and Leach, J. P. (2020). Drug withdrawal in the epilepsy monitoring unit – The patsalos table, *Seizure* **75**: 75–81.

Kleitman, N. (1982). Basic rest-activity cycle – 22 Years Later, *Sleep* **5**(4): 311–317.

Kothare, S. V. and Zarowski, M. (2011). Sleep and epilepsy: Common bedfellows, *Journal of Clinical Neurophysiology* **28**(2): 101–102.

Kramer, M. A. and Cash, S. S. (2012). Epilepsy as a disorder of cortical network organization, *The Neuroscientist* **18**(4): 360–372.

Kramer, M. A., Eden, U. T., Kolaczyk, E. D., Zepeda, R., Eskandar, E. N. and Cash, S. S. (2010). Coalescence and fragmentation of cortical networks during focal seizures, *Journal of Neuroscience* **30**(30): 10076–10085.

Kramer, M. A., Eden, U. T., Lepage, K. Q., Kolaczyk, E. D., Bianchi, M. T. and Cash, S. S. (2011). Emergence of persistent networks in long-term intracranial EEG recordings, *The Journal of Neuroscience* **31**(44): 15757–15767.

Kramer, M. A., Ostrowski, L. M., Song, D. Y., Thorn, E. L., Stoyell, S. M., Parnes, M., Chinappen, D., Xiao, G., Eden, U. T., Staley, K. J., Stufflebeam, S. M. and Chu, C. J. (2019). Scalp recorded spike ripples predict seizure risk in childhood epilepsy better than spikes, *Brain* **142**(5): 1296–1309.

Kuhnert, M.-T., Elger, C. E. and Lehnertz, K. (2010). Long-term variability of global statistical properties of epileptic brain networks, *Chaos: An Interdisciplinary Journal of Nonlinear Science* **20**(4): 043126.

Kwan, P., Arzimanoglou, A., Berg, A. T., Brodie, M. J., Allen Hauser, W., Mathern, G., Moshé, S. L., Perucca, E., Wiebe, S. and French, J. (2009). Definition of drug resistant epilepsy: Consensus proposal by the ad hoc task force of the ILAE commission on therapeutic strategies: Definition of drug resistant epilepsy, *Epilepsia* **51**(6): 1069–1077.

Kwan, P. and Brodie, M. J. (2000). Early identification of refractory epilepsy, *New England Journal of Medicine* **342**(5): 314–319.

Lachner-Piza, D., Kunz, L., Brandt, A., Dümpelmann, M., Thomschewski, A. and Schulze-Bonhage, A. (2021). Effects of spatial memory processing on hippocampal ripples, *Frontiers in Neurology* **12**: 620670.

Lagarde, S., Bonini, F., McGonigal, A., Chauvel, P., Gavaret, M., Scavarda, D., Carron, R., Régis, J., Aubert, S., Villeneuve, N., Giusiano, B., Figarella-Branger, D., Trebuchon, A. and Bartolomei, F. (2016). Seizure-onset patterns in focal cortical dysplasia and neurodevelopmental tumors: Relationship with surgical prognosis and neuropathologic subtypes, *Epilepsia* **57**(9): 1426–1435.

Lagarde, S., Buzori, S., Trebuchon, A., Carron, R., Scavarda, D., Milh, M., McGonigal, A. and Bartolomei, F. (2019). The repertoire of seizure onset patterns in human focal epilepsies: Determinants and prognostic values, *Epilepsia* **60**(1): 85–95.

Lamberts, R. J., Gaitatzis, A., Sander, J. W., Elger, C. E., Surges, R. and Thijs, R. D. (2013). Postictal generalized EEG suppression, *Neurology* **81**(14): 1252–1256.

Langdon-Down, M. and Russell Brain, W. (1929). Time of day in relation to convulsions in epilepsy, *The Lancet* **213**(5516): 1029–1032.

Lee, D. D. and Seung, H. S. (1999). Learning the parts of objects by non-negative matrix factorization, *Nature* **401**(6755): 788–791.

Leguia, M. G., Andrzejak, R. G., Rummel, C., Fan, J. M., Mirro, E. A., Tcheng, T. K., Rao, V. R. and Baud, M. O. (2021). Seizure cycles in focal epilepsy, *JAMA neurology* **78**(4): 454–463.

Lehnertz, K., Geier, C., Rings, T. and Stahn, K. (2017). Capturing time-varying brain dynamics, *EPJ Nonlinear Biomedical Physics* **5**: 2.

Lehnertz, K., Rings, T. and Bröhl, T. (2021). Time in brain: How biological rhythms impact on EEG signals and on EEG-derived brain networks, *Frontiers in Network Physiology* **1**.

Leite Góes Gitai, D., De Andrade, T. G., Dos Santos, Y. D. R., Attaluri, S. and Shetty, A. K. (2019). Chronobiology of limbic seizures: Potential mechanisms and prospects of chronotherapy for mesial temporal lobe epilepsy, *Neuroscience & Biobehavioral Reviews* **98**: 122–134.

Leng, Y., Musiek, E. S., Hu, K., Cappuccio, F. P. and Yaffe, K. (2019). Association between circadian rhythms and neurodegenerative diseases, *The Lancet. Neurology*

18(3): 307–318.

Leopold, D. A., Murayama, Y. and Logothetis, N. K. (2003). Very slow activity fluctuations in monkey visual cortex: Implications for functional brain imaging, *Cerebral Cortex* **13**(4): 422–433.

Li, H., Wang, C. and Zhao, D. (2015). An improved EMD and its applications to find the basis functions of EMI signals, *Mathematical Problems in Engineering* **2015**: e150127.

Li, P., Fu, X., Smith, N. A., Ziobro, J., Curiel, J., Tenga, M. J., Martin, B., Freedman, S., Cea-Del Rio, C. A., Oboti, L., Tsuchida, T. N., Oluigbo, C., Yaun, A., Magge, S. N., O'Neill, B., Kao, A., Zelleke, T. G., Depositario-Cabacar, D. T., Ghimbovschi, S., Knoblach, S., Ho, C.-Y., Corbin, J. G., Goodkin, H. P., Vicini, S., Huntsman, M. M., Gaillard, W. D., Valdez, G. and Liu, J. S. (2017). Loss of CLOCK results in dysfunction of brain circuits underlying focal epilepsy, *Neuron* **96**(2): 387–401.e6.

Lin, Y. and Wang, Y. (2017). Neurostimulation as a promising epilepsy therapy, *Epilepsia Open* **2**(4): 371–387.

Litt, B., Esteller, R., Echauz, J., D'Alessandro, M., Shor, R., Henry, T., Pennell, P., Epstein, C., Bakay, R., Dichter, M. and Vachtsevanos, G. (2001). Epileptic seizures may begin hours in advance of clinical onset: A report of five patients, *Neuron* **30**(1): 51–64.

Liu, H., Yang, Y., Wang, Y., Tang, H., Zhang, F., Zhang, Y. and Zhao, Y. (2018). Ketogenic diet for treatment of intractable epilepsy in adults: A meta-analysis of observational studies, *Epilepsia Open* **3**(1): 9–17.

Liu, Y., Razavi Hesabi, Z., Cook, M. and Kuhlmann, L. (2022). Epileptic seizure onset predicts its duration, *European Journal of Neurology* **29**(2): 375–381.

Loddenkemper, T. (2012). Chrono-epileptology: Time to reconsider seizure timing, *Seizure* **21**(6): 411.

Loddenkemper, T., Lockley, S. W., Kaleyias, J. and Kothare, S. V. (2011). Chronobiology of epilepsy: Diagnostic and therapeutic implications of chrono-epileptology,

Journal of Clinical Neurophysiology **28**(2): 146–153.

Loddenkemper, T., Vendrame, M., Zarowski, M., Gregas, M., Alexopoulos, A. V., Wyllie, E. and Kothare, S. V. (2011). Circadian patterns of pediatric seizures, *Neurology* **76**(2): 145–153.

Logan, R. W. and McClung, C. A. (2019). Rhythms of life: Circadian disruption and brain disorders across the lifespan, *Nature Reviews Neuroscience* **20**(1): 49–65.

Lopes da Silva, F., Blanes, W., Kalitzin, S. N., Parra, J., Suffczynski, P. and Velis, D. N. (2003). Epilepsies as dynamical diseases of brain systems: Basic models of the transition between normal and epileptic activity, *Epilepsia* **44 Suppl 12**: 72–83.

Löscher, W. and Klein, P. (2021). The pharmacology and clinical efficacy of antiseizure medications: From bromide salts to cenobamate and beyond, *CNS Drugs* **35**(9): 935–963.

Lubin, A., Nute, C., Naitoh, P. and Martin, W. B. (1973). EEG delta activity during human sleep as a damped ultradian rhythm, *Psychophysiology* **10**(1): 27–35.

Lv, Y., Yuan, R. and Song, G. (2016). Multivariate empirical mode decomposition and its application to fault diagnosis of rolling bearing, *Mechanical Systems and Signal Processing* **81**: 219–234.

Ly, J. Q. M., Gaggioni, G., Chellappa, S. L., Papachilleos, S., Brzozowski, A., Borsu, C., Rosanova, M., Sarasso, S., Middleton, B., Luxen, A., Archer, S. N., Phillips, C., Dijk, D.-J., Maquet, P., Massimini, M. and Vandewalle, G. (2016). Circadian regulation of human cortical excitability, *Nature Communications* **7**(1): 11828.

Mandic, D. P., ur Rehman, N., Wu, Z. and Huang, N. E. (2013). Empirical mode decomposition-based time-frequency analysis of multivariate signals: The power of adaptive data analysis, *IEEE Signal Processing Magazine* **30**(6): 74–86.

Manganaro, S., Loddenkemper, T. and Rotenberg, A. (2017). The need for antiepileptic drug chronotherapy to treat selected childhood epilepsy syndromes and avert the harmful consequences of drug resistance, *Journal of Central Nervous System Disease*

9.

Manohar, S., Thongprayoon, C., Cheungpasitporn, W., Mao, M. A. and Herrmann, S. M. (2017). Associations of rotational shift work and night shift status with hypertension: A systematic review and meta-analysis, *Journal of Hypertension* **35**(10): 1929–1937.

Marciani, M. G. and Gotman, J. (1986). Effects of drug withdrawal on location of seizure onset, *Epilepsia* **27**(4): 423–431.

Mardia, K. V. (1976). Linear-circular correlation coefficients and rhythmometry, *Biometrika* **63**(2): 403–405.

Mardia, K. V. and Jupp, P. E. (eds) (1999). *Directional Statistics*, Wiley Series in Probability and Statistics, John Wiley & Sons, Inc., Hoboken, NJ, USA.

Martín, A., Kim, J., Kurniawan, J. F., Sempionatto, J. R., Moreto, J. R., Tang, G., Campbell, A. S., Shin, A., Lee, M. Y., Liu, X. and Wang, J. (2017). Epidermal microfluidic electrochemical detection system: Enhanced sweat sampling and metabolite detection, *ACS Sensors* **2**(12): 1860–1868.

Martin, K., Jackson, C. F., Levy, R. G. and Cooper, P. N. (2016). Ketogenic diet and other dietary treatments for epilepsy, *Cochrane Database of Systematic Reviews* .

Martino, J. K., Freelance, C. B. and Willis, G. L. (2018). The effect of light exposure on insomnia and nocturnal movement in Parkinson's disease: An open label, retrospective, longitudinal study, *Sleep Medicine* **44**: 24–31.

Matos, H. d. C., Koike, B. D. V., Pereira, W. d. S., de Andrade, T. G., Castro, O. W., Duzzioni, M., Kodali, M., Leite, J. P., Shetty, A. K. and Gitaí, D. L. G. (2018). Rhythms of core clock genes and spontaneous locomotor activity in post-status epilepticus model of mesial temporal lobe epilepsy, *Frontiers in Neurology* **9**: 632.

Maturana, M. I., Meisel, C., Dell, K., Karoly, P. J., D'Souza, W., Grayden, D. B., Burkitt, A. N., Jiruska, P., Kudlacek, J., Hlinka, J., Cook, M. J., Kuhlmann, L. and

Freestone, D. R. (2020). Critical slowing down as a biomarker for seizure susceptibility, *Nature Communications* **11**.

Meisel, C., Bailey, K., Achermann, P. and Plenz, D. (2017). Decline of long-range temporal correlations in the human brain during sustained wakefulness, *Scientific Reports* **7**(1): 11825.

Meisel, C., Schulze-Bonhage, A., Freestone, D., Cook, M. J., Achermann, P. and Plenz, D. (2015). Intrinsic excitability measures track antiepileptic drug action and uncover increasing/decreasing excitability over the wake/sleep cycle, *Proceedings of the National Academy of Sciences* **112**(47): 14694–14699.

Milton, J. G. (2010). Epilepsy as a dynamic disease: A tutorial of the past with an eye to the future, *Epilepsy & Behavior* **18**(1): 33–44.

Mitsis, G. D., Anastasiadou, M. N., Christodoulakis, M., Papathanasiou, E. S., Papacostas, S. S. and Hadjipapas, A. (2020). Functional brain networks of patients with epilepsy exhibit pronounced multiscale periodicities, which correlate with seizure onset, *Human Brain Mapping* **41**(8): 2059–2076.

Molina-Carballo, A., Muñóz-Hoyos, A., Rodríguez-Cabezas, T. and Acuña-Castroviejo, D. (1994). Day-night variations in melatonin secretion by the pineal gland during febrile and epileptic convulsions in children, *Psychiatry Research* **52**(3): 273–283.

Molina-Carballo, A., Muñoz-Hoyos, A., Sánchez-Forte, M., Uberos-Fernández, J., Moreno-Madrid, F. and Acuña-Castroviejo, D. (2007). Melatonin increases following convulsive seizures may be related to its anticonvulsant properties at physiological concentrations, *Neuropediatrics* **38**(3): 122–125.

Moran, M., Lynch, C., Walsh, C., Coen, R., Coakley, D. and Lawlor, B. (2005). Sleep disturbance in mild to moderate Alzheimer's disease, *Sleep Medicine* **6**(4): 347–352.

Naftulin, J. S., Ahmed, O. J., Piantoni, G., Eichenlaub, J. B., Martinet, L. E., Kramer, M. A. and Cash, S. S. (2018). Ictal and preictal power changes outside of the seizure focus correlate with seizure generalization, *Epilepsia* **59**(7): 1398–1409.

Nair, D. R., Laxer, K. D., Weber, P. B., Murro, A. M., Park, Y. D., Barkley, G. L., Smith, B. J., Gwinn, R. P., Doherty, M. J., Noe, K. H., Zimmerman, R. S., Bergey, G. K., Anderson, W. S., Heck, C., Liu, C. Y., Lee, R. W., Sadler, T., Duckrow, R. B., Hirsch, L. J., Wharen, R. E., Tatum, W., Srinivasan, S., McKhann, G. M., Agostini, M. A., Alexopoulos, A. V., Jobst, B. C., Roberts, D. W., Salanova, V., Witt, T. C., Cash, S. S., Cole, A. J., Worrell, G. A., Lundstrom, B. N., Edwards, J. C., Halford, J. J., Spencer, D. C., Ernst, L., Skidmore, C. T., Sperling, M. R., Miller, I., Geller, E. B., Berg, M. J., Fessler, A. J., Rutecki, P., Goldman, A. M., Mizrahi, E. M., Gross, R. E., Shields, D. C., Schwartz, T. H., Labar, D. R., Fountain, N. B., Elias, W. J., Olejniczak, P. W., Villemarette-Pittman, N. R., Eisenschenk, S., Roper, S. N., Boggs, J. G., Courtney, T. A., Sun, F. T., Seale, C. G., Miller, K. L., Skarpaas, T. L., Morrell, M. J. and RNS System LTT Study (2020). Nine-year prospective efficacy and safety of brain-responsive neurostimulation for focal epilepsy, *Neurology* **95**(9): e1244–e1256.

Nasseri, M., Pal Attia, T., Joseph, B., Gregg, N. M., Nurse, E. S., Viana, P. F., Worrell, G., Dümpelmann, M., Richardson, M. P., Freestone, D. R. and Brinkmann, B. H. (2021). Ambulatory seizure forecasting with a wrist-worn device using long-short term memory deep learning, *Scientific Reports* **11**(1): 21935.

Nei, M., Ho, R. T. and Sperling, M. R. (2000). EKG abnormalities during partial seizures in refractory epilepsy, *Epilepsia* **41**(5): 542–548.

Noachtar, S. and Peters, A. S. (2009). Semiology of epileptic seizures: A critical review, *Epilepsy & Behavior* **15**(1): 2–9.

Ochoa-Urrea, M., Lacuey, N., Vilella, L., Zhu, L., Jamal-Omidi, S., Rani, M. R. S., Hampson, J. P., Dayyani, M., Hampson, J., Hupp, N. J., Tao, S., Sainju, R. K., Friedman, D., Nei, M., Scott, C., Allen, L., Gehlbach, B. K., Reick-Mitrisin, V., Schuele, S., Ogren, J., Harper, R. M., Diehl, B., Bateman, L. M., Devinsky, O., Richerson, G. B., Zhang, G.-Q. and Lhatoo, S. D. (2021). Seizure clusters, seizure severity markers, and SUDEP risk, *Frontiers in Neurology* **12**.

Oguni, H. (2004). Diagnosis and treatment of epilepsy, *Epilepsia* **45**(s8): 13–16.

Oken, B. and Chiappa, K. (1988). Short-term variability in EEG frequency analysis, *Electroencephalography and Clinical Neurophysiology* **69**(3): 191–198.

Opherk, C., Coromilas, J. and Hirsch, L. J. (2002). Heart rate and EKG changes in 102 seizures: Analysis of influencing factors, *Epilepsy Research* **52**(2): 117–127.

Pacia, S. V. and Ebersole, J. S. (1997). Intracranial EEG substrates of scalp ictal patterns from temporal lobe foci, *Epilepsia* **38**(6): 642–654.

Panagiotopoulou, M., Papasavvas, C. A., Schroeder, G. M., Thomas, R. H., Taylor, P. N. and Wang, Y. (2022). Fluctuations in EEG band power at subject-specific timescales over minutes to days explain changes in seizure evolutions, *Human Brain Mapping* .

Pandolfo, G. (2015). Circular statistics in R, *Journal of Applied Statistics* **42**(4): 918–919.

Panteliadis, C. P., Vassilyadi, P., Fehlert, J. and Hagel, C. (2017). Historical documents on epilepsy: From antiquity through the 20th century, *Brain and Development* **39**(6): 457–463.

Parrino, L., Grassi, A. and Milioli, G. (2014). Cyclic alternating pattern in polysomnography: What is it and what does it mean?, *Current Opinion in Pulmonary Medicine* **20**(6): 533–541.

Parvizi, J. and Kastner, S. (2018). Human intracranial EEG: Promises and limitations, *Nature neuroscience* **21**(4): 474–483.

Patel, P. and Moshé, S. L. (2020). The evolution of the concepts of seizures and epilepsy: What's in a name?, *Epilepsia Open* **5**(1): 22–35.

Pattnaik, A. R., Ghosn, N. J., Ong, I. Z., Revell, A. Y., Ojemann, W. K. S., Scheid, B. H., Bernabei, J. M., Conrad, E., Sinha, S. R., Davis, K. A., Sinha, N. and Litt, B. (2022). A quantitative tool for seizure severity: Diagnostic and therapeutic applications.

Pavlova, M. K., Lee, J. W., Yilmaz, F. and Dworetzky, B. A. (2012). Diurnal pattern of seizures outside the hospital: Is there a time of circadian vulnerability?, *Neurology* **78**(19): 1488–1492.

Payne, D. E., Dell, K. L., Karoly, P. J., Kremen, V., Gerla, V., Kuhlmann, L., Worrell, G. A., Cook, M. J., Grayden, D. B. and Freestone, D. R. (2021). Identifying seizure risk factors: A comparison of sleep, weather, and temporal features using a Bayesian forecast, *Epilepsia* **62**(2): 371–382.

Payne, D. E., Karoly, P. J., Freestone, D. R., Boston, R., D'Souza, W., Nurse, E., Kuhlmann, L., Cook, M. J. and Grayden, D. B. (2018). Postictal suppression and seizure durations: A patient-specific, long-term iEEG analysis, *Epilepsia* **59**(5): 1027–1036.

Peng, W., Danison, J. L. and Seyal, M. (2017). Postictal generalized EEG suppression and respiratory dysfunction following generalized tonic–clonic seizures in sleep and wakefulness, *Epilepsia* **58**(8): 1409–1414.

Pensel, M. C., Schnuerch, M., Elger, C. E. and Surges, R. (2020). Predictors of focal to bilateral tonic-clonic seizures during long-term video-EEG monitoring, *Epilepsia* **61**(3): 489–497.

Perucca, E., Brodie, M. J., Kwan, P. and Tomson, T. (2020). 30 years of second-generation antiseizure medications: Impact and future perspectives, *The Lancet Neurology* **19**(6): 544–556.

Perucca, P., Dubeau, F. and Gotman, J. (2014). Intracranial electroencephalographic seizure-onset patterns: Effect of underlying pathology, *Brain* **137**(1): 183–196.

Pewsey, A. and García-Portugués, E. (2021). Recent advances in directional statistics, *TEST* **30**(1): 1–58.

Philippu, A. (1988). Regulation of blood pressure by central neurotransmitters and neuropeptides, *Reviews of Physiology, Biochemistry and Pharmacology, Volume 111*, Reviews of Physiology, Biochemistry and Pharmacology, Springer, Berlin, Heidelberg, pp. 1–115.

Philippu, A. (2019). Neurotransmitters are released in brain areas according to ultradian rhythms: Coincidence with ultradian oscillations of EEG waves, *Journal of Chemical Neuroanatomy* **96**: 66–72.

Philipsen, A., Hornyak, M. and Riemann, D. (2006). Sleep and sleep disorders in adults with attention deficit/hyperactivity disorder, *Sleep Medicine Reviews* **10**(6): 399–405.

Pitkänen, A., Löscher, W., Vezzani, A., Becker, A. J., Simonato, M., Lukasiuk, K., Gröhn, O., Bankstahl, J. P., Friedman, A., Aronica, E., Gorter, J. A., Ravizza, T., Sisodiya, S. M., Kokaia, M. and Beck, H. (2016). Advances in the development of biomarkers for epilepsy, *The Lancet. Neurology* **15**(8): 843–856.

Polychronopoulos, P., Argyriou, A. A., Sirrou, V., Huliara, V., Aplada, M., Gourzis, P., Economou, A., Terzis, E. and Chroni, E. (2006). Lunar phases and seizure occurrence: Just an ancient legend?, *Neurology* **66**(9): 1442–1443.

Potruch, A., Khoury, S. T. and Ilan, Y. (2020). The role of chronobiology in drug-resistance epilepsy: The potential use of a variability and chronotherapy-based individualized platform for improving the response to anti-seizure drugs, *Seizure - European Journal of Epilepsy* **80**: 201–211.

Pritchard III, P. B. (1991). The effect of seizures on hormones, *Epilepsia* **32**(s6): S46–S50.

Proix, T., Truccolo, W., Leguia, M. G., Tcheng, T. K., King-Stephens, D., Rao, V. R. and Baud, M. O. (2021). Forecasting seizure risk in adults with focal epilepsy: A development and validation study, *The Lancet. Neurology* **20**(2): 127–135.

Quigg, M. (2000). Circadian rhythms: Interactions with seizures and epilepsy, *Epilepsy Research* **42**(1): 43–55.

Quigg, M., Straume, M., Menaker, M. and Bertam, E. H. (1998). Temporal distribution of partial seizures: Comparison of an animal model with human partial epilepsy, *Annals of Neurology* **43**(6): 748–755.

Rakers, F., Walther, M., Schiffner, R., Rupprecht, S., Rasche, M., Kockler, M., Witte, O. W., Schlattmann, P. and Schwab, M. (2017). Weather as a risk factor for epileptic

seizures: A case-crossover study, *Epilepsia* **58**(7): 1287–1295.

Ramgopal, S., Shah, A., Zarowski, M., Vendrame, M., Gregas, M., Alexopoulos, A. V., Loddenkemper, T. and Kothare, S. V. (2012). Diurnal and sleep/wake patterns of epileptic spasms in different age groups: Diurnal Patterns of Epileptic Spasms, *Epilepsia* **53**(7): 1170–1177.

Ramgopal, S., Thome-Souza, S. and Loddenkemper, T. (2013). Chronopharmacology of anti-convulsive therapy, *Current Neurology and Neuroscience Reports* **13**(4): 339.

Ramgopal, S., Vendrame, M., Shah, A., Gregas, M., Zarowski, M., Rotenberg, A., Alexopoulos, A. V., Wyllie, E., Kothare, S. V. and Loddenkemper, T. (2012). Circadian patterns of generalized tonic–clonic evolutions in pediatric epilepsy patients, *Seizure* **21**(7): 535–539.

Rao, V. R., G. Leguia, M., Tcheng, T. K. and Baud, M. O. (2021). Cues for seizure timing, *Epilepsia* **62**(S1): S15–S31.

Re, C. J., Batterman, A. I., Gerstner, J. R., Buono, R. J. and Ferraro, T. N. (2020). The molecular genetic interaction between circadian rhythms and susceptibility to seizures and epilepsy, *Frontiers in Neurology* **11**: 520.

Rehman, N. and Mandic, D. P. (2010). Multivariate empirical mode decomposition, *Proceedings of the Royal Society A: Mathematical, Physical and Engineering Sciences* **466**(2117): 1291–1302.

Rieke, C., Mormann, F., Andrzejak, R., Kreuz, T., David, P., Elger, C. and Lehnertz, K. (2003). Discerning nonstationarity from nonlinearity in seizure-free and preseizure EEG recordings from epilepsy patients, *IEEE Transactions on Biomedical Engineering* **50**(5): 634–639.

Rilling, G., Flandrin, P. and Goncalves, P. (2003). On empirical mode decomposition and its algorithms, *In Proceedings of IEEE-EURASIP Workshop on Nonlinear Signal and Image Processing NSIP-03* .

Rilling, G., Flandrin, P., Goncalves, P. and Lilly, J. M. (2007). Bivariate empirical mode decomposition, *IEEE Signal Processing Letters* **14**(12): 936–939.

Roehri, N., Pizzo, F., Lagarde, S., Lambert, I., Nica, A., McGonigal, A., Giusiano, B., Bartolomei, F. and Bénar, C.-G. (2018). High-frequency oscillations are not better biomarkers of epileptogenic tissues than spikes: HFOs are not better than spikes, *Annals of Neurology* **83**(1): 84–97.

Roenneberg, T. and Merrow, M. (2016). The circadian clock and human health, *Current biology: CB* **26**(10): R432–443.

Rojas, A., Górriz, J. M., Ramírez, J., Illán, I. A., Martínez-Murcia, F. J., Ortiz, A., Gómez Río, M. and Moreno-Caballero, M. (2013). Application of Empirical Mode Decomposition (EMD) on DaTSCAN SPECT images to explore Parkinson Disease, *Expert Systems with Applications* **40**(7): 2756–2766.

Rose, A. B., McCabe, P. H., Gilliam, F. G., Smith, B. J., Boggs, J. G., Ficker, D. M., Moore, J. L., Passaro, E. A. and Bazil, C. W. (2003). Occurrence of seizure clusters and status epilepticus during inpatient video-EEG monitoring, *Neurology* **60**(6): 975–978.

Rosenow, F. (2001). Presurgical evaluation of epilepsy, *Brain* **124**(9): 1683–1700.

Rothman, S. M. and Mattson, M. P. (2012). Sleep disturbances in Alzheimer's and Parkinson's diseases, *NeuroMolecular Medicine* **14**(3): 194–204.

Rybak, Y. E., McNeely, H. E., Mackenzie, B. E., Jain, U. R. and Levitan, R. D. (2007). Seasonality and circadian preference in adult attention-deficit/hyperactivity disorder: Clinical and neuropsychological correlates, *Comprehensive Psychiatry* **48**(6): 562–571.

Ryvlin, P., Rheims, S., Hirsch, L. J., Sokolov, A. and Jehi, L. (2021). Neuromodulation in epilepsy: State-of-the-art approved therapies, *The Lancet Neurology* **20**(12): 1038–1047.

Saggio, M. L., Crisp, D., Scott, J. M., Karoly, P., Kuhlmann, L., Nakatani, M., Murai, T., Dümpelmann, M., Schulze-Bonhage, A., Ikeda, A., Cook, M., Gliske, S. V., Lin, J., Bernard, C., Jirsa, V. and Stacey, W. C. (2020). A taxonomy of seizure dynamotypes, *eLife* **9**.

Sakoe, H. and Chiba, S. (1978). Dynamic programming algorithm optimization for spoken word recognition, *IEEE Transactions on Acoustics, Speech, and Signal Processing* **26**(1): 43–49.

Salami, P., Borzello, M., Kramer, M. A., Westover, M. B. and Cash, S. S. (2022). Quantifying seizure termination patterns reveals limited pathways to seizure end, *Neurobiology of Disease* **165**: 105645.

Salami, P., Peled, N., Nadalin, J. K., Martinet, L.-E., Kramer, M. A., Lee, J. W. and Cash, S. S. (2020). Seizure onset location shapes dynamics of initiation, *Clinical Neurophysiology* **131**(8): 1782–1797.

Salanova, V., Witt, T., Worth, R., Henry, T. R., Gross, R. E., Nazzaro, J. M., Labar, D., Sperling, M. R., Sharan, A., Sandok, E., Handforth, A., Stern, J. M., Chung, S., Henderson, J. M., French, J., Baltuch, G., Rosenfeld, W. E., Garcia, P., Barbaro, N. M., Fountain, N. B., Elias, W. J., Goodman, R. R., Pollard, J. R., Troster, A. I., Irwin, C. P., Lambrecht, K., Graves, N., Fisher, R. and For the SANTE Study Group (2015). Long-term efficacy and safety of thalamic stimulation for drug-resistant partial epilepsy, *Neurology* **84**(10): 1017–1025.

Sánchez-Barceló, E. J., Mediavilla, M. D. and Reiter, R. J. (2011). Clinical uses of melatonin in pediatrics, *International Journal of Pediatrics* **2011**: 1–11.

Savvidis, C. and Koutsilieris, M. (2012). Circadian rhythm disruption in cancer biology, *Molecular Medicine* **18**(9): 1249–1260.

Schauwecker, P. E. (2012). The effects of glycemic control on seizures and seizure-induced excitotoxic cell death, *BMC Neuroscience* **13**(1): 94.

Scheich, H. (1969). Interval histograms and periodic diurnal changes of human alpha rhythms, *Electroencephalography and Clinical Neurophysiology* **26**(4): 442.

Schevon, C. A., Weiss, S. A., McKhann, G., Goodman, R. R., Yuste, R., Emerson, R. G. and Trevelyan, A. J. (2012). Evidence of an inhibitory restraint of seizure activity in humans, *Nature Communications* **3**(1): 1060.

Schindler, K., Gast, H., Stieglitz, L., Stibal, A., Hauf, M., Wiest, R., Mariani, L. and Rummel, C. (2011). Forbidden ordinal patterns of periictal intracranial EEG indicate deterministic dynamics in human epileptic seizures: Forbidden patterns in iEEG, *Epilepsia* **52**(10): 1771–1780.

Scholtens, LH., Lange, SC. and van den Heuvel, MP. (2021). Simple brain plot.

Schroeder, G. M., Chowdhury, F. A., Cook, M. J., Diehl, B., Duncan, J. S., Karoly, P. J., Taylor, P. N. and Wang, Y. (2022). Multiple mechanisms shape the relationship between pathway and duration of focal seizures, *Brain Communications* **4**(4): fcac173.

Schroeder, G. M., Diehl, B., Chowdhury, F. A., Duncan, J. S., de Tisi, J., Trevelyan, A. J., Forsyth, R., Jackson, A., Taylor, P. N. and Wang, Y. (2020). Seizure pathways change on circadian and slower timescales in individual patients with focal epilepsy, *Proceedings of the National Academy of Sciences* .

Schroeder, G. M., Karoly, P. J., Maturana, M., Panagiotopoulou, M., Taylor, P. N., Cook, M. J. and Wang, Y. (2022). Chronic iEEG recordings and interictal spike rate reveal multiscale temporal modulations in seizure states.

Scott, J. M., Gliske, S. V., Kuhlmann, L. and Stacey, W. C. (2021). Viability of preictal high-frequency oscillation rates as a biomarker for seizure prediction, *Frontiers in Human Neuroscience* **14**: 612899.

Serin, Y. and Acar Tek, N. (2019). Effect of circadian rhythm on metabolic processes and the regulation of energy balance, *Annals of Nutrition and Metabolism* **74**(4): 322–330.

Shah, P., Ashourvan, A., Mikhail, F., Pines, A., Kini, L., Oechsel, K., Das, S. R., Stein, J. M., Shinohara, R. T., Bassett, D. S., Litt, B. and Davis, K. A. (2019). Characterizing the role of the structural connectome in seizure dynamics, *Brain* **142**(7): 1955–1972.

Shannahoff-Khalsa, D. (1991). Lateralized rhythms of the central and autonomic nervous systems, *International Journal of Psychophysiology* **11**(3): 225–251.

Shouse, M. N., Martins da Silva, A. and Sammaritano, M. (1996). Circadian rhythm, sleep, and epilepsy, *Journal of Clinical Neurophysiology* **13**(1): 32.

Simeone, T. A., Simeone, K. A., Stafstrom, C. E. and Rho, J. M. (2018). Do ketone bodies mediate the anti-seizure effects of the ketogenic diet?, *Neuropharmacology* **133**: 233–241.

Sinha, S. (2006). Do seizures in patients with refractory epilepsy vary between wakefulness and sleep?, *Journal of Neurology, Neurosurgery & Psychiatry* **77**(9): 1076–1078.

Smeets, V. M., van Lierop, B. A., Vanhoutvin, J. P., Aldenkamp, A. P. and Nijhuis, F. J. (2007). Epilepsy and employment: Literature review, *Epilepsy & Behavior* **10**(3): 354–362.

Smith, S. (2005). EEG in the diagnosis, classification, and management of patients with epilepsy, *Journal of Neurology, Neurosurgery, and Psychiatry* **76**(Suppl 2): ii2–ii7.

Smyk, M. K. and van Luijtelaar, G. (2020). Circadian rhythms and epilepsy: A suitable case for absence epilepsy, *Frontiers in Neurology* **11**: 245.

Spencer, D. C., Sun, F. T., Brown, S. N., Jobst, B. C., Fountain, N. B., Wong, V. S. S., Mirro, E. A. and Quigg, M. (2016). Circadian and ultradian patterns of epileptiform discharges differ by seizure-onset location during long-term ambulatory intracranial monitoring, *Epilepsia* **57**(9): 1495–1502.

Spencer, S. S., Spencer, D. D., Williamson, P. D. and Mattson, R. H. (1981). Ictal effects of anticonvulsant medication withdrawal in epileptic patients, *Epilepsia* **22**(3): 297–307.

Staba, R. J., Stead, M. and Worrell, G. A. (2014). Electrophysiological biomarkers of epilepsy, *Neurotherapeutics* **11**(2): 334–346.

Stafstrom, C. E. and Carmant, L. (2015). Seizures and epilepsy: An overview for neuroscientists, *Cold Spring Harbor Perspectives in Medicine* **5**(6).

Stam, C. J. (2005). Nonlinear dynamical analysis of EEG and MEG: Review of an emerging field, *Clinical Neurophysiology* **116**(10): 2266–2301.

Steriade, M., Nunez, A. and Amzica, F. (1993). Intracellular analysis of relations between the slow (< 1 Hz) neocortical oscillation and other sleep rhythms of the electroencephalogram, *The Journal of Neuroscience* **13**(8): 3266–3283.

Stirling, R. E., Cook, M. J., Grayden, D. B. and Karoly, P. J. (2021). Seizure forecasting and cyclic control of seizures, *Epilepsia* **62**(S1).

Strijkstra, A. M., Beersma, D. G. M., Drayer, B., Halbesma, N. and Daan, S. (2003). Subjective sleepiness correlates negatively with global alpha (8–12 Hz) and positively with central frontal theta (4–8 Hz) frequencies in the human resting awake electroencephalogram, *Neuroscience Letters* **340**(1): 17–20.

Suffczynski, P., Lopes da Silva, F., Parra, J., Velis, D., Bouwman, B., van Rijn, C., van Hese, P., Boon, P., Khosravani, H., Derchansky, M., Carlen, P. and Kalitzin, S. (2006). Dynamics of epileptic phenomena determined from statistics of ictal transitions, *IEEE Transactions on Biomedical Engineering* **53**(3): 524–532.

Sunderam, S., Osorio, I. and Frei, M. G. (2007). Epileptic seizures are temporally interdependent under certain conditions, *Epilepsy Research* **76**(2): 77–84.

Tauste Campo, A., Principe, A., Ley, M., Rocamora, R. and Deco, G. (2018). Degenerate time-dependent network dynamics anticipate seizures in human epileptic brain, *PLOS Biology* **16**(4): e2002580.

Taylor, P. N., Papasavvas, C. A., Owen, T. W., Schroeder, G. M., Hutchings, F. E., Chowdhury, F. A., Diehl, B., Duncan, J. S., McEvoy, A. W., Miserocchi, A., de Tisi, J., Vos, S. B., Walker, M. C. and Wang, Y. (2022). Normative brain mapping of interictal intracranial EEG to localize epileptogenic tissue, *Brain* **145**(3): 939–949.

Taylor, P. N., Sinha, N., Wang, Y., Vos, S. B., de Tisi, J., Miserocchi, A., McEvoy, A. W., Winston, G. P. and Duncan, J. S. (2018). The impact of epilepsy surgery on the structural connectome and its relation to outcome, *NeuroImage: Clinical* **18**: 202–214.

Temkin, N. R. and Davis, G. R. (1984). Stress as a risk factor for seizures among adults with epilepsy, *Epilepsia* **25**(4): 450–456.

Tibshirani, R. (1996). Regression shrinkage and selection via the Lasso, *Journal of the Royal Statistical Society: Series B (Methodological)* **58**(1): 267–288.

Todorova, K. S., Velikova, V. S., Kaprelyan, A. G. and Tsekov, S. T. (2013). Seizure severity as an alternative measure of outcome in epilepsy, *Journal of IMAB - Annual Proceeding (Scientific Papers)* **19**(3): 433–437.

Toffa, D. H., Touma, L., Meskine, T. E., Bouthillier, A. and Nguyen, D. K. (2020). Learnings from 30 years of reported efficacy and safety of vagus nerve stimulation (VNS) for epilepsy treatment: A critical review, *Seizure - European Journal of Epilepsy* **83**: 104–123.

Tong, S., Li, Z., Zhu, Y. and Thakor, N. V. (2007). Describing the nonstationarity level of neurological signals based on quantifications of time-frequency representation, *IEEE Transactions on Biomedical Engineering* **54**(10): 1780–1785.

Torres, M. E., Colominas, M. A., Schlotthauer, G. and Flandrin, P. (2011). A complete ensemble empirical mode decomposition with adaptive noise, *2011 IEEE International Conference on Acoustics, Speech and Signal Processing (ICASSP)*, IEEE, Prague, Czech Republic, pp. 4144–4147.

Truccolo, W., Donoghue, J. A., Hochberg, L. R., Eskandar, E. N., Madsen, J. R., Anderson, W. S., Brown, E. N., Halgren, E. and Cash, S. S. (2011). Single-neuron dynamics in human focal epilepsy, *Nature Neuroscience* **14**(5): 635–641.

Ułamek-Kozioł, M., Czuczwar, S. J., Januszewski, S. and Pluta, R. (2019). Ketogenic diet and epilepsy, *Nutrients* **11**(10): 2510.

ur Rehman, N. and Aftab, H. (2019). Multivariate variational mode decomposition, *IEEE Transactions on Signal Processing* **67**(23): 6039–6052.

Ur Rehman, N. and Mandic, D. (2010). Empirical mode decomposition for trivariate signals, *IEEE Transactions on Signal Processing* **58**(3): 1059–1068.

Ur Rehman, N. and Mandic, D. P. (2011). Filter bank property of multivariate empirical mode decomposition, *IEEE Transactions on Signal Processing* **59**(5): 2421–2426.

Urrestarazu, E., Chander, R., Dubeau, F. and Gotman, J. (2007). Interictal high-frequency oscillations (100–500 Hz) in the intracerebral EEG of epileptic patients, *Brain* **130**(9): 2354–2366.

Usami, K., Matsumoto, R., Kobayashi, K., Hitomi, T., Shimotake, A., Kikuchi, T., Matsuhashi, M., Kunieda, T., Mikuni, N., Miyamoto, S., Fukuyama, H., Takahashi, R. and Ikeda, A. (2015). Sleep modulates cortical connectivity and excitability in humans: Direct evidence from neural activity induced by single-pulse electrical stimulation: SPES-induced CCEP & high gamma in sleep, *Human Brain Mapping* **36**(11): 4714–4729.

Usui, N., Terada, K., Baba, K., Matsuda, K., Nakamura, F., Usui, K., Yamaguchi, M., Tottori, T., Umeoka, S., Fujitani, S., Kondo, A., Mihara, T. and Inoue, Y. (2011). Clinical significance of ictal high frequency oscillations in medial temporal lobe epilepsy, *Clinical Neurophysiology* **122**(9): 1693–1700.

van Campen, J. S., Hompe, E. L., Jansen, F. E., Velis, D. N., Otte, W. M., van de Berg, F., Braun, K. P. J., Visser, G. H., Sander, J. W., Joels, M. and Zijlmans, M. (2016). Cortisol fluctuations relate to interictal epileptiform discharges in stress sensitive epilepsy, *Brain* **139**(6): 1673–1679.

van Eeghen, A. M., Numis, A. I., Staley, B. A., Therrien, S. E., Thibert, R. L. and Thiele, E. A. (2011). Characterizing sleep disorders of adults with tuberous sclerosis complex: A questionnaire-based study and review, *Epilepsy & Behavior* **20**(1): 68–74.

van Putten, M. J. A. M. (2020). Basics of the EEG, *in* M. J. van Putten (ed.), *Dynamics of Neural Networks: A Mathematical and Clinical Approach*, Springer, Berlin, Heidelberg, pp. 129–152.

Verbeek, M. M., Leen, W. G., Willemsen, M. A., Slats, D. and Claassen, J. A. (2016). Hourly analysis of cerebrospinal fluid glucose shows large diurnal fluctuations, *Journal of Cerebral Blood Flow & Metabolism* **36**(5): 899–902.

Vetter, C., Devore, E. E., Wegrzyn, L. R., Massa, J., Speizer, F. E., Kawachi, I., Rosner, B., Stampfer, M. J. and Schernhammer, E. S. (2016). Association between

rotating night shift work and risk of coronary heart disease among women, *JAMA* **315**(16): 1726.

Vidaurre, D., Smith, S. M. and Woolrich, M. W. (2017). Brain network dynamics are hierarchically organized in time, *Proceedings of the National Academy of Sciences* **114**(48): 12827–12832.

Videnovic, A. and Zee, P. C. (2015). Consequences of circadian disruption on neurologic health, *Sleep medicine clinics* **10**(4): 469–480.

Wagner, F. B., Eskandar, E. N., Cosgrove, G. R., Madsen, J. R., Blum, A. S., Potter, N. S., Hochberg, L. R., Cash, S. S. and Truccolo, W. (2015). Microscale spatiotemporal dynamics during neocortical propagation of human focal seizures, *NeuroImage* **122**: 114–130.

Wallace, E., Wright, S., Schoenike, B., Roopra, A., Rho, J. M. and Maganti, R. K. (2018). Altered circadian rhythms and oscillation of clock genes and sirtuin 1 in a model of sudden unexpected death in epilepsy, *Epilepsia* **59**(8): 1527–1539.

Wang, Y., Trevelyan, A. J., Valentin, A., Alarcon, G., Taylor, P. N. and Kaiser, M. (2017). Mechanisms underlying different onset patterns of focal seizures, *PLOS Computational Biology* **13**(5): e1005475.

Wirrell, E. C., Nabbout, R., Scheffer, I. E., Alsaadi, T., Bogacz, A., French, J. A., Hirsch, E., Jain, S., Kaneko, S., Riney, K., Samia, P., Snead, O. C., Somerville, E., Specchio, N., Trinka, E., Zuberi, S. M., Balestrini, S., Wiebe, S., Cross, J. H., Perucca, E., Moshé, S. L. and Tinuper, P. (2022). Methodology for classification and definition of epilepsy syndromes with list of syndromes: Report of the ILAE Task Force on Nosology and Definitions, *Epilepsia* **63**(6): 1333–1348.

Worrell, G. A., Parish, L., Cranstoun, S. D., Jonas, R., Baltuch, G. and Litt, B. (2004). High-frequency oscillations and seizure generation in neocortical epilepsy, *Brain* **127**(7): 1496–1506.

Wu, H., Liu, Y., Liu, L., Meng, Q., Du, C., Li, K., Dong, S., Zhang, Y., Li, H. and Zhang, H. (2021). Decreased expression of the clock gene Bmal1 is involved in the

pathogenesis of temporal lobe epilepsy, *Molecular Brain* **14**: 113.

Wu, J. Y., Sankar, R., Lerner, J. T., Matsumoto, J. H., Vinters, H. V. and Mathern, G. W. (2010). Removing interictal fast ripples on electrocorticography linked with seizure freedom in children, *Neurology* **75**(19): 1686–1694.

Wu, Z. and Huang, N. E. (2004). A study of the characteristics of white noise using the empirical mode decomposition method, *Proceedings of the Royal Society of London. Series A: Mathematical, Physical and Engineering Sciences* **460**(2046): 1597–1611.

Wu, Z. and Huang, N. E. (2009). Ensemble empirical mode decomposition: A noise-assisted data analysis method, *Advances in Adaptive Data Analysis* **1**: 1–41.

Wulff, K., Porcheret, K., Cussans, E. and Foster, R. G. (2009). Sleep and circadian rhythm disturbances: Multiple genes and multiple phenotypes, *Current Opinion in Genetics & Development* **19**(3): 237–246.

Xue, X., Zhou, J., Xu, Y., Zhu, W. and Li, C. (2015). An adaptively fast ensemble empirical mode decomposition method and its applications to rolling element bearing fault diagnosis, *Mechanical Systems and Signal Processing* **62–63**: 444–459.

Yalýn, Ö., Arman, F., Erdoğan, F. and Kula, M. (2006). A comparison of the circadian rhythms and the levels of melatonin in patients with diurnal and nocturnal complex partial seizures, *Epilepsy & Behavior* **8**(3): 542–546.

Yamadera, H., Ito, T., Suzuki, H., Asayama, K., Ito, R. and Endo, S. (2000). Effects of bright light on cognitive and sleep–wake (circadian) rhythm disturbances in Alzheimer-type dementia, *Psychiatry and Clinical Neurosciences* **54**(3): 352–353.

Yang, S., Yamazaki, S., Cox, K. H., Huang, Y.-L., Miller, E. W. and Takahashi, J. S. (2022). Coupling-dependent metabolic ultradian rhythms in confluent cells, *Proceedings of the National Academy of Sciences* **119**(45): e2211142119.

Yegnanarayan, R., Mahesh, S. D. and Sangle, S. (2006). Chronotherapeutic Dose Schedule of Phenytoin and Carbamazepine in Epileptic Patients, *Chronobiology International* **23**(5): 1035–1046.

Yuan, M. and Lin, Y. (2006). Model selection and estimation in regression with grouped variables, *Journal of the Royal Statistical Society: Series B (Statistical Methodology)* **68**(1): 49–67.

Zamponi, N., Passamonti, C., Cesaroni, E., Trignani, R. and Rychlicki, F. (2011). Effectiveness of vagal nerve stimulation (VNS) in patients with drop-attacks and different epileptic syndromes, *Seizure* **20**(6): 468–474.

Zhou, D., Wang, Y., Hopp, P., Kerling, F., Kirchner, A., Pauli, E. and Stefan, H. (2002). Influence on ictal seizure semiology of rapid withdrawal of carbamazepine and valproate in monotherapy, *Epilepsia* **43**(4): 386–393.

Zhuang, X., Yang, Z. and Cordes, D. (2020). A technical review of canonical correlation analysis for neuroscience applications, *Human Brain Mapping* **41**(13): 3807–3833.